Environmentally Benign Production of Ionic Liquids in CO_2-Expanded Systems

By

Sylvia Ogechi Nwosu

Submitted to the graduate degree program in Chemical and Petroleum Engineering and the Graduate Faculty of the University of Kansas in partial fulfillment of the requirements for the degree of Doctor of Philosophy.

_____

Chairperson* Aaron M. Scurto

_____

Committee Members: Raghunath V. Chaudhari

_____

Lawrence Weatherley

_____

Susan Williams

_____

Jon Tunge

Date Defended: July 6th, 2012

The Dissertation Committee for Sylvia O. Nwosu
certifies that this is the approved version of the following dissertation

Environmentally Benign Production of Ionic Liquids
in
CO_2-Expanded Systems

_____

Chairperson Aaron M. Scurto

Date approved: 23rd July 2012

Environmentally Benign Production of Ionic Liquids in CO_2-Expanded Systems

Sylvia O. Nwosu

The need to reduce air pollution in chemical manufacturing processes continues to drive the search for alternative solvents. Ionic Liquids (ILs) have emerged in recent years as a promising solution. In contrast to traditional organic solvents, ILs have negligible volatility, which eliminates air emissions and harmful worker exposure concerns. Various combinations of cations and anions afford distinct properties to an IL, such as melting point, solvation properties, and phase behavior; thus making it possible to molecularly *design* or engineer ILs for specific tasks across many chemical sectors.

Unfortunately, many ILs are synthesized and processed using the very organic solvents which they are purportedly replacing. Despite the exponential growth in this field, very little work focuses on developing alternative synthesis and production methods for ILs. The objective of this dissertation is to investigate novel economically viable and environmentally benign methodologies for ionic liquid production.

Three solvent platforms: 1) conventional organic solvents; 2) compressed and supercritical CO_2; 3) CO_2-Expanded DMSO are considered for the synthesis of IL synthesis. A full understanding of the kinetics and effects of solvent in the synthesis of ILs is of great importance for optimally selecting a benign and economically viable solvent for IL production. Empirical LSER expression, correlating kinetic rate constant with solvent polarity was obtained, which will facilitate rapid data generation needed for engineering production processes of different ILs in varied solvent systems. While some general trends for these Mentshukin-type reactions are widely known, quantitative second (2^{nd}) order rate constants are reported here.

The use of CO_2 in the synthesis of ILs has many advantages over conventional solvents. CO_2 induces IL-solvent mixtures to split into IL-rich and organic solvent-rich phases that can be decanted or extracted for easy separations, simply by controlling pressure,

temperature and CO_2 loading. This work demonstrates that CO_2 is a flexible and tunable solvent for the synthesis of the model IL 1-hexyl-3-methylimidazolium bromide ([HMIm][Br]). Previously, our group has found that among ten organic solvents, DMSO has the highest kinetic rate for the synthesis of [HMIm][Br]). Although DMSO is a relatively environmentally benign solvent, it is beset with a high boiling point (189^oC), rendering it both economically and environmentally non-feasible as a solvent option. The synthesis and processing of ILs in gas-expanded DMSO alleviates these issues. Furthermore, gas expanded liquids reduce the amount of organic solvent needed for the reaction. This work, for the first time, leverages the kinetic benefits of DMSO and the thermodynamic advantages of benign CO_2 for the production of ILs. Specifically, this study explored another promising solvent media; CO_2 expanded liquid DMSO (CXLs).Non-complex separation schemes are proposed from mixture phase behavior. Kamlet-Taft polarity parameters for CO_2 expanded DMSO are also reported.

Experimental high-pressure phase equilibria data were measured and modeled for CO_2 binary, ternary and pseudo-binary systems encountered in the synthesis of [HMIm][Br]. Unique chemical and thermodynamic behaviors are observed in the IL-synthesis mixtures. Using estimated critical properties to correlate the vapor-liquid equilibrium, the Peng-Robinson equations of state, with van der waals 2-parameter mixing rules, were found to sufficiently correlate data. The phase equilibrium data allow better understanding and kinetic characterization of the synthesis of ILs with CO_2. Results have important ramifications on the kinetics and process constraints of an actual IL synthesis in high pressure systems. Design considerations for optimizing solvents ratio, kinetic properties and separations are discussed.

Here, the systematic risk assessment methodology was extended to ILs systems. Environmental assessments of different IL synthesis routes studied here are performed and presented. Potential issues (unit operations that have the most impact on the environment and profitability) in the life cycle of the processes are identified. Green sustainable methodology was extended to applications of ILs *viz* cellulose valorization and processing, separations and the fabrication of cellulosic materials.

Acknowledgement

No bird soars too high if he soars with his own wings. - ***William Blake***

I am indebted to a number of people who made this all possible. First, I would like to express my deepest gratitude to my advisor, Professor Aaron Scurto, for his inspiration, mentorship, encouragement and patience during my time at the University of Kansas (KU). I am grateful to my committee members, Professors Susan Williams, Laurence Weatherley, Raghunath Chaudhari and Jon Tunge for their time and guidance in reviewing this dissertation.

I am thankful to my colleagues: Wei Ren, Jay Schliecher, Azita Ahossieni, Aravind Gangu, and Dave Minnick. It was an honor learning, working, troubleshooting alongside you and most especially solving problems together. You taught me the importance of TEAMWORK. Several undergraduate researchers made significant contributions to the experimental work: Kevin Livengood, Will Smith, John Dibaggio, Chirsty Cheung and Ming Tan. Thank you for working so hard, teaching me patience and helping me learn to teach. Dr. Claudia Bode, I thank you for your enthusiasm and creative ideas when editing my presentations, written work and posters for effective communication. I will take along many lessons learned into my future career.

My professional families at the Department of Chemical and Petroleum Engineering (CPE) and the Center for Environmentally Beneficial Catalysis (CEBC) have helped me enormously. Your smiles and kind words made the day's work bearable. I would like to give my special thanks to Mr. Alan Walker and Mr. Scott Ramskill for their willingness to help with equipment setup and maintenance. To Drs Andrew Danby and Michael Lundin, I appreciate you both for always lending strong hands and experienced eyes for equipment troubleshooting. I am grateful to Mike Mendez at Aspen Technologies, who spent hours helping me troubleshoot Aspen software issues. I thank Justin Douglas and Sarah Neuenswander for help with NMR spectroscopy.

I am especially grateful to the Emily Taylor Women Resources Center at KU (KU4KU Women Elevator Fund), Kathy Rose Mockery, Mary Mba, Angela Oguna, and Mrs

Florence Boldridge. The value of your steadfast support throughout my challenges of balancing motherhood and research work is unquantifiable.

Of course without funding none of my work would have been possible. Thus, I want to acknowledge my funding sources, the NSF-ERC Center for Environmentally Benign Catalysis, the US National Science Foundation (NSF CBET-0626313), and the University of Kansas Graduate Studies Diversity Fellowship 2011-2012.

I want to express my deepest gratitude to my FAMILY. Truly you have shown me it takes a village to raise a child. These past five years have not been easy. I acknowledge the long trips from Nigeria, Jamaica, the UK, Tennessee, Texas, North Carolina and South Dakota to meet needs or simply to cheer us on: Marlon and I are forever indebted to you. I thank you for spiritual, emotional, and financial support during this challenging time. Our lives are so much richer because you are in it.

Thank you to our mothers for their selfless effort in making my load lighter especially with childcare. As a mother of three young boys, your support has been invaluable in allowing me to achieve this goal. To my Sons, Munachi, Uzoma and Ikechi, you make this accomplishment so much sweeter.

To my husband, Marlon Hugh Johnson, I am one lucky girl! I am married to my love, best friend, biggest fan and prayer partner. Thank you for believing in me always. Love is an action word; *Marlon, you do love!*

I reserve my gratitude to my father, Nze Ignatius.O. Nwosu, till the end. Without your confidence in me, none of my achievements would have been possible. Thank you for believing in, and supporting, the crazy dreams of your little girl. You are a true father and I will always love you.

Above all, I thank God! *Chukwu imela!*

For *Mom*, In Loving Memory

LoLo Felicia C. Nwosu

Thank you! You are not forgotten.

Table of Contents

LIST OF FIGURES

1. AN INTRODUCTION TO IONIC LIQUIDS

Across today's chemical industry, energy security and environmental protection are a paramount global priority. Sustainable chemical technology advances are not only welcomed, but deemed critical. For instance, there continues to be an overwhelming need for improving solvent media in age-old chemical processes. Several commonly used volatile organic solvents are especially harmful to the environment and human health because of their high vapor pressures.

Ionic liquids (IL), which have virtually no vapor pressure and negligible volatility, have created a "buzz" in the scientific community because of their potential as environmentally-friendly solvents. In addition to preventing air pollution, researchers can molecularly tune IL properties, as well as design new IL solvents for various applications, such as catalysis, separations, electrochemistry, fuel cell, and biotechnology applications. The number and diversity of publications and patents associated with novel applications of these solvents continues to as presented in Figure 1.1.

Although ILs have the potential to be greener alternative solvents, more research is needed across their entire life cycle to establish overall environmental impacts. One area that is especially important but frequently overlooked is the synthesis methodologies for ILs. Paradoxically, many ILs are synthesized and processed using the very organic solvents that they are purportedly designed to replace (pyridine, diethyl ether, hexane, acetonitrile, toluene, trichloroethane (TCE) etc). [1, 2]

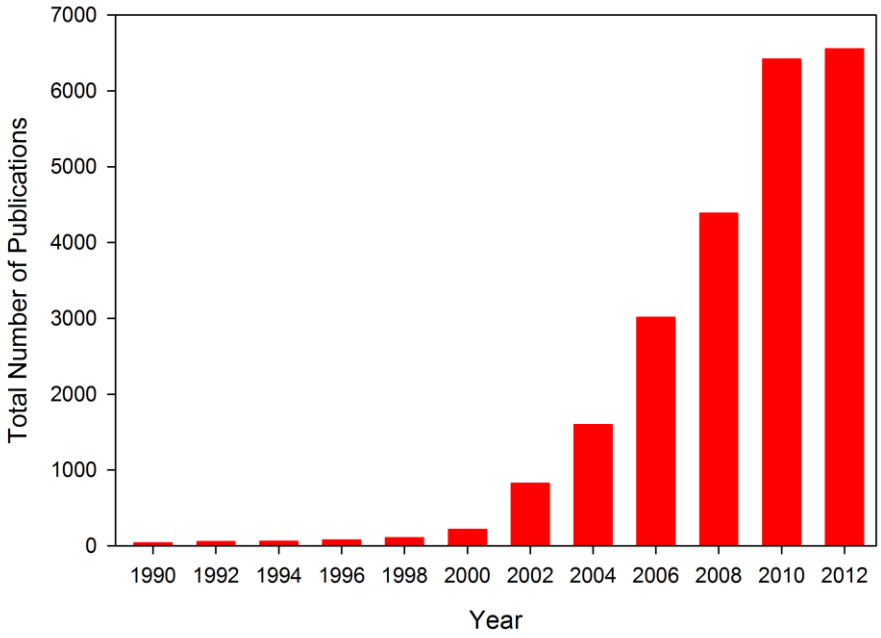

Figure 1.1 IL Research Trend from Scifinder

While interest in ILs is growing exponentially, very little work focuses on finding environmentally benign and economically viable IL synthesis and production methods. Most literature reports of IL syntheses are primarily concerned with making relatively small quantities to study physicochemical properties or for other small-scale applications. Furthermore, ILs are still not cost competitive with traditional solvents, costing as high as 5-20 times more.[3] Although the price of ILs is declining because of higher demand, high costs are a major deterrent to their full industrial launch. Large scale production could further bring down the costs; unfortunately, a lack of adequate kinetic data for the synthesis process[4-7] and transport properties data make engineering efficient continuous synthesis processes impossible.

This research focuses on identifying and studying new, environmentally benign routes—so called "greener" solvents—for the synthesis of ILs. Gas expanded liquids (GXLs), which are another promising solvent media, might be useful in accomplishing these goals. GXLs such as CO_2 expanded liquids (CXL) offer the flexibility of highly tunable reaction media for use in various applications. Furthermore, carbon dioxide (CO_2) was found to induce many IL-solvent mixtures to split into IL-rich and solvent-rich phases that can be decanted, or, at higher pressures, extracted by near- or super-critical CO_2. The synthesis and processing of ILs in a CO_2-expanded media may alleviate aforementioned efficiency and cost concerns while minimizing the use of organic solvents in the synthesis of ILs.

For the first time, here the kinetic benefits of a polar aprotic solvent, dimethyl sulfoxide (DMSO), and the thermodynamic advantages of environmentally benign CO_2 for the production of ILs. Results show the combined benefits of implementing DMSO (a relatively benign solvent) and CO_2 for the synthesis of a model IL compound known as 1-hexyl-3-methylimidazolium bromide ([HMIm][Br]). Experimentally obtained thermodynamic, kinetic and physical property data were modeled for the critical design and optimization of IL production. The results indicate that the chemical and thermodynamic phenomena must be understood to optimize these systems for IL production. Most importantly, practical separation processes are proposed. Environmental impacts of all proposed routes are quantified and compared against traditional techniques. These methods are extended to applications of ILs in biomass processing *viz* biomass conversion separations (LLE) and the fabrication of cellulosic

materials. This research provides engineering design considerations and recommendations that will help to minimize environmental impacts and energy consumption of IL production technologies.

1.1 Ionic Liquids: Countless Combinations

ILs are low melting salts. They are comprised mainly of cations and anions that are liquid at, or near, room temperature (with T_m < 100°C). Commonly studied cations include 1-alkyl-3-methylimidazolium (abbreviated $[Cnmim]^+$, where n = number of carbon atoms in a linear alkyl chain), N-alkylpyridinium ($[Cnpy]^+$), tetraalkylphosphonium and tetraalkylammonium cations. These cations can be combined with either organic or inorganic anions, including halide, acetate, hexafluorophosphate, tetrafluoroborate, trifluoromethylsulfonate, nitrate, etc. Innumerable molecular combinations are theoretically possible ($>10^{18}$) [8], with various combinations of cations and anions affording distinct physicochemical properties such as melting point, polarity, viscosity, stability, solvation properties, and phase behavior of the resultant IL. It is thus possible to molecularly engineer ILs for specific tasks. Figure 1.2 illustrates some possible combinations of anion, cations and cation substituents.[9]

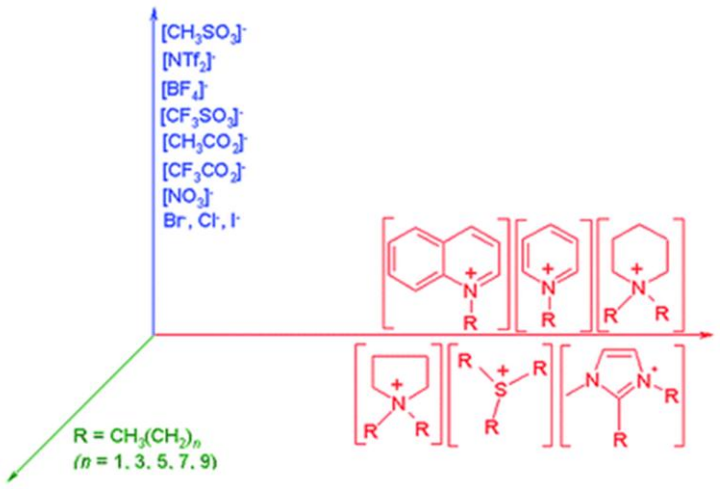

Figure 1.2 Commonly used cations and anions. [9]

1.2 Properties of ILs

Solvents are selected for engineering applications based on their specific physical and chemical properties. In fact, engineering process requirements are translated into quantitative parameters, which can then be achieved by tuning relevant physicochemical properties of the chemical. This can be accomplished for ILs mainly by the choice of anion and cation. This design flexibility positively contrasts ILs, as solvent media, against traditional solvents. Table 1. 1 presents a general comparison of ILs and traditional organic solvents, adapted from Seddon and Plechkova.[10]

Table 1. 1 Comparing general properties of Ionic Liquid and Organic Solvents [10]

Property	**Organic Solvents**	**Ionic liquids**
Number of Solvents	>1000	>1,000,000
Applicability	Single function	Multifunction
Catalytic ability	Rare	Common and tunable
Chirality	Rare	Common and tunable
Vapor pressure	follows Clausius-Clapeyron equation	Negligible vapor pressure
Flammability	Usual Flammable	Usual nonflammable
Solvation	Weakly solvating	Strongly Solvating
Polarity	Convention polarity concepts apply	Polarity concept questionable
Tuneability	Limited range of solvents available	Virtually unlimited range means" designer solvents"
Cost	Cheap	2 -100 times cost of normal solvent
Recyclability	Green imperative	Economic imperative
Viscosity/cP	0.2-100	22-40,000
Density/g cm^{-3}	0.6-1.7	0.8-3.3
Refractive index	1.3-1.6	1.5-2.2

1.2.1 **IL Melting Points**

ILs are typically found in the lower end of the liquidus range, with low melting points (T_m), making this class of solvents very attractive for many applications. Cation and anion choice has been shown to affect T_m. For instance, studies show that bulky ions often have lower T_m compared to smaller ions such as chloride or bromide. However, it is important to note that several ILs do form glass at relatively mild temperatures, and these glass transition temperatures can be easily mistaken for melting points.[11]

1.2.2 **IL Viscosity and Density**

Viscosities affect diffusion of solutes and govern mass transfer for systems involving solvents. Mass transfer is a critical phenomenon affecting the choice of unit operation, such as stirring and pumping, and can consequently become an economic driver for processes involving viscous products.

In comparison to traditional organic solvents, ILs are more viscous (on the order of several magnitudes) with viscosities typically within 10 to 1000 mPa·s at room temperature. For example, [HMim][TF_2N][12] is 71.0 mPa·s, water 0.894 mPa·s and acetone 0.306 mPa·s at 25 °C, respectively. Viscosities decrease significantly with temperature. Ambient temperature viscosity values of many IL systems are widely published in the literature. Studies show that the viscosity temperature dependence in ILs does not always follow the usual Arrhenius behavior observed in conventional organic solvents. Density is an important physical property for most applications. Most ILs are more dense than water. Typical viscosity and densities of common ILs pulled from the NIST database are shown in Table 1.2 [13].

Table 1. 2: Ionic Liquids - Physical properties at 298.1K [13]

Name	Abbreviation	Molecular Weight (g/mol)	Viscosity (Pa-s)	Melting Point [a] (K)	Heat Capacity at Constant Pressure [a] (J/K/mol)	Thermal Conduct-ivity [a] W/M/K	Cost [b] $/KG	Specific Density (kg/m^3) [a]
1-butyl-3-methylimidazolium Chloride	[BMIm][Cl]	174.67	40.89	340.10	322.7	-	278	1080.00
1-ethyl-3-methylimidazolium tetrafluoroborate	[EMIm][BF_4]	197.97	0.067	247.10	306.5	-	1,110	1247.90
1-hexyl-3-methylimidazolium tetrafluoroborate	[HMIm][BF_4]	254.08	0.314	-	416.0	0.158	-	1153.10
1-butyl-3-methylimidazolium trifluoromethane sulfonate	[BMIm][OTf]	288.29	0.099	286.10	417.2	0.147	-	1302.00
1-Butyl-3-methylimidazolium hexafluorophosphate	[BMIm][PF_6]	284.18	0.450	283.10	397.6	0.145	-	1360.00
1-ethyl-3-methylimidazolium ethylsulfate	[EMIm][$EtSO_4$]	236.29	0.098	236.29	378.0	0.181	274	1242.30
1-hexyl-3-methylimidazolium bis(trifluoromethylsulfonyl)imide	[HMIm][TF_2N]	447.42	0.068	266.00	583	0.127	1,134	1365.90
N-butyl-N-methylpyrrolidinium bis(trifluoromethanesulfonyl)imide	[BMpyrr][[TF_2N]	422.41	0.075	255.10	629	0.125	-	1394.00
1-hexylpyridinium bis(trifluromethylsulfonyl)imide	[HPy] [TF_2N]	444.42	0.080	273.00	612	-	-	-

[a]Data taken from NIST IL Database and References within [b] From Sigma Aldrich

1.2.3 **Solvent Parameters**

Understanding solute or co-solvent behavior chemistry, especially solvent polarity, is useful for designing reaction and separation processes. Polarity is a strong indicator, often employed to predict or describe solvent/solute or co-solvent interactions. There are many ways in the literature to measure polarity, including dielectric constant (***ε***), cohesive pressure (***c***), Hildebrand solubility parameter (***δ***), miscibility numbers (***M***-number) and dipole moment of solvent molecules (***μ*).** Multi-parameter solvent polarity scales such as Kamlet-Taft (K-T) parameters give a better picture of polarity: the π* scale of dipolarity/polarizability captures dipole−dipole polarizability effects, the α scale indicates hydrogen-bond-donor (HBD) acidity, and the β scale, hydrogen-bond accepting (HBA) basicity. The *KT* parameters divide "polarity" into 3 different contributions, as opposed to

1-parameter approaches which use dielectric constant, dipole moment, $E_T(30)$, etc., and qualitatively do not correlate the rate constant data for the various solvents. In this study, Kamlet-Taft solvent polarity measurement methods are discussed in detail. The solvent properties of ILs are also investigated using these approaches. ILs have been found to have solvent polarities that were largely determined by the ability of the salt to act as an HBD and/or HBA, and the degree of localization of the charge on the anions.[11] Studies show that increasing the chain length of alkyl substituents on either the cations or anions can increase the hydrophobicity of the ionic liquids.[14, 15]

1.2.4 **Thermodynamic properties**

The century-old petrochemical industry utilizes conventional thermodynamic methods (such as UNIFAC) to model, correlate, and predict separations for various mixtures of well characterized compounds. The NIST IL database (IL thermo) currently contains about 22,935 data points for pure IL data and 53,614 data points for binary and ternary systems.[16] The mirage of possible combinations of cations and anions makes it impractical to experimentally test all individual ILs systems. Thus, it is not surprising that there is scant binary and ternary data in the literature for systems involving ILs. There is a need for robust predictive thermodynamic tools.

Quantitative structure–property relationships (QSPR) have been employed to predict IL thermodynamic properties.[17-19] In the past, researchers employed several techniques to estimate thermodynamic properties, from molecular dynamics (MD) using atomistic force fields, to classical activity coefficient based models such as UNIQUAC and NRTL.

Computational MD approaches require prior insight into force field magnitude. Such insight would need to be developed specifically for IL systems, and will be time consuming.

Currently, group contribution methods (GCMs) are the most widely accepted way of predicting activity coefficients and other thermodynamic physical data of liquid mixtures. However, while GCMs approximate the interaction energy of a system by the sum of functional group interaction energies, these methods do not account for several other molecular interactions. As a result, GCMs provide limited information, while relying heavily on experimental data.

The Conductor-like Screening Model (COSMO) is a quantum chemical method based on a dielectric continuum model. Here, the ideal screening charge density is first computed. Klamt and co-workers[16, 20-26] extended COSMO to real fluids in COSMO-Real Solvents (COSMO-RS) for thermodynamic computations. Compared to traditional GCMs, the COSMO-RS approach to chemical thermodynamics takes a completely different point of view. Computation starts from the molecular surface via a quantum chemical method. The charge density σ is the most significant descriptor and is used to determine the interaction energies. It replaces the empirical interaction parameters usually used in traditional chemical engineering models such as UNIQUAC and UNIFAC. [27] A unique σ-profile can be computed for every molecule; Figure 1.3 presents σ-profiles of the minimum conformers of the acetate anion.[28] COSMO-RS has

been applied to LLE of binary systems of ILs and common solvents such as alcohols, hydrocarbons, ethers, ketones and water.

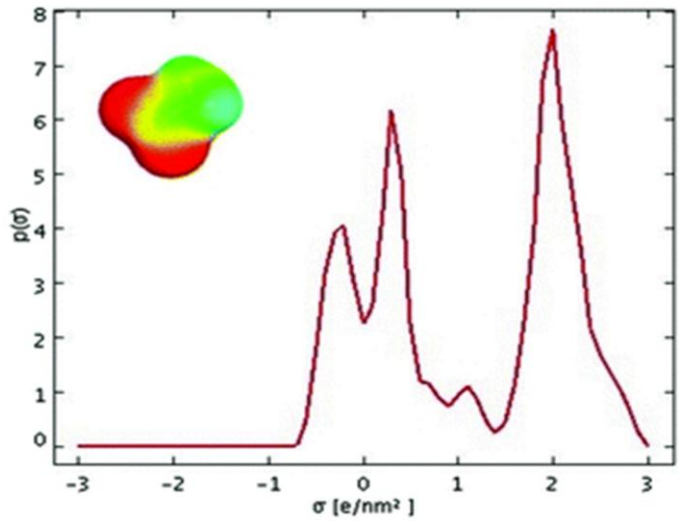

Figure 1.3: σ-profiles of the minimum conformers of acetate anion. [28]

1.2.5 **Impurity: Water Content, Trace Compounds**

Seddon et al [29], for the first time, studied the effect of impurities e.g., water, chloride, and co-solvents on the physical properties of imidazolium-based ILs and found that the viscosity dramatically increased with higher chloride impurities. Since that study, a number of studies have shown the influence of water and other trace impurities on different IL properties such as solubility, density, viscosity, etc. of the ionic liquids. These findings will be particularly important when designing large-scale industrial processes. However, the extent to which this is a problem depends on the application, and will vary widely with the kind of IL being utilized. For example, in biomass

investigations, water is known to cause cellulose aggregation and decreased solubility. Swatloski *et al.*,[30] attribute this to competitive hydrogen bonding to the cellulose fiber network: this problem is noteworthy, since most ILs that dissolve cellulose are hydrophilic. Another example occurs in catalysis: highly moisture-sensitive catalysts can be deactivated by even the smallest amounts of water.[11] Also, in homogenous catalysis, trace amounts of halides are known to coordinate to the transition-metal centers of catalysts, negatively affecting the rate of reaction.[31]

Difficulty in purifying or cleaning is often a barrier to using ILs for certain processes. Handling ILs under an inert atmosphere, especially for moisture-sensitive applications, is highly recommended. Appropriate storage of ILs will further increase shelf life and minimize impurities.

1.3 Applications of Ionic Liquids

The literature comprehensively covers recent advances and applications of ILs across many areas of chemical engineering from industrial investigations[10] to fundamental academic research efforts. The following is a selection of academic research investigations showcasing how ILs can be potentially advantageous in various areas.

1.3.1 *IL in Biomass Processes:*

The US Department of Energy's Biomass program outlined national goals for replacing 30% of fossil fuel use with bio-fuels by 2030.[32] This ambitious (and arguably

optimistic) mandate provides a strong impetus for the development of cutting-edge technologies in the renewable fuels area. Furthermore, many bio-renewable chemicals are excellent substitutes for making a wide variety of chemical products, ranging from polymers to pharmaceuticals. ILs have high potential as powerful solvents for biomass processes, offering several advantages. Biomass hydrolysis in ILs has been catalyzed using transition metals, mineral or solid acids and the IL itself. Researchers have found that ILs enhance selectivity in the conversion of monosaccharides to platform chemicals, depending on the water content and the acidity of the medium. There are several ongoing research efforts in the area of biomass processing catalysis, employing ILs as a solvent media, catalyst, heat transfer fluid, separating agent or a combination of these. For example, Swatloski *et al.*,[30] showed that 1-butyl-3-methylimidazolium chloride (BMImCl) can dissolve up to 25 w/w % of cellulose. Figure 1.4 highlights a few more examples of common ILs that have been used for cellulose dissolution in the literature.[33]

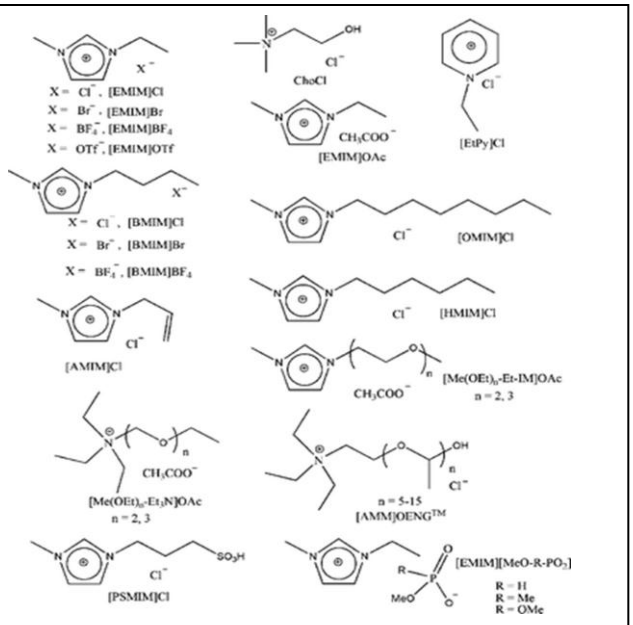

Figure 1.4 Examples of commonly use ILs in cellulose dissolution and biomass processing[33]

1.3.2 **Catalysis in a Supported Ionic Liquid Phase (SILP)**

ILs have been extensively considered for catalysis in both homogeneous and heterogeneous systems. Often in these systems, mass transfer issues encountered due to the high viscosity of ILs become a major deterrent in employing ILs for catalytic purposes. Supported IL catalysis (SILP) partially circumvents this drawback. SILP combines the advantages of two technologies: the unique properties of ILs and "supports" to immobilize homogeneous transition metal complexes in a reaction system. In this technology, the IL is simply dispersed uniformly over a support material such as silica, as shown in Figure 1.5.[34] The IL layer can facilitate transport to or from the active site,

enhancing reaction selectivity. Optimally derived SILP systems have been shown to be potentially superior to conventional catalysts when used in fixed-bed reactors.[34-38] Recently, SILP has been extended to separation and gas purification applications.

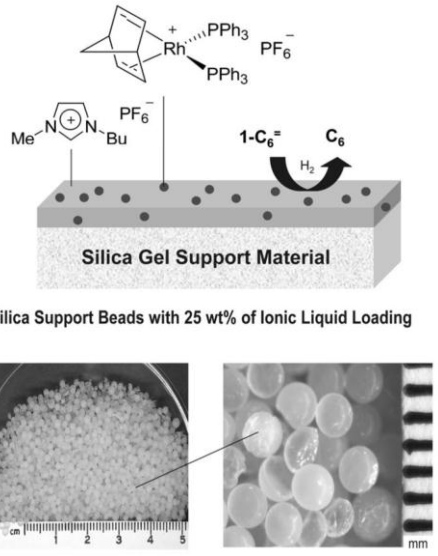

Figure 1.5 SILP system[34]

1.3.3 *Ionic Liquids for Liquid-Liquid Separations and Fermentation*

Distillation remains the most commonly used separation method. But this method is highly energy intensive, accounting for 60% to 80% of the cost in most mature chemical processes. Energy savings can be obtained by switching from enthalpy driven separation schemes to entropically driven routes.[39]

Take for example fermentation, where microorganisms catalyze reactions at, or near, ambient conditions. After a series of transformations by different enzymes, products are excreted from the cells into an aqueous fermentation broth, forming very dilute solutions. Often, fermentation microorganisms have minimal tolerance for these bio-products. For instance, ethanol concentration is limited to 5 to 10% (v/v) in the broth while only about 2 wt % of n-butanol can be tolerated.[40, 41] Sequestering desired products from this aqueous phase is often challenging. Methods currently employed for fermentation separations include: gas stripping, membrane separations (e.g. micro-/ultra-filtration, pervaporation), adsorption, liquid chromatography, etc. [40, 42] Some of these methods are implemented *in situ* or *ex situ* (downstream). A wide variety of extractive fermentation systems have been reported in the literature, with most focused on ethanol fermentation.[40, 43-48] In the literature, several studies have screened for optimal extraction solvents in fermentation using selectivity, distribution coefficient and biocompatibility. Long chain alkyl- alcohols and ketones [49-51] are optimal for these processes; however, these conventional solvents have relatively high volatility and present air pollution issues. The schematic in Figure 1.6 shows a process flow sheet for n-butanol recovery from fermentation broth using an IL.[41]

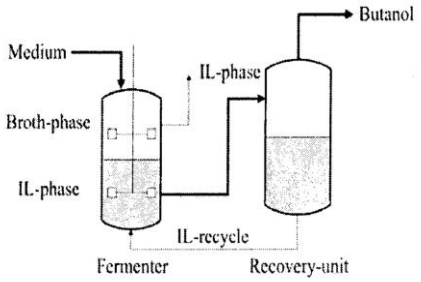

Figure 1.6: Process flow sheet of butanol recovery from fermentation broth [41]

Recent advances have embraced non-conventional solvents and extraction techniques for the separation and purification of various biomolecules through partitioning of liquid phases. Solvent extraction (or liquid-liquid distribution, the International Union of Pure and Applied Chemistry (IUPAC) preferred terminology) is the separation of a solute from a mixture by utilizing the preferential dissolution (partition) of that solute between two practically immiscible liquid phases.[40] Several studies have shown ILs as effective separating agents that can potentially result in high-purity products. ILs alleviate the concerns of transport and reuse often associated with solid salts. In IL systems, phase separation can be achieved by manipulating the hydrophobicity or hydrophilicity of the IL. An ideal IL with high selectivity and desired distribution coefficient may be designed to achieve higher separation efficiency, consequently lowering needed heat duties for separation processes. Additionally, because ILs are nonvolatile, they provide a wider operating temperature range.

1.3.4 **Ionic Liquids in CO_2 Capture: CO_2 Photo Reduction**

Researchers have shown optimism for the conversion of solar energy to chemical fuels; this is supported by the growing trend of literature published in this area (solar energy harvesting and photochemical conversion). CO_2 can be reduced in water vapor or solvent, via light-induced reactions using photocatalysts, to C1 and C2 hydrocarbons, such as methanol and methane. Photosensitizers *viz* metal complexes, e.g TiO_2, metal chalcogenides (CdS, CdSe, ZnS) and other metal oxides (ZnO, MgO) etc., are used to absorb visible or UV radiation in the wavelength range of 200–900 nm. The overall

reaction for CO_2 reduction to methanol is presented in equation (1). This has been observed in both liquid and gas phases [52]:

$$CO_2 + 2H_2O \xrightarrow{h\nu} CH_3OH + \frac{3}{2}O_2 \quad (1)$$

CO_2 is a stable form of carbon: these reactions are thermodynamically unfavorable processes and thus require large energy input. Grimes' group [53] observed a twenty times (20x) higher conversion rate using sunlight versus UV illumination for the photocatalytic conversion of CO_2 to hydrocarbon on high surface area Titania (TiO_2) nanotube arrays. CO_2 conversion chemistry is complex; very little is still known about the reaction mechanisms. However, TiO_2 based photocatalysts have been used to convert CO_2 to useful compounds, both in gas and aqueous phase photoreactions. To date, yields and conversion are still too low for this route to be commercially viable.

Titania (TiO_2) is relatively cheap with a low toxicity and, in the Anatase form, considered the perfect candidate for UV illumination.[54] Several composites of titania (copper, etc) have been employed for CO_2 reduction.[55-57] Catalyst complexes are designed to capture visible light for reaction. These efforts are mainly directed towards heuristic optimizations of TiO_2-based photocatalysts. Still, very limited data is available for the comparison of conversion efficiencies and quantum yields of various TiO_2-based catalysts. ILs may present useful advantages in photo-catalysis. For example, for the photocatalytic reduction in supercritical CO_2, an IL offers good mass-transport properties where catalyst and electron-donor solubility issues may arise.[58] Yan *et al.*,[59]

recently modeled the adsorption of CO_2 on the rutile surface in an IL using Molecular Dynamics (MD) simulations (Figure 1.7).[59] The TiO_2, when acted upon by light, generates electron-hole pairs. The carbon, because of its conductive nature, helps with the separation of charge (i.e. keeps the electrons and holes apart). So far, ILs that have been considered for use in the CO_2 photo-reduction include tetrafluoroborate, nitrates and hexafluorophosphate anions (BF_4, NO_3 and PF_6 respectively). Molecular dynamic (MD) modeling by Yan *et al*., indicates that different anions are absorbed on the surface of the catalyst differently. [59] They show that NO_3 anions exhibited a highly ordered surface organization; this was not the case for the PF_6 anions. Additionally, the hydrophobicity of the IL may increase the selectivity of the surface, favoring CO_2 absorption over the anion.

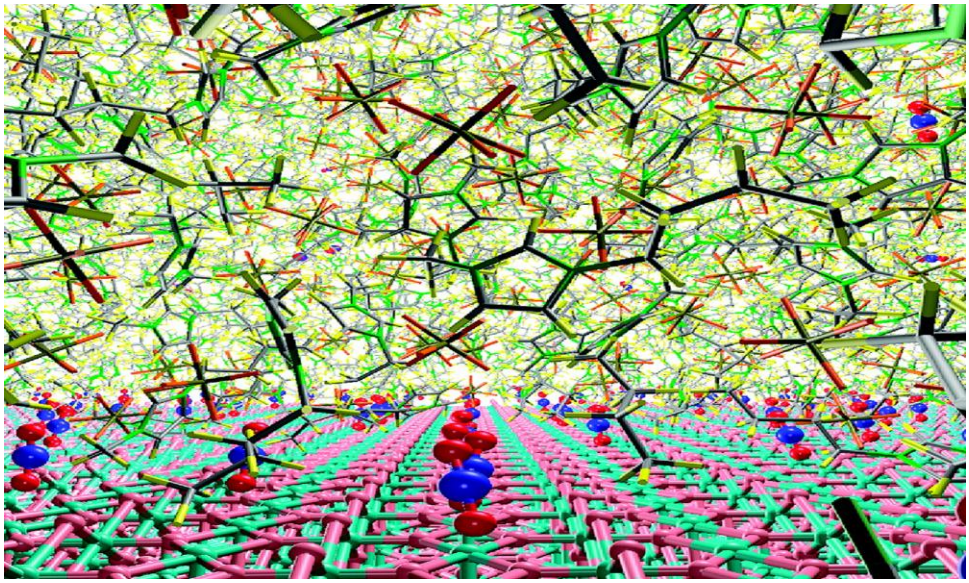

Figure 1.7: MD simulation showing structure of the TiO_2 (110) interfacial region (green, N atom; yellow, H atom; gray, C atom on imidazolium ring; tan, P atom;orange, F atom; blue, C atom on CO_2; red, O atom on CO_2; cyan, Ti; pink, O atom on TiO_2). [59]

1.4 Current Barriers to IL Implementation

While novel applications of ILs continue to emerge in the scientific communities, researchers must cross a variety of hurdles before wide scale adoption of ILs in industry can be achieved. At the laboratory level, researchers must overcome impurities (such as water content and discoloration), viscosity, and separation (ties into recovery and recyclability of the IL) challenges. As described early, many ILs are synthesized and processed using the very organic solvents which they are intended to replace [1, 2]. Cost of ILs is also a major concern, admittedly less so as it trends down with increasing demand for ILs, and works such as this dissertation yield better production techniques. Profitability will require the development of efficient recycling methods, perhaps by phase separation techniques that exploit properties such as hydrophobicity or hydrophilicity of the IL. For example, Blanch and coworkers [60] recovered ILs via the "salting out effect". They demonstrated the possibility of partially separating an IL from an aqueous solution by adding water-structuring species, such as potassium phosphate, to induce phase separation. Their technique decreased water concentration in the IL, thereby reducing evaporation-related energy costs.

IL toxicity is yet another topic of formidable debate. Limited toxicological data and knowledge about basic physicochemical characteristics further hinders widespread implementation of ILs. Until very recently, few reports have been published on the safety of ILs. Although negligible vapor pressure of ILs could reduce air-born exposure of workers, current production methods are still not benign, ultimately affecting overall life cycle analysis and the environmental impact of using ILs as alternative solvents.

1.5 Synthesis of Ionic Liquids

There are a variety of different methods for synthesizing ILs. Most commonly, ILs are synthesized by a quaternization reaction of a substituted amine or phosphine followed by anion exchange if needed. However, there are several alternative halide-free techniques.[61-64] Processing techniques must also factor in heat dissipation, since IL synthesis reactions are highly exothermic.

Some ILs or their intermediates are either viscous liquids or are solids with elevated melting-points. Processing solids requires different techniques than liquids. As an example, the liquid-phase reaction between 1-methylimidazole and 1-bromoethane forms 1-ethyl-3-methylimidazolium bromide ([HMIm][Br]), which is a solid compound at room-temperature and melts to a viscous liquid at 76°C.[65] These problems with heat and processing are often solved by the use of a solvent: the product IL and/or reactants can be kept in a relatively low-viscosity solution that can be separated by distillation. While solvent-free processing is often considered ideal, this does not seem generally practical for ILs.

Extensive investigations of solvent effects on the transition state during the formation of ionic compounds emphasize the importance of solvent selection. Menshutkin, while studying nucleophilic substitution reactions (S_N2) between amines with haloalkanes in 23 solvents, reported large solvent effects on these kinds of reactions,[66-69] and others have shown that these kinds of reactions are highly solvent dependent.

A full understanding of the kinetics and effects of solvent in the synthesis of ILs is of great importance for the industrial production of ILs. This work presents the effects of solvents on the synthesis of selected imidazolium, pyridinium and methylpyrrolidinium IL. Figure 1.8 presents the example of 1-hexyl-3-methylimidazolium bromide, one of the systems studied.

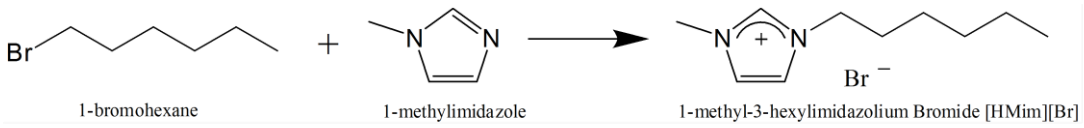

Figure 1.8 Reaction between 1-methylimidazole and 1-bromohexane forming 1-hexyl-3-methylimidazolium bromide [HMIm][Br].

1.5.1 **Gas Expanded Liquids**

In an attempt to reduce the use of volatile organic solvents in chemical processes**,** researchers have explored Gas Expanded Liquids (GXL), as a solvent media. GXLs are composed of a compressible gas (such as CO_2) dissolved in an organic solvent phase, as illustrated in Figure 1.9. This type of system uses significantly less organic solvent, which minimizes waste, volatile emissions and solvent costs. Carbon dioxide (CO_2), in particular, is a common gas used to expand solvents due to the environmental and economic advantages it presents.

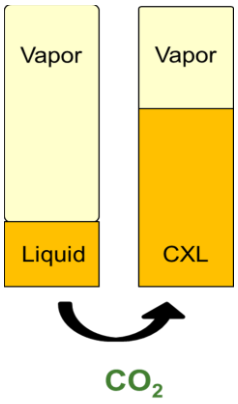

Figure 1.9 Illustrating GXL

The application of GXL technology has been studied for many processes in catalysis, nanotechnology and pharmaceuticals. An extensive review by Jessop and Subramaniam[70] classifies GXLs into Types I, II and III, based on the solvent to be expanded. Type I liquids are those solvents not able to dissolve enough CO_2 for a large solvent volume expansion: water would fall in this category. Type II liquids readily dissolve large amounts of CO_2: common solvents such as acetone, ethanol, DMSO etc. are examples of Type II GXLs. In contrast, Type III liquids do not expand much, even though they dissolve relatively large amounts of CO_2. ILs and liquid polymers are typical examples of Type III fluids.

Properties of supercritical fluids, such as density and viscosity, can be fine-tuned for a specific task by varying pressure and temperature. This feature makes GXLs attractive for reactions and separation. For instance, CO_2 in the liquid phase has been shown to significantly improve transport properties of systems. Ahosseini *et al*.,[12] have shown that CO_2 decreases the viscosity of ILs, reporting an 80% drop in viscosity of [HMIm][Tf_2N] at about 60 bar of CO_2 at 40°C. This reduction in viscosity translates into better diffusivity, which results in better reaction mass transfer. As new applications emerge, a clear understanding of these often complicated systems becomes necessary. Phase behavior data is needed to engineer and select conditions for processes involving GXL. Although binary data for organic solvents and CO_2 systems are available in the literature, ternary or higher component mixture data available for many other solvent systems is meager.

1.5.2 **Synthesis of Ionic Liquids in a CO_2 Expanded System**

Synthesizing imidazolium-based ILs using compressed CO_2 as a solvent has many advantages over traditional solvents.[71-73] CO_2 is relatively abundant naturally, and is considered a "green", more environmentally friendly solvent[74]. Literature reports have shown fast and sensitive organic synthesis can be achieved with high levels of functionality, controllability and energy efficiency in supercritical CO_2. With moderate critical conditions (31°C, 71 bar), CO_2 affords product separation by pressure tuning the system. Simple product sequestration reduces process steps and energy demands that would have been otherwise required from energy intensive distillation processes.

Our groups, and others, have shown that CO_2 has relatively high solubility in most ILs.[75-78] Unlike organic compounds, which partition into the CO_2 phase and CO_2 becomes miscible or critical with organic compounds and solvents at higher pressures, ILs are immeasurably insoluble in a compressed CO_2 phase to elevated pressures of 400+bar.[79-81] Thus for IL synthesis, reactants can be rendered miscible by choice of temperature, pressure and composition, but the product will remain insoluble in this solvent. This phenomenon may be used to extract or purify the IL from residual reactants and impurities by varying CO_2 pressure. This allows for separation of CO_2 solvent without cross contamination between the CO_2 and the IL.

1.6 Dissertation Objectives

This dissertation identifies and presents novel techniques, useful to both industry and researchers, for synthesizing ILs via a process that minimizes negative human and environmental impact. This work successfully demonstrates how gas expanded DMSO is a beneficial solvent media for IL synthesis. Ramifications of phase behavior and kinetics on large scale GXLs are also presented. Phase transitions in equilibria, such as vapor-liquid, vapor-liquid-liquid, liquid-liquid, etc. must be understood to determine optimal operating conditions for multiphase gas expanded systems. To unravel these unknowns, experimentally observed chemical and thermodynamic complexities typical of complex organic mixtures (mixtures of ionic liquids, 1-methylimidazole, 1-bromohexane and dimethylsulfoxide) are modeled. These data can serve as a basis for predicting behavior in future applications.

Further, experimentally-obtained physical property data, phase equilibria data and kinetic data critical for designing and optimizing IL production are presented. Most importantly, simple separation processes are proposed along with detailed comparative environmental assessments of the proposed routes. Results and methods can be extended to other engineering applications. This work reinforces the importance of green engineering principles and demonstrates how ILs can be produced without compromising sustainable engineering principles.

1.7 Outline of Chapters

The next chapter details experimental procedures and the methodology employed for this study. This includes an overview of the high pressure static VLE apparatus, autoclave procedure for global phase behavior study, NMR and ReactIR for kinetic analysis, and UV-Vis for polarity measurements at ambient and high pressures. Ionic synthesis procedures and chemicals are also presented in this chapter. Chapter 3 presents an overview of thermodynamic theories and models that are employed in this study.

Experimentally obtained kinetic, thermodynamic and thermo-physical data needed to engineer efficient continuous processes for IL synthesis are described in Chapter 4. This chapter also includes a description of high-pressure phase equilibria (including CO_2 solubility, volume expansion, and mixture critical points) measurements and models for the binary, ternary and pseudo-binary systems involved in the synthesis of a model imidazolium ionic liquid 1-hexyl-3-methylimidazolium bromide ([HMIm][Br]). The results have important ramifications on the kinetics and process constraints of an actual IL synthesis. The Peng-Robinson equation of state, with van der waals 2-parameter mixing rules, are used with estimated critical properties to correlate the vapor-liquid equilibrium. The phase equilibrium data will allow better understanding and kinetic characterization of the synthesis of ILs with CO_2. The global phase behavior was observed for 1-methylimidazole. Also, density ρ, viscosity η, thermal conductivity λ, diffusivity D_{ij} , kinetic rate constant k , activity coefficient γ_i are obtained for different concentrations of solvent and the product IL for ambient pressure systems. Design

considerations for optimizing solvents ratio, kinetic properties and separations are discussed.

A full understanding of the kinetics and solvent effects in the synthesis of ionic liquids (IL) is of great importance for optimally selecting a benign solvent for IL production. Chapter 5 thus follows with a detailed presentation of kinetic and polarity analysis for the synthesis of different ILs in various traditional solvent systems. The kinetics for the synthesis of 1-alkyl-3-methyl-imidazolium halide, 1-hexyl-pyridium bromide and 1-hexyl-1-methylpyrrolidinium bromide ionic liquids are investigated with different alkyl halides, branched alkyl halides and various solvent-to-reactant concentrations. While some general trends (the type of leaving group, the relative reactivity of the electrophile, and the structure/sterics of the alkyl group) for these Mentshukin-type reactions are widely known, the quantitative second (2^{nd}) order rate constants are reported here. Varying reactant concentration ratios are found to affect the rate constant through changes in polarity: these findings are rationalized in terms of the Kamlet-Taft polarity parameters of the reaction mixture.

Chapter 6 presents results on the kinetic study of CO_2 as a solvent for the synthesis of 1-hexyl-3-methylimidazolium bromide ([HMIm][Br]), at different pressures and at temperatures 313.15 K and 333.15 K. The synthesis route afforded the flexibility to tune the rate of reaction by controlling pressure loading of CO_2. The rate of reaction under certain conditions is found to be as attractive as using conventional organic solvent. The rate of reaction decreases with increasing CO_2 pressure for imidazolium-based ionic

liquids, especially when operating above the mixture critical point. Also, it has been demonstrated that phase equilibrium as well as the solubility of CO_2 play a significant role in understanding kinetics by decoupling the various effects of compressed CO_2. This chapter also showcases the synthesis of IL in CO_2 expanded DMSO systems. Here we leverage the kinetic benefits of DMSO and the thermodynamic advantage of environmentally benign CO_2 for the production of ILs. Non-complex separation schemes are proposed from mixture phase behavior. Kamlet Taft polarity parameters for CO_2 expanded DMSO are reported.

Environmental and economic assessment of different IL synthesis solvent platforms is presented in chapter 7. This section marries results from both experiments and modeling to evaluate proposed novel routes for IL production. Potential "hot" spots (unit operations that have the most impact on environmental and profitability) in the life cycle of the processes are identified. While a full LCA for this process is beyond the scope of this current work, resulting engineering recommendations will serve as design best practice for consideration in future implementations.

The greener, more sustainable approach for synthesizing ILs was extended to new proposed separations schemes for other applications of ILs viz cellulose valorization and processing, separations and the fabrication of cellulosic materials. These findings are presented in chapter 8. Finally, recommendations and future work are presented in Chapter 9.

References

[1] P.T. Anastas, J.C. Warner, Green Chemistry Theory and Practice, Oxford University Press, New York, 1998.

[2] P.T. Anastas, J.B. Zimmerman, Peer Reviewed: Design Through the 12 Principles of Green Engineering, Environ. Sci. Tech., 37 (2003) 94A-101A.

[3] J. Brennecke, E. Maginn, Ionic liquids: Innovative fluids for chemical processing, AICHE J, 47 (2001) 2384-2389.

[4] P. Bonhôte, A.-P. Dias, N. Papageorgiou, K. Kalyanasundaram, M. Grätzel, Hydrophobic, highly conductive ambient-temperature molten salts, Inorg. Chem., 35 (1996) 1168-1178.

[5] W.T. Ford, R.J. Hauri, D.J. Hart, Syntheses and properties of molten tetraalkylammonium tetraalkylborides, J. Org. Chem., 38 (1973) 3916-3918.

[6] N. Karodia, S. Guise, C. Newlands, J.-A. Andersen, Clean catalysis with ionic solvents - phosphonium tosylates for hydroformylation Chem Comm, (1998) 2341-2342.

[7] M.S. Selvan, M.D. McKinley, R.H. Dubois, J.L. Atwood, Liquid-liquid equilibria for toluene plus heptane+1-ethyl-3-methylimidazolium triiodide and toluene plus heptane+1-butyl-3-methylimidazolium triiodide J. Chem. Eng. Data, 45 (2000) 841-845.

[8] J.D. Holbrey, K.R. Seddon, Ionic Liquids, Clean Technologies and Environmental Policy, 1 (1999) 223-236.

[9] A. Stark, Ionic liquids in the biorefinery: a critical assessment of their potential, Energy & Environmental Science, (2011).

[10] N.V. Plechkova, K.R. Seddon, Applications of ionic liquids in the chemical industry, Chemical Society Reviews, 37 (2008) 123-150.

[11] T. Welton, Room-Temperature Ionic Liquids. Solvents for Synthesis and Catalysis, Chemical Reviews, 99 (1999) 2071-2084.

[12] A. Ahosseini, A. Scurto, Viscosity of Imidazolium-Based Ionic Liquids at Elevated Pressures: Cation and Anion Effects, International Journal of Thermophysics, 29 (2008) 1222-1243.

[13] J.G. Huddleston, A.E. Visser, W.M. Reichert, H.D. Willauer, G.A. Broker, R.D. Rogers, Characterization and comparison of hydrophilic and hydrophobic room temperature ionic liquids incorporating the imidazolium cation, Green Chemistry, 3 (2001).

[14] K.G. Furton, R. Morales, Effect of anion chain length on the solvent properties of liquid tetrabutylammonium alkylsulfonate salts studied by gas—liquid chromatography, Analytica Chimica Acta, 246 (1991) 171-179.

[15] P.H. Shetty, P.J. Youngberg, B.R. Kersten, C.F. Poole, Solvent properties of liquid organic salts used as mobile phases in microcolumn reversed-phase liquid chromatography, Journal of Chromatography A, 411 (1987) 61-79.

[16] M. Diedenhofen, A. Klamt, COSMO-RS as a tool for property prediction of IL mixtures--A review, Fluid Phase Equilibria, 294 (2010) 31-38.

[17] J.F. Brennecke, E.J. Maginn, Ionic liquids: innovative fluids for chemical processing, AIChE Journal, 47 (2001) 2384-2389.

[18] R.L. Harris, R.E. Wood, H.L. Ritter, The Structure of Liquid Aluminum Chloride, Journal of the American Chemical Society, 73 (1951) 3151-3155.

[19] A.R. Katritzky, A. Lomaka, R. Petrukhin, R. Jain, M. Karelson, A.E. Visser, R.D. Rogers, QSPR correlation of the melting point for pyridinium bromides, potential ionic liquids, Journal of chemical information and computer sciences, 42 (2002) 71-74.

[20] M. Diedenhofen, F. Eckert, A. Klamt, Prediction of Infinite Dilution Activity Coefficients of Organic Compounds in Ionic Liquids Using COSMO-RS†, J. Chem. Eng. Data, 48 (2003) 475-479.

[21] A. Klamt, Comments on "A Priori Phase Equilibrium Prediction from a Segment Contribution Solvation Model", Ind. Eng. Chem. Res, 41 (2002) 2330-2331.

[22] A. Klamt, F. Eckert, COSMO-RS: a novel and efficient method for the a priori prediction of thermophysical data of liquids, Fluid Phase Equilibria, 172 (2000) 43-72.

[23] A. Klamt, F. Eckert, W. Arlt, COSMO-RS: An Alternative to Simulation for Calculating Thermodynamic Properties of Liquid Mixtures, Annual Review of Chemical and Biomolecular Engineering, 1 (2010) 101-122.

[24] A. Klamt, F. Eckert, M. Diedenhofen, M. Beck, First Principles Calculations of Aqueous pKa Values for Organic and Inorganic Acids Using COSMO- RS Reveal an Inconsistency in the Slope of the pKa Scale, J. Phys. Chem. A, 107 (2003) 9380-9386.

[25] A. Klamt, V. Jonas, T. Burger, J. Lohrenz, Refinement and parametrization of COSMO-RS, J. Phys. Chem. A, 102 (1998) 5074-5085.

[26] A. Klamt, G. Schüürmann, COSMO: a new approach to dielectric screening in solvents with explicit expressions for the screening energy and its gradient, Journal of the Chemical Society, Perkin Transactions 2, 1993 (1993) 799-805.

[27] F. Eckert, A. Klamt, Fast solvent screening via quantum chemistry: COSMO RS approach, AIChE Journal, 48 (2002) 369-385.

[28] J. Kahlen, K. Masuch, K. Leonhard, Modelling cellulose solubilities in ionic liquids using COSMO-RS, Green Chemistry, 12 (2010) 2172-2181.

[29] K.R. Seddon, A. Stark, M.J. Torres, Influence of chloride, water, and organic solvents on the physical properties of ionic liquids, Pure Appl. Chem, 72 (2000) 2275-2287.

[30] R.P. Swatloski, S.K. Spear, J.D. Holbrey, R.D. Rogers, Dissolution of Cellose with Ionic Liquids, Journal of the American Chemical Society, 124 (2002) 4974-4975.

[31] P. Bonhôte, A.-P. Dias, N. Papageorgiou, K. Kalyanasundaram, M. Grätzel, Hydrophobic, Highly Conductive Ambient-Temperature Molten Salts†, Inorganic Chemistry, 35 (1996) 1168-1178.

[32] M. Himmel, S. Ding, D. Johnson, W. Adney, M. Nimlos, J. Brady, T. Foust, Biomass recalcitrance: engineering plants and enzymes for biofuels production, Science, 315 (2007) 804.

[33] H. Tadesse, R. Luque, Advances on biomass pretreatment using ionic liquids: An overview, Energy Environ. Sci., (2011).

[34] C.P. Mehnert, Supported ionic liquid catalysis, Chemistry-A European Journal, 11 (2005) 50-56.

[35] C.P. Mehnert, R.A. Cook, N.C. Dispenziere, M. Afeworki, Supported ionic liquid catalysis-A new concept for homogeneous hydroformylation catalysis, Journal of the American Chemical Society, 124 (2002) 12932-12933.

[36] A. Riisager, R. Fehrmann, S. Flicker, R. van Hal, M. Haumann, P. Wasserscheid, Very Stable and Highly Regioselective Supported Ionic-Liquid-Phase (SILP) Catalysis: Continuous-Flow Fixed-Bed Hydroformylation of Propene, Angewandte Chemie International Edition, 44 (2005) 815-819.

[37] A. Riisager, R. Fehrmann, M. Haumann, P. Wasserscheid, Supported Ionic Liquid Phase (SILP) Catalysis: An Innovative Concept for Homogeneous Catalysis in Continuous Fixed-Bed Reactors, European journal of inorganic chemistry, 2006 (2006) 695-706.

[38] A. Riisager, R. Fehrmann, M. Haumann, P. Wasserscheid, Catalytic SILP Materials, Regulated Systems for Multiphase Catalysis, (2008) 149-161.

[39] G. Stephanopoulos, Challenges in engineering microbes for biofuels production, Science, 315 (2007) 801.

[40] T. Gu, Liquid Liquid partitioning methods for bioseperations, Academic Publisher, New York, 2000.

[41] F.W. Santangelo, A. E.; Gorak, A.; Pitner, W.; Schulte, M. , Purification of biofuels using ionic liquids, in: B.A. Moyer (Ed.) Solvent Extraction: Fundamentals to Industrial Applications, Proceedings of ISEC 2008 International Solvent Extraction Conference,,, Canadian Institute of Mining, Metallurgy and Petroleum, Montreal, Que, Tucson, AZ, United States, 2008, pp. 931-936.

[42] A. Daugulis, Integrated reaction and product recovery in bioreactor systems, Biotechnology Progress, 4 (1988) 113-122.

[43] A. Daugulis, D. Swaine, F. Kollerup, C. Groom, Extractive fermentation-integrated reaction and product recovery, Biotechnology Letters, 9 (1987) 425-430.

[44] L. Bruce, A. Daugulis, Solvent selection strategies for extractive biocatalysis, Biotechnology Progress, 7 (1991) 116-124.

[45] V. Yabannavar, D. Wang, Extractive fermentation for lactic acid production, Biotechnology and bioengineering, 37 (1991) 1095-1100.

[46] V. Yabannavar, D. Wang, Bioreactor System with Solvent Extraction for Organic Acid Productiona, Annals of the New York Academy of Sciences, 506 (1987) 523-535.

[47] J. Rydberg, C. Musikas, G.R. Choppin, Principles and Practices of Solvent Extraction, Dekker, New York, 1992

[48] T. Sekine, Y. Hasegawa, Solvent Extraction Chemistry: Fundamentals and Application, Dekker, New York, 1977.

[49] A. Fadeev, M. Meagher, Opportunities for ionic liquids in recovery of biofuels, Chemical Communications, 2001 (2001) 295-296.

[50] A. Kertes, C. King, Extraction chemistry of low-molecular-weight aliphatic alcohols, Chemical Reviews, 87 (1987) 687-710.

[51] S. Roffler, H. Blanch, C. Wilke, In situ extractive fermentation of acetone and butanol, Biotechnology and bioengineering, 31 (1988) 135-143.

[52] J.C.S. Wu, H. Lin, Photo reduction of CO~ 2 to methanol via TiO~ 2 photocatalyst, International Journal of Photoenergy, 7 (2005) 115.

[53] S.C. Roy, O.K. Varghese, M. Paulose, C.A. Grimes, Toward Solar Fuels: Photocatalytic Conversion of Carbon Dioxide to Hydrocarbons, ACS Nano, 4 (2010) 1259-1278.

[54] J. Wu, H.M. Lin, C.L. Lai, Photo reduction of CO2 to methanol using optical-fiber photoreactor, Applied Catalysis A: General, 296 (2005) 194-200.

[55] P. Pathak, M.J. Meziani, L. Castillo, Y.P. Sun, Metal-coated nanoscale TiO2 catalysts for enhanced CO2 photoreduction, Green Chem., 7 (2005) 667-670.

[56] W.N. Wang, J. Park, P. Biswas, Rapid synthesis of nanostructured Cu–TiO2–SiO2 composites for CO2 photoreduction by evaporation driven self-assembly, Catal. Sci. Technol., (2011).

[57] H.C. Yang, H.Y. Lin, Y.S. Chien, J.C.S. Wu, H.H. Wu, Mesoporous TiO 2/SBA-15, and Cu/TiO 2/SBA-15 Composite Photocatalysts for Photoreduction of CO 2 to Methanol, Catalysis letters, 131 (2009) 381-387.

[58] D.C. Grills, E. Fujita, New Directions for the Photocatalytic Reduction of CO2: Supramolecular, scCO2 or Biphasic Ionic Liquid− scCO2 Systems, The Journal of Physical Chemistry Letters, 1 (2010) 2709-2718.

[59] T. Yan, S. Wang, Y. Zhou, Z. Cao, G. Li, Adsorption of CO2 on the Rutile (110) Surface in Ionic Liquid. A Molecular Dynamics Simulation, The Journal of Physical Chemistry C, 113 (2009) 19389-19392.

[60] K. Shill, S. Padmanabhan, Q. Xin, J.M. Prausnitz, D.S. Clark, H.W. Blanch, Ionic liquid pretreatment of cellulosic biomass: Enzymatic hydrolysis and ionic liquid recycle, Biotechnology and Bioengineering, 108 (2011) 511-520.

[61] J.D. Holbrey, W.M. Reichert, R.P. Swatloski, G.A. Broker, W.R. Pitner, K.R. Seddon, R.D. Rogers, Efficient, halide free synthesis of new, low cost ionic liquids: 1,3-dialkylimiadolium salts containing methyl- and ethyl-sulfate anions, Green Chem., 4 (2002).

[62] L. Leclercq, I. Suisse, G. Nowogrocki, F. Agbossou-Niedercorn, Halide-free highly-pure imidazolium triflate ionic liquids: Preparation and use in palladium-catalysis allylic alkylation, Green Chem., 9 (2007) 1097-1103.

[63] M. Ue, M. Takeda, T. Takahashi, M. Takehara, Ionic Liquids with Low Melting Points and Their Application to Double-Layer Capacitor Electrolytes, Electrochem. Solid-State Lett. , 5 (2002) A119-A121.

[64] M. Yoshizawa, M. Hirao, K. Ito-Akita, H. Ohno, Ion conduction in zwitterionic-type molten salts and their polymers, J. Mater. Chem., 11 (2001) 1057-1062.

[65] E.A. Turner, C.C. Pye, R.D. Singer, Use of ab initio calculations toward the rational design of room temperature ionic liquids, J. Phys. Chem. A, 107 (2003) 2277-2288.

[66] N. Menshutkin, Z. Phys. Chem, 5 (1890) 589.

[67] N. Menshutkin, 6 (1890) 41.

[68] C. Reichardt, Solvatochromic dyes as solvent polarity indicators, Chem. Rev., 94 (1994) 2319-2358.

[69] C. Reichardt, Solvents and solvent effects in organic chemistry, 3rd ed., Wiley-VCH, Weinheim, Germany, 2003.

[70] P.G. Jessop, B. Subramaniam, Gas-expanded liquids, Chemical Reviews, 107 (2007) 2666-2694.

[71] W. Wu, W. Li, B. Han, Z. Zhang, T. Jiang, Z. Liu, A green and effective method to synthesize ionic liquids: supercritical CO_2 route, Green Chem., 7 (2005) 701-704.

[72] Z. Zhou, T. Wang, H. Xing, Preparation of ionic liquid N,N'-dialkylimidazolium halide, in: F.Z.S.G. Shuomingshu (Ed.), China, 2005.

[73] Z. Zhou, T. Wang, H. Xing, Butyl-3-methylimidazolium Chloride Preparation in Supercritical Carbon Dioxide, Ind. Eng. Chem. Res., 45 (2006) 525-529.

[74] M. Poliakoff, J.M. Fitzpatrick, T.R. Farren, P.T. Anastas, Green chemistry: science and politics of change, Science, 297 (2002) 807-810.

[75] L.A. Blanchard, Z. Gu, J.F. Brennecke, High-Pressure Phase Behavior of Ionic Liquid/CO2 Systems, J. Phys. Chem. B, 105 (2001) 2437-2444.

[76] M. Nunes da Ponte, Phase equilibrium-controlled chemical reaction kinetics in high pressure carbon dioxide, J. Supercrit. Fluids, 47 (2009) 344-350.

[77] W. Ren, B. Sensenich, A.M. Scurto, High-Pressure Phase Equilibria of Carbon Dioxide (CO2)+ n-Alkyl-Imidazolium Bis (trifluoromethylsulfonyl) amide Ionic Liquids, The Journal of Chemical Thermodynamics, (2009).

[78] A.M. Scurto, S. Aki, J.F. Brennecke, CO2 as a separation switch for ionic liquid/organic mixtures, J. Am. Chem. Soc, 124 (2002) 10276-10277.

[79] R. Dohrn, G. Brunner, High-pressure fluid-phase equilibria: experimental methods and systems investigated (1988–1993), Fluid Phase Equil., 106 (1995) 213-282.

[80] T. Kraska, K.O. Leonhard, D. Tuma, G.M. Schneider, Correlation of the solubility of low-volatile organic compounds in near-and supercritical fluids. Part I: applications to adamantane and ß-carotene, J. Supercrit. Fluid., 23 (2002) 209-224.

[81] D.J. Miller, S.B. Hawthorne, Determination of Solubilities of Organic Solutes in Supercritical CO2 by Online Flame Ionization Detection, Anal. Chem., 67 (1995) 273-279.

2. Experimental Methods

2.1 Vapor Liquid Equilibrium Method

2.1.1 Static High-Pressure Apparatus

A synthetic method based on material balances was used for solubility measurements. The apparatus used for this study has been described in detail by Ren and Scurto [2, 3] and will be overviewed here. The setup consists of a view cell, high pressure syringe pump, a water bath and high-precision pressure and temperature measurement (see Figure 2.1). The equilibrium cell is fabricated from stainless steel and rated for a pressure of about 275 bar. It is equipped with a high-pressure gauge glass window for observing phase interfaces and phase transitions. A cathetometer is used to measure the height of the liquid, which is converted to a volume by a separate calibration of the view-cell. Prior to running vapor-liquid equilibrium experiments, the instrumentation and water bath were allowed to thermally equilibrate.

A known amount of solute was weighed on a high-precision scale (Ohaus Analytical Standard, with 0.0001 g accuracy) and injected into the cell. Then, the view cell was pressurized to a specified pressure and the sample vigorously stirred to ensure equilibrium. Phase equilibria data calculations are based on the mass balance by determining the amount of gas delivered from a high-pressure/high-precision pump, the moles/mass of gas in the headspace above the liquid, and volume in the tubing/lines to the equilibrium cell. The mass of gas in the liquid phase was calculated by subtracting the

mass of gas in the lines and headspace above the liquid from the total mass of gas injected into the system.

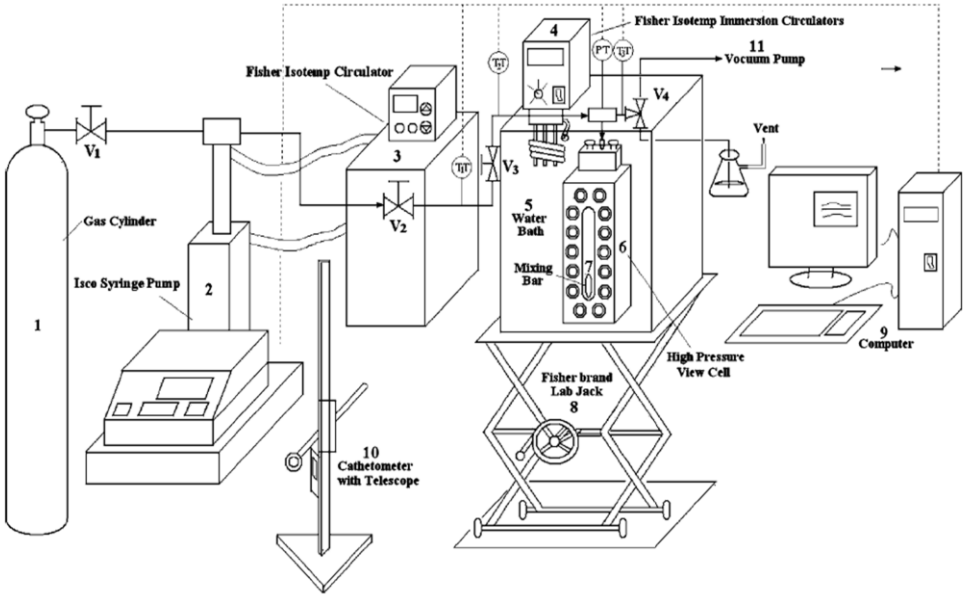

Figure 2.1 Static Cell for vapor liquid Equilibria Setup[2]

2.1.2 **Autoclave- Global Phase Behavior**

An autoclave view cell was used to accurately study the global phase behavior of 1-methylimidazole. The design is similar to Leitner et al. [5] and was modified by our group [6] . The set-up, shown in Figure 2.2 is equipped with two HIP (High Pressure Equipment, Inc.) valves, a magnetic stir bar, two view windows, and an Omega digital pressure gauge (model DPG5500B, accurate to within + 0.25% of full scale). The temperature of the autoclave cell was maintained at the desired temperature using an IKA

RET basic C hotplate fitted with an IKA ETS-D4 fuzzy logic controller, which has an accuracy of greater than + 1^{o}C.

In this study, three different types of phase behavior transitions were observed: vapor liquid (VLE) to vapor-liquid-liquid (VLLE); VLLE to liquid-liquid (LLE); and VLE, VLLE or LLE to critical transitions including upper-critical (UCEP) and lower critical endpoints (LCEP). To observe global phase behavior, known amounts of sample were loaded into the autoclave cell and the cell then equilibrated to the desired temperature. CO_2 was slowly metered into the cell via a high-pressure syringe pump (Teledyne-Isco, Inc., model 100DM) to the desired pressure. With stirring, the pressure was slowly raised continuously, until the first sign of the phase transition. The vessel was then slightly vented to a pressure right below the transition, and allowed to re-equilibrate. The process was repeated until the transition pressure was reproducible within ±0.5 bar. This process was performed at different temperatures at constant pressure, and was continued until temperatures were reproducible to approximately ±0.5°C. The amount of initial loading of sample was varied to accommodate volume expansion of the liquid, especially for conditions close to the mixture critical points.

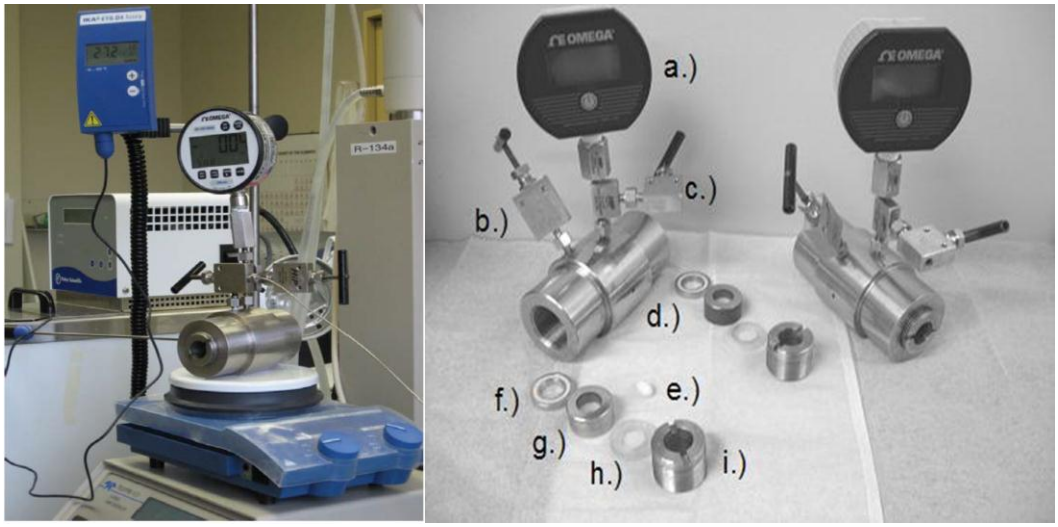

Figure 2.2 Assembled and dismantled autoclaves.[3, 4] a.) Pressure gauge b.) 90o HIP valve c.) straight HIP valve d.) hole in autoclave body for temperature probe e.) magnetic stirbar f.) Teflon o-ring and Teflon o-ring holder g.) Metaglas windows h.) acrylic spacer/gasket (to protect window) i.) threaded nut

2.2 Kinetic Study

Reactions kinetics were experimentally measured via nuclear magnetic resonance (NMR) spectroscopy and *in-situ* real-time, high-pressure attenuated total reflection infrared (ATR-IR) spectroscopy. Figure 2.3 illustrates a typical quaternization reaction observed between 1-methylimidazole and 1-bromohexane forming 1-hexyl-3-methylimidazolium bromide [HMIm][Br]. The reaction rates were confirmed to be 2^{nd} order/bimolecular according to the expression [7]:

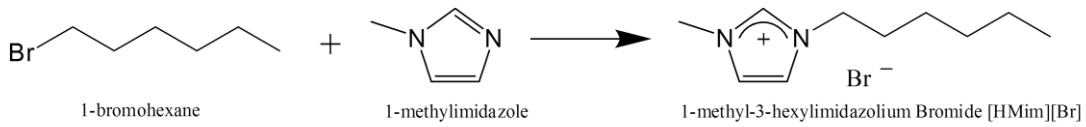

Figure 2.3 Reaction between 1-methylimidazole and 1-bromohexane forming 1-hexyl-3-methylimidazolium bromide [HMIm][Br].

$$r_{IL} = -r_{M\,\mathrm{Im}} = -r_{BrHex} = -\left(\frac{\partial C_{M\,\mathrm{Im}}}{\partial t}\right) = kC_{M\,\mathrm{Im}}C_{BrHex} \qquad \text{Eqn. 2-1}$$

or alternatively[8]:

$$r_{IL} = -r_{M\,\mathrm{Im}} = C^0_{M\,\mathrm{Im}}\left(\frac{\partial X}{\partial t}\right) = k(C^o_{M\,\mathrm{Im}} - C^o_{M\,\mathrm{Im}}X)(C^o_{BrHex} - C^o_{M\,\mathrm{Im}}X) \qquad \text{Eqn. 2-2}$$

Where *r* is the reaction rate based on component *i*, *k* is the kinetic constant, C_i^o the initial concentrations of the components (molarity), and *X* is the fractional conversion. When the initial concentrations of the two reactants are equal (1:1 stoichiometry), $r_{IL} = -r_{M\,\mathrm{Im}} = C^0_{M\,\mathrm{Im}}\left(\frac{\partial X}{\partial t}\right) = k(C^o_{M\,\mathrm{Im}} - C^o_{M\,\mathrm{Im}}X)(C^o_{BrHex} - C^o_{M\,\mathrm{Im}}X)$ Eqn. 2-2 becomes:

$$r_{IL} = -r_{M\,\mathrm{Im}} = C^0_{M\,\mathrm{Im}}\left(\frac{\partial X}{\partial t}\right) = k\left(C^o_{M\,\mathrm{Im}}\right)^2(1-X)^2 \qquad \text{Eqn. 2-3}$$

$$\frac{X}{C^o_{M\,\mathrm{Im}}(1-X)} = kt \qquad \text{Eqn. 2-4}$$

The kinetic constant *k* may be obtained by graphing the experimental data to a linearized form of Eqn. 2-4. However, this often introduces unnecessary error or undue emphasis

on certain time regimes; hence the need for a non-linear regression approach using SigmaPlot 2000, implemented in this study.

2.2.1 **High Pressure Kinetic Study**

2.2.1.1 ReactIR

A ReactIR™ iC10 reaction analysis system (from Mettler Toledo) equipped with SiComp IR probe (chemical resistant silicon film as the ATR element) located at the bottom and a CN76000 series temperature control (Omega Engineering, Stamford, CT) was used to monitor real-time mid-infrared spectra. The maximum working pressure of the probe is approximately 103 bars. Reactions were carried out in a 50 cm^3 high-pressure autoclave reactor (Model 4592 micro bench top reactor, Parr Instrument Company) set with a magnetically driven 4-blade impeller (stirrer speed ranges from 0 to 1700 rpm) for mixing. Two electric heating elements were fitted around the external reactor wall to provide the energy needed to maintain constant reactor temperature. The reactor temperature and the impeller rotating speed were controlled via a Parr 4843 controller and monitored via a LabView 8.6 data acquisition system (Figure 2.4 represents schematic of setup).

.

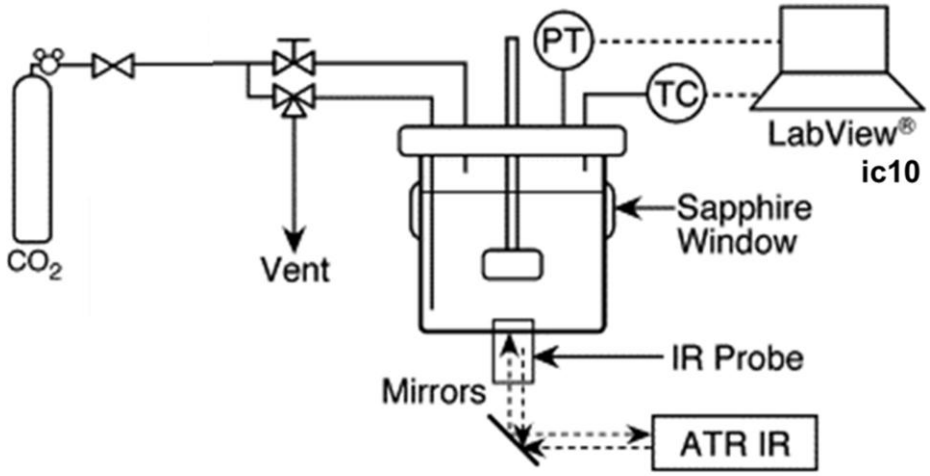

Figure 2.4 Schematic of REactIR setup

The reactor was allowed to heat up to the desired temperature and then charged with reactants weighed out with a Mettler Toledo XS205 dual range balance. Once the reactants were loaded, CO_2 was used to pressurize reactor to a known pressure. Each spectrum was the Fourier transformation of 200 scans collected over the spectral ranges of 4000-650 cm^{-1}, within a time period of less than 1 min and with an instrument resolution of 4 cm^{-1}. Figure 2.5 presents the time dependent spectral data for an experimental run at 40°C and at 90 bar pressure. The characteristic peak of 1-methyimidazole assigned to the imidazolium-ring HCCH antisymmetric stretching at 1516.97 cm^{-1} and the corresponding peak for [HMIm][Br] at 1569.16 cm^{-1}; these can be seen decreasing and increasing respectively over the reaction period in Figure **2.5**. The changes in the absorption over the reaction time for 1-methylimidazole were used to compute the conversion [9]:

$$X = 1 - \frac{peak\ height\ at\ time\ t}{peak\ height\ at\ time\ t = 0} \qquad \text{Eqn. 2-5}$$

The peak height at time = 0 represents the absorbance of 1-methylimidazole when the reaction is initiated. Results were compared with runs carried out using the NMR analysis: the differences in the kinetic constant obtained were within ± 6.0%.

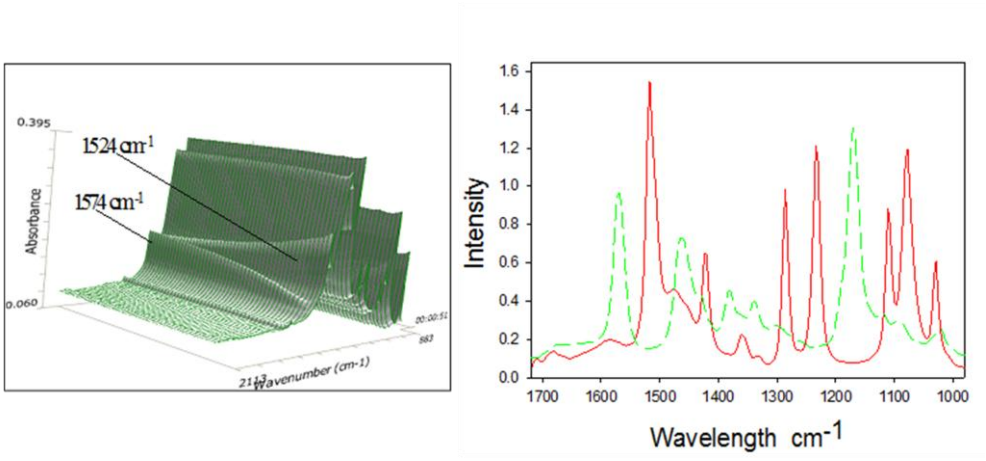

Figure 2.5 (a) Characteristic FTIR absorption spectrum with time for the synthesis of [HMIm][Br] from 1-bromohexane and 1-methylimidazole at 40°C (b) FTIR spectrum for reactant 1-methylimidazole) and product ([HMIm][Br])

2.2.1.2 Check ReactIR against established NMR technique

This section compares data obtained using ReactIR (described above) and an established methodology using Bruker AMX-500 Fourier transform H-NMR spectrometer for the

reaction of 1-methylimidazole and 1-bromoheaxane in acetonitrile (ACN) at 40^{o}C and ambient pressure to produce the ionic liquid 1-hexyl-3-methylimidazolium bromide (HmimBr).[10] 1-methyl-imidazole, 1-bromohexane and ACN were charged into reactor at 1:1:20 mole ratio respectively. Figure 2.6 presents the spectra for pure components at 40^{o}C and at ambient pressure. Calibration data was collected for 1-methylimidazole spectra at known concentrations to calculate concentration (Calibration plot for 1-methylimidazole is shown in Figure 2.7 at 1524 cm^{-1})

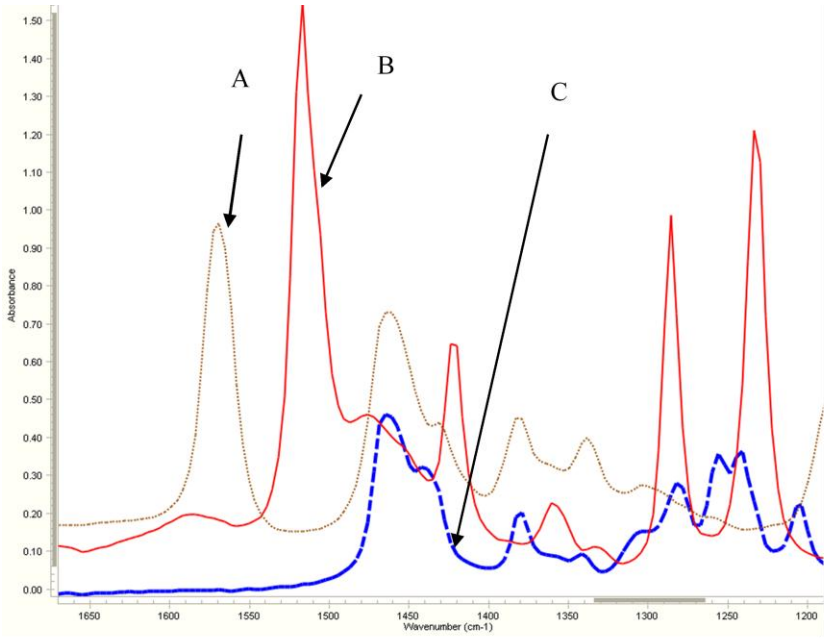

Figure 2.6 A) HmimBr (B) 1-methyl imidazole, (C) 1-bromohexane FTIR spectra with solvent subtraction.

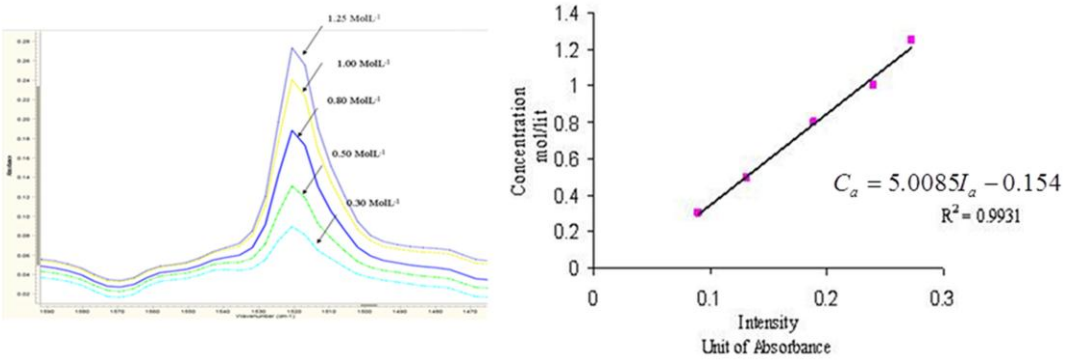

Figure 2.7 Calibration Spectra (a) and chart (b) for 1-methyl-imidazole at 1524cm-1

Concentration can be calculated using intensity values, using calibration data obtained using the ReactIR for 1-methylimidazole.

$$C_a = 5.0085I_a - 0.154$$

Where C_a is concentration of methyl imidazole in moles per liter ($molL^{-1}$) and I_a the intensiy measured in units of absorbance. Conversions were obtained using:

$$X_a = 1 - \frac{C_a}{C_{ao}}$$

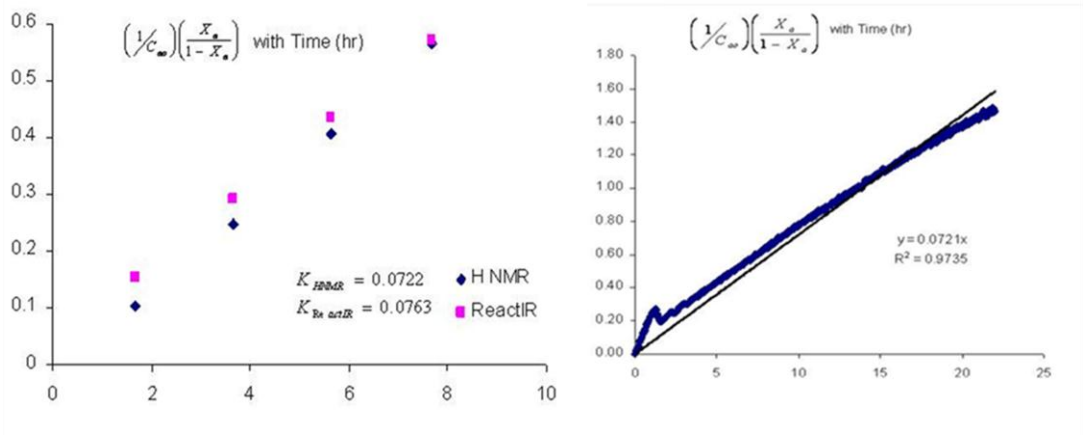

Figure 2.8 obtaining K value Equation 2-1-4

Figure 2.8 shows results obtained using and ReactIR corroborated those obtained via 1H NMR studies, within an error limit of ± 3% of percent conversion. In situ real time FTIR monitoring is a valuable method for kinetic study for these systems where sampling with NMR can be problematic. For high pressure runs, initial concentration of the 1-methylimidazole was computed using final volume data furnished by previously obtained volume expansion and VLE data (see section 1.1 for method) for the reaction mixture and CO_2. Slightly higher conversion values observed in the ReactIR are due to temperature excursions especially at the beginning of the reaction before equilibrium is reached, Jovanovic and Dube [11] observed similar issues when using ReactIR of real time monitoring of reactions. We find that this effect on the results obtained is minimal at the temperatures studied.

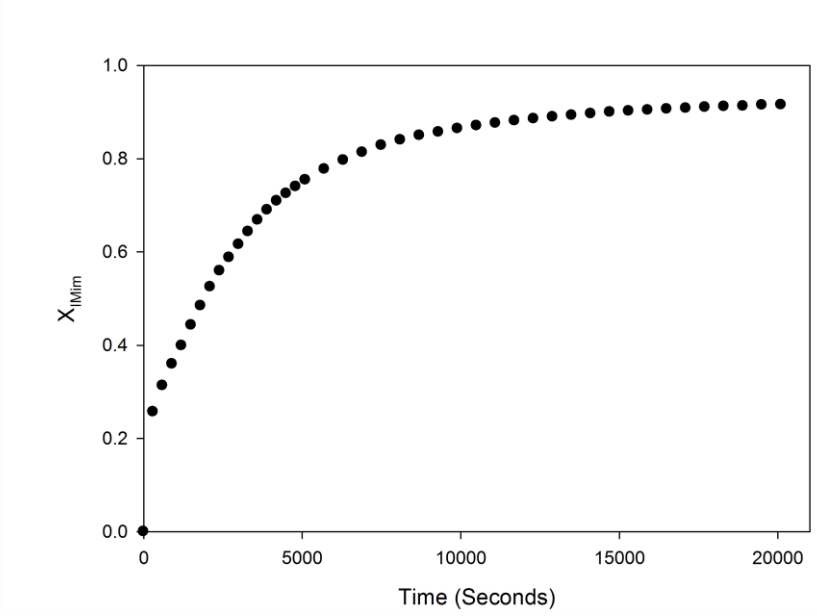

Figure 2.9 Conversion with time for the synthesis of [HMIm][Br] from 1-bromohexane and 1-methylimidazole in CO2 at 30 bar and 40°C, CMiM,0 = 4.37 mol L^{-1}

2.2.2 **Autoclave**

The autoclave view cell was used to carry out reactions at pressures higher than the limits of the ReactIR™ probe. The autoclave cell temperature was maintained at the desired level using an IKA RET basic C hotplate fitted with an IKA ETS-D4 fuzzy logic controller having an accuracy of greater than $\pm$ 1^{o}C. Initially, the autoclave was preheated to the desired temperature; weighed amounts of reactants were then added to the autoclave. It was purged twice using carbon dioxide to remove all oxygen. The autoclave was then pressurized while the mixture was continuously stirred. At specified periods, the temperature, pressure, time, and any observations were recorded; the autoclave was then submerged in an ice bath to quench the reaction. A convenient organic solvent (such as

acetonitrile and acetone), with minimal or no NMR peak overlap with reactants and product, was used to trap the vapor phase. The extracted autoclave content was added to the mixture collected from the venting vapor and mixed thoroughly. Samples were analyzed using ^{1}H NMR.

2.2.3 **Ambient Pressure Kinetics Technique**

For ambient pressure kinetic study, with or without solvents was conducted at three different temperatures using a multi-well reactor block from Chemglass, Inc. (model number CG-1991-03) which holds sixteen (16) standard 20 mL scintillation vials. The temperature and stirring of the reactor block was maintained using an IKAMAG RET basic hotplate equipped with an ETS-D4 fuzzy logic temperature controller which maintained the temperature to $\pm$1°C. Samples were analyzed using a Bruker 400 MHz Nuclear Magnetic Resonance (NMR) spectrometer periodically. The accuracy of this method to determine conversion X has been estimated at ±1%.

2.2.4 **NMR**

Nuclear magnetic resonance (NMR) spectroscopy is based on the magnetic properties of atomic nulcei. The nuclear magnetic moment of a nucleus interacting with an external magnetic field B_0 yields a nuclear magnetic energy level diagram. The absorption of energy is detected and amplified as a spectral line known as the resonance signal.[12] Gunther presents detailed analysis of the physics of NMR spectroscopy. Commonly used atoms for NMR investigations include ^{1}H, ^{19}F, ^{31}P, and the isotope ^{13}C. In this study, proton NMR (^{1}H NMR) was used for calculating the rates of reactions by integrating

specified reactants and product chemical shifts, using deuterated chloroform (chloroform-d) as the locking solvent. Samples were analyzed using a Bruker 400MHz Nuclear Magnetic Resonance (NMR) spectrometer. Typically, the time duration between sample extraction and NMR analysis was less than 5 minutes; further conversion during this time was negligible due to the relatively slower kinetic rates at ambient conditions and the more dilute concentrations after adding the deuterated chloroform. The conversion over time was determined by tracking the disappearance of the reactant and the appearance of the product peaks on the NMR spectrum product. For instance, the reaction shown in Figure 2.3 for the quaternization reaction between 1-methylimidazole and 1-bromohexane, The methyl peaks for the reactant, 1-methylimidazole and the corresponding methyl peaks for [HMIm][Br] at δ_H ~3.65ppm and δ_H ~4.16ppm respectively Figure 2.10 are integrated to determine the fractional conversion, X, using the following equation:

$$X = \frac{C^0_{M\,\mathrm{Im}} - C_{M\,\mathrm{Im}}}{C^0_{M\,\mathrm{Im}}} = \frac{N_{IL}}{N^0_{M\,\mathrm{Im}}} = \frac{N_{IL}}{N_{M\,\mathrm{Im}} + N_{IL}} = \frac{I_{\delta_H\,4.16}}{I_{\delta_H\,4.16} + I_{\delta_H\,3.65}} \quad \text{Eqn 2-6}$$

where N_X is the number of moles of specie X at any point in time, N^0 is initial amount of limiting reactant, and I is the peak area at each of the chemical shifts being analyzed. For further details of the NMR technique, see Schleicher [6]. The accuracy of this method to determine X has been estimated at ±1%. Sample NMR spectra for reactants (1-methylimidazole and 1-bromohexane) and product [HMim][Br] are shown in Figure 2.10 (a) [6] Figure 2.10 (b) presents the NMR spectra and labels for the corresponding *N*,*N*-

hexylmethylpyrrolidinium bromide and *N*-hexylpyridinium bromide bromide systems all studied here.

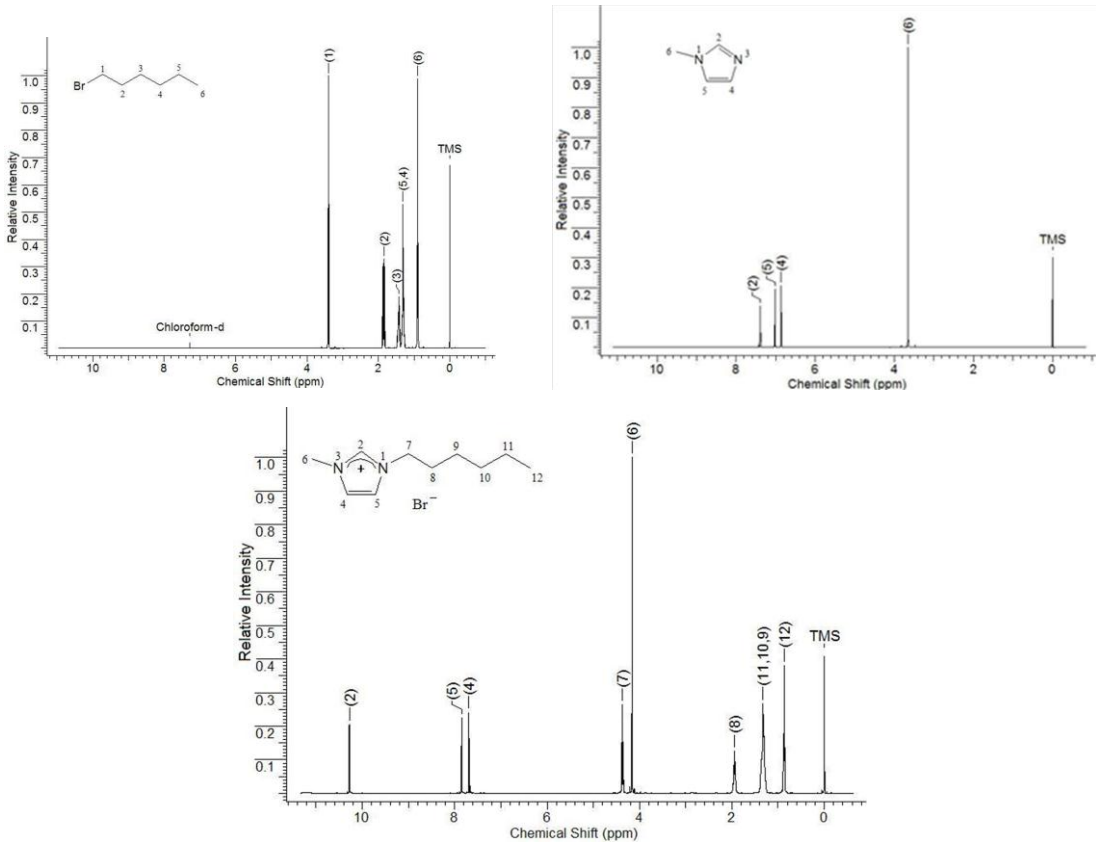

Figure 2.10 ^{1}H NMR in chloroform-d Bruker 400 MHz (a) 1-methylimidazole 1H NMR in chloroform-d Bruker 400 MHz 1H NMR: δ(ppm)= 3.65 (s, 3 H), 6.86 (s, 1 H), 7.02 (s, 1 H), 7.39 (s, 1, (top left). (b) 1-bromohexane 1H NMR in chloroform-d Bruker 400 MHz 1H NMR: δ(ppm)= 0.90 (t, J=6.85 Hz, 3), 1.32 (m, 4), 1.43 (m, 2 H), 1.85 (q, J=7.44 Hz, 2 H), 3.40 (t, J=6.83 Hz, 2 H) (top right) (c) Bruker 400 MHz 1H NMR: δ(ppm)= 0.87 (t, J=6.82 Hz, 3 H), 1.33 (m, 6 H), 1.95 (q, J=7.05 Hz, 2 H), 4.16 (s, 3 H),4.37 (t, J=7.41 Hz, 2 H), 7.69 (s, 1 H), 7.85 (s, 1 H), 10.28 (s, 1 H) (bottom figure)

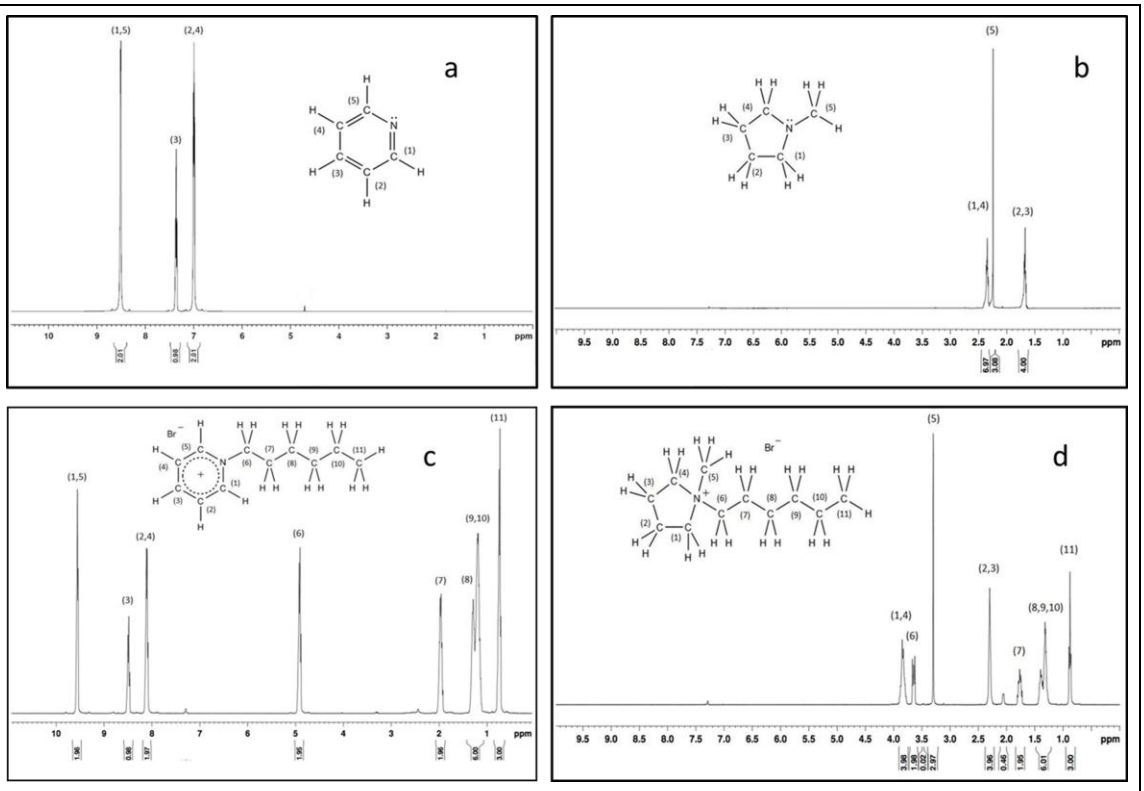

Figure 2.10 (b) : ^{1}H NMR chemical shifts for reactants and product using ^{1}H NMR in chloroform-d **Figure A.** Pyridine ^{1}H NMR without lock-solvent Bruker 500 MHz ^{1}H NMR: δ (ppm) = 8.51 (d, J=1.92Hz, 2 H), 7.36 (t, J=2.10Hz, 1 H), 7.00 (t, J=1.92Hz, 2 H) **Figure B.** *N*-methylpyrrolidine ^{1}H NMR in chloroform-d Bruker 400 MHz ^{1}H NMR: δ (ppm) = 2.34 (t, J=6.72Hz, 4 H), 2.24 (s, 3 H), 1.67 (quin, J=3.36Hz, 4 H) **Figure C.** *N*-hexylpyridinium bromide [HPyrid][Br] ^{1}H NMR in chloroform-d Bruker 400 MHz ^{1}H NMR: δ (ppm) = 9.55 (d, J=6.36Hz, 2 H), 8.48 (t, J=7.62Hz, 1 H), 8.10 (t, J=7.02Hz, 2 H), 4.90 (t, J=7.44Hz, 2 H), 1.97 (quin, J=7.18Hz, 2 H), 1.28 (quin, J=7.38Hz, 2 H), 1.18 (quin, J=3.12Hz, 4 H), 0.73 (t, J=6.96Hz, 3 H) **Figure D.** *N*,*N*-hexylmethylpyrrolidinium bromide [HMPyrrol][Br] ^{1}H NMR in chloroform-d Bruker 400 MHz ^{1}H NMR: δ (ppm) = 3.85 (t, 4 H), 3.64 (t, 2 H), 3.30 (s, 3 H), 2.30 (quin, 4 H), 1.77 (quin, 2 H), 1.40 (quin, 2 H), 1.32 (quin, 4 H), 0.88 (t, 3 H)

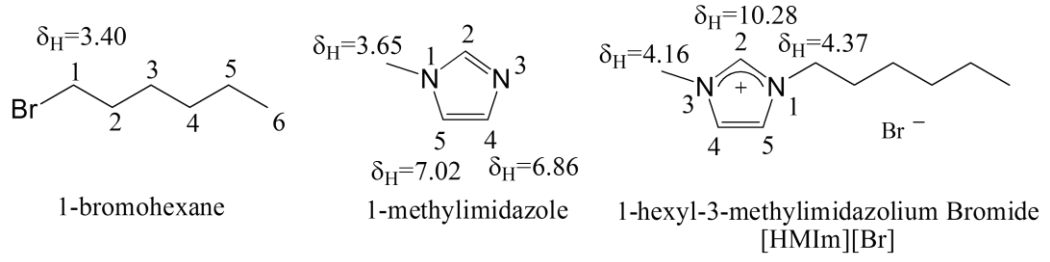

Figure 2.11 : 1H NMR chemical shifts for reactants and product using 1H NMR in chloroform-d

The main shifts examined were δ_H=3.65 on 1-methylimidazole and δ_H=3.40 on 1-bromohexane and the corresponding chemical shifts δ_H=4.16 and δ_H=3.40 on the product respectively. When solvent peaks overlapped, as is the case for this reaction, and methanol at δ_H=3.31 and δ_H=4.87, the chemical shift for 1-methylimidazole at δ_H=7.02 and δ_H=6.86 were used with the corresponding products chemical shift δ_H=10.28.

2.3 Transport Property Measurements

2.3.1 Thermal conductivity and Diffusivity Measurements

Thermal conductivity may be determined via stationary or transient measurements. The stationary method simply relies on a constant temperature profile, while transient methods employ a changing temperature profile, the gradient of which must be accurately determined. The transient hot-wire technique is a widely accepted method to measure thermal conductivity of fluids; the principle has been thoroughly explained by Healy and coworkers.[13] The temperature field of the transient hot-wire instrument, and the fundamental working equation may be expressed as:

$$\frac{\partial T}{\partial t} = a_T * \left(\frac{\partial^2 T}{\partial r^2} + \frac{l}{r} * \frac{\partial T}{\partial r} \right)$$

Eqn 2-7

……

with

$$a_T = \frac{\lambda}{c_p * \rho}$$

where T is temperature, *t* is the elapsed time, a is the thermal diffusivity of the fluid and r is the radius of the hot wire. Eqn 2-7 is a classic numerical problem was solved by Carslow and Jaeger [14] to

$$T - T_o = -\frac{q}{4 * \pi * \lambda} * E_i\left(-\frac{r^2}{4 * a_T * t}\right) \qquad \text{Eqn 2-8}$$

where E is the Euler-Mascheroni constant. At time t_0 (5ms) after heat transfer starts

$$E_i = \gamma + \ln x - \frac{x}{1*1!} + \frac{x^2}{2*2!} - \frac{x^3}{3*3!} + ...$$

with Eqn 2-9

$$\gamma = 0.5772$$

Since $t >> \frac{r^2}{4 * a_T}$, then Eqn 2-8 becomes:

$$T - T_o = \frac{q}{4 * \pi * \lambda} * \left(\ln \frac{4 * a_T * t}{r^2} - 0.5772\right) \qquad \text{Eqn 2-10}$$

Between t_1 and t_2, the solution of heat transfer on the surface of the heated wire (r approaches r_o) becomes:

$$\lambda = \frac{q_1 + q_2}{8 * \pi * (T_2 - T_1)} * \ln \frac{t_2}{t_1} \qquad \text{Eqn 2-11}$$

and the thermal diffusivity can be computed from:

$$a_T = \frac{r_o^2}{4*t} * \exp\left(\frac{4*\pi*\lambda}{q} * T + 0.5772\right) \quad \text{Eqn 2-12}$$

2.3.1.1 Lambda Cell

The LAMBDA measuring system, from Flucon Fluid Control GmbH (Germany), is the transient short-hot-wire cell used in this study for obtaining thermal heat conductivity, and thermal diffusivity data. The lambda unit uses a platinum wire of a diameter of about 100 μm and length about 35mm, and which are welded to platinum lead terminals. This lead terminal is supported by a circular Teflon plate having a diameter of 24mm and a thickness of 5mm. Platinum lead wires for electric heating and voltage measurement were welded to a platinum lead terminal. The maximum volume of the stainless-steel pressure-resistant cell is approximately 65 cm^3. Temperature is controlled by a circulating bath connected to the jacketed sample vessel, and can vary within a range of 25-400^oC within an accuracy of ±1%, at a frequency of about 20s. The PC controller calculates the actual energy input for each point of measurement of the temperature profile. Although impurities such as water content affect transport properties (viscosity, for example) of samples especially IL, Valkenburg et al., [15] showed that this effect was relatively small for thermal conductivity at around ± 0.8%. Pan and coworkers [16] corroborated this trend with a difference of ±1.2%.

2.3.1.2 Procedure

First, the setup is calibrated using a solvent with properties similar to test subject and with known parameters, for systems studied here, methanol was used to calibrate the

lambda unit. For reference, Density (at 15^{o}C and thermal conductivity data (over working temperature range) was obtained for Methanol from REFPROP (calibration and REFPROP data used is presented in the appendix). After calibration, the temperature bath is set to desired temperature and allowed to equilibrate over 30-45 minutes. Data is accumulated over time in-situ using accompanying Lambda software. Thermal conductivity and diffusivity are directly obtained by the setup; however with known density of sample, the heat capacity may be computed. Table 2.1 compares literature data with experimental data at ambient temperature.

Table 2. 1 Lambda Unit Verification (Literature Data from REFPROP database)

			Thermal Conductivity (mW/mK)			Thermal Diffusivity (m^2/sec)		
Compound	Water Content (ppm)	Temp C	Exp	Lit	% Diff	Exp	Lit	% Diff
Methanol	701.690	21.1	202.383	202.020	0.180	9.28E-08	1.02E-07	8.91
Ethanol	1213.920	21.9	169.000	165.910	1.863	8.94E-08	8.30E-08	7.72
Decane	60.060	22.0	133.436	130.260	2.438	8.60E-08	8.19E-08	5.01
Cyclohexane	28.650	22.0	119.980	124.620	3.723	8.48E-08	8.96E-08	5.44
Average % Difference					2.051			6.770

2.3.2 **Viscosity**

2.3.2.1 Ambient Pressure

The viscosity of liquids at ambient pressure was measured using a Wells-Brookfield Cone and Plate (DV-III ULTRA) Viscometer / Rheometer. Here, a rotating cone is immersed in the sample fluid between the cone and a stationary flat plate. This is then driven by a calibrated beryllium-copper spring; the viscose drag of the fluid against the

cone is measured by the spring deflection. This deflection is measured with a rotary transducer. The resistance to the rotation of the cone produces a torque that is proportional to the shear stress in the fluid. The torque is read off a digital display and converted to absolute centipoise units (mPa·s) from pre-calculated range charts. Temperature is controlled using a constant temperature circulating bath connected to the jacketed sample cup. The system is accurate to within ±1.0% of the working range. Reproducibility is to within ±0.2%. Working temperature range is from 0°C to 100°C with the accuracy of ±0.1°C. Hence the full scale viscosity range for the DV-III Ultra model can be calculated from:

$$\text{viscosity}[cP] = TK * SMC * \frac{10{,}000}{RPM} \quad \text{Eqn 2-14}$$

Where TK is the DV-III Ultra Torque constant, for this model (0.09373), SMC is the spindle multiplier constant (this instrument uses a CP42 spindle, with corresponding constant, 0.64).

2.3.2.2 High Pressure

A high pressure viscometer was obtained using a modified Cambridge Applied Systems (currently Cambridge Viscosity, Inc.) Model ViscoPro 2000 System 4- SPL-440 equipped with Viscolab software. A detailed description of the apparatus has been described in detail by Ahosssieni and Scurto [1, 17] and will be overviewed here. The apparatus is operated based on annular flow around an axially oscillating piston. The apparatus is made up of a temperature controlled oven which houses the high pressure viscometer sensor (connected to a precision pressure transducer (PT)) and a resistance

temperature detector (RTD). The testing chamber consists of a piston and electromagnetic coils: two magnetic coils inside the sensor body oscillate the piston over a fixed distance, forcing the fluid to flow through the annular space between the rod and chamber. One magnetic coil applies a constant force on the piston while the other determines the position of the piston. The roles of the coils reverse when the piston reaches the end of the cycle and changes direction. The time required for the rod to complete a cycle can be directly correlated to the dynamic viscosity of the fluid. The viscosity reading is the average of 20 viscosity measurements and is reported with the standard deviation of those measurements. A volume of approximately 30-40 mL of sample was metered into the $30cm^3$ Jerguson view-cell, a stainless steel high pressure metering pump (Eldex Laboratories, Inc., Model 1020 BBB-4), and the pressure was slowly increased to desired pressures using a Teledyne- Isco, Inc. syringe pump (model 260D) (8). A Micropump, Inc. (model 415A) recirculation pump (9) is used to draw the sample liquid from the view-cell, transport it through the viscometer sensor (2) and then back to the top of the view-cell, where the material falls through the gas phase back to the liquid layer. This recirculation allows for a rapid approach to equilibrium, while being able to monitor the change in viscosity over time. Equilibrium is usually achieved in approximately 30 minutes for each pressure studied. The error in viscosity, based upon the sampling average of 20 measurements, is reported at each point. This apparatus can be used to obtain viscosity measurements within the range of 0.2 to 10,000 cP (mPa・s), and up to a maximum pressure of 137.9 MPa between 233.15 K to 463.15 K. The NIST-traceable calibration was accurate to 0.0084% full-scale. The maximum deviation of

temperature from the set-point temperature for all data was 0.1 K, with the average deviation being ±0.07K.

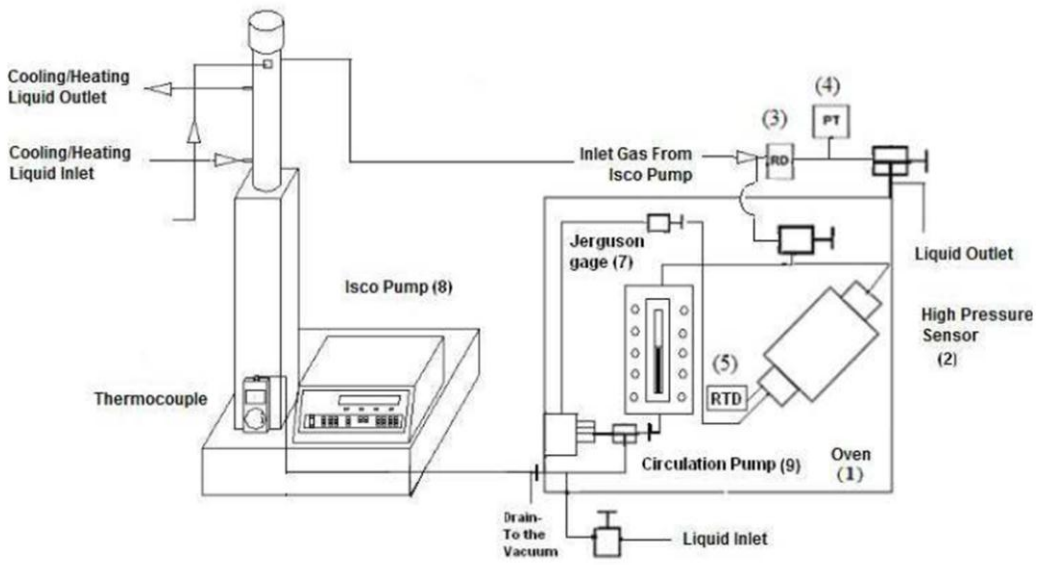

Figure 2.12: A schematic of the high pressure viscometer setup[1] (1)oven (2) high pressure sensor (3) rupture disc (4) pressure (5) RTD temperature probe (6) high pressure generator (is not shown here) (7)Jerguson view cell (8) syringe pump (9) Micropump recirculation system.

2.3.3 **Densitometer**

Density ρ, is defined as mass divided by volume and is a highly temperature dependent property. For mixtures, the density of the mixture is a function of composition. In this study, density was measured using an Anton Parr U-tube oscillating densitometer (DMA 4500). This instrument is based on Anton Parr's law of harmonic oscillation, where an electronically excited sample vibrates at its characteristic frequency. The characteristic

frequency changes depending on the density of the sample. Density can computed from determining this characteristic frequency of the sample. A sample (approximately 2 mL) is typically introduced into the U-shaped borosilicate glass tube. The U-tube oscillating densitometer is straightforward and accurate, with repeatability within ±0.00001 gr/cm^3 and measuring range 0 g/cm^3 to 1.5 g/cm$^{3.}$ Temperature of the sample in the measuring cell is precisely measured using an ultra-accurate platinum sensor with an accuracy ±0.03^{o}C.

2.4 Polarity Studies

2.4.1 Kamlet Taft parameters

Kamlet, Taft, *et. al.*[18-21] take a multi-parameter approach to describing solvent polarity; considering three different scales called the Kamlet Taft (*KT*) parameters. *KT* parameters consist of 3 components namely, acidity (α), basicity (β), and dipolarity/polarizability (π^*). [18, 20-25] The α scale, which measures the solvent's acidity, or ability to donate a proton to a solvent-to-solute hydrogen bond, is also referred to the hydrogen bonding donor ability (HBD) of the solvent. The β scale characterizes the solvent's basicity or ability to accept a proton in a solute-to-solvent interaction, also known as the hydrogen bonding accepting (HBA) strength of the solvent. Finally, the π^* is a measure of the solvent's ability to stabilize a charge or a dipole by the solvent's dielectric effects.[18] Reichardt presents a literature collection of these K-T parameter(α's, β's, and π^*'s) for common solvents.[18, 26]

2.4.1.1 Solvatochromic Probes:

Chemicals that change color due to a change in solvent polarity are often referred to solvatochromic probes. Solvatochromic probes are dyes used to study solvent properties using an Ultraviolet-Visible (UV-Vis) spectrophotometer. Depending on the molecular interactions between the solvatochromic probe and the solvent molecules a shift in the solvatochromic probes' absorbing wavelength is observed in different solvents. Figure 2.13 presents the dyes that are used for this study. Negative solvatochromism's characteristic is a blue shift also known as a hypsochromic shift, observed with increasing solvent polarity. A red shift is seen for a positive solvatochromism and is also referred to as a bathochromic shift, observed with decreasing solvent polarity. These different shifts occur due to the difference in dipole moment between the ground and excited states of the chromophore, which manifests as a strong dependence of absorption and emission spectra with the solvent polarity. The variation in the position, intensity, and shape of the absorption spectra correlates with specific solute/solvent interactions.

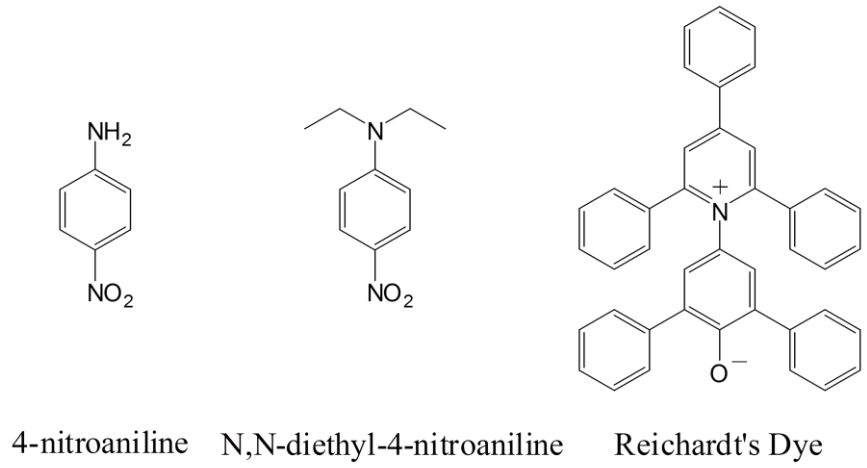

Figure 2.13: Solvatochromic probes used in this study

2.4.2 **Method**

There are many different solvatochromic probes that can be used to determine the *KT* parameters. Different sets of dyes produce slightly different quantitative results: comparisons with other studies should be made only with similar dye sets. π^* for each solvent was calculated using N,N-diethyl-4-nitroaniline, a dye only affected by polarizability with no effect of solvent acidity or basicity[18]:

$$\pi^* = \left[\frac{27.52kK - \nu(1)_{Max}}{3.18kK} \right] \qquad \text{Eqn 2-15}$$

where π^* is the dipolarity/polarizability parameter, kK is kiloKaysers (1000kK = cm $^{-1}$),[27] and $\nu(1)_{Max}$ is the maximum absorbing wavelength for Dye 1 (cm^{-1}). Cyclohexane (π^*=0.00) and dimethyl sulfoxide (π^*=1.00) are used as references.

The basicity component β was calculated using probes 4-nitroaniline and N,N-diethyl-4-nitroaniline.[20] Hexamethylphosphoramide is used as a reference solvent with β=1. The equation used in calculating all β values is: [20]

$$\beta = \left[\frac{1.035\nu(1)_{Max} - \nu(2)_{Max} + 2.64kK}{2.80kK} \right] \quad \text{Eqn 2-16}$$

The acidity of the solvent, α was calculated using N,N-diethyl-4-nitroaniline/Reichardt's Dye. In HBD solvents, Reichardt's dye showed hypsochromic shifts, resulting from both the HBD ability and the dipolarity/polarizability. The π^* parameter obtained in is used to compute α using $\pi^* = \left[\frac{27.52kK - \nu(1)_{Max}}{3.18kK} \right]$ Eqn 2-15 [18]

$$\alpha = \left[\frac{\nu(3)_{Max} - 10.60kK - 5.12kK(\pi^* - 0.23\delta)}{5.78kK} \right] \quad \text{Eqn 2-17}$$

where $\nu(3)_{Max}$ is the maximum absorbing wavelength for Dye 3 (cm^{-1}) and δ is the "polarizability correction term" (0 for non-chlorinated solvents aliphatic solvents, 0.5 for polychlorinated aliphatics, and 1.0 for aromatic solvents).[18] The kinetic rate constants

were correlated with the *KT* parameters using a Linear Solvation Energy Relationship (LSER) method [26]:

$$\ln k = \ln k^{o} + A\alpha + B\beta + C(\pi^{*} - D\delta) \quad \text{Eqn 2-18}$$

The regressed coefficients, *A*, *B*, C, and *D* quantify the individual effects of the polarity parameter on the kinetic rate. The regression was done using SigmaPlot 2000 version 6.00. Further, Reichardt's dye was also used to determine polarity based on the $E_T(30)$ scale[26]:

$$E_T(30) = hc\nu(3)_{Max} N_A \quad \text{Eqn 2-19}$$

where $E_T(30)$ is a scale of polarity with units of kcal/mol, *h* is Planck's constant, *c* is the speed of light, $\nu(3)_{Max}$ is the maximum absorbance for Reichardt's dye, and N_A is Avogadro's number. Experimental values obtained for α, β, and π* were found to be within ±0.01 of literature values.

2.4.3 **Polarity Measurements**

In this study, the solvatochromic probes *N*,*N*-diethyl-4-nitroaniline, 4-nitroaniline, and Reichardt's dye were used to calculate the three solvent parameters α, β, and π^*. All *KT* parameters and $E_T(30)$ values were obtained from solutions with the appropriate dyes, using a Varian Cary 300 Bio Ultra violet-Visible (UV-Vis) Spectrophotometer with a dual cell Peltier accessory temperature controller. The temperature was maintained at the standard 25°C. The wavelengths of maximum absorption of the dyes were related to the

KT parameters using the standard formulas.[26] The LSER coefficients were regressed using the non-linear optimization techniques in the Sigma-Plot 2000 version 6.0 software.

2.4.3.1 UV-Vis

The solvatochromic probe studies for solvents and reaction mixtures were performed using a Varian Cary 300 Bio UV-Visible Spectrophotometer with a Dual Cell Peltier Accessory Temperature Controller, supplied with Cary WinUV software version 3.00.

2.4.3.1.1 Ambient Pressure

A one centimeter path-length cuvette was used for all ambient pressure studies. Before beginning any experiments, the UV-Vis spectrophotometer was allowed to warm up for at least one hour and a validation on the instrument performance verified prior to taking any scans. Once preheated, 3 mL of the solvent was added to the cuvette and a background spectrum taken for the solvent. Three mg of the solvatochromic probe was then added to a 20 mL vial containing 3 mL of solvent. The vial was then mixed; 50 μL was drawn and placed in the cuvette containing the 3 mL of solvent. The cuvette was then mixed and placed in the UV-Vis spectrophotometer. A quick scan was made from 800-200 nanometers (nm), at a rate of 600nm/min, to narrow the region where the solvatochromic probe had a maximum absorbance. Once the scan was complete, the maximum absorbance for each probe was noted along with the corresponding wavelength. For the 4-nitroaniline and *N*,*N*-diethyl-4-nitroaniline solvatochromic probes,

the maximum absorbances occurred between 300-420 nm. The Reichardt's dye solvatochromic probe has a high absorbance in the ultraviolet and visible region, with the wavelength of interest for Reichardt's dye in the visible region between 800-550 nm. Once the maximum absorbance was determined for each solvatochromic probe, the sweep width was narrowed to ±150 nm around the maximum absorbing wavelength of interest, and the scan rate decreased to 200 nm/min. If the maximum absorbance for the probe was greater than 1.0 or less than 0.6, the cuvette was diluted or concentrated accordingly. A scan was taken and the wavelength at the maximum absorbance recorded for calculating the *KT* parameters. Each set of data was replicated three times to obtain a standard deviation.

2.4.3.1.2 High pressure

All *KT* parameters and $E_T(30)$ values were obtained from solutions with the appropriate dyes using a Varian Cary 300 Bio Ultra violet-Visible (UV-Vis) Spectrophotometer, procedure is similar to previous section except for apparatus was adapted for high pressure runs. Here, a high pressure stainless steel optical cell fitted with sapphire windows (Meller Optics MSW062/125**),** 0.625 inches in diameter and 0.125 inches thick was used instead of the cuvette. CO_2 was metered into the cell to desired concentrations/pressures using a high pressure syringe pump. The wavelengths of maximum absorption of the dyes were related to the *KT* parameters using standard formulas described above. [28]

2.5 Ionic Liquid Synthesis

2.5.1 **[HMim][Br]**

1-hexyl-3-methylimidazolium bromide was prepared by quanternization reaction of 1-methylimidazole with small excess amount of 1-bromohexane in acetonitrile at 40°C under an argon atmosphere with stirring for three days. The solvent was removed using a rotary evaporator under reduced pressure at 40°C and then dried under high vacuum ($<10^{-4}$ Torr) at 50°C for several days. The IL's water content was measured as 3.19 ppm, while the bromide content was below 6 ppm. ^{1}H-NMR spectra were recorded on a Bruker 400 NMR spectrometer using TMS as a reference for ^{1}H chemical shifts. The water content was measured using Mettler Toledo DL32 Karl Fisher Coulometer. Bromide content was determined by a Cole Parmer Bromide Electrode (27502-05) equipped with an Oakton Ion 510 series meter. ^{1}H NMR chemical shifts (relative to TMS internal standard) and coupling constants J/Hz for [HMIm][Br] ^{1}H NMR in chloroform-d were δ(ppm)= 0.87 (t, J=6.82 Hz, 3 H), 1.33 (m, 6 H), 1.95 (q, J=7.05 Hz, 2 H), 4.16 (s, 3 H), 4.37 (t, J=7.41 Hz, 2 H), 7.69 (s, 1 H), 7.85 (s, 1 H), 10.28 (s, 1 H). The water content was 0.28 wt % as measured by Karl Fisher analysis (Mettler Toledo DL32 Karl Fisher).

2.5.2 **[HMim][TF_2N]**

1-hexyl-3-methylimidazolium bis(trifluoromethylsulfonyl) imide ([HMIm][Tf_2N]) was prepared from the anion exchange of [HMIm][Br] with Li[Tf_2N] in deionized water, as described in the literature.[29] The denser, hydrophobic, IL phase is decanted and washed six to eight times with a volume of water approximately twice that of the IL. The

IL was then dried under vacuum. Water content was 125 ppm, and Br content less than 8 ppm. 1H NMR chemical shifts (relative to TMS internal standard) and coupling constants J/Hz: δ=8.65 (s, 1H), 7.39(t, 1H, J=1.8), 7.37(t, 1H, J=1.5), 4.17 (t, 2H, J=7.4), 3.93(s, 3H), 1.87(m, 2H), 1.32(m, 6H) 0.87(t, 3H, J=6.53).

2.5.3 **[EMim][Acetate]**

1-ethyl-3-methylimidazolium acetate ([EMIm][Acetate]) was prepared from the anion exchange of [EMIm][Br] with potassium acetate in ethanol as described in the patent literature. [30] [EMIm][Br] was first synthesized similar to procedure described above for [HMIm][Br]. Precipitated potassium acetate salt was vacuum filtered from the ethanol/[EMim][Acetate] mixture at a low temperature. The ethanol was removed from the IL using a rotary evaporator and then dried under vacuum. The IL was dried under vacuum at 50^{o}C for 2 days to remove volatile impurities. The IL appears to be very hydrophilic; Karl Fischer analysis showed water content of water 1500 ppm.

2.6 Materials

1-methylimidazole (CAS 616-47-7) 99+% and 1-bromohexane (CAS 111-25-1) 99+% were obtained from Sigma Aldrich. 1-methylimidazole was distilled and further dried using a Type 4 Angstrom Molecular sieve obtained from Fisher Scientific. Coleman Instrument grade CO_2 and Argon (extra dry, grade 99.998%) were obtained from Airgas Inc. 1-bromohexane was used as received. Acetonitrile (>99.9%) and chloroform d (>99.6%) were purchased from Acros. Reagents pyridine (>99%), 1-bromohexane

(>99%), were obtained from Acros Organics. Solvents acetonitrile (>99.9%), acetone (>99.9%), methanol (>99.9%), chlorobenzene (99.9%), dichloromethane (99.8%), dimethylsulfoxide (>99%), cyclopentanone (>99%), ethyl lactate (>98%), 2-butanone (>99.7%), and cyclohexane (>99.9%) were all obtained from Sigma Aldrich, while ethyl formate (>98%) was purchased from Acros Organics. Solvatochromic probe 4-nitroaniline (>99%) was purchased from Sigma Aldrich; N,N-diethyl-4-nitroaniline (97%) was purchased from Oakwood Products Inc., and Reichardt's Dye (>90%) was purchased from Fluka. All starting materials were distilled and kept under argon gas prior to use. All solvents were dried using 3Å or 4Å molecular sieves. The solvatochromic probes Reichardt's Dye, 4-nitroaniline, and N,N-diethyl-4-nitronaniline were used as received.

References

[1] A. Ahosseini, Homogeneous Catalysis and Mass Transfer in Biphasic Ionic Liquid systems with compressed CO_2 and oragnaic compounds, in: Chemical and Petroleum Engineering, Univeristy of Kansas, Lawrence, 2010.

[2] W. Ren, High-Pressure Phase Equilibria of Ionic Liquids and Compressed Gases for Applications in Reactions and Absorption Refrigeration, in: Chemical and Petroleum Engineering, University of Kansas, Lawrence, 2009.

[3] W. Ren, A.M. Scurto, High-pressure phase equilibria with compressed gases, Review of scientific instruments, 78 (2007) 125104-125104-125107.

[4] J. Schleicher, Masters Thesis, in, MS Thesis, University of Kansas, 2007.

[5] W. Leitner, Supercritical carbon dioxide as a green reaction medium for catalysis, Acc. Chem. Res., 35 (2002) 746-756.

[6] J. Schleicher, in, University of Kansas, Lawrence, Kansas, USA, 2007.

[7] J. Schleicher, A.M. Scurto, Kinetics and solvent effects in the synthesis of ionic liquids: imidazolium, Green Chem., Published Online: DOI: 10.1039/b808364a (2009) in press.

[8] O. Levenspiel, Chemical Reaction Engineering, Third ed., Wiley, New York, 1998.

[9] R. Jovanovic, M.A. Dubé, In-Line Monitoring of Butyl Acrylate/Vinyl Acetate Emulsion Copolymerizations Using ATR–FTIR Spectroscopy, Polym. React. Eng., 11 (2003) 233-257.

[10] J.C. Schleicher, A.M. Scurto, Kinetics and solvent effects in the synthesis of ionic liquids: imidazolium, Green Chem., 11 (2009) 694-703.

[11] R. Jovanović, M.A. Dubé, In-Line Monitoring of Butyl Acrylate/Vinyl Acetate Emulsion Copolymerizations Using ATR–FTIR Spectroscopy, Polymer Reaction Engineering, 11 (2003) 233-257.

[12] B. Bode, The importance of density for transport quantities of liquids under high pressure, Erdöl, Erdgas, Kohle, 107 (1991).

[13] J. Healy, J. De Groot, J. Kestin, The theory of the transient hot-wire method for measuring thermal conductivity, Physica B+ C, 82 (1976) 392-408.

[14] H.S.J. Carslaw, J.C, Conduction of heat in solids, 2nd ed., Oxford University Press, 1950.

[15] M.E.V. Valkenburg, R.L. Vaughn, M. Williams, J.S. Wilkes, Thermochemistry of ionic liquid heat-transfer fluids, Thermochimica Acta, 425 (2005) 181-188.

[16] J. Pan, X. Li, J. Wu, EquationThermal Conductivity of Liquid 1, 1, 1, 3, 3, 3-Hexafluoropropane (HFC-236fa) from 253 K to 373 K and Pressure up to 30 MPa, Fluid Phase Equilibria, (2011).

[17] A. Ahosseini, A. Scurto, Viscosity of Imidazolium-Based Ionic Liquids at Elevated Pressures: Cation and Anion Effects, International Journal of Thermophysics, 29 (2008) 1222-1243.

[18] M.J. Kamlet, J.M. Abboud, M.H. Abraham, R.W. Taft, Linear Solvation Energy Relationship. 23. A Comprehensive Collection of the Solvatochromic Parameters, pi*, alpha, beta, and Some Methods for Simplifying Solvatochromic Equation, J. Org. Chem., (1983) 2877-2887.

[19] M.J. Kamlet, T.N. Hall, J. Boykin, R.W. Taft, Linear Solvation Energy Relationship. 6. Additions to the Correlations with the pie star Scale of Solvent Polarity, J. Org. Chem., 44 (1979) 2599-2604.

[20] M.J. Kamlet, R.W. Taft, The Solvatochromic Comparison Method. I. The beta-scale of Solvent Hydrogen-Bond Acceptor (HBA) Basicities, J. Amer. Chem. Soc., (1976) 377-383.

[21] M.J. Kamlet, R.W. Taft, The Solvatochromic Comparison Method. 2. The alpha-scale of Solvent Hydrogen-Bond Donor (HBD) Acidities, J. Amer. Chem. Soc., (1976) 2886-2894.

[22] J. Lu, C. Liotta, C. Eckert, Spectroscopically Probing Microscopic Solvent Properties of Room- Temperature Ionic Liquids with the Addition of Carbon Dioxide, J. Phys. Chem., (2003) 3995-4000.

[23] Y. Migron, Y. Marcus*, Polarity and Hydrogen-bonding Ability of Some Binary Aqueous-Organic Mixtures, J. Chem. Soc., Faraday Trans., 87 (1991) 1339-1343.

[24] M.J. Muldoon, C.M. Gordon*, I.R. Dunkin, Investigations of Solvent-Solute Interactions in Room Temperature Ionic Liquids using Solvatochromic Dyes, RSC, (2001) 433-435.

[25] A. Oehlke, K. Hofmann, S. Spange*, New Aspects on Polarity of 1-alkyl-3-methylimidazolium Salts as Measured by Solvatochromic Probes, New J. Chem., (2006) 533-536.

[26] C. Reichardt, Solvent and Solvent Effects in Organic Chemistry 3ed., Wiley-VCH, Weinheim, Germany, 2003.

[27] T. Yokoyama, R.W. Taft, M.J. Kamlet, The Solvatochromic Comparison Method. 3. Hydrogen Bonding by Some 2-Nitroaniline Derivatives, J. Am. Chem. Soc., 98 (1976) 3233-3237.

[28] C. Reichardt, Solvents and solvent effects in organic chemistry, 3rd ed., Wiley-VCH, Weinheim, Germany, 2003.

[29] P. Nockemann, K. Binnemans, K. Driesen, Purification of imidazolium ionic liquids for spectroscopic applications, Chemical physics letters, 415 (2005) 131-136.

[30] L. Zhang, J. Ji, D. Deng, Z. Shu, X. Chen, Method for preparing acetic acid-type ionic liquid, in, Zhejiang University of Technology, Peop. Rep. China . 2008, pp. 10pp.

3. Thermodynamics

Thermodynamics of Phase Equilibrium

Across the chemical industry, separation remains the most energy- (and consequently, cost-) intensive of process segments. A thorough understanding of thermodynamics is crucial for developing separation processes. Thermodynamic models that are valid over various temperature, pressure and composition conditions become important for the prediction and optimization of chemical processes. Although phase equilibrium modeling is considered a mature subject, it is, in reality, still far from perfect. Ionic liquid (IL) mixtures provide a high level of complexity: few studies for these systems are available in the literature. This chapter overviews the models employed in this study for correlating and predicting the thermodynamics of organic systems encountered in IL synthesis and processing in both CO_2 and gas expanded systems.

3.1. Criteria for Phase Equilibrium

This study presents phase equilibrium data for binary and multi-component systems with CO_2 at high pressures. Phase equilibrium criteria are the basis of thermodynamic computations. The vapor and liquid phases of a pure component are said to be at equilibrium when the temperature, pressure and chemical potentials are equal in both phases. Similarly, in a mixture, phases are said to be in equilibrium, when the pressure, temperature and partial molar Gibbs free energy (chemical potential) of a given specie are equal in all phases in which the specie is present. A mixture with specie *i* at

temperature T and pressure P with chemical potential μ in two phases (I and II) in equilibrium can be expressed as:

$$\mu_i^I = \mu_i^{II}$$
$$T^I = T^{II}$$
$$P^I = P^{II}$$

The chemical potential can be related to the fugacity by

$$\mu_i - \mu_i^o = \mu^o + RT \ln \frac{\bar{f}_i}{\bar{f}_i^o}$$

$$\frac{\bar{f}_i}{y_i P} \to 0 \quad \text{as} \quad P \to 0$$

where the superscript o represents a reference state, and for a component *i* in a mixture of ideal gas, the fugacity is simply its partial pressure (Py_i). At low pressures, all systems approach ideal gas behavior. The equilibrium criteria expression, in terms of fugacity, then becomes:

$$\bar{f}_i^I(T,P) = \bar{f}_i^{II}(T,P)$$

At times, a dimensionless fugacity coefficient $\bar{\varphi}$ is used, as:

$$\bar{\varphi}_i = \frac{\bar{f}_i}{P} \ .$$

Thermodynamics relates mixture compositions to (the harder to obtain) chemical potential. Systems can be accurately described and predicted provided appropriate models are employed.

3.1.1. Vapor-Liquid Equilibrium

The equilibrium criterion for vapor-liquid phase equilibrium is expressed as

$$f_i^L(T,P,x_i) = f_i^V(T,P,y_i)$$

with superscripts L and V indicating the liquid and vapor phases for components *i* in the mixture. At low pressures, the vapor phase can be assumed to be ideal, and an activity coefficient model sufficiently describes the liquid phase. This assumption fails at higher pressures as the non-idealities in the vapor phase must then be accounted for. An equation of state (EoS) is typically used to obtain the component fugacity in the vapor and liquid phases, in terms of temperature, pressure and composition. The relatively simple Peng-Robinson (PR) EoS provides sufficient correlation, and thus is employed throughout this study to predict and correlate experimental data for the binary and multicomponent mixtures encountered in high pressure IL synthesis reactions. The fugacity coefficient of each component *i* in the liquid and vapor phases can be calculated by integrating the following expression using a single equation of state of choice (here, PR EoS):

$$\ln \varphi_i^v = \frac{1}{RT}\int_{\underline{V}^v}^{\infty}\left[\left(\frac{\partial P}{\partial n_i}\right)_{T,\underline{V},n_j} - \frac{RT}{\underline{V}}\right]d\underline{V} - \ln\frac{P\underline{V}^v}{n_T RT}$$

$$\ln \varphi_i^L = \frac{1}{RT}\int_{\underline{V}^L}^{\infty}\left[\left(\frac{\partial P}{\partial n_i}\right)_{T,\underline{V},n_j} - \frac{RT}{\underline{V}}\right]d\underline{V} - \ln\frac{P\underline{V}^L}{n_T RT}$$

Here, the term n_i is the number of moles of component *i*; n_T is the total number of moles in each phase.

3.2. Equations of State (EoS)

Equations of State (EoS) describe chemical systems using mathematical representations of thermodynamic functions at given sets of physical conditions, such as temperature, pressure and molar volume. The simplest form of a thermodynamic EoS is the ideal gas law,

$$PV = nRT$$

which describes a hypothetical gas, assuming:

- collisions between molecules are perfectly elastic,
- molecular interactions between the molecules of the gas are negligible,
- and molecules have no volume.

While the ideal gas EoS is a useful approximation, it is extremely limited. To improve the ideal gas equation approximation for real fluids, several EoS have been developed. A thorough discussion of the different kinds of EoS may be found in the Thermodynamic literature[11]. Two-parameter-cubic EoS, coupled with classical van der waals mixing rules, are the most common modeling tool for VLE of many chemicals, including organic mixtures.

3.2.1. Peng Robinson Equation of State

The reactants and IL product systems in this study were modeled with the Peng Robinson (PR) EoS:

$$P = \frac{RT}{\underline{V} - b_m} - \frac{a_m}{\underline{V}(\underline{V} + b_m) + b_m(\underline{V} - b_m)}$$

where $\underline{V}$ is molar volume, a_m is the mixture attractive parameter and b_m is the mixture co-volume parameter. Typically, in the EoS, fundamental phase stability criteria is used at the critical point to ensure the correct prediction of the critical temperature and pressure, T_c and P_c, respectively: the critical point is where the spinodal stability locus and the VLE binodal co-existence locus meet[1]:

$$\left(\frac{\partial P}{\partial V}\right)_{T_c} = \left(\frac{\partial^2 P}{\partial V^2}\right)_{T_c} = 0$$

For the PR EoS this becomes;

$$a_m(T) = \left(0.4577235\frac{R^2 T_c^2}{P_c}\right)\alpha(T)$$

and

$$b_m = 0.077796\frac{RT_c}{P_c}$$

The term $\alpha(T)$ ensures that the vapor pressure calculated at other temperatures is accurate: it is unity at critical conditions.

$$\alpha(T) = \left[1 + \kappa(1 - \sqrt{T/T_c}\right]^2$$

For hydrocarbons and organic gases, κ can be expressed as

$$\kappa = 0.37464 + 1.54226\omega - 0.26992\omega^2$$

The Pitzer acentric factor ω is defined as :

$$\omega = -1.0 - \log_{10}\left[\frac{P^{vap}(T_r = 0.7)}{P_c}\right]$$

$$T_r = T / T_c$$

Once T_c, P_c and ω are known, the two-parameter (a,b) EoS can be computed and used to completely predict the equilibrium of a given system. For a better VLE description, researchers have extended the $\alpha(T)$ term for non-hydrocarbon systems[2, 3], an example of which is the PR Stryjek and Vera (PRSV) equation.[3]

3.3. Mixing Rules

Mixing rules furnish the EoS with the compositional dependencies for predicting phase behaviors of mixtures. The mixture parameters for the van der waal 2-parameter mixing rule (vdW2) are:

$$a_m = \sum_i \sum_j x_i x_j a_{ij} \qquad a_{ij} = (1 - k_{ij}) \sqrt{a_{ii} a_{jj}}$$

$$b_m = \sum_i \sum_j x_i x_j b_{ij} \qquad b_{ij} = (1 - l_{ij}) \frac{b_{ii} + b_{jj}}{2}$$

Binary interaction parameters k_{ij} and l_{ij} of the systems are obtained when EoS predictions are fitted to experimentally obtained phase equilibrium or volumetric data.

3.4. Estimation of Equation of State Parameters:

While many pure-component critical properties for the PR-EoS parameters are available in the literature, others remain absent. Such unavailable parameters, especially for IL systems, can be estimated using group-contribution methods such as the Joback group-contribution method [5]. These methods assign values for weighting sub-constituents, or the ‘groups’ of a molecule, to obtain the overall critical properties of the chemical. The

method estimates critical temperature using boiling point data: in this study, the experimental normal boiling point is used in the Joback method to predict the critical properties of 1-methylimidazole [6] and 1-bromohexane [7]. As the IL under consideration does not have a known boiling point, the Joback method is used to compute all of its properties. The acentric factors for 1-bromohexane and 1-methylimidazole are computed from the predicted critical properties and experimental vapor pressure (normal and reduced boiling points) using the standard expression [8]:

$$\omega = -\log P_r^{sat}(T_r = 0.7) - 1$$

where the subscript *r* indicates the property has been normalized by the critical point value. However, for the IL [HMIm][Br], no vapor pressure data is available, and the Lee-Kesler relationship is used in calculating the acentric factor[9]:

$$\omega = \frac{\alpha}{\beta}$$

$$\alpha = -\ln\frac{P_c}{P(atm)} - 5.92714 + \frac{6.09648}{\theta} + 1.28862\ln\theta - 0.169347\theta^6$$

$$\beta = 15.2518 - \frac{15.6875}{\theta} - 13.4721\ln\theta + 0.43577\theta^6$$

where $\theta = \frac{T_b}{T_c}$.

3.5. High Pressure Phase Behavior

Phase diagrams are based on solutions to phase equilibrium equations. The phase behavior of binary systems varies with temperature and pressure. To understand phase diagrams, the Gibbs phase rule comes into play, expressed simply as

$$F = m + 2 - \pi$$

where F is the degree of freedom, m is number of components and π is the number of phases. At the critical point, physical properties of the phases in equilibrium become identical. Thus, per the Gibbs Phase Rule, in imposing an additional π -1 reduction to the degree of freedom, a three component system may have as many as 5 phases. Van Konynenburg and Scott[10] present a general classification for the behavior of most binary high-pressure systems (Figure 3. 1). Most binary systems can be classified using six phase types, with a variety of fluid phase behavior near the critical points which can be sufficiently described using van der Waals EoS and mixing rules. An upper critical solution temperature (UCST) is the point at which a two phase system (heterogeneous) becomes a one phase system (homogeneous) when temperature is raised, while a lower critical solution temperature (LCST) is the point at which a homogeneous system becomes a two phase system when the temperature is increased. On the T-x coexistence curve, the LCST occurs at T_{min}, while the UCST occurs at T_{max}.

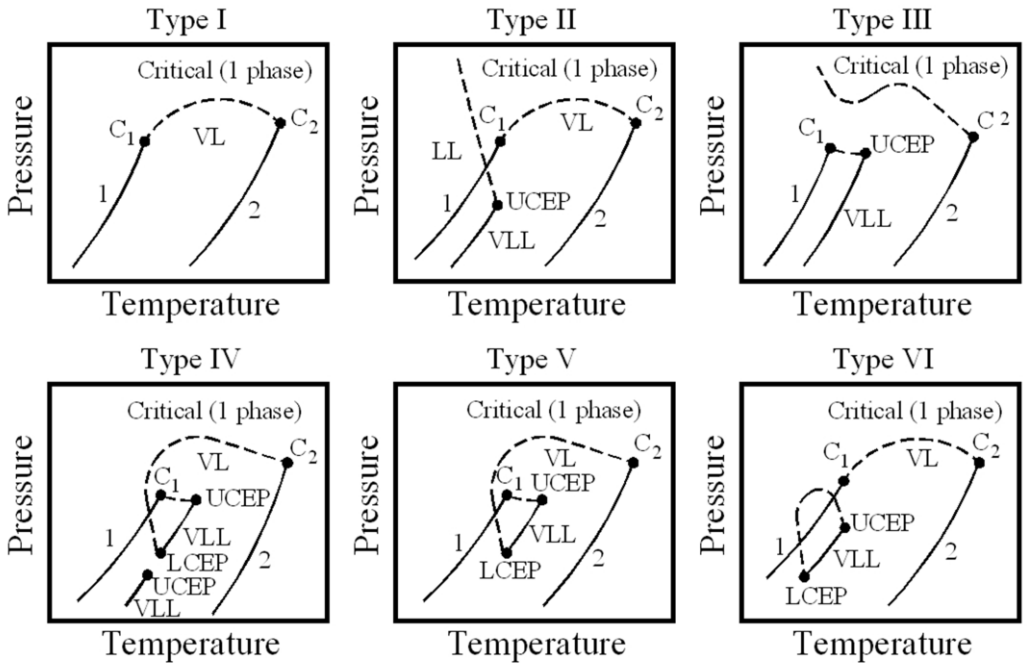

Figure 3. 1 Six types of phase behavior for binary systems [10]

In Type I phase behavior (the simplest classification), there is one critical line that begins and ends at the pure component's critical points, forming a critical locus. This type behavior is common with components having similar chemical properties. In less ideal mixture systems, regions of immiscibility are more likely to occur, resulting in Types II-VI phase behavior. Type II phase behavior has two critical lines: one critical locus, as in a Type I system, plus another critical line occurring as an upper critical end point (UCEP), which is a transition point when the two liquid layers become miscible with each other, resulting in VLE. Type III phase behavior has two separate critical loci; one joining the critical point of component 1, C_1, to the UCEP, and a second which is connected to the

critical point of component 2 (the less volatile component) and rises with pressure. Type IV and V phase behavior are quite similar to each other. Both Type IV and V feature a critical locus which spans between the critical point of component one to a UCEP, and a second locus which connects the pure critical point for component two to a lower critical endpoint (LCEP). The LCEP is similar to an UCEP, in that the two liquid phases become miscible with each other, resulting in VLE. A Type VI situation has a third critical line (another region of immiscibility) below the LCEP, with a corresponding UCEP.

3.5.1. Stability Analysis

Multiple roots may result from evaluating equifugacity equations: not all are physical. This is because fugacity equality is not a sufficient condition for phase equilibria. A search for the global minimum of the Gibbs free energy, often implemented in traditional algorithms, is used to evaluate phase stability. The Gibbs free energy minimization condition is thermodynamically sufficient to test for system stability in a given thermodynamic state. Towards this end, derivative methods[11] and tangent plane distance analysis[12, 13] are most commonly used. In tangent plane analysis, points *(z)* at a given temperature and pressure are analyzed by the distance between the Gibbs free energy of mixing and the plane tangent to the Gibbs surface at any composition.

$$\left(\frac{\partial \tilde{g}_m}{\partial x_i} - \frac{\partial \tilde{g}_m}{\partial x_n}\right) - \left(\frac{\partial \tilde{g}_m}{\partial x_i} - \frac{\partial \tilde{g}_m}{\partial x_n}\right)_{x=z} = 0$$

$$D(x,z) = \tilde{g}_m(x) - \tilde{g}_m(z) - \sum_{i=1}^{n}\left(\frac{\partial \tilde{g}_m}{\partial x_n}\right)_{x=z}(x_i - z_i)$$

If the tangent distance *D* is negative for any value of x, the Gibbs energy surface is below the tangent plane, and thus the phase of composition z being tested is unstable. The system is stable if the value of *D* is never negative in the composition. Using the PR EoS, the dimensionless molar Gibbs energy of mixing at a given pressure and temperature is:

$$\tilde{g}_m(x) = \frac{P\underline{V}}{RT} + \ln\frac{RT}{\underline{V} - b_m} + \frac{a_m}{b_m \times 2\sqrt{2} \times RT}\ln\left(\frac{\underline{V} + \left(1-\sqrt{2}\right)b_m}{\underline{V} + \left(1+\sqrt{2}\right)b_m}\right) + \sum_{i=1}^{n} x_i \ln x_i - \sum_{i=1}^{n} x_i \tilde{g}_i^0$$

3.6. Computation; PE2000

The correlation, regression and prediction of the high-pressure equilibria are implemented in the PE2000 modeling software, developed by Pfohl *et al.*[14] Several studies have employed this software package as a tool to correlate and predict phase equilibria. PE2000 gives the user the flexibility of using any of its 40 different equations of state (EoS), coupled with as many as seven (7) different mixing rules for correlating and predicting phase equilibria. PE2000 optimizes the binary interaction parameters by minimizing one of four objective functions, namely absolute, absolute square, relative and relative square. For parameter fitting, PE2000 utilizes the Simplex-Nelder-Mead algorithm[15] for regression. The Simplex-Nelder-Mead algorithm is a direct search algorithm that requires initial guesses for the interaction parameters and locates the optimum based on the concept of a simplex. A simplex is a polytope of *N* + 1 vertices in *N* dimensions (a triangle in this case). The approach starts with an initial simplex: for every iteration, the technique generates a new test position by extrapolating the behavior of the objective function measured at each test point. The algorithm then chooses whether to replace the worst point with the new test point - iteration continues until the diameter

of the simplex is less than the set threshold. As such, the Nelder-Mead method is a local search algorithm that does not guarantee the resulting optimum to be global, as the result is dependent on the initial guess. Various initial guesses are utilized to avoid local minima in the regression. In this work, the deviation calculated by PE2000 is based on the mole fractions of the coexisting phases at certain temperature and pressure. The objective function chosen for the systems in this study is the average absolute relative deviation (%AARD) of the liquid mole fractions (x_i):

$$\%AARD = \frac{100}{n}\sum_{i=1}^{n}\left|\frac{x_i^{\exp} - x_i^{calculated}}{x_i^{\exp}}\right|$$

The resulting k_{ij} and l_{ij} parameters for systems modeled are presented in their respective sections.

References

[1] J. Tester, W.;Modell, Michael., Thermodynamics and its Applications, 3rd Edition ed., Prentic-Hall, Inc, Upper Saddle River, New Jersey, 1997.

[2] P.M. Mathias, T.W. Copeman, Extension of the Peng-Robinson equation of state to complex mixtures: evaluation of the various forms of the local composition concept, Fluid Phase Equilibria, 13 (1983) 91-108.

[3] R. Stryjek, J. Vera, PRSV: An improved peng—Robinson equation of state for pure compounds and mixtures, The Canadian journal of chemical engineering, 64 (1986) 323-333.

[4] S.I. Orbey Hasan; Sandler, Modelling vapor-liquid equilibria:cubic equation of state and their mixing rules, Cambridge University Press, 1998.

[5] K.G. Joback, R.C. Reid, Estimation of pure-component properties from group-contributions, Chemical Engineering Communications (Print), 57 (1987) 233-243.

[6] Aldrich Catalog: Handbook of Fine Chemicals, Aldrich Chemical, 2008.

[7] J. Dykyj, S. J, R.C. Wilhoit, M. Frenkel, K.R. Hall, Landolt-Börnstein Numerical Data and Functional Relationships in Science and Technology: New Series, in: K.R. Hall (Ed.) Vapor Pressure of Chemicals, Springer, Berlin, 1999.

[8] R.C. Reid, J.M. Prausnitz, B.E. Poling, The properties of gas and liquids, MacGraw-Hill, New York, (1987).

[9] B.I. Lee, M.G. Kesler, A generalized thermodynamic correlation based on three-parameter corresponding states, AIChE Journal, 21 (1975).

[10] P.H. Van-Konynenburg, R.L. Scott, Critical lines and phase equilibriums in binary Van der Waals mixtures, Philos. Trans. R. Soc., 298 (1980) 495-540.

[11] J.M. Prausnitz, R.N. Lichtenthaler, E.G. de Azevedo, Molecular thermodynamics of fluid-phase equilibria, Prentice Hall, 1998.

[12] L.E. Baker, A.C. Pierce, K.D. Luks, Gibbs energy analysis of phase equilibria, Old SPE Journal, 22 (1982) 731-742.

[13] M.L. Michelsen, The isothermal flash problem. Part I. Stability, Fluid Phase Equilibria, 9 (1982) 1-19.

[14] O. Pfohl, S. Petkov, G. Brunner, PE 2000 A Powerful Tool to Correlate Phase Equilibria, Herbert Utz Verlag, Munich, 2000.

[15] J.A. Nelder, R. Mead, A simplex method for function minimization, Computer J., 7 (1965) 308.

4. Understanding Thermodynamics and Transport Properties in IL Synthesis Systems

4.1 Introduction

An understanding of phase equilibrium is essential in determining the kinetics and reactor/process engineering for ionic liquid (IL) synthesis systems. Figure 4. 1 presents chemical structures of chemicals encountered in this chapter. Additionally phase behavior studies of CO_2 expanded systems add insight necessary to design or propose energy efficient separation, i.e. CO_2 extraction and flash separations discussed in Chapter 7. To comprehend the process phenomena occurring in IL high pressure systems, vapor-liquid equilibrium (VLE) data and phase behavior data were experimentally obtained (Chapter 2 presents methods) and correlated with conventional thermodynamic models (See Chapter 3). VLE data was also needed for computing initial molarity in order to quantify the reaction rate constant. Volume expansion data are used to compute molarity necessary for the computation of *k* constants obtained in Chapter 6 and for reactor design studies in Chapter 7. Further, VLE data and phase behavior studies shed light on optimal composition, pressure and temperature for IL synthesis and product recovery.

This chapter presents physico-chemical properties (viscosity, density, thermal conductivity, and thermal diffusivity) for high pressure DMSO/CO_2 mixture system and ambient pressure physical property data for different solvent (acetone) ratios to product IL [HMIm][Br] are also presented here.

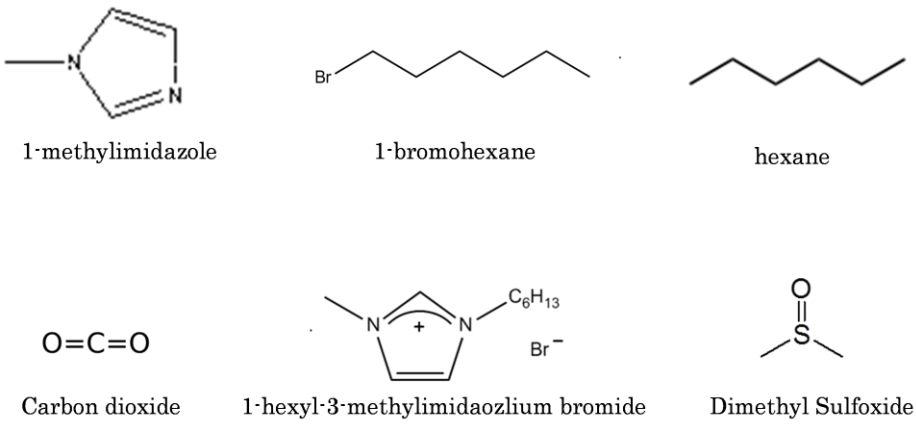

Figure 4. 1 Structure of chemicals studied.

4.2 Thermodynamic Data-Compressed CO_2 with ILs, N-heterocycles, haloalkanes, and Solvents

4.2.1 Literature Survey of CO_2 with ILs, N-heterocycles, and haloalkanes

Few VLE studies of CO_2 with either N-containing heterocycles or haloalkanes exist in the literature. Brennecke and coworkers[2] and Chen *et al.*,[4] published the only known VLE study of 1-methylimidazole and CO_2 at isotherms 293.15, 309.75 and 323.15 K, and to pressures of 15 bar to 85 bar. The CO_2/pyridine system has been studied by two groups.[5, 6] Brunner[5] measured vapor-liquid and liquid-liquid phase equilibria in the CO_2/pyridine system between 304.21 K and 620.2 K, at pressures from 7.38 MPa to 19.14 MPa. Studies have shown that primary amines, as well as secondary amines, may react with CO_2 in a reversible reaction to form carbamic acids. [7-9] With approximately

10 bar of CO_2, 1-methylimidazole, a tertiary amine (unsaturated N-heterocycle) used for this study, had no observed reaction with CO_2 within NMR sensitivity. [10] Thamanavat *et al.*,[11] recently observed both VLE and liquid–liquid equilibrium (LLE) for the CO_2/pyrrole system at temperatures between 313 K and 333 K, and pressures between 8.4 MPa and 15.1 MPa. CO_2 solubility in alkylimidazolium-based ILs has received much of attention of late [2, 12-16]. However, none of these ILs has a halide anion, and thus, no equilibrium data exists for those ILs produced in the initial alkylation synthesis step.

4.2.2 VLE Data

The Peng Robinson equation of state (PR EoS) was employed to model the reactants and IL product systems in this study. The binary interaction parameters k_{ij} and l_{ij} of these systems were fitted to the data, and are summarized in Table 4. 2. The pure component critical properties for the PR-EoS parameters were only available for CO_2 and DMSO. The critical properties for 1-methylimidazole, 1-bromohexane and [HMIm][Br] were estimated using the Joback group contribution method. [17] The Joback method can either compute T_b or can use an experimental T_b to compute the *Tc, Pc,* The experimental normal boiling points were used in the Joback method to predict the critical properties of 1-methylimidazole [18] and 1-bromohexane. [19] As the IL [HMIm][Br] does not have a known boiling point, the Joback method was also used to compute its critical properties. Using the standard expression [20], the acentric factors for 1-bromohexane and 1-methylimidazole were computed from the predicted critical properties and experimental vapor pressure (from a Clausius-Clapeyron extrapolation using the normal and reduced

boiling points). For [HMIm][Br], however, no vapor pressure data is available, and the Lee-Kesler relationship was used for calculating the acentric factor.[21] A summary of the critical and equation of state parameters are found in Table 4. 1.

Table 4. 1. Critical Properties of Pure Components.

Substance	*Tc* [K]	*Pc* [bar]	*Tb* [K]	*ω*
1-bromohexane	624.88	33.61	428.45[a]	0.346[b]
1-methylimidazole	742.38	55.61	471.15[c]	0.279[d]
1-Methyl-3-hexyl-imidazolium bromide	841.07	26.68	608.80	0.607
DMSO[e]	729.00	56.50	464.00	0.281
Carbon dioxide	304.10	73.80	195.00	0.225

[a] ref [19]. [b] were computed from vapor pressure data from ref [19]. [c] obtained from ref [18]; [d] computed from vapor pressure data from ref [18], [e] was obtained from NIST database in ASPEN PLUS

Table 4. 2. Summary of binary interaction parameters and modeling fit.

System	T [K]	k_{ij}	l_{ij}	% AARD
1-bromohexane/CO_2	313.15	0.058	-0.026	0.66
	333.15	0.060	-0.014	5.28
1-methylimidazole/CO_2	313.15	0.036	-0.014	0.43
	333.15	0.058	0.002	2.47
DMSO/CO_2	313.15	0.045	-0.064	1.64
	333.15	0.040	-0.069	1.90
[HMim][Br]/CO_2	313.15	0.045	-0.064	6.36
	333.15	0.040	-0.069	1.50
1:1 Mixture:1-bromohexane (3),	313.15	[a]	[a]	5.53
1-methylimidazole (2)-CO_2 (1)	333.15	[a]	[a]	4.67

[a] parameters above *with* $k_{23} = l_{23} = 0$

4.2.3 Global Phase Behavior and Equilibria of CO_2/1-Methyimidazole

The global phase behavior of 1-methylimidazole and CO_2 was measured experimentally between 275.15 K and 333.15 K and 1 to 160 bars and is listed in Table 4. 3. Figure 4. 2 illustrates that a vapor-liquid-liquid (VLLE) exists well beyond the critical point of pure

CO_2. Chapter 2 overviews the thermodynamics and phase behavior theories presented in this section. This VLLE region exists between the lower critical end point (LCEP), at 304.05 K and 68.5 bar, and the upper critical end point (UCEP), at 313.95 K and 80.6 bar. The mixture critical points connect the LCEP to the critical point of pure 1-methylimidazole, but were only measured to 313.15 K. This is indicative of type IV or V phase behavior, according to Scott and van Konynenburg's classification scheme.[22] A second upper critical endpoint (UCEP) and region of VLLE and LLE was observed between 275.15 K and 304.05 K, and may indicate a Type V system. However, as a Type IV system also has another UCEP at lower temperatures, further cryogenic measurements at much lower temperatures would be needed to verify the Type V behavior.

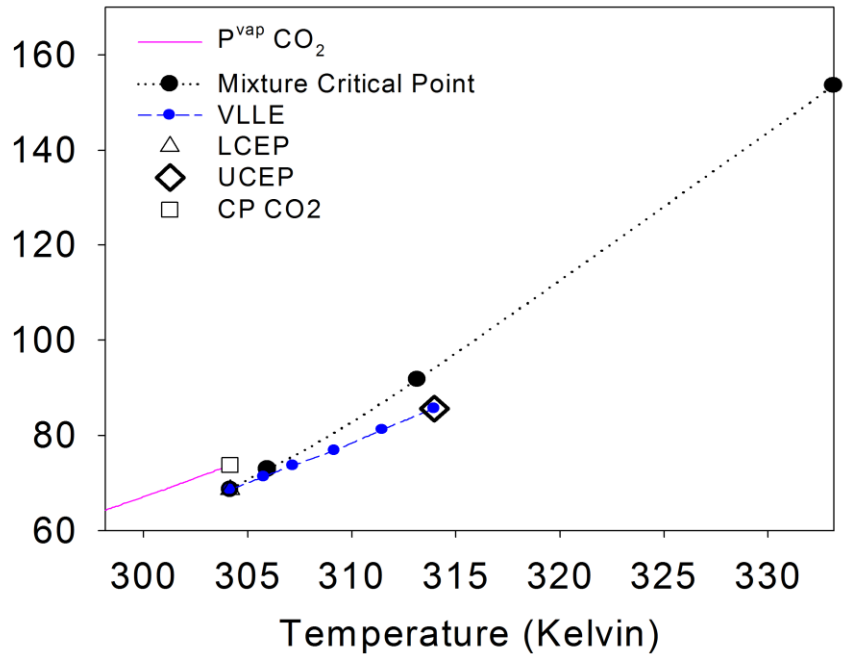

Figure 4. 2 Global Phase behavior for 1-methylimidazole/CO_2 Binary System. Lines are smoothed data.[3]

Pyrrole is structurally similar to imidazole, as it is an unsaturated 5-membered N-heterocycle, but with only one nitrogen. For the system of pyrrole/CO_2, Thamanavat *et al.*, [11] observed VLE, VLLE, LLE, and mixture critical points. They were able to predict the global phase behavior over a wide range of conditions using the Patel-Teja equation of state model, with parameters fitted to their data. They concluded that the pyrrole/CO_2 system is a Type IV system according to the classification of Scott and van Konynenburg [22], since a second UCEP was predicted at very low temperatures.

Table 4. 3 Global Phase behavior for 1-methylimidazole/CO_2 Binary System.

Temperature [K]	Pressure [bar]	# of Phases
304.05	68.48	LCEP
305.75	71.30	3
307.15	73.65	3
309.15	76.75	3
311.45	81.03	3
313.95	85.64	UCEP

Mixture Critical Points

Temperature [K]	Pressure [bar]
306.05	72.89
309.25	84.61
313.15	91.77
333.15	153.52

The vapor-liquid equilibrium (VLE) data for 1-methylimidazole/CO_2 system was measured at 313.15 K and 333.15 K and listed in Table 4. 4. At 313.15 K, the system was just below the upper critical endpoint (UCEP). For our particular loading of CO_2 to 1-methyl-imidazole, VLE exists until a pressure of 82.97 bar was reached, after which there was a phase transition to vapor-liquid-liquid equilibrium (VLLE) and then liquid-liquid equilibrium (liquid-fluid), as shown in Figure 4. 3. The equilibrium terminated in a mixture critical point at 91.77 bar. Technically, a region of VLE exists above 82.97 bar at very high loadings of CO_2 and would end in another mixture critical point. However, this region was not experimentally measured. The system at 333.15 K is above the UCEP and thus VLE exists until the mixture critical point at 153.52 bar. The system pyridine (6-membered N-hetercycle)/CO_2 was measured between 304.2 K and 620.2 K and Type I or II behavior was reported.[5]

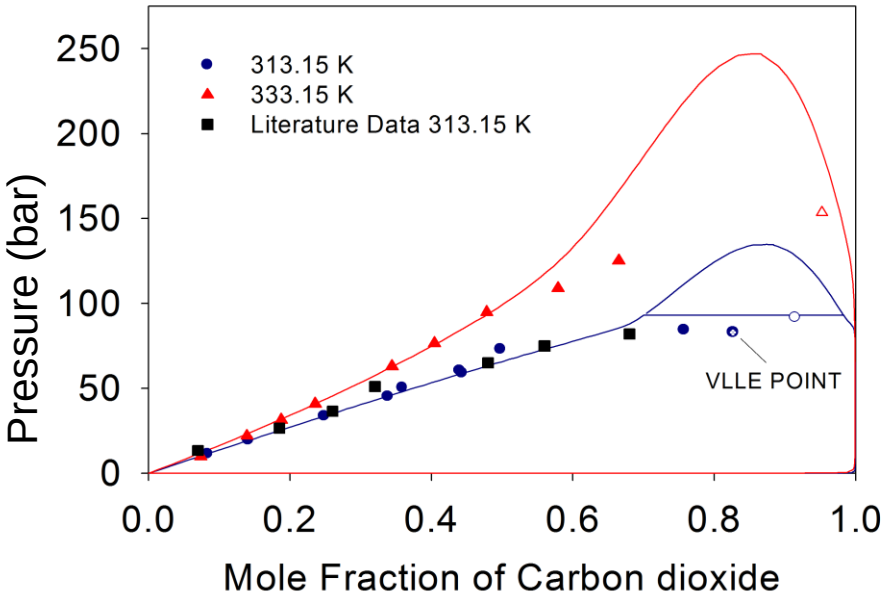

Figure 4. 3 CO_2 Solubility in 1- methylimidazole at 313.15 K (Experimental and Literature data [[2]]) and 333.15 K. Lines in this figure and for the rest of the figures are PR-vdW2 model.

Using estimated equation of state (critical) properties, the Peng-Robinson equation of state and the van der Waals 2-parameter mixing rules were used to correlate the 1-methylimidazole/CO_2 system. As shown in Figure 4. 3, the model satisfactorily correlates the bubble point data below approximately 90 bar for both isotherms; the binary interaction parameters and model fit (%AARD) are found in Table 4. 2. These parameters were fit solely to the VLE data. However at 313.15 K, which has a region of VLLE, LLE, and a mixture critical point, the model predicted the VLLE pressure at 93 bar and the lower liquid composition at 0.70, which were approximately 12.09 % higher and 15.33 % lower, respectively, than the experimental data. In addition, the predicted mixture critical

point was estimated at 134.66 bar and 0.8737 mole fraction, which were 46.73 % higher and 4.45 % lower, respectively, than the experimental data. Poor EoS mixture critical point predictions using just VLE data has been reported by other researchers,[23] especially for highly polar substances.

4.2.4 Phase Equilibrium of CO_2/1-bromohexane

The VLE data for the 1-bromohexane/CO_2 system at 313.15 K and 333.15 K is listed in Table 4. 4 This system does not have any known regions of liquid-liquid immiscibility (to ~2°C) or VLLE and probably represents a Type II system according to Scott and van Konynenburg.[22] However, further studies in cryogenic conditions would be necessary to confirm this hypothesis. From Figure 4. 4, at 313.15 K, vapor-liquid equilibrium exists until the mixture critical point at 84.90 bar and 0.968 mole fraction CO_2.

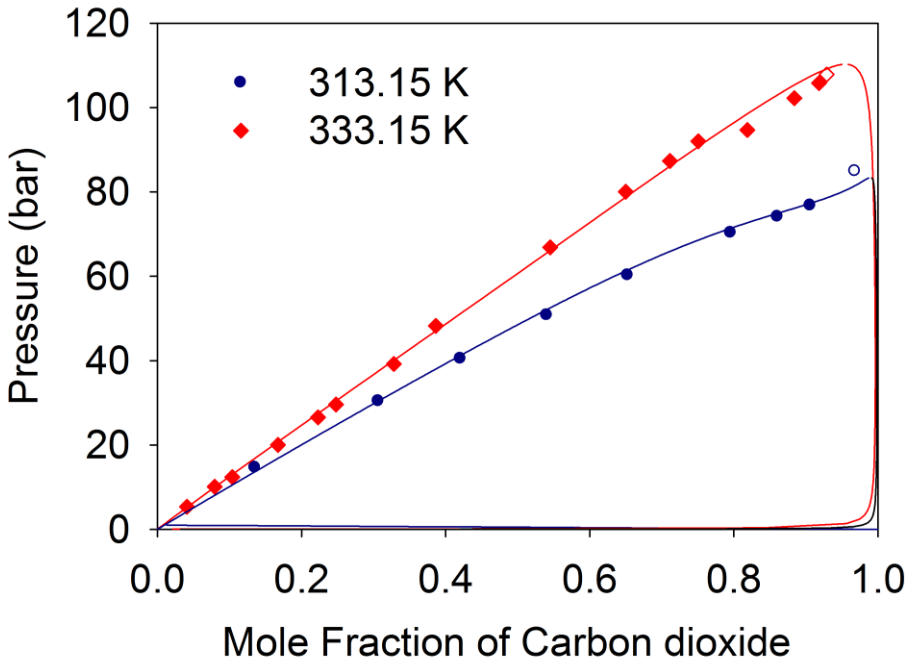

Figure 4. 4 CO_2 Solubility in 1-bromohexane at 313.15 K and 333.15 K.

At 333.15 K, VLE exists until the mixture critical point at 107.81 bar and 0.929 mole fraction CO_2. The only other phase equilibrium study of haloalkanes with CO_2 known to the author is with the CO_2/chlorobutane system studied by Wang *et al.*[24] The system of hexane/CO_2 has been measured by Ohgaki and Katayama [1] at 313.15 K and is plotted in Figure 4. 5. Carbon dioxide is more soluble in n-hexane compared to 1-bromohexane. At 60 bar, the mole fraction of CO_2 in n-hexane was measured at 0.80 mole fraction, while 1-bromohexane was lower at 0.65 mole fraction of CO_2. The Peng-Robinson equation of state and the van der waals 2-parameter mixing rules were used to correlate the 1-bromohexane/CO_2 system using estimated equation of state (critical) properties. As shown in Figure 4. 4 the model performed very well through both the bubble point data and, surprisingly, the mixture critical points. The predicted mixture critical points were

approximately at 83.3 bar and 0.987 mole fraction (compared to 84.9 bar and 0.968 mole fraction CO_2 experimentally) at 313.15 K, and at 110.2 bar and 0.950 mole fraction (compared to 107.8 bar and 0.929 mole fraction CO_2 experimentally) at 333.15 K. The binary interaction parameters and model fit (%AARD) are listed in Table 4. 2. [25]

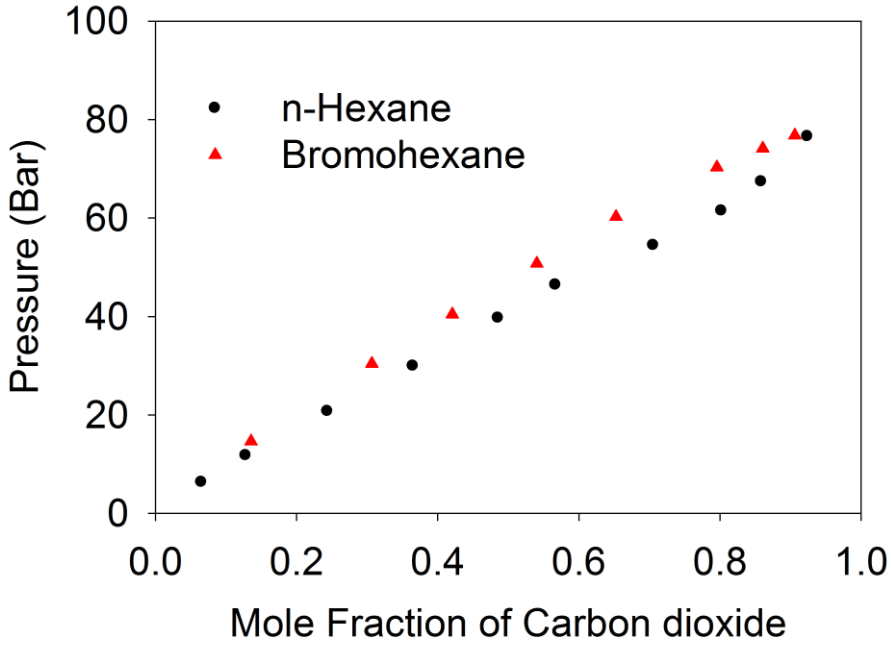

Figure 4. 5 CO_2 Solubility in n-hexane [1] and 1-bromohexane at 313.15 K

4.2.5 Equilibrium of CO_2/DMSO

VLE data for DMSO/CO_2 system at 313.15 K and 333.15 K was measured and is also listed in Table 4. 4. Dimethyl sulfoxide (DMSO) is a powerful polar aprotic solvent that

dissolves both polar and nonpolar compounds. Organic compounds including proteins and biodegradable polymers are highly soluble in DMSO, making the solvent very attractive for use in the pharmaceutical sector. It is commonly employed in supercritical particle generation processes such as Supercritical Anti-Solvent (SAS) processes. Gas-expanded DMSO systems are uniquely advantageous for IL synthesis reactions; the aprotic solvent features a high reaction constant and CO_2 tunability, which can be leveraged for separation. However, in order to optimize or design such processes, VLE and physical properties of binary and ternary mixtures of DMSO and CO_2 must be understood. Although VLE data for the binary CO_2/DMSO system is published in the literature, the results are inconsistent; this is not surprising, as DMSO is notorious for water contamination, which is known to affect VLE data. Water content for the sample used in this study was measured at 150 ppm using the Karl Fisher, methods descried in chapter 2.[26] Peter and co-workers [27, 28] measured phase equilibrium data for the DMSO/CO_2 binary system and the ternary CO_2/DMSO/water system, between 280 and 370K and at pressures up to 15MP. Andreatta *et al*.,[27] observed partial liquid miscibility in the DMSO/ CO_2 system at high CO_2 concentrations. Although not confirmed, they predicted a Type IV fluid phase behavior for CO_2/DMSO. Gonazalez *et al.*,[25] presents experimental data for CO_2/DMSO at 309.44 K, 314.49 K, 321.28 K and 328.94 K. The PR EOS and the van der waals 2-parameter mixing rules were sufficient to correlate the DMSO/CO_2 system using available critical property data obtained from the literature (shown in Table 4. 1). Resulting data from modeling are shown in Figure 4. 6 and binary parameters presented in Table 4. 2. DMSO behaves as a typical organic system, with high amounts of CO_2 solubilizing in the liquid at higher pressures. The

observed critical points for 313.15 K and 333.15 K are 85.74 bar (at x_{co2}, 0.9463) and 141.6 bar (at x_{co2}, 0.9367), respectively.

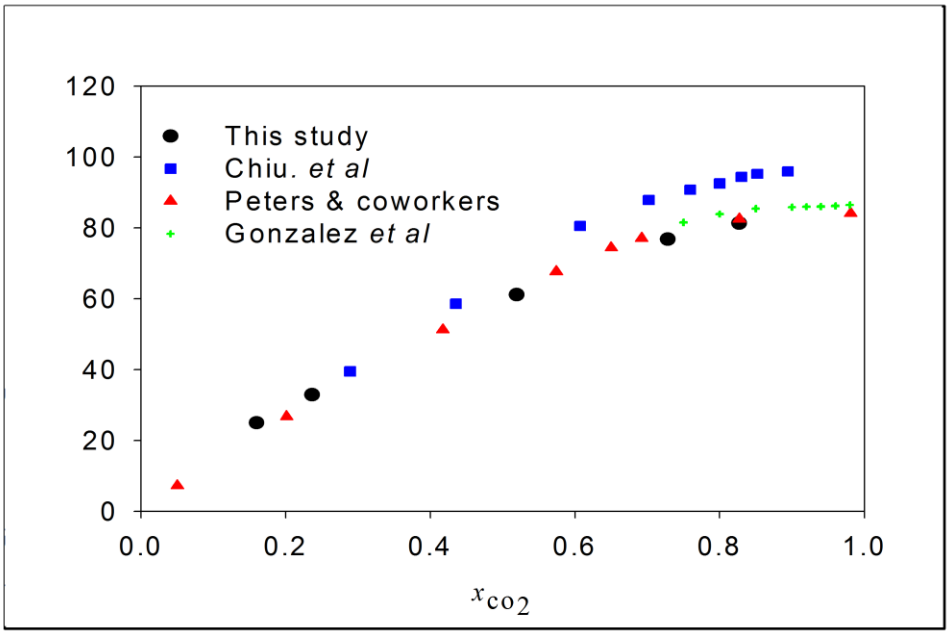

Figure 4. 6 Bubble point for the binary system of CO_2/DMSO at 40C and 60C with comparison with the literature.

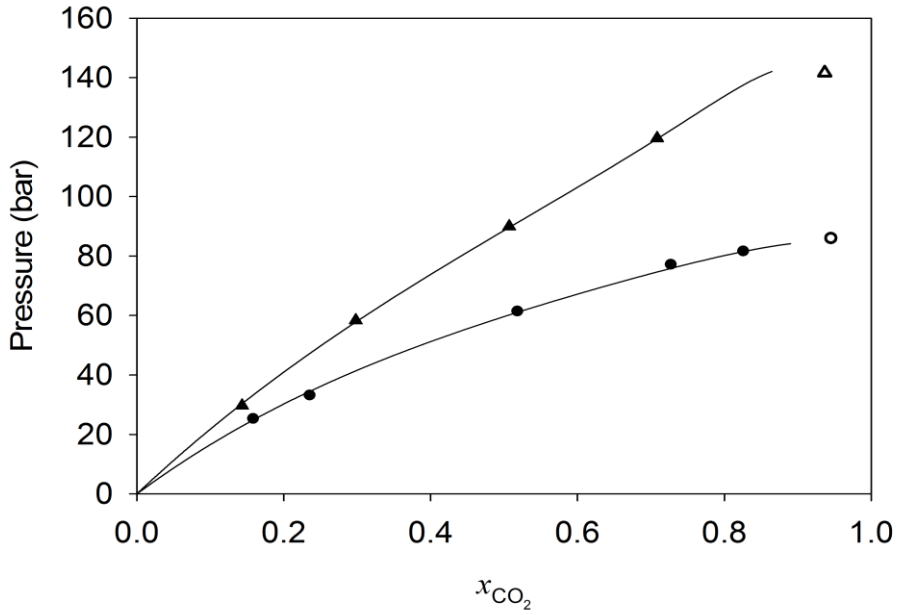

Figure 4. 7 VLE data for the binary system of CO_2/DMSO at 40C and 60C (---) Model data (Δ) 60° C (o) 40° C

Table 4. 4 Vapor liquid equilibrium experimental data and mixture critical points of the ionic liquid synthesis systems with CO_2.

T [K]	*P [bar]*	x_{CO2}	$\Delta V/V_0$	$\underline{V}^L$ *[cm³/mol]*
1-bromohexane/CO_2				
313.15				
	14.64	0.1355 ± 0.0031	0.049 ± 0.001	135.25
	30.41	0.3067 ± 0.0035	0.143 ± 0.001	118.27
	40.43	0.4206 ± 0.0033	0.241 ± 0.002	107.27
	50.76	0.5405 ± 0.0027	0.374 ± 0.002	94.18
	60.24	0.6527 ± 0.0019	0.625 ± 0.002	84.19
	70.30	0.7957 ± 0.0008	1.366 ± 0.002	72.06
	74.12	0.8607 ± 0.0004	2.259 ± 0.003	67.70
	76.79	0.9062 ± 0.0002	3.722 ± 0.005	66.07
	84.90[cpe]	0.9681 ± 0.0002		62.49
333.15				
	5.37	0.0411 ± 0.0008	0.0104 ± 0.0005e	148.71
	10.10	0.0794 ± 0.0009	0.0254 ± 0.0005	144.88
	12.37	0.1038 ± 0.0034	0.0149 ± 0.0014	146.44
	20.00	0.1673 ± 0.0013	0.0619 ± 0.0005	135.72
	26.52	0.2230 ± 0.0046	0.0677 ± 0.0014	133.57
	29.61	0.2480 ± 0.0016	0.1024 ± 0.0006	127.24
	39.20	0.3283 ± 0.0017	0.1517 ± 0.0006	118.73
	48.23	0.3864 ± 0.0057	0.1938 ± 0.0015	117.94
	66.85	0.5451 ± 0.0016	0.3929 ± 0.0006	97.26
	80.03	0.6501 ± 0.0013	0.6241 ± 0.0007	87.21
	87.36	0.7113 ± 0.0003	0.6557 ± 0.0019	97.66
	91.98	0.7508 ± 0.0009	1.0433 ± 0.0009	78.17
	107.81[cp]	0.9289 ± 0.0001		70.69
1-methylimidazole/CO_2				
313.15				
	11.44	0.0837 ± 0.0022	0.001 ± 0.002	82.14
	19.55	0.1413 ± 0.0028	0.029 ± 0.002	79.07
	33.68	0.2484 ± 0.0035	0.097 ± 0.002	73.80
	45.07	0.3385 ± 0.0038	0.182 ± 0.002	70.47
	59.04e	0.4431 ± 0.0042	0.323 ± 0.002	69.97
	72.96	0.4977 ± 0.0096	0.567 ± 0.002	62.49
	82.97[vll]	0.8267 ± 0.0006	2.865 ± 0.004	53.59[e]
	91.77[cp]	0.9144 ± 0.0003	[e]	59.62
333.15				
	9.90	0.0737 ± 0.0017	0.001 ± 0.001	81.14
	22.02	0.1391 ± 0.0024	0.026 ± 0.001	77.34
	31.43	0.1878 ± 0.0030	0.062 ± 0.001	75.50
	40.96	0.2357 ± 0.0035	0.098 ± 0.001	73.46
	63.07	0.3441 ± 0.0046	0.196 ± 0.001	68.65
	76.56	0.4044 ± 0.0056	0.277 ± 0.002	66.58
	94.79	0.4783 ± 0.0085	0.418 ± 0.002	64.73
	108.99	0.5791 ± 0.0065	0.558 ± 0.002	57.38
	125.13	0.6648 ± 0.0048	0.633 ± 0.002	55.54
	153.52cp	0.9521 ± 0.0003		50.27

Table 4. 4 (Cont'd) Vapor liquid equilibrium experimental data and mixture critical points of the ionic liquid synthesis systems with CO_2.

T [K]	*P [bar]*	x_{CO2}	$\Delta V/V_0$	$\underline{V}^L$ *[cm^3/mol]*
[HMIm][Br]/CO_2				
313.15				
	30.90	0.135 ± 0.008	0.016 ± 0.001	229.74
	53.80	0.201 ± 0.013	0.052 ± 0.001	219.57
	75.01	0.285 ± 0.017	0.069 ± 0.001	199.56
	90.05	0.356 ± 0.022	0.077 ± 0.001	181.22
	128.00	0.489 ± 0.028	0.271 ± 0.001	169.78
333.15				
	31.32	0.085 ± 0.007	0.0255 ± 0.0009	229.33
	50.84	0.132 ± 0.011	0.0564 ± 0.0009	224.20
	72.24	0.206 ± 0.016	0.0705 ± 0.0009	207.68
	93.45	0.288 ± 0.030	0.0841 ± 0.0009	188.74
	128.70	0.393 ± 0.031	0.0970 ± 0.0009	162.73
	148.91	0.468 ± 0.026	0.1174 ± 0.0009	145.34
DMSO/CO_2				
313.15	25.08	0.1595 ± 0.0067	0.433 ±0.005	74.97
	32.96	0.2365 ±0.0073	0.516 ±0.005	72.06
	61.19	0.5194 ±0.0079	1.140 ±0.007	64.02
	76.90	0.7283 ±0.0085	2.451 ±0.010	58.38
	81.39	0.8269 ±0.0035	4.144 ±0.015	55.43
	85.74^{cp}	0.9463 ±0.0003		61.69
333.15	29.70	0.1433±0.0069	0.237±0.004	57.00
	58.37	0.2981±0.0134	0.384±0.004	65.34
	89.94	0.5072±0.0272	0.898±0.005	62.91
	119.62	0.7084±0.0090	1.922±0.009	45.85
	1441.6^{cp}	0.9367±0.0004		59.88
1:1:5 Reactants (1-bromohexane and 1-methylimidazole)& DMSO/CO_2				
313.15	36.42	0.3029±0.0068	0..307±0.004	68.29
	55.87	0.5141±0.0062	0.710±0.005	62.28
	64.81	0.6499±0.0591	1.059±0.005	54.02
	83.24^{cp}	0.9447±0.0003		63.02
2:5 [HMim][Br]&DMSO/CO_2				
313.15	30.26	0.0944±0.0123	0.027±0.003	94.58
	61.52	0.2587±0.0254	0.221±0.004	92.09
	77.66	0.3647±0.0619	0.360±0.004	87.89
1:1:20 (1-bromohexane, 1-methylimidazole &DMSO)/CO_2				
313.15	29.70	0.2233±0.0059	0.240±0.004	64.83
	55.60	0.4517±0.0069	0.645±0.004	60.70
	64.63	0.6398±0.3527	0.920±0.005	46.55
	86.14^{cp}	0.9395±0.0003		60.49

Table 4. 4 (Cont'd) Vapor liquid equilibrium experimental data and mixture critical points of the ionic liquid synthesis systems with CO_2.

T [K]	*P [bar]*	x_{CO2}	$\Delta V/V_0$	$\underline{V}^L$ *[cm³/mol]*
2:20 [HMim][Br] & DMSO/CO_2				
313.15	27.76	0.1453±0.0079	0.111±0.003	76.65
	41.49	0.2430±0.0097	0.212±0.004	74.06
	60.33	0.4000±0.0121	0.436±0.004	69.55
	69.00	0.49733±0.029	0.634±0.004	66.30
1:1 1-bromohexane & 1-methylimidazole/CO_2				
313.15				
	36.54	0.3006 ± 0.0024	0.152 ± 0.002	96.12
	49.81	0.4420 ± 0.0016	0.286 ± 0.002	85.65
	60.57	0.5654 ± 0.0012	0.510 ± 0.002	78.30
	70.56	0.7128 ± 0.0008	0.995 ± 0.003	68.38
	78.46	0.8715 ± 0.0002	3.026 ± 0.005	61.73
	79.82	0.9024 ± 0.0001	4.276 ± 0.006	61.47
	87.53[cp]	0.9616 ± 0.0001		57.68
333.15				
	28.45	0.1948 ± 0.0052	0.042 ± 0.002	118.62
	39.01	0.2481 ± 0.0059	0.043 ± 0.002	104.22
	62.90	0.4217 ± 0.0083	0.111 ± 0.002	98.14
	79.06	0.5048 ± 0.0061	0.188 ± 0.001	82.38
	96.80	0.6534 ± 0.0077	0.596 ± 0.002	73.49
	107.81	0.8447 ± 0.0013	3.908 ± 0.004	68.76
	111.75[cp]	0.9128 ± 0.0006		75.32

a volume expansion: ; cp= mixture critical point; vll= vapor-liquid-liquid equilibrium points.

Volume expansion: $\frac{\Delta V}{V_0} = \frac{V_m(T,P) - V_0(T, P = 1\,\text{bar})}{V_0(T, P = 1\,\text{bar})}$

4.2.6 Phase Equilibrium of CO_2/1-Hexyl-3-methylimidazolium Bromide ([HMIm][Br])

The VLE of the [HMIm][Br]/CO_2 system was measured at 313.15 K and 333.15 K and is listed Table 4. 4. As seen in Figure 4. 8, the phase behavior of CO_2 with this IL has no mixture critical points. While a number of imidazolium IL/CO_2 phase equilibrium studies have appeared in the literature,[2, 12-14, 16] this is the first one known to the authors that uses a halide anion. Comparing ILs with the [HMIm] cation from current work from our

laboratory [10], as well as from literature results [12, 16], the solubility of CO_2 increases in the order of [Br]<<[BF_4]<[PF_6]<[Tf_2N]. The bromide anion significantly decreases the solubility of CO_2. The Peng-Robinson equation of state (PR EoS) and the van der Waals 2-parameter (vdW-2) mixing rules were used to correlate the [HMIm][Br]/CO_2 system using estimated critical properties. As shown in Figure 4. 8 , the model performs very well through the bubble point data for both isotherms. The binary interaction parameters and model fit (% AARD) are found in Table 4. 2.

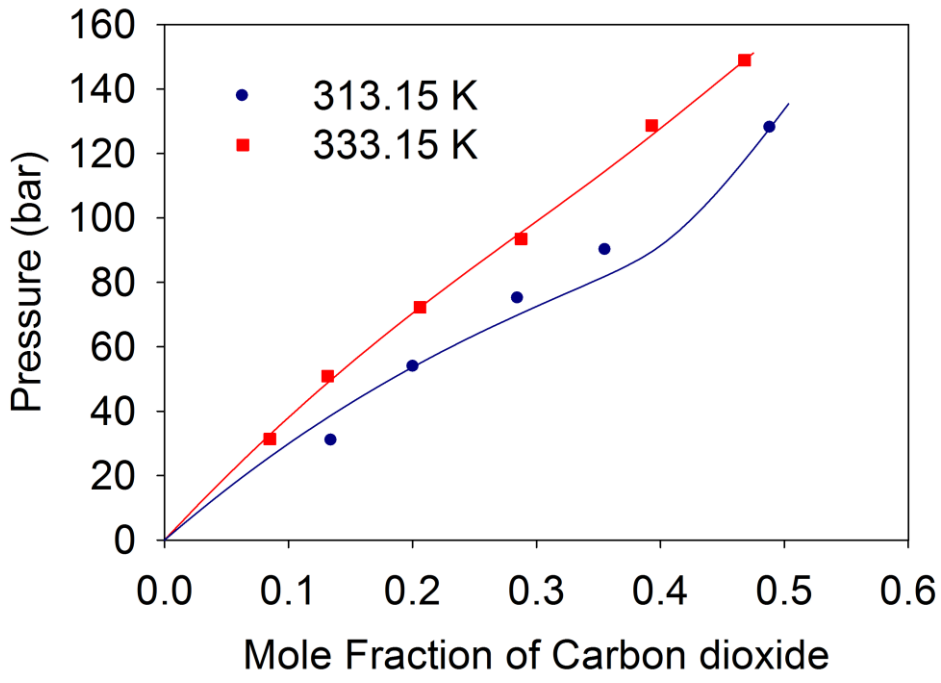

Figure 4. 8 CO_2 Solubility in [HMim][Br] at 313.15 K and 333.15 K.

4.2.7 Ternary Phase Equilibria of CO_2/1-bromohexane/1-methylimidazole

In an actual CO_2-expanded reaction mixture, equal molar ratios of 1-bromohexane and 1-methylimidazole would exist in equilibrium with the CO_2 system. The bubble points of this system were measured at 313.15 K and 333.15 K and listed in Table 4. 4. As the two components react with each other, great care was taken to reduce the influence of the product IL, [HMIm][Br] on the solubility data as will be discussed here. In a concurrent study [29], the 2nd order kinetic rate constant was measured for this system over a broad pressure range. The kinetic data indicates that the reaction is slightly faster at lower CO_2 pressure conditions and that the reaction is not significant (less than 3 % conversion) at 313.15 K for time periods less than 1 hour. In addition, the CO_2 acts as a diluent which reduces the concentration (molarity), decreasing the reaction rate. Thus, these equilibrium data were measured over several different runs to minimize the influence of the IL product. Figure 4.9 illustrates the solubility of CO_2 (component 1) in a mixture of 1-methylimidazole (2) and 1-bromohexane (3), where the reactants are in a 1:1 mole ratio. The solubility in the binary systems is also plotted in the Figure 4. 10 (a). At lower pressures, the 1:1 mixture appears to have CO_2 solubility that is the average of the individual solubilities; at the higher pressure data, the mixture solubility is closer to that of 1-methylimidazole.

The ternary system was predicted using the PR-EoS and vdW-2 mixing rules, utilizing the binary interaction parameters as previously regressed (Table 4. 2). Normally, the interaction parameters of the 1-methylimidazole and 1-bromohexane would be regressed from lower-pressure vapor-liquid equilibrium data. However, these are absent from the literature: the k_{23} and l_{23} terms were set to zero. The solubility of CO_2 in the 1:1 reactant

mixture was predicted and plotted in Figure 4.9; this assumes that one of the components does not significantly partition into the vapor phase, as this would change this 1:1 ratio. As shown, the prediction is quite good at lower pressures, but deviates slightly at the higher pressures. However, as seen by the model performance (Table 4. 2), an adequate prediction is still achieved.

The mixture critical points of the ternary mixture are 87.53 bar and 0.962 mole fraction CO_2 at 313.15 K and 111.75 bar, 0.913 mole fraction CO_2 at 333.15 K. As the 1-methylimidazole/CO_2 system is characterized by a region of VLLE and LLE at 313.15 K, and 1-bromohexane/CO_2 has just VLE, it is interesting that the ternary mixture has no multi-phase phenomenon, with only VLE present and a mixture critical point. Instead, the ternary mixture critical point has a critical composition similar to the binary mixtures. However, the ternary mixture's critical pressure is 2.63 bar greater than that of 1-bromohexane/CO_2, and 4.24 bar less than that of the 1-methylimidazole at 313.15K. At 333.15K, the ternary mixture's critical point is similarly 3.94 bar greater than that of 1-bromohexane/CO_2, but is much lower (41.25 bar) than that of the 1-methylimidazole.

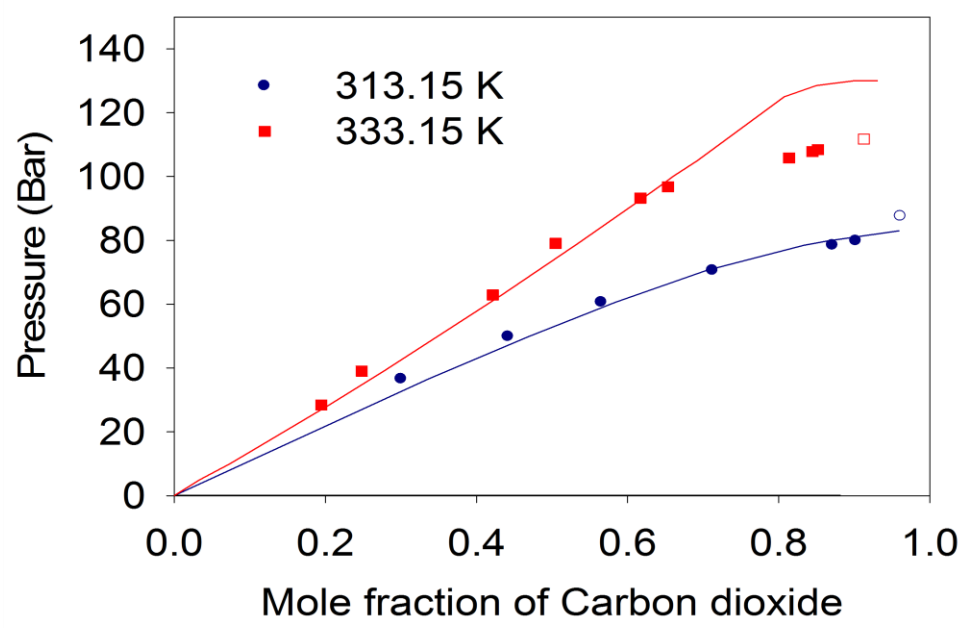

Figure 4.9 CO_2 solubility in 1:1 mixture (1-methylimidazole + 1-bromohexane) at 313.15 K and 333.15 K.

Figure 4. 10 (b) also illustrates the difference in the solubility of CO_2 between the 1:1 reaction mixture of (1-bromohexane/1-methylimidazole) and the product IL, [HMIm][Br]. As seen, [HMIm][Br] has far less solubility of CO_2 that does the 1:1 mixture. For instance, at 313.15 K and approximately 70 bar (see dashed line), the solubility of CO_2 in 1:1 reaction mixture is 0.796 mole fraction, while in the IL it is only approximately 0.26 mole fraction of CO_2. This has ramifications on the reaction, especially in biphasic situations (CO_2-expanded mixture): as the reaction conversion increases, CO_2 will try to escape from the liquid into the vapor phase.

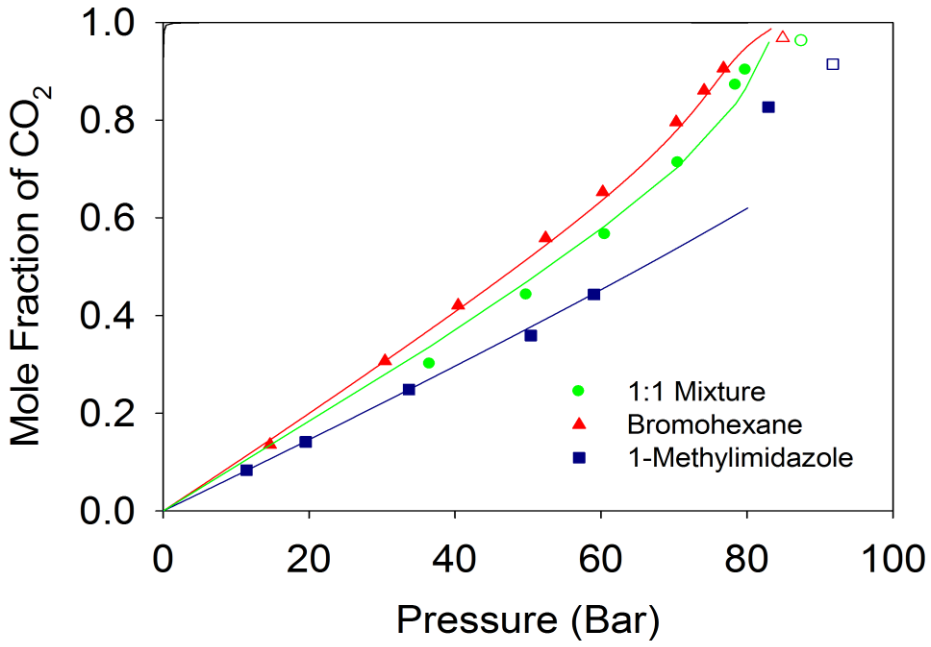

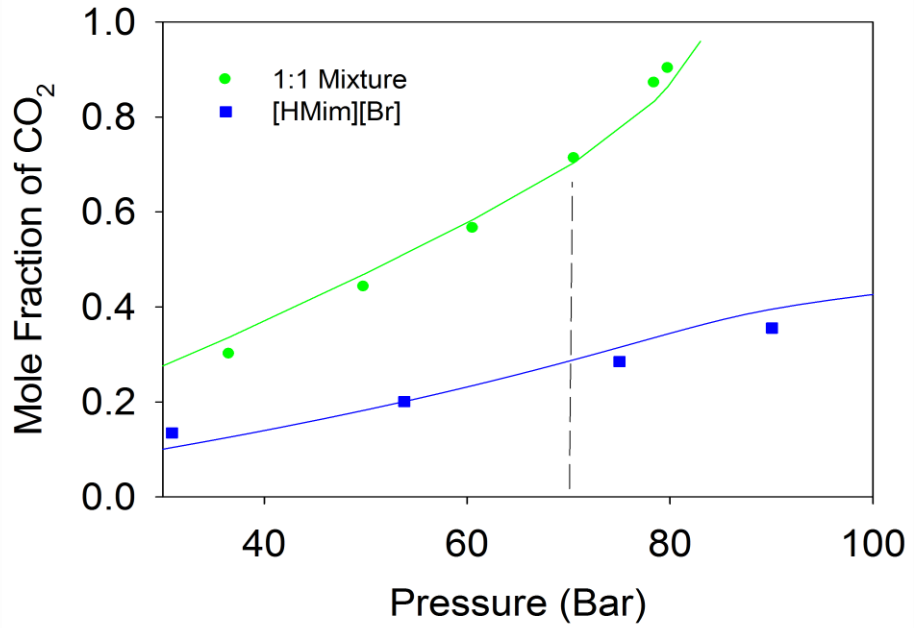

Figure 4. 10 a.) Mole fraction of CO_2 in the liquid phase versus Pressure data taken at 313.15 K for reactants and for the 1:1 mole ratio reactant mixture (TOP) b.) Mole fraction of CO_2 in the liquid phase versus Pressure data taken at 313.15 K for the 1:1 mole ratio reactant mixture and [HMim][Br].(BOTTOM)

In a batch system, this could increase the pressure as the reaction progresses and must be taken into consideration for safety precautions. However, this can actually be advantageous for IL production in CO_2. As the IL is removed from the pressurized reactor, it will contain lower amounts of CO_2 than the reaction mixture, thus there will be less CO_2 makeup or recompression needed, improving the economics of the system.

4.2.8 Multicomponent Phase Equilibria of CO_2/1-bromohexane/1-methylimidazole/DMSO and CO_2/[HMim][Br] /DMSO

Investigations were carried out on a ternary CO_2/DMSO/[HMim][Br] (product) mixture and pseudo-ternary mixture of CO_2/1-bromohexane/1-methylimidazole/DMSO. VLE data of the multicomponent mixture CO_2/DMSO/1:1-reactant-mixture furnishes data used to compute molarity and subsequently, *k* constants. The bubble points of this system were measured at 313.15 K and 333.15 K, and listed in Table 4. 4. Figure 4. 12 compares mixture VLE with CO_2 at 40^o C for different initial molar ratios of reactants to DMSO compared with resulting product mixtures. At higher conversions (i.e., as reaction progresses in an IL synthesis system), the expanded system will move toward the solubility trends observed in the CO_2/DMSO/[HMim][Br] ternary system, especially at lower solvent ratios of the DMSO to reactants. The CO_2/1-bromohexane/1-methylimidazole/DMSO multicomponent mixtures appear to have CO_2 solubility closest to that of the DMSO binary. For the CO_2/1-bromohexane/1-methylimidazole/DMSO mixtures, VLLE regions were observed at 40^oC, and eventually at higher pressures, a mixture critical point was observed. For 1 1-bromohexane:1 1-methylimidazole:5

DMSO, a VLLE region occurred at 86 bar, and then the mixture critical point occurred at 89.19 bar. Similarly when the solvent ratio was 1 1-bromohexane:1 1-methylimidazole:20 DMSO, the VLLE occurred at 84.3 bar and the mixture critical point was at 86.14 bar. For the CO_2/DMSO/[HMIm][Br] system (2 HMIMBr : 5 DMSO), representative of a true reaction mixture at 100% conversion, VLLE occurred 81.32 bar and, as pressure increased, a K point occurred at 85.87 bar. No mixture critical point was observed for this system. A 29% temperature difference in K point was observed for the 2 [HMIm][Br]:20 DMSO system at a K-point of 121.57 bar, and the VLLE region occurred at 94.64 bar. This implies that, to be able to leverage CO_2 extraction for effective separation of DMSO from the system after reaction, optimal solvent ratio/amount has to be carefully selected. Operating temperature, pressure and loading will be other design criteria to be considered for optimal separations. Additionally, the CO_2 solubility should be expected to vary over reaction time, as illustrated in Figure 4.11 (arrows).

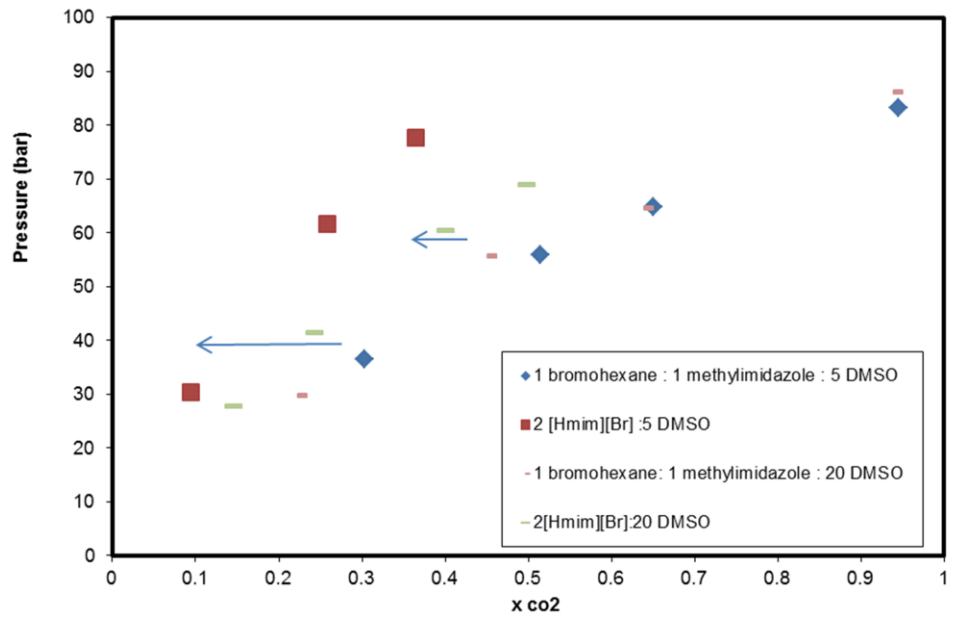

Figure 4.11 Vapor-Liquid Equilibrium with CO_2 at 40C for different initial molar ratios of reactants to DMSO compared with resulting product mixtures

4.3 Volume Expansion

For reactions conducted in CO_2-expanded liquids, the volume expansion is an important mixture property, especially as the volume changes as a function of the pressure and sometimes conversion. For reactions conducted above the mixture critical point, the concentration is simply the moles divided by the volume of the vessel. However, when operating below the mixture critical point, the relation between the pressure and volume of the liquid phase is important, as most reaction kinetic expressions are based upon concentration, i.e. moles per unit volume.[30] Often the volume is reported as volume expansion, which is the relative change in mixture volume compared to the initial volume (without any CO_2), i.e., $(V_m\text{-}V_0)/V_0$, where subscripts *m* and *0* are for the mixture volume

at any given pressure and for the initial volume of the liquid phase without CO_2 pressure, respectively. The volume expansion of all of the liquids increases with rising CO_2 pressure; technically, the volume expansion reaches infinity at the mixture critical point, as the fluid will fill whatever volume that it occupies. Figure 4. 13 indicates that the volume expansion of all of the liquids increases with increasing pressure, as seen with other organic liquids in CO_2.[31] However, at a constant temperature and pressure, the volume expansion of 1-bromohexane is larger than 1-methylimidazole. For instance at 313.15 K and 70 bar of CO_2, the volume expansion of 1-bromohexane is 136.56 %, and this pressure corresponds to a CO_2 solubility of approximately 0.796 mole fraction. For 1-methylimidazole, the volume expansion is 51.51 % at 313.15 K and 70 bar (approximately 0.486 mole fraction of CO_2).

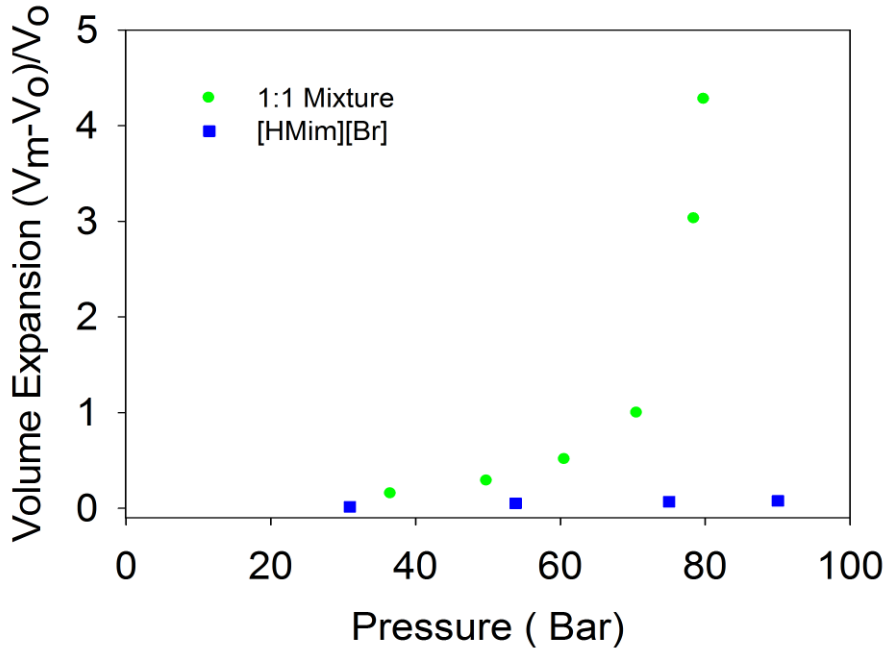

Figure 4. 12 Volume Expansion of the liquid phase versus Pressure data taken at 313.15 K for the 1:1 mole ratio reactant mixture and [HMim][Br]

Figure 4. 12 illustrates the volume expansion difference between that of the 1:1 reactant mixture and that of the product, [HMIm][Br], with CO_2. The volume expansion of [HMIm][Br] at 70 bar of CO_2 is only approximately 6.47 % at 313.15 K (approximately 0.265 mole fraction of CO_2), while the volume expansion of the 1:1 mixture is 99.46 % at 70 bar (approximately 0.713 mole fraction of CO_2). [HMIm][Br], like some other ILs, has very low volume expansion compared to traditional organic solvents.[30] Blanchard *et al.*,[2] attributed this to the strong Coulombic forces between the ions: separation of those ions by dissolution of the CO_2 would result in too large of a thermodynamic penalty.

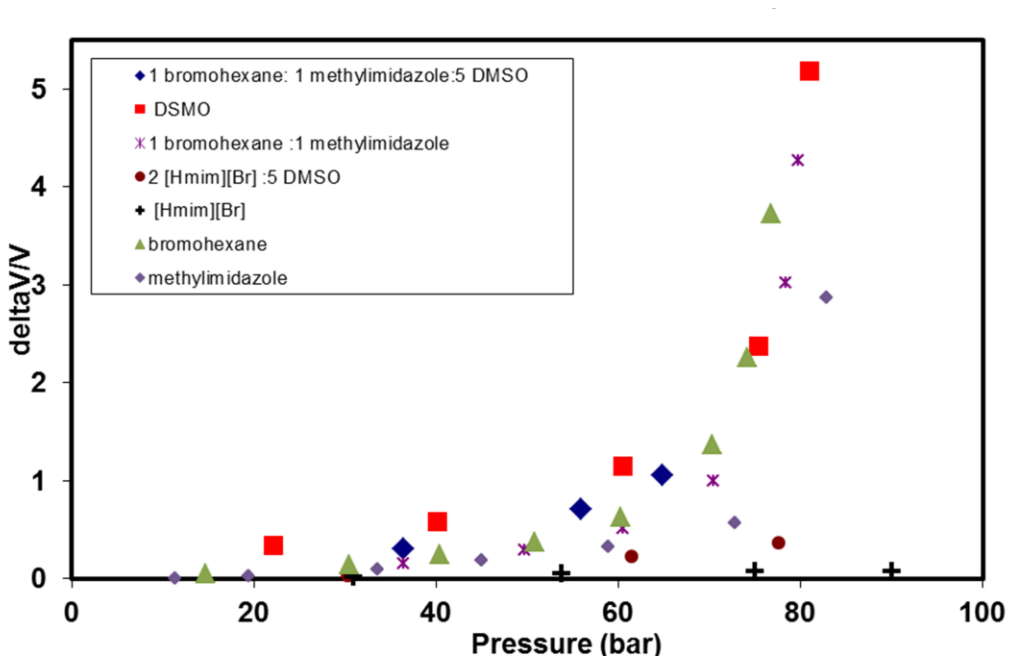

Figure 4. 13 Volume Expansion of the liquid phase versus Pressure data taken at 313.15 K for CO_2 binaries and multicomponent IL synthesis system.

As shown, the volume expansion for the IL is significantly smaller than the reactant mixture, especially at higher pressures. This would indicate that, as conversion increases, the volume will decrease, assuming a single liquid phase. However, in most real systems, the product IL will be mostly insoluble in the CO_2-expanded reactant phase and will separate, forming a 3 phase systems; vapor-liquid-liquid equilibrium (VLLE). In this case, the denser IL will form a liquid layer at the bottom that does not expand much, despite some amounts of dissolved CO_2; the middle liquid layer will be a reactant-rich phase expanded with CO_2; and a mostly CO_2 vapor phase will exist at the top. Thus, a CO_2-expanded reactant phase (VLE) will first convert to a 3-phase system (VLLE), and

then back to a 2-phase system (VLE) at complete conversion. During the intermediate VLLE stage, the IL may be removed in a continuous reaction system. The purity of this IL will depend on the extent of reactant (mainly 1-methylimidazole) partitioning into the IL phase.

4.4 High Pressure Transport Property Data (Viscosity, Thermal conductivity, Heat Capacity, and Thermal diffusivity) for CO_2-expanded DMSO System

Viscosity, thermal conductivity, and thermal diffusivity were measured for the liquid phase of the DMSO/CO_2 binary over a range of pressures, at 40^{o}C and at 60^{o}C. Results obtained are presented in Table 4.5 and Table 4.7.

A modified ViscoPro 2000 System (SPL-440), equipped with Viscolab software, was used for DMSO/CO_2 high pressure viscosity measurements (see chapter 2). The apparatus is operated based on annular flow around an axially oscillating piston. In order to validate the viscometer measurement obtained from the ViscoPro 2000 System, ambient pressure viscosity for DMSO was obtained using a Wells-Brookfield Cone and Plate (DV-III ULTRA) Viscometer / Rheometer. The viscosity of pure DMSO was found to be within 3.5% at 40 C and 0.5 % of literature data. Because DMSO is extremely hydrophilic, a Karl Fisher analysis was performed for the DMSO sample used for both analyses, of which the result was 50 ppm.

DMSO is a Newtonian fluid, and its viscosity was found to decrease with temperature. Calvignac *et. al.*[32, 33], used a falling ball viscometer to obtain viscosity measurements

for CO_2 expanded DMSO system. This is the only literature data available for this system; we compare our data in Figure 4.14. CO_2 composition for this (our) study was obtained from extrapolating experimental data presented in the VLE section. At a given isotherm, viscosity of the liquid phase was found to decrease exponentially with CO_2 composition (as with pressure). For example, at 40^oC, the viscosity of the solvent was found to decrease by 80% at 81.38 bar, from its original 1.561 cP to 0.310 cP, as shown in Figure 4.15. Table 4.5 summarizes viscosity data at the two temperatures studied. There is a steeper drop in viscosity at 40^oC, compared to the trend observed at 60^oC, which is due higher CO_2 dissolution. At high CO_2 compositions, the temperature effect was found to diminish.

Thermal conductivity and thermal diffusivity data were obtained using the Lambda system (based on the transient short hot wire method, as detailed in Chapter 2). Thermal conductivity data for gas expanded fluids are scare in the literature. Recently, Tomida and co- workers [34], using transient hot wire methods, measured the thermal conductivity for 1-Butyl-3-methyliidazolium hexafluorophosphate [BMim][PF_6]/CO_2, 1-butyl-3-methylimidazlium tetrafluoroborate 1-methylimidazole [BMim][BF_4]/CO_2 and 1-methylimidazole/CO_2 expanded liquid phases (up to $x$$CO_2$ = 0.42) from 294 K to 334 K, at pressures 10.0MPa and 20MPa. They found that the thermal conductivities of the systems observed, especially the ILs, have very weak CO_2 composition dependence. The thermal conductivity of 1-methylimidazole decreased slightly with CO_2 composition (only 8%, compared to pure 1-methylimidazole), from $x$$CO_2$ =0, which yielded the highest thermal conductivity, up to $x$$CO_2$=0.42, the highest mole fraction of CO_2 they

observed. No thermal diffusivity data was reported. To the best of our knowledge, no experimental data exists for thermal conductivity, and diffusivity of a DMSO-CO_2 system under pressure.

Our experimental pressure range was from 0-72 bar at 40^{o}C and 60^{o}C isotherms. Composition of CO_2 was extrapolated from the VLE data presented previously. While viscosity measurements are known to be sensitive to impurities, i.e. water content, Valkenburg *et. al.*,[35] found this not to be the case for thermal conductivity measurements. A slight (0.8%) difference in thermal conductivity was found for samples of 1,2-diethyl-3-propylimidazolium bis(trifluorosulfonyl)imide with water content 500 ppm and 2000 ppm. This work introduces new perspectives on the determination of physical properties such as thermal conductivity and thermal diffusivity for organic systems under high pressure. These three properties were found to decrease slightly with CO_2 composition/solubility. The trends we observed are similar to that previously noted for the organic solvent 1-methylimidazole. These properties were found to have a weak CO_2 composition dependence - changes were minimal, even up to xCO_2 = 0.82 at the 40^{o}C isotherm. Compared to the pure DMSO (at 0 bar), the changes observed for thermal conductivity, heat capacity and thermal diffusivity for the CO_2/DMSO system at 72 bar (the highest pressure observed) were 0.04 %, 0.01% and 0.03%, respectively.

Table 4.5 High pressure viscosity of the DMSO/CO_2 system at 40°C and 60°C

Temp °C	Pressure (bar)	Viscosity (cP)	xCO_2
40	0.00	1.561±0.0073	0.000
40	19.31	1.155±0.0054	0.089
40	34.34	0.933±0.0035	0.265
40	47.86	0.667±0.0050	0.423
40	70.55	0.407±0.0011	0.689
40	81.38	0.310±0.0006	0.816
60	0.00	1.122±0.0052	0.000
60	21.79	0.851 ±0.0039	0.066
60	41.24	0.708 ±0.0020	0.169
60	57.79	0.608 ±0.0022	0.257
60	79.45	0.453 ±0.0021	0.371
60	94.90	0.369 ±0.0014	0.453
60	118.07	0.318 ±0.0015	0.576

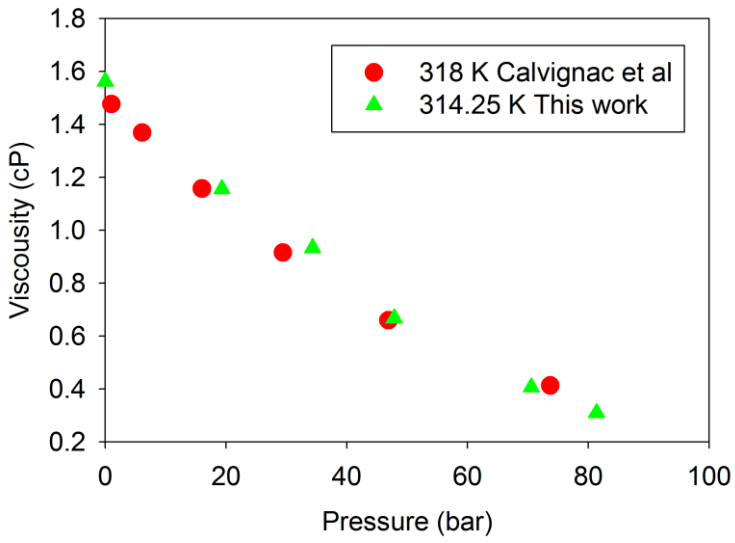

Figure 4.14 Comparing literature viscosity data for DMSO/CO_2 system

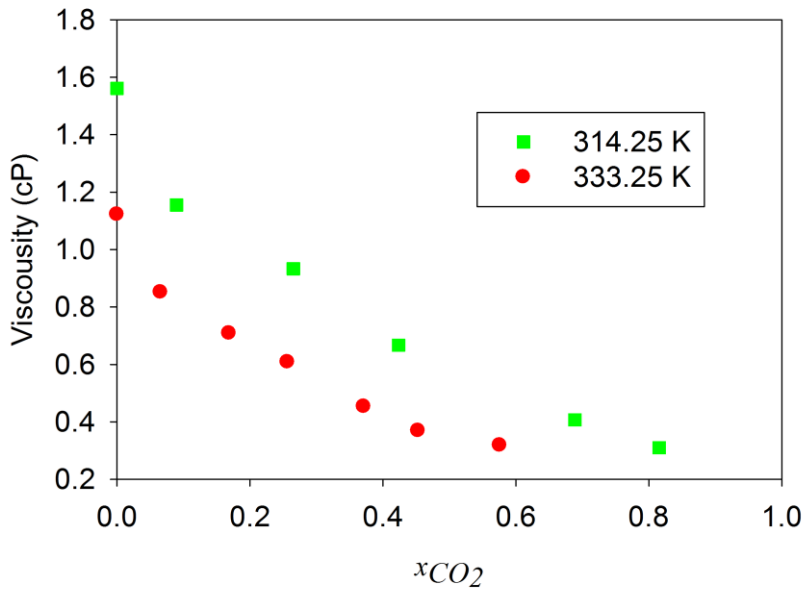

Figure 4.15 High pressure viscosity data for DMSO/CO_2 system at 40°C and 60°C

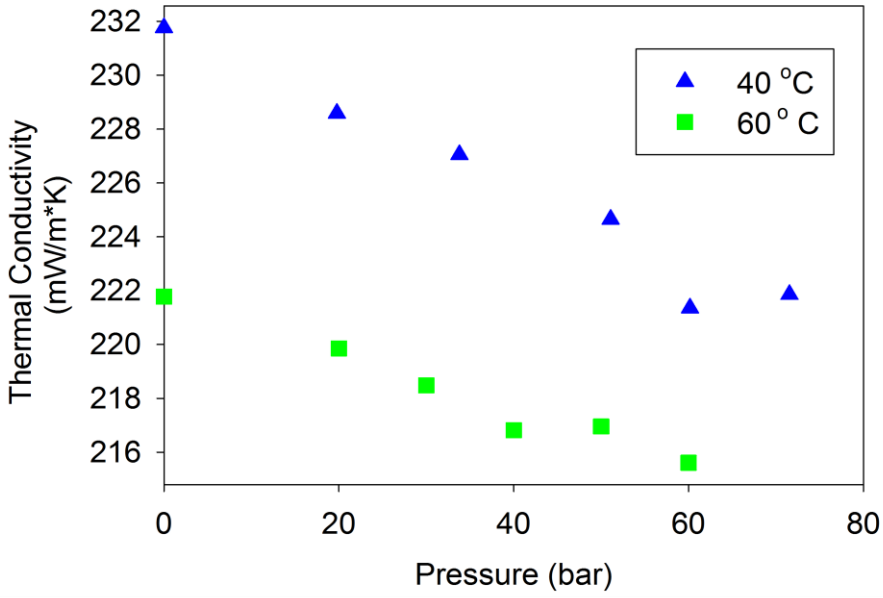

Figure 4.16 High pressure thermal conductivity of DMSO/CO_2 System at 40°C and 60°C

Table 4. 6 High pressure transport data for DMSO/CO_2 system at 40°C and 60°C

T/K	Pressure (bar)	xCO_2	Thermal Conductivity (mW/m*K)	Thermal Diffusivity (m^2/sec) x 10^{-8}
313.15	0	0.000	231.77	9.581
	20	0.095	228.58	9.547
	34	0.259	227.05	9.531
	51	0.461	224.65	9.507
	60	0.567	221.35	9.472
	72	0.701	221.85	9.477
333.15	0	0.000	221.78	9.477
	20	0.056	219.85	9.457
	30	0.109	218.48	9.443
	40	0.162	216.81	9.425
	50	0.215	216.95	9.427
	60	0.268	215.60	9.413

4.4.1 Solvent Ratio Effect on Transport Properties

Encountering mixtures of IL and organic solvents is expected in IL applications.[35] In IL processes, recovering and recycling the IL become key determinants of the economic feasibility of using the technology. For the design of efficient separations, mixture data is important.[36, 37] This information is essential for efficient design of unit operations that are heavily dependent on heat transfer, such as chemical reactors and heat exchangers. Overall heat transfer coefficient, U_a, a design parameter that measures the rate at which heat is transferred between the fluid and its surroundings, must be determined. Typically,

it is estimated from dimensionless correlations using physical properties (e.g. thermal conductivity, density, viscosity, thermal diffusivity etc.) of the fluid.

Most literature work focuses on water mixtures of ILs and the effect of chloride concentration on the properties of the IL. In IL production systems, these properties are important, as the IL product must be recovered from the solvent employed for synthesis. In this work, viscosity, density, thermal conductivity, and thermal diffusivity were measured over various molar ratios of solvent (acetone) and products. The temperature dependence of these properties was investigated. Density decreased with temperature, but this effect was more pronounced at mixtures of higher than 50% concentration; at 75% concentration of the solvent, the density of the mixture was reduced by 15%. This trend was expected, as mixture density is typically a function of the pure component densities and the concentration of the components in the mixture. Acetone has lower density than the IL: as the composition of acetone increases, the density of the mixture would therefore decrease. Seddon *et al*.,[38] studied the effect of water, ethanenitrile, trimethylethanenitrile, 2-propenenitrile, 1-methylimidazole, toluene, 1,4-dimethylbenzene, and 1,2-dimethoxyethane on the viscosity of [C4mim][BF_4] and [C4mim][PF_6]. The addition of co-solvents significantly reduced the viscosity and density of the ILs, especially when a solvent with a high dielectric constant is involved. They found that the viscosity of the mixture reduced with molar fraction, and that the concentration of the IL/molecular solvent mixtures had a stronger effect on the viscosity than did temperature, regardless of the polarity of solvents studied.

The viscosity of the IL/organic solvent mixtures was a strong function of molar fraction, which represents the amount of the molecular solvents in the mixture. Brennecke and coworkers[37] investigated density and viscosity of binary mixtures of water and ILs (1-ethyl-3-methylimidazolium trifluoroacetate, 1-ethyl-3-methylimidazolium ethylsulfate, and 1-ethyl-3-methylimidazolium trifluoromethanesulfonate) at atmospheric pressure at 278.15 to 348.15 K. They also observed that composition has a greater influence than temperature on density and viscosity. The mixture density and viscosity were affected by both temperature and composition; the density decreases as both temperature and water composition in the systems increase. For instance, at 25^{o}C, the 25% mixture had 85% higher viscosity than the 50% mixture; viscosity was further reduced by 99% in a 75% mixture. In practice, this implies that the handling of highly viscous product IL can be circumvented simply by controlling the composition of solvent chosen for synthesis. Although much lower viscosity and better transport properties may be achieved with higher solvent concentrations, it must be noted that this would require more energy and cost to recover the product IL. Process design and optimization must prioritize these criteria and balance reaction conditions appropriately. For example, the engineer should factor in pump costs, reaction rate constant, equipment or construction material, solvent cost and, most importantly, energy requirements for separations.

Thermal conductivities of ILs and their binary mixture is meager in the literature. Qun *et.al*.,[39] measured the thermal conductivity of mixtures of acetone using the transient hot-wire method at some selected temperatures between 253.15 K to 303.15 K. Diebold and co-workers [40] measured thermal diffusivity of several room-temperature ILs

(RTILs) using the transient grating method. They show that the anion affects the thermal diffusivity of the IL; they found that, for an IL with the same cation for example $[BMIm]^+$, changing the anion from $[BF_4]^-$ to $[Tf_2N]^-$ would result in a slight decrease in thermal diffusivity and thermal conductivity. No effect was observed for the size of the cation.

At atmospheric pressure, Ge *et al.*,[18] measured the thermal conductivities of eleven ionic liquids over a temperature range from 293 K to 353 K, using the transient hot-wire method. The thermal conductivities were found to be between 100- 200 $mW \cdot m^{-1} \cdot K^{-1}$; pure [HMim][Br] thermal conductivity in this study was found to be within this range at 140.98 $mW \cdot m^{-1} \cdot K^{-1}$ 25.05°C and 198.28 $mW \cdot m^{-1} \cdot K^{-1}$ at 40 and 50°C . The pure [HMim][Br] thermal diffusivity found in this study was comparable to the diffusivity of pure $[BMim][BF_4]$, which is 30% higher than that of $[HMim][Tf_2N]$. [40]

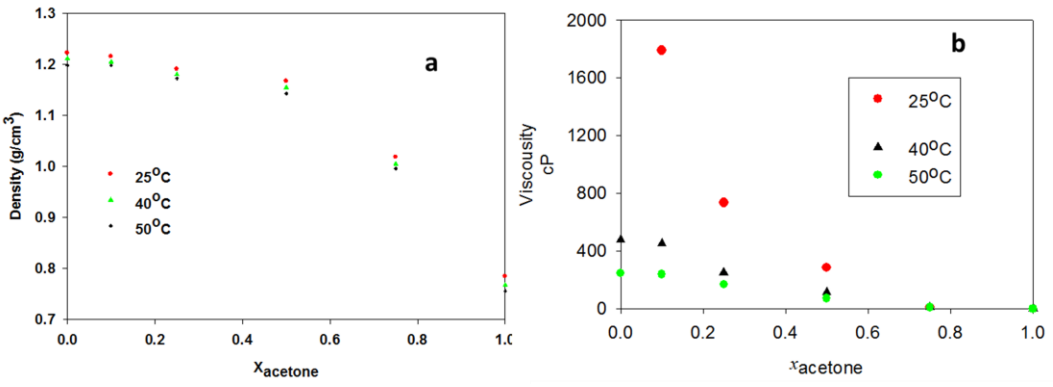

Figure 4.17 (a) Density and viscosity (b) with concentration of acetone at 25, 40 and 50 C

Table 4. 7 Transport Data constant with concentration of acetone at 25 C, 40 C and 50 C

xAcetone	T (^{o}C)	Thermal Conductivity	Thermal Diffusivity
1	25.00	262.19	9.91
1	40.01	295.43	10.27
1	50.01	295.87	10.28
0.1	25.01	195.64	9.21
0.1	40.00	190.57	9.16
0.1	50.01	185.75	9.11
0.5	25.00	197.09	9.22
0.5	40.00	192.94	9.18
0.5	50.00	191.29	9.17
0	50.05	191.48	9.17
0	40.01	191.28	9.17
0	25.05	140.98	8.67

4.5 **Summary**

The use of CO_2 systems for the production of ILs has many advantages over conventional solvents. However, the phase behavior and equilibrium must be carefully understood. The global phase behavior of 1-methylimidazole was investigated from 275.15 K to 333.15 K and was found to be a Type V system (or potentially IV), using the classification scheme of Scott and van Konynenburg, with regions of vapor-liquid equilibrium, vapor-liquid-liquid equilibrium, liquid-liquid equilibrium, upper and lower critical endpoints, as well as mixture critical points.

The solubility and volume expansion of CO_2 in 1-methylimidazole, 1-bromohexane, DMSO, 1:1 mixture of 1-methylimidazole and 1-bromohexane and [HMIm][Br] were determined at 313.15 K and 333.15 K for pressures ranging from 10-160 bar. The Peng-

Robinson Equation of State with van der Waals 2-parameter mixing rules was used with estimated critical properties to well correlate the vapor-liquid equilibrium. The phase equilibrium data will allow better understanding and kinetic characterization of the synthesis of ILs with CO_2.

Viscosity, thermal conductivity, heat capacity and thermal diffusivity were measured for the liquid phase of the DMSO/CO_2 binary over a range of pressures, at 40^{o}C and at 60^{o}C. Viscosity data was compared with the only literature data available for this system. The viscosity of the liquid phase was found to decrease exponentially with CO_2 composition (as with pressure). Viscosity decreased with temperature. Thermal conductivity and thermal diffusivity were measured over a 0-72 bar pressure range at 40^{o}C and 60^{o}C isotherms. These properties were found to decrease slightly with CO_2 composition/solubility.

At ambient pressure conditions, solvent concentration was found to be important in selecting optimal reaction conditions for IL synthesis. Viscosity, density, thermal conductivity and diffusivity data were obtained for different mole fractions of acetone (x_{acetone}. 0, 0.1, 0.25, 0.5, 0.75 and 1). Similarly, molar fraction was found to be stronger determinant of the viscosity and density of the mixture, compared to temperature. Thermal conductivity and diffusivity data are reported for the IL/acetone mixture.

References

[1] K. Ohgaki, T. Katayama, Isothermal Vapor-Liquid Equilibrium for Binary Systems Containing Carbon Dioxide at High Pressures: n-Hexane-Carbon Dioxide and Benzene-Carbon Dioxide Systems, J. Chem. Eng. Data, 21 (1976) 53-55.

[2] L.A. Blanchard, Z. Gu, J.F. Brennecke, High-Pressure Phase Behavior of Ionic Liquid/CO2 Systems, J. Phys. Chem. B, 105 (2001) 2437-2444.

[3] V.T. Wyatt, D. Bush, J. Lu, J.P. Hallett, C.L. Liotta, C.A. Eckert, Determination of solvatochromic solvent parameters for the characterization of gas-expanded liquids, The Journal of Supercritical Fluids, 36 (2005) 16-22.

[4] S.N.V.K. Aki, B.R. Mellein, E.M. Saurer, J.F. Brennecke, High-pressure phase behavior of carbon dioxide with imidazolium-based ionic liquids, The Journal of Physical Chemistry B, 108 (2004) 20355-20365.

[5] E. Brunner, Fluid mixtures at high pressures. V: Phase separation and critical phenomena in 18 binary mixtures containing bither pyridine or ethanoic acid, J. Chem. Thermo., 19 (1987) 823-835.

[6] H.S. Byun, C. Kwak, High Pressure Phase Behavior Measurement for Binary Carbon Dioxide-Pyridine and Carbon Dioxide-Isobutyronitrile Systems, Kor. J. Chem. Eng., 38 (2000) 366-372.

[7] Z.J. Dijkstra, A.R. Doornbos, H. Weyten, J.M. Ernsting, C.J. Elsevier, J.T.F. Keurentjes, Formation of carbamic acid in organic solvents and in supercritical carbon dioxide, J. Supercrit. Fluid., 41 (2007) 109-114.

[8] E.M. Hampe, D.M. Rudkevich, Exploring reversible reactions between CO2 and amines, Tetrahedron, 59 (2003) 9619-9625.

[9] I. Omae, Aspects of carbon dioxide utilization, Catalysis Today, 115 (2006) 33-52.

[10] J. Schleicher, in, University of Kansas, Lawrence, Kansas, USA, 2007.

[11] K. Thamanavat, T. Sun, A.S. Teja, High-pressure phase equilibria in the carbon dioxide+ pyrrole system, Fluid Phase Equilibria, 275 (2009) 60-63.

[12] S. Aki, B.R. Mellein, E.M. Saurer, J.F. Brennecke, High-pressure phase behavior of carbon dioxide with imidazolium-based ionic liquids, J. Phys. Chem. B, 108 (2004) 20355-20365.

[13] J.L. Anthony, E.J. Maginn, J.F. Brennecke, Solubilities and thermodynamic properties of gases in the ionic liquid 1-n-butyl-3-methylimidazolium hexafluorophosphate, J. Phys. Chem. B, 106 (2002) 7315-7320.

[14] L.A. Blanchard, Z. Gu, J.F. Brennecke, Ionic Liquids and Supercritical CO_2, in: R.D. Rogers, K.R. Seddon, S. Volkov (Eds.) Green Industrial Applications of Ionic Liquids

Proceedings of the NATO Advanced Research Workshop held in Heraklion, Crete, Greece, 12-16 April 2000, Springer, 2003, pp. 403.

[15] W. Ren, A.M. Scurto, High-Pressure Phase Equilibria of Carbon Dioxide (CO2) + n-Alkyl-Imidazolium Bis(trifluoromethylsulfonyl)amide Ionic Liquids Submitted, (2009).

[16] A. Shariati, S. Raeissi, C. Peters, CO_2 Solubility in Alkylimidazolium-Based Ionic Liquids, in: T.M. Letcher (Ed.) Developments and Applications in Solubility, Royal Society of Chemistry, Cambridge, 2007, pp. 131-149.

[17] K.G. Joback, R.C. Reid, Estimation of pure-component properties from group-contributions, Chemical Engineering Communications (Print), 57 (1987) 233-243.

[18] R. Ge, C. Hardacre, P. Nancarrow, D.W. Rooney, Thermal Conductivities of Ionic Liquids over the Temperature Range from 293 K to 353 K, Journal of Chemical & Engineering Data, 52 (2007) 1819-1823.

[19] J. Dykyj, S. J, R.C. Wilhoit, M. Frenkel, K.R. Hall, Landolt-Börnstein Numerical Data and Functional Relationships in Science and Technology: New Series, in: K.R. Hall (Ed.) Vapor Pressure of Chemicals, Springer, Berlin, 1999.

[20] R.C. Reid, J.M. Prausnitz, B.E. Poling, The properties of gas and liquids, MacGraw-Hill, New York, (1987).

[21] B.I. Lee, M.G. Kesler, A generalized thermodynamic correlation based on three-parameter corresponding states, AIChE Journal, 21 (1975).

[22] P.H. Van Konynenburg, R.L. Scott, Critical lines and phase equilibriums in binary Van der Waals mixtures, Philos. Trans. R. Soc. London, Ser. A, 298 (1980) 495-540.

[23] A.M. Scurto, C.M. Lubbers, G. Xu, J.F. Brennecke, Experimental measurement and modeling of the vapor–liquid equilibrium of carbon dioxide+ chloroform, Fluid Phase Equilibria, 190 (2001) 135-147.

[24] B. Wang, J. He, D. Sun, R. Zhang, B. Han, Solubility of chlorobutane, ethyl methacrylate and trifluoroethyl acrylate in supercritical carbon dioxide, Fluid Phase Equilibria, 239 (2006) 63-68.

[25] A.V. Gonzalez, R. Tufeu, P. Subra, High-Pressure Vapor- Liquid Equilibrium for the Binary Systems Carbon Dioxide+ Dimethyl Sulfoxide and Carbon Dioxide+ Dichloromethane, J. Chem. Eng. Data, 47 (2002) 492-495.

[26] A. Andreatta, L. Florusse, S. Bottini, C. Peters, Phase equilibria of dimethyl sulfoxide (DMSO)+ carbon dioxide, and DMSO+ carbon dioxide+ water mixtures, The Journal of Supercritical Fluids, 42 (2007) 60-68.

[27] A. Kordikowski, A. Schenk, R. Van Nielen, C. Peters, Volume expansions and vapor-liquid equilibria of binary mixtures of a variety of polar solvents and certain near-critical solvents, The Journal of Supercritical Fluids, 8 (1995) 205-216.

[28] S. Nwosu, J. Schleicher, A.M. Scurto, Kinetics and Polarity Effects for the synthesis of ionic liquids in compressed CO_2 Manuscript in preparation, (2009).

[29] A.M. Scurto, H. Keith, B. Subramaniam, Gas-Expanded Liquids (GXLs): Fundamentals and Applications, in: K.W. Hutchenson, A.M. Scurto, B. Subramaniam (Eds.) Gas Expanded Liquids and Near-Critical Media: Green Chemistry and Engineering ACS Symposium Series 1006, Washington, D.C., 2009, pp. 3-37.

[30] R. Marr, T. Gamse, Use of supercritical fluids for different processes including new developments—a review, Chem. Eng. Proc., 39 (2000) 19-28.

[31] B. Calvignac, E. Rodier, J.J. Letourneau, J. Fages, Development of Characterization Techniques of Thermodynamic and Physical Properties Applied to the CO_2/DMSO Mixture, International Journal of Chemical Reactor Engineering, 7 (2009) 46.

[32] B. Calvignac, E. Rodier, J.J. Letourneau, P. Vitoux, C. Aymonier, J. Fages, Development of an improved falling ball viscometer for high-pressure measurements with supercritical CO2, The Journal of Supercritical Fluids, 55 (2010) 96-106.

[33] D. Tomida, S. Kenmochi, T. Tsukada, K. Qiao, C. Yokoyama, Thermal Conductivities of Imidazolium-Based Ionic Liquid+ CO 2 Mixtures, International Journal of Thermophysics, 31 (2010) 1888-1895.

[34] M.E.V. Valkenburg, R.L. Vaughn, M. Williams, J.S. Wilkes, Thermochemistry of ionic liquid heat-transfer fluids, Thermochimica Acta, 425 (2005) 181-188.

[35] Y. Wang, D. Chen, X. OuYang, Viscosity Calculations for Ionic Liquid− Cosolvent Mixtures Based on Eyring's Absolute Rate Theory and Activity Coefficient Models, Journal of Chemical & Engineering Data, 55 (2010) 4878-4884.

[36] K.N. Marsh, J.A. Boxall, R. Lichtenthaler, Room temperature ionic liquids and their mixtures—a review, Fluid Phase Equilibria, 219 (2004) 93-98.

[37] H. Rodríguez, J.F. Brennecke, Temperature and Composition Dependence of the Density and Viscosity of Binary Mixtures of Water + Ionic Liquid, Journal of Chemical & Engineering Data, 51 (2006) 2145-2155.

[38] K.R. Seddon, A. Stark, M.J. Torres, Influence of chloride, water, and organic solvents on the physical properties of ionic liquids, Pure Appl. Chem, 72 (2000) 2275-2287.

[39] L. Qun-Fang, L. Rui-Sen, N. Dan-Yan, H. Yu-Chun, Thermal Conductivities of Some Organic Solvents and Their Binary Mixtures, Journal of Chemical & Engineering Data, 42 (1997) 971-974.

[40] C. Frez, G.J. Diebold, C.D. Tran, S. Yu, Determination of Thermal Diffusivities, Thermal Conductivities, and Sound Speeds of Room-Temperature Ionic Liquids by the Transient Grating Technique, Journal of Chemical & Engineering Data, 51 (2006) 1250-1255.

5. Synthesis of Ionic Liquids in Conventional Solvents.

5.1.Introduction

ILs are synthesized in a one- or two-step process. First, a quarternization reaction is performed to obtain a halide, alkyl-sulfate, etc. compound whose anion can then be exchanged if necessary. The anion-exchange step involves the derived precursor and a metal salt or acid to produce the desired IL with a different anion. This work focuses on the first step in IL synthesis, the quaternization reaction. Limited kinetic data for the synthesis of ILs hinders their efficient laboratory-scale, as well as widespread use. Only a few literature studies report quantitative kinetic constants for the production of ILs. Common IL parent cations classes include imidazolium, pyridinium, pyrrolidinium, phosphonium, and ammonium cations. Most investigations reported in the literature are focused on imidazolium-based ILs.

The myriad possible combinations of these cations and anions (an extensive array of options) warrant an understanding of the use of empirical methods to estimate IL data. It is impossible to experimentally test all these systems, hence, an in depth chemical understanding is necessary for performing rapid optimization searches for ILs with prime properties for given applications. Empirical expressions can enable researchers to utilize quantitative kinetic data in predicting time needed for desired conversions, while optimizing for solvent and temperature, in order to make more informed decisions regarding IL synthesis. Additionally, kinetic data is necessary for reaction engineering implemented for large scale production of ionic liquids that will inherently drive lower

costs for ILs. While many factors come into play in the selection of green solvents, high kinetic rates and yields remain priorities in the production of any chemical. Additionally, early stage solvent selection heuristics must also consider product recovery/separations; human/environmental impact of the solvent is also a crucial part of designing a sustainable processes. We find that some environmentally benign solvents may yield slow reaction rates in energy-intensive separations processes; a balance must thus be found between human and environmental impact and economics (yield, cost, energy for separation) for a given process. In chapter 7, we revisit this concern in detail.

In this section, we focus on optimal solvent selection, based heavily on productivity/high reaction rate, via a meta-heuristic approach: understanding molecular level phenomena such as polarity/solvent effects, steric hindrance, leaving group effects on IL synthesis reaction. The emergence of green chemistry morphs traditional perspectives, forcing researchers to look at "old" chemistry in new light. Menshutskin reactions between amines and alkyl halides are well-studied in the chemistry literature, long before the rise of ILs in importance [3-7]: investigations at the time were far from concerned about the "green" production of IL. Recently, our group presented Kamlet-Taft parameters in a LSER regression that quantitatively correlated the kinetics of reaction with solvent parameters. Here, we extend that work to the pyridinium and methylpyrrolidinium IL classes. The quantitative 2^{nd} order kinetic rate constants for these systems in various solvents at 25°C, 40°C, and 60°C were obtained and are reported here. In all, this chapter presents kinetic data for the synthesis of:

- 1-hexyl-pyridinium bromide [HPyrid][Br]

- 1-hexyl-1-methylpyrrolidinium bromide [HMPyrrol][Br]
- Several 1-alkyl-3-methyl-imidazolium halide ILs with different alkyl halides
- Solvent ratio effect on a model IL synthesis.

Empirical LSER expressions obtained here are useful for quick rate of reaction estimates for IL systems where no such data is available; this will expedite development of future IL applications. Chemical structures for compounds studied in this chapter are illustrated in Figure 5. 1.

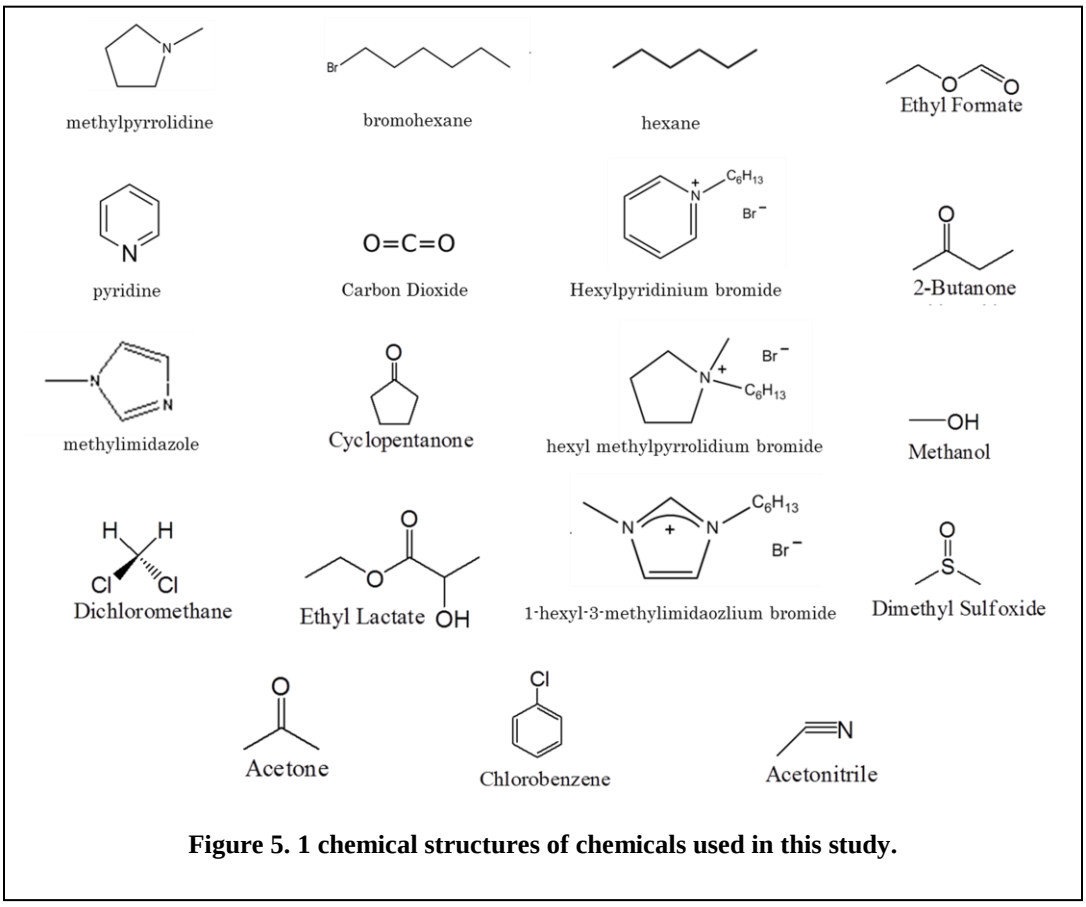

Figure 5. 1 chemical structures of chemicals used in this study.

5.2.Kinetic Theory: an Overview

The classical Arrhenius equation shows rate of reaction dependence on temperature. Arrhenius argued that reactants must overcome an energy barrier, known as the activation energy (E_a), to transform into products. This minimum energy can be justified by kinetic theory from statistical mechanics. Molecules react if they collide along their lines-of-center with a relative kinetic energy that exceeds E_a. At higher temperatures, the molecules in a solution have greater kinetic energy, and thus collide much faster, lowering the overall activation energy of the system. This can be expressed as:

$$k = k_o \exp^{\left(-\frac{E_a}{RT}\right)} \qquad \text{Eqn 5. 1}$$

where E_a is the activation energy, R is the gas constant, T is temperature, and k_o is the frequency factor (a measure of the frequency of collisions between the reactant molecules).

5.3. Solvent Effects: an Overview

The IL alkylation synthesis reaction proceeds via a Menchutskin-type second-order nucleophilic substitution (S_N2) reaction. Menchustkin's work demonstrated solvent effects on the quaternization reaction of triethylamine and iodoethane in 23 solvents.[8] He showed that these types of reactions (tertiary amines with primary haloalkanes) are

dramatically influenced by solvent choice. Since this work, these types of effects have been extensively studied and published in the chemistry literature. The transition state theory is a widely accepted justification for solvent effects in homogeneous chemical reactions.[1, 9-11] It states that solvents can modify the Gibbs energy of activation by differential solvation of the reactants and the activated complex. Reactants must first get to a higher energy state (transition state) to proceed. Solvents can alter the Gibbs energy of activation ($\Delta G^{\neq}$) via enthalpic and entropic effects, affecting the chemical reaction. The $\Delta G^{\neq}$ can be altered when reactants' energy is stabilized /destabilized by solvation, or when the activated complex is stabilized /destabilized, also by solvation at the transition state (See Figure 5. 2[1]).

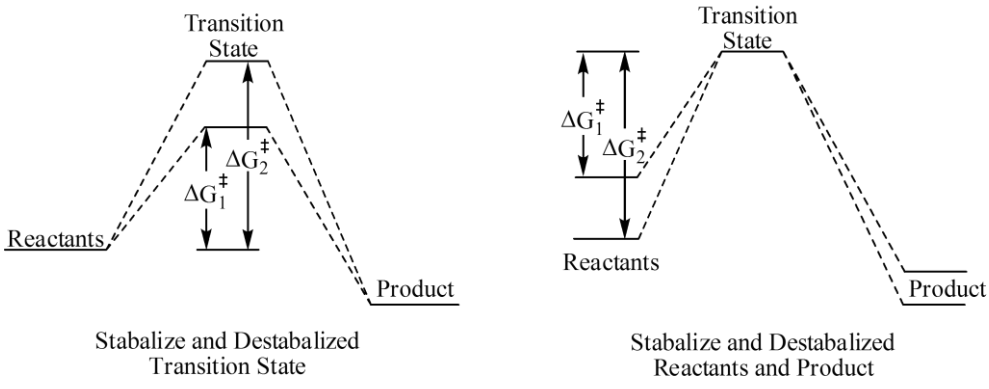

Figure 5. 2 Gibbs Free Energy of transition**[1]**

Reichardt[12] illustrates this theory using a hypothetical reaction,

$$A + B \leftrightarrow (AB)^{\neq} \rightarrow C$$

The transition state theory assumes that the reactants and activated complex are in pseudo-equilibrium, so that the rate constant for the transition state is:

$$K^{\neq} = \frac{a_{(AB)^{\neq}}}{a_A a_B} \qquad \text{Eqn 5. 2}$$

where *a* represent activities or adjusted composition, accounting for non-ideality. The theory also assumes that the formation of products does not affect the equilibrium between the reactants and the transition state. The reaction rate is determined by the rate at which the activation complex energy barrier is overcome in the direction of product formation. Hence, the reaction rate *k* is proportional to $K^{\neq}$, and from statistical mechanics [1, 9], can be related per

$$k = \frac{k_B T}{h} K^{\neq} \qquad \text{Eqn 5. 3}$$

where k_B is the Boltzmann's constant, *k* is the rate constant, and *h* is Planck's constant. From Eyring's equation, equilibrium constants can be expressed as [1, 9]

$$\Delta G^{\neq} = \Delta H^{\neq} - T\Delta S^{\neq} = -RT \ln K^{\neq} \qquad \text{Eqn 5. 4}$$

where $\Delta G^{\neq}$ is the Gibbs free energy of activation, $\Delta H^{\neq}$ is the Enthalpy of activation, $\Delta S^{\neq}$ is the Entropy of activation, *T* is temperature, *R* is the gas constant, and $K^{\neq}$ is the thermodynamic equilibrium constant for the activated complex. Combining both equations, *k* can be expressed as [1, 9]

$$k = \frac{k_B T}{h} \exp\left(-\frac{\Delta H^{\neq}}{RT}\right) \exp\left(\frac{\Delta S^{\neq}}{R}\right) \qquad \text{Eqn 5. 5}$$

This equation can be rearranged to the general linear form $y=mx+b$, as follows:

$$\ln\left(\frac{k}{T}\right) = -\frac{\Delta H^{\neq}}{RT} + \ln\left(\frac{k_B}{h}\right) + \frac{\Delta S^{\neq}}{R} \qquad \text{Eqn 5. 6}$$

5.3.1. **Hughes and Ingold Rules**

Hughes and Ingold used a simple qualitative solvation model to describe solvent effects. Hughes, Ingold *et al.*[1, 13-15] examined a number of organic substitution and elimination reactions for differences in rates of reaction, based on the charge difference (neutral, positive, or negative) between the reactants and activated complex. They show that all nucleophillic and elimination reactions can be classified based on the charge types of the reaction species. The Hughes Ingold rules can be summarized as follows [1, 13-15]:

(1) For a given chemical reaction, an increase in solvent polarity will result in an increase in reaction rate if the charge density in its activated complex (transition state) is greater than the initial reactants.

(2) An increase in solvent polarity will decrease the rate of reaction, if the charge density is lower in its activation complex than in the initial reactants.

(3) There will have no solvent effect on a chemical reaction where the charge density of its activated complex is similar to that of the initial reactants.

5.3.2. **Solvent Effects and Polarity Scales Overview**

Menshutkin demonstrated that the rate of reaction is influenced heavily by the "polarity" of the reaction mixture or solvent.[16, 17] This bimolecular second order (S_N2) proceeds

by a nucleophilic back-side attack by the entering atom, which has an unshared pair of electron and readily donates in the bond formation (illustrated in Figure 5. 3).

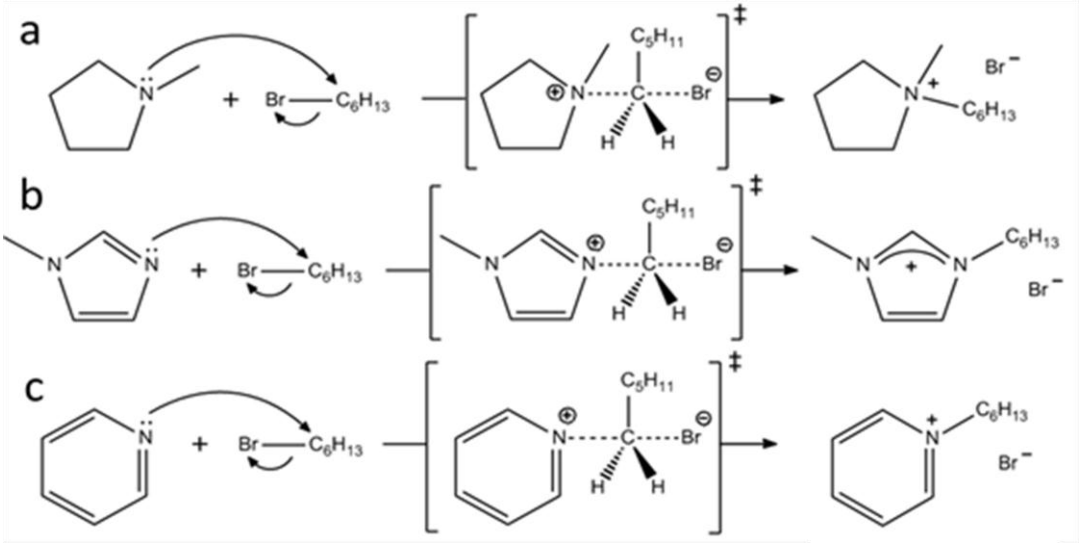

Figure 5. 3 Transition state for the reaction between methylpyrrolidine (a), 1-methylimidazole (b) pyridine (c) and 1-bromohexane.

Polarity effects are encountered when polar transition state of a reaction, interact with a solvent media through dipole-dipole mechanisms, as well as the charge formed on the leaving halide group interacting with solvent e.g. hydrogen bonding, etc.. Solvent "polarity" is defined by several different properties of solvent *viz* dipole moment, dielectric constant, hydrogen bond accepting ability, polarizability, etc. Solvatochromic scales are used to quantify various solvent properties. Solvatochromic parameters are indicative of certain solute/probe-solvent interactions and have been used to describe polarity. Although one-parameter scales for polarity, such as dipole moment, dielectric

constant, the $E_T(30)$ scale, etc.[1, 18, 19] have been found to qualitatively correlate rate constants, they are often not sufficient to quantitatively correlate reaction rates. Kosower presented a correlation between Z –value and *log k* for Menchutskin; however, it was limited to alcoholic solvents.[6] The Z- value is defined as the transition energy for the longest wavelength absorption band observed for 1-ethyl-4-cabomethoxypyridinium iodide) in a solvent. Abraham[20], in a study with 68 solvents, found that under half of the solvents were rationalized with the electrostatic continuum effect, hence the need to employ additional methodologies that account for other effects such as polarizability, hydrogen bonding, charge-transfer interactions etc.

Kamlet Taft (*KT*) parameters differentiate various independent solute-solvent interactions, *viz.* acidity (α), basicity (β), and dipolarity/polarizability (π^*), that sum "polarity". Linear Solvation Energy Relationships (LSERs) such as solubility of a solute, thermodynamic properties, and rates of reaction correlate well with Kamlet and Taft, this has been widely applied. [21-24] The LSER method performs the regression to correlate the physicochemical property such as kinetic rate constants, *k*, with the solvent-dependent physicochemical properties, α, β, and π^*:[12]

$$XYZ = XYZ_o + a\alpha + b\beta + p\pi^* \quad \text{Eqn 5. 7}$$

where the magnitude of the solvent-dependent physicochemical property are given by *XYZ* (for a given solvent) and *XYZo* (in a reference solvent). Coefficients, *a*, *b*, *p*, and *d* quantify the susceptibility of the property to the independent parameters (acidity α, basicity β, and dipolarity/polarizability π^*). In this study, *KT* parameters are used to

describe polarity effects on kinetic rate constants, the form of $XYZ = XYZ_o + a\alpha + b\beta + p\pi^*$ Eqn 5. 7 utilized is:

$$\ln k = \ln k^o + a\alpha + b\beta + p(\pi^* - d\delta) \qquad \text{Eqn 5. 8}$$

Regressed coefficients, *a, b, p,* and *d* quantify the effect of the different constituents of polarity on kinetic rate. δ is the polarizability correction term, which is equal to 0.0 for non-chlorinated solvents, 0.5 for polychlorinated solvents, and 1.0 for aromatic solvents. [22]

5.4. Solvent Effects in Synthesis of Halide ILs

Several studies have shown that the kinetic rate constant for these types of reactions strongly correlate with polarity parameters (e.g. Kamlet Taft). Recently, our group published K-T parameter regressed expressions for the synthesis of [HMim][Br] of 1-methylimidazole and 1-bromohexane, in 20 solvents.[2] The study showed that kinetic rate constants are strong functions of the dipolarity/polarizability parameter (π^*) and the basicity (β), but are negatively affected by acidity (α). For instance, reaction rates in methanol, despite the large dipole moment and high π^* and β, were among the slowest, due the solvent's high α (hydrogen bond donating ability). In this section we extend this investigation to the reactions of 1-bromohexane with (1) pyridine and (2) n-methylpyrrolidine. *KT* parameters of reactants and solvents are summarized and presented in Table 5. 1 for reference.

Table 5. 1 Kamlet Taft Parameters[a]				
Solvent[a]	α	β	π^*	$E_T(30)$ (kcal mol^{-1})
Dimethyl Sulfoxide	-0.013 ± 0.003	0.724 ± 0.009	1.032 ± 0.004	45.11 ± 0.02
Acetonitrile	0.230 ± 0.009	0.376 ± 0.012	0.787 ± 0.012	45.62 ± 0.02
Cyclopentanone	-0.085 ± 0.005	0.565 ± 0.004	0.748 ± 0.003	39.85 ± 0.01
Acetone	0.110 ± 0.002	0.523 ± 0.012	0.715 ± 0.002	42.58 ± 0.03
2-Butanone	0.053 ± 0.004	0.568 ± 0.004	0.675 ± 0.002	41.06 ± 0.06
Dichloromethane	0.042 ± 0.003	-0.020 ± 0.014	0.790 ± 0.004	40.88 ± 0.02
Ethyl Formate	0.094 ±0.035	0.412 ± 0.075	0.570 ± 0.042	40.19 ±0.11
Chlorobenzene[a]	0.051 ± 0.004	0.080 ± 0.009	0.624 ± 0.004	36.91 ± 0.02
Ethyl Lactate	0.642 ± 0.004	0.633 ± 0.010	0.689 ± 0.002	51.01 ± 0.04
Methanol	0.909 ± 0.006	0.629 ± 0.009	0.697 ± 0.006	55.53 ± 0.04
1-methylimidazole	0.232 ± 0.012	0.712 ± 0.016	0.961 ± 0.014	44.85 ± 0.01
1-bromohexane	0.014 ± 0.07	-0.009 ± 0.011	0.500 ± 0.01	37.9± 0.70
Pyridine[b]	0.00	0.64	0.87	40.5
a Taken from ref .[25] and b Taken from ref.[12]				

5.4.1. **Solvent Effects in Synthesis of Hexyl Pyridinium Bromide**

Pyridinium ILs are thought to have less environmental impact than their imidazolium counterparts. This is mainly based on the fact that pyridinium ILs are more biodegradable by comparison.[26] These environmental advantages have increased the level of interest in this class of IL. Further, Pyridinium-based ILs are currently a lower-cost alternative to imidazolium-based ILs.[27] Pyridinium salts have been employed in antimicrobial applications, as cationic surfactants, polymer components, chromatographic supports, and as reagents in catalysis. Additionally, this class of IL has excellent thermal stability: in particular, dimethylaminopyridinium bis(trifluoromethylsulfonyl)imide salts are confirmed to have the best thermal stability of all ILs experimentally investigated to

date.[28] This particular property fosters technology development using this IL class in applications where thermal stability is imperative or at the forefront, driving demand. As they are generally more viscous than the equivalent imidazolium compounds[28], the need for, and choice of, an optimal solvent for processing pyridinium salts is critical. Pyridinum ILs can be synthesized from halide precursors, such as 1-hexyl-pyridinium bromide [HPy][Br], used in this study (see Figure 5. 4).

The reaction between pyridine and alkyl halide is a well-studied Menshutskin model reaction[3-7], a "guinea pig" system for classical solvent effect investigation. The reactivity of pyridine has long been explained using LSER relationships. One such study by Elshafie and Fouli [29] presents nucleophilic rate constants for pyridine, piperidine, 2,4,6-trimethyl pyridine and 2,3,4 picolines with ethyl iodide in different aprotic and protic solvents, using Kamlet Taft (*KT*) parameters α, β, and π^*. Hossain and Morshed[30] studied the reaction between pyridine and benzyl bromide in methanol, acetone and acetonitrile: they found the order of reactivity to be acetonitrile>methanol> acetone. Reinheim et al., [31] studied the rate of the reaction of pyridine with ethyl bromide and ethyl iodide in benzene, chlorobenzene, bromobenzene, and iodobenzene. The rate constant increase was proportional to the polarizability of the solvent, attributed to the interaction of the solvent with the leaving halide in the transition state. Kondo *et al.*,[5] studied the reaction of triethylamine and pyridine with methyliodide in an acetonitrile and methanol mixture using linear correlation free energy.

We present solvent effects on the kinetics in the synthesis of [HPy][Br] in a wide variety of conventional and low-toxicity organic solvents. Figure 5. 5 shows conversion over time obtained from a typical run of 1-bromohexane and pyridine at 40^{o} C in acetonitrile. When benzylbromide and pyridine are reacted in the methanol[30], previous studies showed methanolysis occurring simultaneously with the desired Menchshutskin reaction. NMR verification indicates that no such reactions occurred for 1-bromohexane systems in this study. Our results will demonstrate that greener solvents can be utilized for producing ILs while optimizing for high rates of reaction.

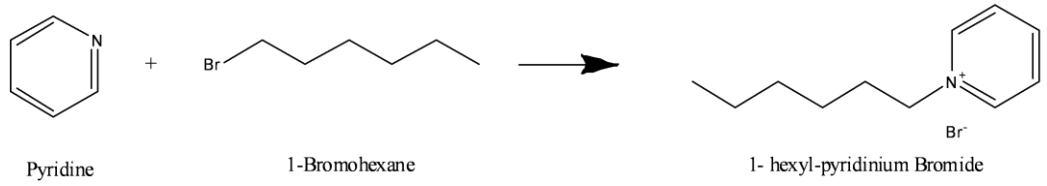

Figure 5. 4 Reaction between pyridine and 1-bromohexane forming 1-hexyl-pyridinium bromide [HPyr][Br].

For each reaction system, the mole ratio of reactants to solvent was maintained at 1:1:20 to avoid concentration effects on the bulk polarity from the reactant and/or product. The reaction was conducted at three different temperatures (25°C, 40°C, and 60°C) and the data regressed to obtain Arrhenius parameters. All rates of reaction at 25°C, 40°C, and 60°C were regressed assuming 2^{nd} order kinetics and are presented in Table 5. . Similar to what obtained for the synthesis of [HMim][Br][2] and [BMim][Cl][32], two phases (IL-rich and reactant/solvent-rich) were observed at conversions greater than 6% in the chlorobenzene solvent system. With higher conversions, a sonicator was used to ensure

proper mixing before taking a uniform sample that is later dissolved in solvent forming a homogeneous mixture. Of all the solvents studied, the rate of reaction was greatest in DMSO and slowest in chlorobenzene; the rate constant with DMSO was more than two orders of magnitude higher than that of chlorobenzene. The natural log of *k* was fit to the LSER coefficients based on the *KT* parameters (acidity α, basicity β, and dipolarizability π^*, as previously described) and are as follows:

$25\ ^{o}C \quad \ln k = -19.58 + 0.10\alpha - 1.61\beta + 8.50(\pi^* - 0.22\delta) \qquad R^2 = 0.9876 \qquad$ Eqn 5. 9

$40\ ^{o}C \quad \ln k = -18.88 + 0.35\alpha - 2.58\beta + 9.84(\pi^* - 0.22\delta) \qquad R^2 = 0.9887 \qquad$ Eqn 5. 10

$60\ ^{o}C \quad \ln k = -17.29 + 0.66\alpha - 2.42\beta + 9.71(\pi^* - 0.16\delta) \qquad R^2 = 0.9933 \qquad$ Eqn 5. 11

Experimental data correlated well with calculated data, evidenced by R^2 values close to unity, and illustrated in Figure 5. 6. From the regression expressions above, observe that the π^* parameter (dipolarity/polarizability) has the largest positive effect on the reaction rate, followed by the α parameter (acidity). The β parameter (basicity) has a negative effect on the rate of reaction. For an optimal reaction rate, a solvent with a high π^* and α should then be chosen. Kamlet-Taft parameters in a LSER regression can quantitatively correlate the kinetics of reaction with the K-T parameters of the solvent. Table 5. lists the solvents investigated for 1-bromohexane with pyridine, in order of decreasing rate of reaction.

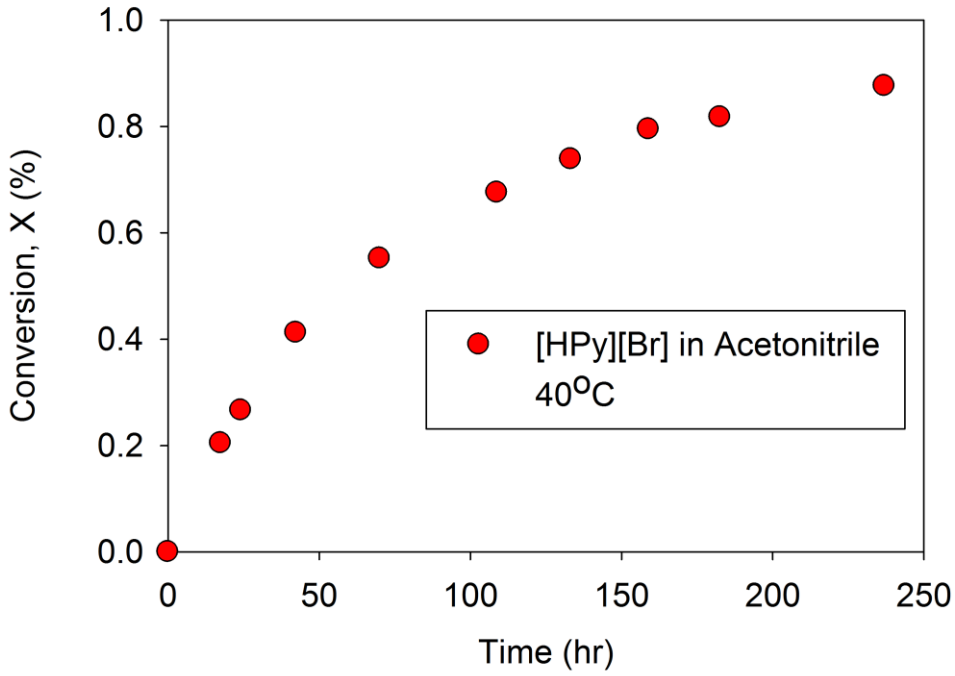

Figure 5. 5 Concentration versus time for the formation of [HPy][Br] in acetonitrile at 40°C, Cpyridine,0=0.454 mol/L

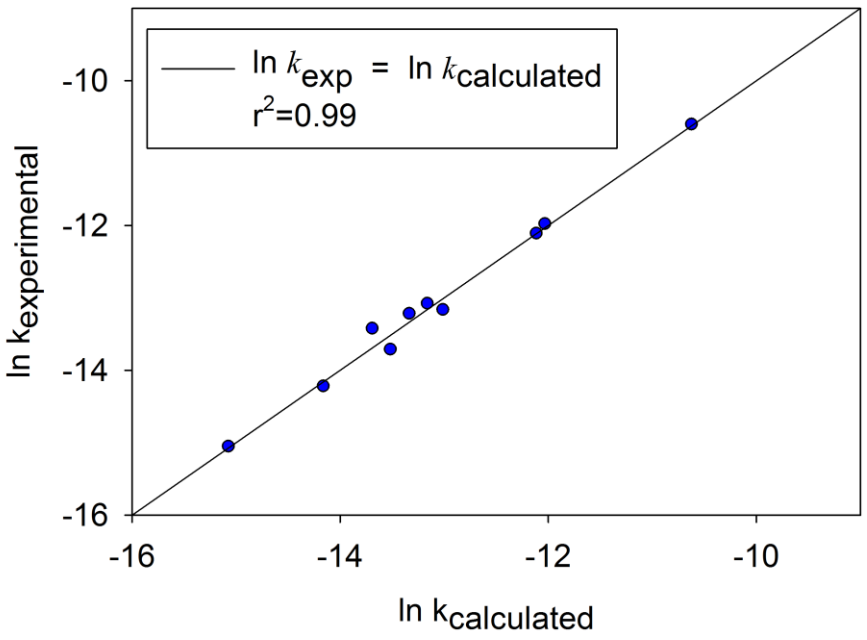

Figure 5. 6 LSER results for the synthesis of [HPy][Br] in 10 different solvents at 40°C.

Table 5. 1. Rates of reaction and kinetic parameters.

	k x10^7 [M^{-1} sec^{-1}]			k_o x10^{-7}	E_a	$\Delta H^{\ddagger}$	$\Delta S^{\ddagger}$
Solvent	25°C	40°C	60°C	[$M^{-1}sec^{1}$]	[kJ/mol]	[kJ/mol]	[J/mol/K]
DMSO	65.33± 2.06	246.00±	1180.00 ± 130[b]	0.60	68.27	65.65	-123.96
Acetonitrile	16.67±0.99	62.30±2.33	306.00±0.57	0.18	68.68	66.06	-134.00
Dichloromethane	9.36±0.21	54.50±6.19	[b]	873.85	91.16	88.62	-63.11
Acetone	5.91±0.07	20.70±0.23	[b]	0.01	64.84	62.30	-155.20
Cyclopentanone	5.72±0.37	19.00±0.39	103.00±6.23	0.05	68.39	65.77	-144.21
Methanol	4.83	18.00±0.09	101.00±16.00	0.18	71.84	69.22	-133.90
2-Butanone	4.34	14.70±0.58	191.00±4.74	211.01	90.00	87.38	-75.19
Ethyl Lactate	3.62	11.00±2.43	89.40±9.2	0.70	76.15	73.53	-122.67
Ethyl Formate	2.52	6.61±0.12	[b]	0.00	49.91	47.37	-212.38
Chlorobenzene[c]	0.93±0.03	2.88±0.36	24.30±0.47	0.32	77.60	74.98	-129.15

a.) Reaction conducted at 1:1:80 mole ratio pyridine:1-bromohexane:dimethyl sulfoxide due to high exothermicity of more concentrated solutions. b.) Exceeds boiling point of solvent; c.) Mixture split into two phases during reaction.

5.4.2. Solvent Effects on Rate Constant in the Synthesis of 1-hexyl-methylpyrollidium Bromide

Cho *et al.*, [33] found methylpyrrolidinium bromide least toxic compared to the toxicities of tetrabutylphosphonium, tetrabutylammonium, 1-butyl-3-methylimidazolium and 1-butyl-3-methylpyridinium bromides. Only a few studies have considered synthesis of the pyrrolidinium class of ILs despite the fact that these classes of IL are important solvents, owing to their electrolytic stability and electronic conductivity being higher than those of many other liquids. Solvent effect studies were extended to the synthesis of the IL 1-hexyl-1-methylpyrrolidinium bromide [HMPyrrol][Br]. This reaction proceeds as illustrated in Figure 5.7.

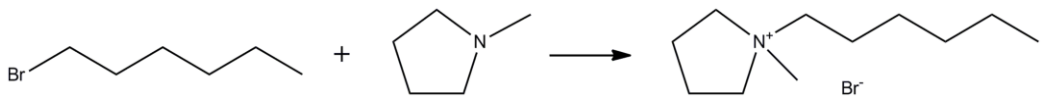

Figure 5. 7 Reaction Between 1-Methylpyrrolidine and 1-Bromohexane forming 1-Hexyl-1-methylpyrrolidinium bromide [HMPyrrol][Br]

Figure 5.8 illustrates a typical reaction conversion over time for 1-Hexyl-1-methylpyrrolidinium bromide [HMPyrrol][Br] synthesis in methanol at 25°C. In this study, four solvent routes were used, namely DMSO, acetonitrile, acetone, methanol, as well as the neat reaction. DMSO was the fastest solvent medium for this reaction; methanol was the slowest. The experimentally obtained rate constants were regressed with K-T parameters to yield:

$25\ ^{o}C$ $\ln k = -14.59 - 1.48\alpha - 4.71\beta + 10.72\pi^{*}$ $R^2 = 0.9999$ Eqn 5. 12

$40\ ^{o}C$ $\ln k = -13.44 - 0.09\alpha - 4.99\beta + 10.34\pi^{*}$ $R^2 = 0.9999$ Eqn 5. 13

$60\ ^{o}C$ $\ln k = -13.55 + 0.94\alpha - 5.10\beta + 11.76\pi^{*}$ $R^2 = 0.9999$ Eqn 5. 14

A strong correlation was attained (r^2 of 1), as illustrated in Figure 5.9. From regression expressions, the π^{*} parameter (dipolarity/polarizability) has the largest positive effect on the reaction rate, while the β parameter (basicity) has a negative effect on the rate of reaction. For an optimal reaction rate, a solvent with a high π^{*} and a low β should be selected. The resulting empirically derived LSER equations will accelerate quick generation of reaction rate constants needed for large scale production of methylpyrrolidinium ILs. The kinetic rate constants, activation energies and frequencies for the reaction in different solvents are shown in Table 5. 2.

Table 5. 2. Rates of reaction and kinetic parameters. [a]

	k x10[6] [M^{-1} sec^{-1}]			k_o x10^{-6}	E_a
Solvent	25°C	40°C	60°C	[M^{-1} sec^{-1}]	[kJ/mol]
DMSO	968.60 ± 235.23	1656.66± 84.93	5826.01 ± 1756.77[a]	0.027	42.73
Acetonitrile	257.69 ± 24.38	745.90 ± 21.36	2476.25± 353.0	0.579	53.35
Acetone	71.17 ± 6.28	172.08 ± 11.49	448.63 ± 24.35	0.003	43.38
Methanol	10.94 ± 0.10	78.60 ± 17.83	448.53 ± 51.90	23200	87.23
Neat[b]	[c]	2.91 + 0.01	[c]		

a)1-Methylpyrrolidine:1-bromohexane :20 Solvent mole ratio b) 1-Methylpyrrolidine:1-bromohexane = 1:1 by mole. c) Neat reaction only performed at 40°C to due to poor mixing in solid phase reaction mixture

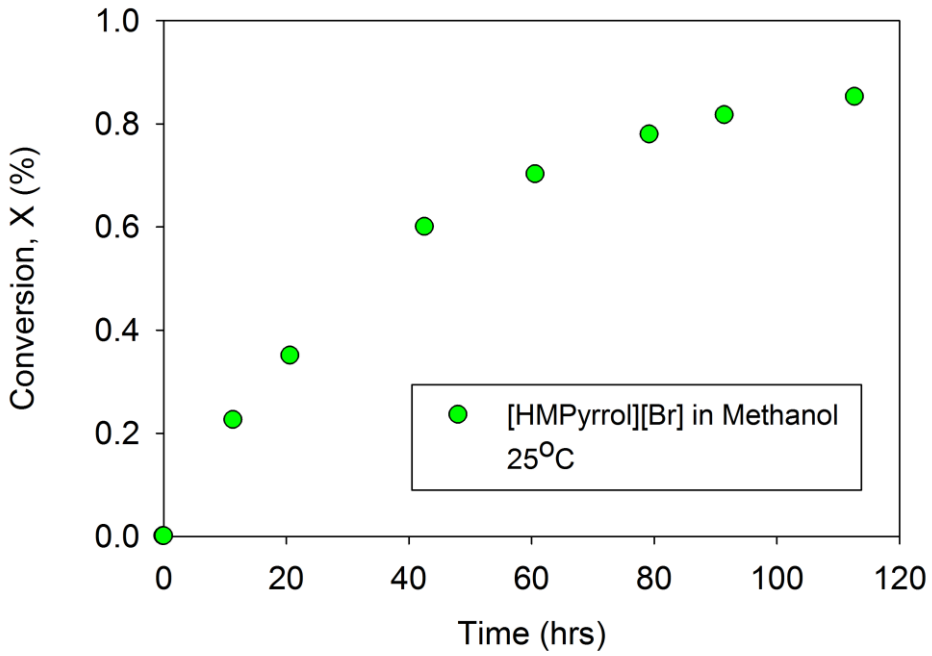

Figure 5.8 Conversion versus time for the formation of [HMPyrrol][Br] in Methanol at 25°C, CMPyrrol,0 = 0.944 mol/L

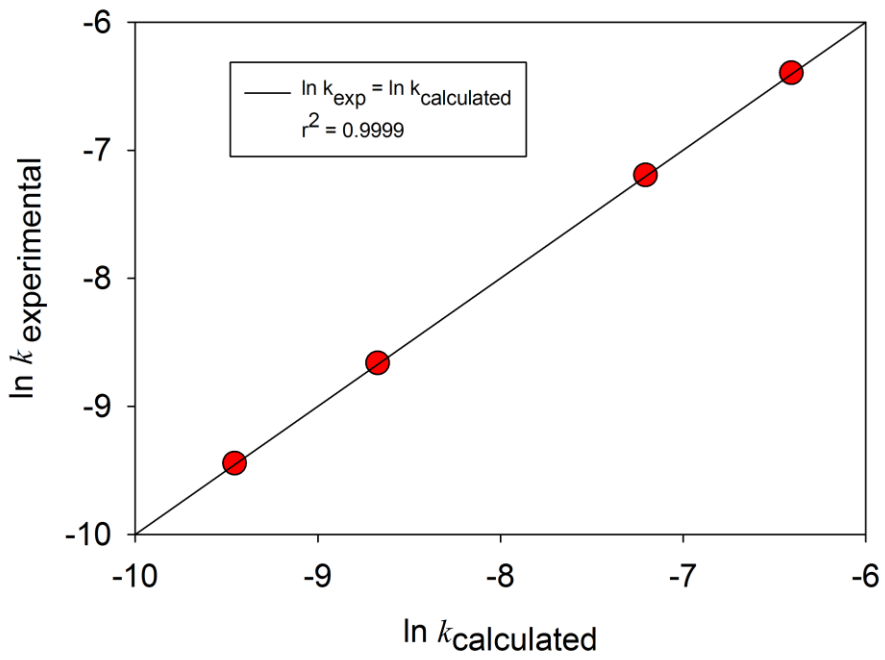

Figure 5.9 *k* computed from LSER equations with kexperimental for the 10 solvents used in this study at 40°C.

The neat scenario was the slowest observed. In the neat run, the solid IL forms rapidly, falling out of solution; at higher conversion, mixing becomes very difficult. Melting point of the pure IL was investigated to shed light on optimal reaction conditions for a neat scenario. The melting point of hexylmethylpyrrolidinium bromide was determined. The IL sample used for melting point determination was synthesized via a neat reaction with excess 1-methylpyrrolidine. At greater than 99% conversion, the IL was purified using $ScCO_2$ at 60°C and 150 bar. In addition, hexylmethylpyrrolidinium bromide synthesized from a neat reaction of equimolar amounts of 1-methylpyrrolidine and 1-bromohexane, and without CO_2 purification treatment, was also measured. Results are summarized in Table 5. 3. The melting point data was found to be very sensitive to the purity of the IL.

We observed that trace amounts of the reactants changed the melting point dramatically. This is will be very important when condensation methods (typically used for solid ILs) are used for product recovery of this IL.

Table 5. 3 Hexylmethylpyrrolidinium Bromide Melting Point

Sample	Temperature (°C)
Not Purified	161.7 ± 0.58
CO_2-Purified	137.3 ± 2.89

5.4.3. **Solvent Effects: Summary**

From the three classes of ILs studied, 1-methylpyrrolidine had the highest reaction rate. This can be explained by considering the effect of acid-base equilibria in these reactions; the nucleophilicity of the amine. For example, in acetoniritile solvent at 40^{o}C, the reaction rate constant for the synthesis reaction of the corresponding bromide IL with 1-bromohexane was 745.9 x 10^{-6} M^{-1} sec^{-1}, 21 x 10^{-6} M^{-1} sec^{-1} and 6.2 x 10^{-6} M^{-1} sec^{-1} for methylpyrrolidinium, 1-methylimidazole and pyridine respectively. These three nitrogen-containing reactants are Lewis bases, which donate a pair of electrons to a Lewis acid (in this study, 1-bromohexane) to form a conjugate acid and base, respectively. For these S_N2 type reactions, a lower transition state energy is realized when the electron pair is donated easily, thus, a faster rate of reaction. Sloan and Koch[37] found that reaction rates of different amines with (acyloxy)alkyl α–halides depend on both the nucleophilicity of the amines and the leaving group ability of halides. For example, in methanol, they found that the order of nucleophilicity was piperidine ($n_{CH_3I} = 7.30$) > pyrrolidine ($n_{CH_3I} = 7.23$) > imidazole ($n_{CH_3I} = 4.97$) when CH_3I was the leaving group. Also, Elsaffie and Fouli

[29] found that the rate constant for the reaction of piperidine with ethyliodide in DMSO was much faster than other pyridines because of piperidine high basicity.

This study covers reasonable temperature range for potential syntheses, as well as a variety of solvents. As expected, the reaction rates increased with temperature for all systems. In aprotic solvents such as DMSO or acetonitrile, the nitrogen free electron pair do not hydrogen bond compared to a protic solvent such as methanol. For instance in methanol, solvation by hydrogen bonding contributes to the inaccessibility of the nitrogen free electron pair by the alkyl group.[20, 38] Consistently, polar aprotic DMSO was found to have the fastest reaction rate for all three classes of ILs considered. Acetone, an aprotic solvent, still ranks as a relatively good candidate for the synthesis of pyridinium and pyrrolidinium halide ILs. These findings corroborate our group's previous findings for imidazolium systems.

Due to the formation of solids in the neat reaction, the two model ILs systems studied here, *viz* [HMPyrrol][Br] and [HPy][Br], reinforce the importance of using solvents for synthesis, unless the reactor used is kept at a temperature well above the melting point of the IL (in these cases, temperatures far in excess of 100°C). This study furnished substantial kinetic rate constants and engineering parameters needed for efficient reactor design.

5.5. Steric, Electronic and Chain Length Effect on Menchutskin Reactions

Here, the synthesis of 1-alkyl-3-methyl-imidazolium ILs will be investigated with a variety of alky halide substituents. While the 1-hexyl-3-methyl-imidazolium cation is often used for a variety of chemistries and applications, there are numerous other types of substituents (*R*-groups) that are desirable for influencing the different IL physical and chemical properties from a variety of starting materials. While the qualitative effects on S_N2 reaction rates of the structure, sterics, and electronics of alkyl halides with amines (imidazole, pyridine, etc.) are generally well known in organic chemistry, the quantification of kinetic rates is equally important for efficient IL synthesis, and eventual scale-up, for production. The investigation will quantify the effect of the choice of alkyl halide, sterics, alkyl-chain length, and, importantly, the reactant concentration and ratio.

5.5.1. Steric, Electronic, and Chain-length Effects in Ionic Liquids Synthesis

Recently, there have been a number of qualitative literature reports on the synthesis of a variety of both imidazolium and pyridinium ILs with various chain lengths, leaving groups and branched or chiral R groups.[39-42] Appetecchi *et al.* [39], published a study on the effect of the alkyl side group on the synthesis and the electrochemical properties of N-alkyl-N-methylpyrrolidinium bis(trifluoromethanesulfonyl)amide ILs. The study employed side alkyl groups of different lengths and structure for the synthesis of $[PyrrR_1][Tf_2N]$ ILs. Erdmenger *et al.*[40], also synthesized new branched ILs 1-(1-ethylpropyl)-3-methylimidazolium and 1-(1-methylbenzyl)-3-methylimidazolium to study the role of different branched alkyl side chains on imidazolium-based IL

properties. However in these studies, kinetic rate data were not reported. S_N2 reactions, as found in most synthesis methods of ILs, depend on a large number of factors, including the nature of the leaving group, the relative reactivity of the nucleophile, and the structure/sterics of the alkyl group.[43] Again, the qualitative trends are largely known, but the quantification of these is highly important to general research and production of ILs alike.

5.5.2. **Leaving Group**

The effect of the leaving group on the kinetic rate constant was investigated with halo-hexanes at 40°C, both in the neat reaction and in acetonitrile. From previous work with imidazolium synthesis, polar aprotic solvents such as acetonitrile yielded higher reaction rates.[2] Figure 5.10 illustrates the conversion over time for the reaction of 1-methylimidazole and 1-iodohexane in solvent-free conditions at 40°C. The reaction exhibits classic 2^{nd} order behavior, and the second order rate constant is obtained from non-linear regression of the experimental data. Table 5. 4 illustrates the kinetic rate constants for the reaction of 1-halo-hexane with 1-methylimidazole, to produce 1-hexyl-3-methyl-imidazolium chloride ([HMIm][Cl]), 1-hexyl-3-methyl-imidazolium bromide ([HMIm][Br]), and 1-hexyl-3-methyl-imidazolium iodide ([HMIm][I]). Reactivity was found to decrease in the following order: iodide (I) > bromide (Br) > chloride (Cl), along established halide leaving group order.

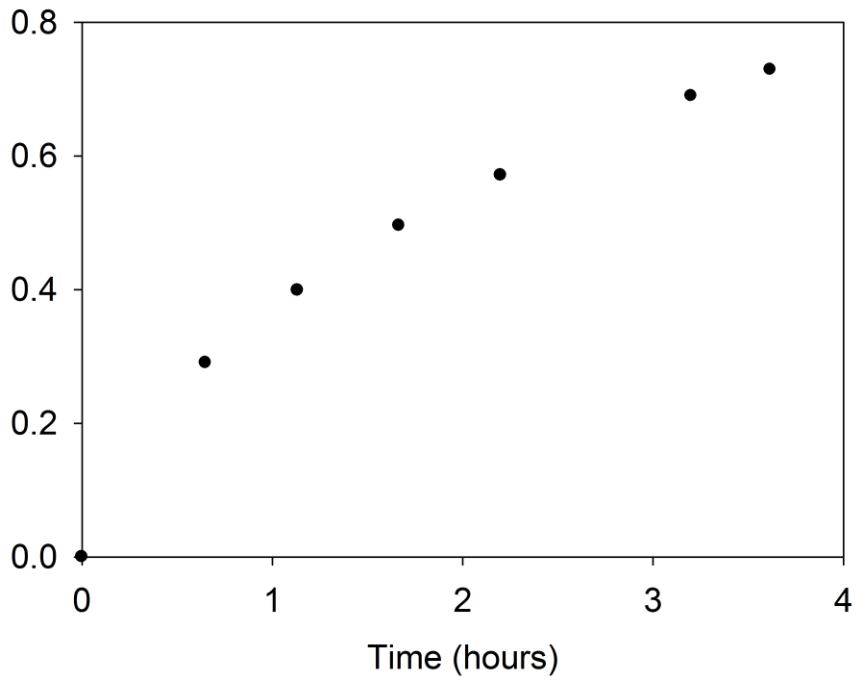

Figure 5.10 Conversion for the reaction of 1-methylimidazole and iodohexane with time at 40°C, CMIM,0= 4.49 mol/L

It is widely known that leaving-groups' abilities highly influence rates of reaction when operating under a second-order nucleophilic substitution (S_N2) reaction. Generally, good leaving-groups form weak conjugate bases for strong acids.[43] This is especially true for halogen leaving-groups. The kinetic rate with 1-iodohexane is over 436 times that of 1-chlorohexane, and more than 187 faster than that of 1-bromohexane in a neat reaction. This trend is expected, since the conjugate acids are in the order of strength HI > HBr > HCl, based on their respective dissociation constant (pK_a) values.[43] Sloan and Koch also found Menchutskin type S_N2 reaction are dependent on the leaving group ability of the halide.[37] As discussed previously[2], polar aprotic solvents produce kinetic rates

sometimes larger than even that of the neat reaction, as the second order rate constant is a strong function of polarity. Thus, the reaction rate in acetonitrile, with the solvent's high π^* and β, and low α, is significantly higher than even in the neat reaction (see Table 5. 5). The reaction with 1-iodohexane is approximately 93% faster in acetonitrile than in the solvent-free condition.

Table 5. 4. Leaving group effect on Rate Constants at 40°C.

	Neat		*Acetonitrile*[a]	
	k x 10^6 [M^{-1} sec^{-1}]	$k_{rel,\,Cl} = k / k_{Cl}$	k x 10^6 [M^{-1} sec^{-1}]	$k_{rel,\,Cl} = k / k_{Cl}$
1-chlorohexane	0.094 ± 0.002	1	0.179 ± 0.01	1
1-bromohexane	17.630 ± 0.060 [a]	187.6	21.56 ± 0.21	120.5
1-iodohexane	41.00 ± 2.090	436.2	79.25 ± 0.77	442.7

Concentration: 0.76 mol/liter (1:1:20 mole ratio, 1-methylimidazole:1-bromohexane:acetonitrile) at 40°C. [a] Ref. [2]

Table 5. 5. *KT* parameters of the reactant, solvent and product.

	Kamlet Taft Parameters[a]		
Solvent	α	β	π^*
Acetonitrile	0.230 ± 0.009	0.376 ± 0.012	0.787 ± 0.012
1-bromohexane	0.014 ± 0.07	-0.009 ± 0.011	0.500 ± 0.01
1-methylimidazole	0.232 ± 0.012	0.712 ± 0.016	0.961 ± 0.014
[HMIm][Br]	0.453 ±0.069	0.562 ± 0.066	0.983 ± 0.037

[a] Ref [2]

5.5.3. **Alkyl-Group Contribution**

The effect of chain length on the kinetic rate was measured: results are presented in Figure 5.11 for the reaction of 1-bromo-alkanes with 1-methylimidazole, in both acetonitrile and a neat reaction (no solvent). When S_N2 type reactions occur through a backside attack of the electrophile, the halo-alkane is often inverted, hindering the addition of methylene groups (i.e. extension of chain length) subsequently deterring the rate of reaction.[2] Figure 5.11 shows a 48% difference in reaction rates of 1-bromoethane and 1-bromopropane in the solvent. Beyond n-propyl-(C_3), incremental increases in methylene units result in only marginal decreases in the reaction rate. The neat reaction was not conducted with 1-bromoethane, due to its low boiling point of 38.4°C; however, boiling point elevation in acetonitrile allowed more facile measurement at 40°C. Generally, this reaction is faster in acetonitrile, although the solvation also seems to reduce the effect of the length of alkyl-group. However, the neat reaction with bromopropane was significantly faster than in acetonitrile. Numerous replicates (>10) were performed for this reaction, with a very small standard deviation. This trend is consistent for the neat reaction, where the rate constants with bromopropane and bromopentane are about 56% higher than that observed for bromodecane.

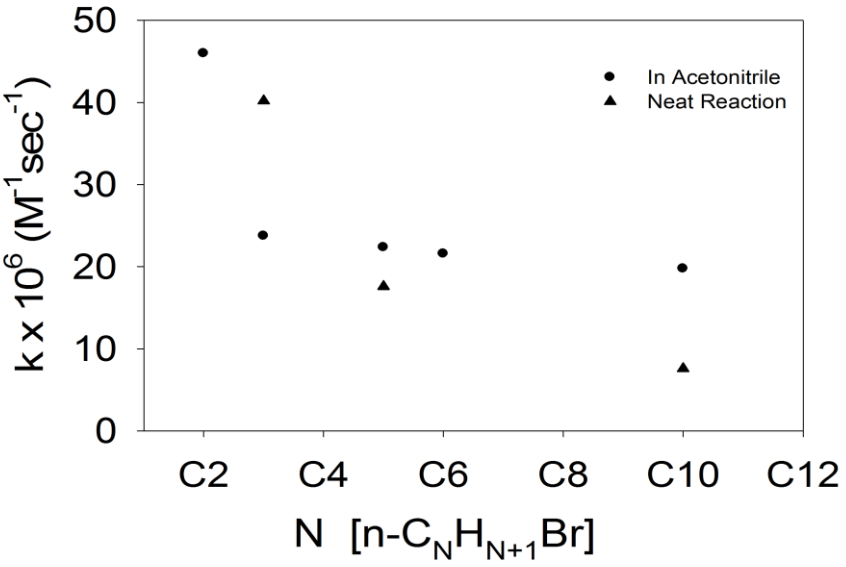

Figure 5.11 Rates of reactions with increasing alkyl chain length of 1-bromo-alkanes with 1-methylimidazole in acetonitrile[2] and solvent-free (neat). C2 is bromoethane, C4 is 1-bromobutane, etc.

5.5.4. **Steric Effects**

The kinetic rate constants of the reaction of 1-methylimidazole with five-carbon bromoalkanes (bromopentanes) were investigated and the results depicted in Table 5. 6. As shown, the location of the point of branching plays a significant role in the kinetic rate of reaction, corroborating a well-discussed trend in the literature.[44, 45] The kinetic rate with 2-bromopentane (racemic) is more than an order of magnitude lower than that observed for 1-bromopentane. As the point of branching (steric hindrance) is located further from the alpha carbon, towards the halide (e.g. 1-bromo-3-methylbutane), the

kinetic rate increases. The reaction with 2-bromo-2-methylbutane was observed over months: only an upper bound is given for the kinetic rate.

Table 5. 6. Reaction between 1-methylimidazole and a number of branched bromoalkanes at 40°C

1-Bromoalkane	Structure	*Neat* k x 10^6 [$M^{-1}sec^{-1}$]	*In Acetonitrile* k x 10^6 [$M^{-1}sec^{-1}$] **[2]**	$k_{rel}{}^{a} = k/k_0$
1-bromopentane	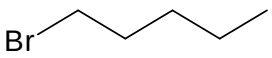	17.60 ± 0.35	22.35 ± 0.40	1
1-bromo-3-methylbutane	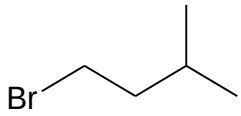	11.00 ± 0.10	14.73 ± 0.02	0.625
2-bromopentane	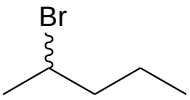	0.68 ± 0.07	1.13 ± 0.05	0.038
2-bromo-2-methylbutane	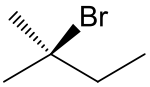	< 0.001	< 0.001	< 5.6 ×10^{-5}

Concentration of 0.76 mol/liter for both reactants. [a] Relative kinetic rate based on that for 1-bromopentane.

Unusually, an S_N1 mechanism has been suggested in the literature for the formation of 1-n-butyl-3-methylimidazolium chloride, as interpreted from transient intermediates observed via *in situ* IR spectroscopy.[46] If this were an S_N1 reaction, branching would stabilize the carbocation and increase the kinetic rate. However, our observations are consistent with a traditional S_N2 mechanism.[43] The reaction rate for experiments conducted in acetonitrile was found to be greater than the k values obtained for the neat version. For rac-2-bromopentane, the reaction was approximately 66% faster in

acetonitrile. However, for 1-bromo-3-methylbutane and 1-bromopentane, the increase was a more modest 30% (approximate). The reaction rate for the highly branched 2-bromo-2-methylbutane did not significantly increase over the course of a month of reaction and only an upper bound is given.

5.5.5. **Solvent Ratio Effect on Properties Kinetic Rate Constant**

Here we consider the effect of solvent ratio/concentration on engineering parameters for IL synthesis systems. We obtained kinetic and transport data (density, heat capacity, viscosity) for various acetone ratios at 50°C, 40°C and 25°C. Four different solvent ratios: 75%, 50%, 25%, and 10% were studied. For each system, i.e., molar ratio of acetone (x_{acetone} 0.00, 0.10, 0.25, 0.50, 0.75, 1.00), the ratio of the reactants are equimolar (1:1). We found a variation, by a factor of 4.3, in observed rate constants across the different systems: and this effect is more pronounced at 60^{o}C, higher temperature than at 40^{o}C as shown in Figure 5. 12.

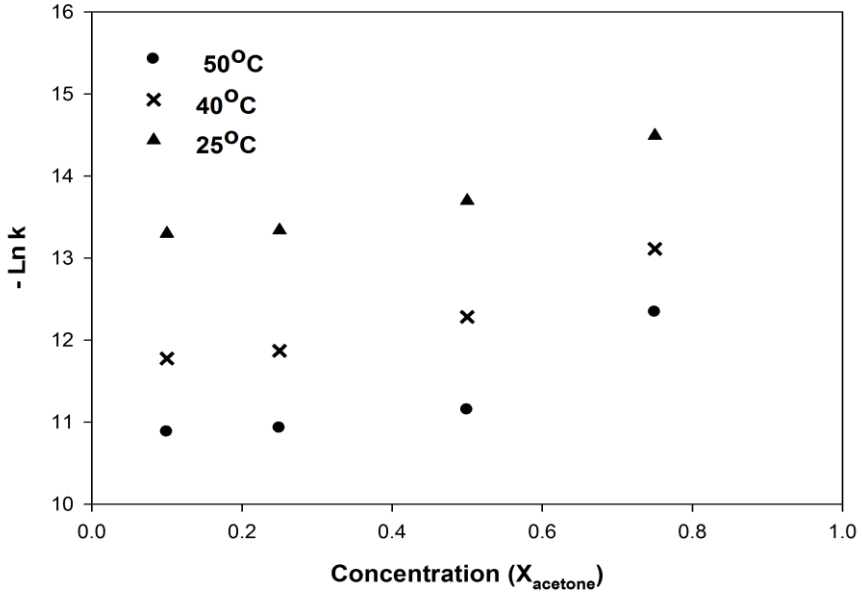

Figure 5. 12 Rate constant with concentration of acetone at 25 C, 40 C and 50 C

5.5.6. Steric, Electronic and Chain Length Effect on Menchutskin Reactions: Summary

There are numerous types of substituent (R-groups) that are desired for different physical and chemical properties of ILs, using a variety of different starting materials. The synthesis of 1-alkyl-3-methyl-imidazolium ILs was investigated with a variety of alky halide substituents. Factors such as the type of leaving group, the relative reactivity of the nucleophile, and the structure/sterics of the alkyl group were observed to affect the rate constant for the synthesis of the precursor imidazolium ILs. Reactivity was found to decrease in the following order: I > Br > Cl. The kinetic rate with 2-bromopentane

(racemic) is over an order of magnitude lower than with 1-bromopentane; both were much higher than the rate constant of 2-bromo-2-methylbutane.

Reference

[1] C. Reichardt, Solvent and Solvent Effects in Organic Chemistry 3ed., Wiley-VCH, Weinheim, Germany, 2003.

[2] J.C. Schleicher, A.M. Scurto, Kinetics and solvent effects in the synthesis of ionic liquids: imidazolium, Green Chem., 11 (2009) 694-703.

[3] M. Gonikberg, V. Zhulin, The pressure effect on the rate of Menshutkin Reactions, Australian Journal of Chemistry, 11 (1958) 285-289.

[4] R.R. Grimm, H.;Wolff, Z. phys. Chem.,'B, 13 (1931) 301.

[5] Y. Kondo, M. Ohnishi, N. Tokura, Solvent Effects under High Pressures. IV. A Procedure for the Estimation of Solvation in the Transition State, Bulletin of the Chemical Society of Japan, 45 (1972) 3579-3583.

[6] N. Pickles, C. Hinshelwood, 292. The influence of solvents on reaction velocity. The interaction of pyridine and methyl iodide and the benzoylation of m-nitroaniline, J. Chem. Soc., (1936) 1353-1357.

[7] H. Thompson, E. Blandon, 290. The mechanism of bimolecular reactions in solution. The addition of methyl iodide to pyridine in several solvents, J. Chem. Soc., (1933) 1237-1240.

[8] N. Menshutkin, Unknown, Z. Physik Chem., 5 (1890) 589.

[9] H. Erying, The activated complex and the absolute rate of chemical reactions, Chem. Rev., 17 (1935) 65-77.

[10] H. Eyring, The Activated Complex in Chemical Reactions, J. Chem. Phys., 3 (1935) 107-115.

[11] W.F.K. Wynne-Jones, H. Erying, The Absolute Rate of Reactions in Condensed Phases, J. Chem. Phys., 3 (1935) 492-502.

[12] C. Reichardt, Solvents and solvent effects in organic chemistry, 3rd ed., Wiley-VCH, Weinheim, Germany, 2003.

[13] E.D. Hughes, Mechanism and kinetics of substitution at a saturated carbon atom, Trans. Faraday Soc., 37 (1941) 603-637.

[14] E.D. Hughes, M.L. Dhar, C.K. Ingold, A.M.M. Mandour, G.A. Maw, L.I. Woolf, Mechanism of elimination reactions. XVI. Constitutional influence in elimination. General discussion, J. Chem. Soc., (1948) 2093-2119.

[15] E.D. Hughes, C.K. Ingold, Mechanism of substitution at a saturated carbon atom. IV. Discussion of constitutional and solvent effects on the mechanism, kinetics, velocity and orientation of substitution, J. Chem. Soc., (1935) 244-255.

[16] T. Nevecna, V. Bekarek, Medium Effect of Binary Solvent Mixtures formed by Diethyl Ether, Acetone, and 1,1,2,2-tetrachloroethane on the Quaternization Reaction of Ethyl Iodide with triethylamine and on Electronic Spectrum of 1-Nitro-2-(4'-Dimethylaminophenyl)Ethylene, Acta Univ. Palack. Olomuc. Fac. Rerum Natur. Chemica XXXI, 108 (1992) 33-37.

[17] A. Skrzypczak, P. Neta, Rate Constants for Reaction of 1,2-di1-methylimidazole with Benzyl Bromide in Ionic Liquids and Organic Solvents, Int. J. Chem. Kinet., 36 (2004) 253-258.

[18] M.J. Muldoon, C.M. Gordon, I.R. Dunkin, Investigations of Solvent-Solute Interactions in Room Temperature Ionic Liquids using Solvatochromic Dyes, J. Chem. Soc. Perkin Trans. 2, (2001) 433-435.

[19] C. Reichardt, Polarity of Ionic Liquids determined empiracally by means of Solvatochromic pyridinium N-phenolate Betain Dyes, Green Chem., 7 (2005) 339-351.

[20] M.H. Abraham, Substitution at saturated carbon. Part VIII. Solvent effects on the free energy of trimethylamine, the nitrobenzyl chlorides, and the trimethylamine–nitrobenzyl chloride transition states, J. Chem. Soc.B, Phys. Org., (1971) 299-308.

[21] M.J. Kamlet, J.L. Abboud, R.W. Taft, The solvatochromic comparison method. 6. The. pi.* scale of solvent polarities, J. Am. Chem. Soc., 99 (1977) 6027-6038.

[22] M.J. Kamlet, J.L.M. Abboud, M.H. Abraham, R.W. Taft, Linear solvation energy relationships. 23. A comprehensive collection of the solvatochromic parameters,. pi.*,. alpha., and. beta., and some methods for simplifying the generalized solvatochromic equation, J. Org. Chem., 48 (1983) 2877-2887.

[23] M.J. Kamlet, T.N. Hall, J. Boykin, R.W. Taft, Linear solvation energy relationships. 6. Additions to and correlations with the. pi.* scale of solvent polarities, J. Org. Chem., 44 (1979) 2599-2604.

[24] M.J. Kamlet, R.W. Taft, The solvatochromic comparison method. I. The. beta.-scale of solvent hydrogen-bond acceptor (HBA) basicities, J. Am. Chem. Soc., 98 (1976) 377-383.

[25] J. Schleicher, Masters Thesis, in, MS Thesis, University of Kansas, 2007.

[26] J.R. Harjani, R.D. Singer, M.T. Garcia, P.J. Scammells, The design and synthesis of biodegradable pyridinium ionic liquids, Green Chemistry, 10 (2008) 436-438.

[27] W.A. Lott, METHODS OF PREPARING SAME, in, Google Patents, 1957.

[28] A.K. Burrell, R.E. Del Sesto, S.N. Baker, T.M. McCleskey, G.A. Baker, The large scale synthesis of pure imidazolium and pyrrolidinium ionic liquids, Green Chem., 9 (2007) 449-454.

[29] S.M.F. Elshafie, F.A, Nucleophilic Reactivity: The influence of solvent on Reaction Velocity between pyridines and ethyliodide Egypt Journal of Chem, 29 (1986) 647-657.

[30] D. Hossain, M.M. Morshed, Kinetics of the Menschutkin Reaction of Pyridine with Benzyl Bromide in Different Solvents, JOURNAL-BANGLADESH ACADEMY OF SCIENCES, 22 (1998) 39-44.

[31] J.D. Reinheimer, J.D. Harley, W.W. Meyers, Solvent Effects in the Menschutkin Reaction, The Journal of Organic Chemistry, 28 (1963) 1575-1579.

[32] A.G. Böwing, A. Jess, Kinetics of single-and two-phase synthesis of the ionic liquid 1-butyl-3-methylimidazolium chloride, Green Chem., 7 (2005) 230-235.

[33] C.-W. Cho, Y.-C. Jeon, T.P.T. Pham, K. Vijayaraghavan, Y.-S. Yun, The ecotoxicity of ionic liquids and traditional organic solvents on microalga Selenastrum capricornutum, Ecotoxicology and Environmental Safety, 71 (2008) 166-171.

[34] J.I. Seeman, J.F. Whidby, The iodomethylation of nicotine. An unusual example of competitive nitrogen alkylation, The Journal of Organic Chemistry, 41 (1976) 3824-3826.

[35] A. Albert, Heterocyclic chemistry: an introduction, Athlone press, 1959.

[36] R. Williams, W. Jencks, F. Westheimer, pKa data Pennsylvania State University, University Park.

[37] K.B. Sloan, S.A.M. Koch, Effect of nucleophilicity and leaving group ability on the SN2 reactions of amines with (acyloxy) alkyl. alpha.-halides: a product distribution study, The Journal of Organic Chemistry, 48 (1983) 635-640.

[38] M.K. Pankova, J.; Zavada,J., Rates of the Menschutkin reaction of alkyldimethylamines. Effect of alkyl structures and solvents, Collection of Czechoslovak chemical communications, 39 (1974).

[39] G.B. Appetecchi, M. Montanino, D. Zane, M. Carewska, F. Alessandrini, S. Passerini, Effect of the alkyl group on the synthesis and the electrochemical properties of N-alkyl-N-methyl-pyrrolidinium bis(trifluoromethanesulfonyl)imide ionic liquids, Electrochim. Acta, 54 (2009) 1325-1332.

[40] T. Erdmenger, J. Vitz, F. Wiesbrock, U.S. Schubert, Influence of different branched alkyl side chains on the properties of imidazolium-based ionic liquids, J. Mater. Chem., 18 (2008) 5267-5273.

[41] W. Li, J. Zhang, B. Li, M. Zhang, L. Wu, Branched quaternary ammonium amphiphiles: nematic ionic liquid crystals near room temperature, Chem. Commun., (2009) 5269 - 5271.

[42] Y. Yoshida, O. Baba, C. Larriba, G. Saito, Imidazolium-Based Ionic Liquids Formed with Dicyanamide Anion: Influence of Cationic Structure on Ionic Conductivity, J. Phys. Chem. B, 111 (2007) 12204-12210.

[43] K.P.C. Vollhardt, N.E. Schore, Organic Chemistry Structure and Function, 3rd ed., W H Freeman and Company, 1998.

[44] A.D. Allen, G. Modena, Nucleophilic substitution reactions of organosilicon compounds. Part II. Reaction mechanisms of some sterically hindered organosilicon chlorides, J. Chem. Soc. , 1957 (1957) 3671-3678.

[45] I. Dostrovsky, E.D. Hughes, C.K. Ingold, Mechanism of substitution at a saturated carbon atom. Part XXXII. The role of steric hindrance (Section G) magnitude of steric effects, range of occurrence of steric and polar effects, and place of the Wagner rearrangement in nucleophilic substitution and elimination, J. Chem. Soc. , 173 (1946).

[46] R. Giernoth, In Situ IR Spectroscopy in Ionic Liquids: Toward the Detection of Reactive Intermediates in Transition Metal Catalysis, in: Ionic Liquids III A: Fundamentals, Progress, Challenges, and Opportunities, American Chemical Society, Washington, DC, 2005, pp. 79-88.

6. Kinetics of the Ionic Liquid 1-Hexyl-3-Methyl-Imidazolium Bromide, using Compressed CO_2

6.1 Synthesis of 1-Hexyl-3-Methyl-Imidazolium Bromide, in Neat CO_2

6.1.1. Introduction

There is growing interest in exploring CO_2 as a solvent in IL synthesis. Synthesizing imidazolium-based ILs with compressed CO_2 as solvent has many advantages over using traditional solvents [1-3]. CO_2 is relatively abundant naturally (As of 2006, at about 381 parts per million (ppm)) and cheap. It is considered a "green", more environmentally friendly, solvent [7]; utilizing CO_2 in synthesis, potentially allows replacement of volatile organic solvent-based processes, which contribute to direct human chemical exposure and to both air and water pollution. Further, using CO_2 (a greenhouse gas) from non-sequestered sources reduces carbon footprint and is sustainable; it can be readily recovered and recycled. Literature reports show that fast and sensitive organic synthesis can be achieved with high levels of functionality, controllability and energy efficiency in supercritical (Sc) CO_2. CO_2 is a gas at ambient conditions, with moderate critical conditions (31°C and 71 bar). Product separation can be easily achieved by tuning the system e.g. reducing pressure. This route would reduce the number of process steps, subsequently reducing energy demand, increasing selectivity and diminishing waste. Our group, as well as others, has indicated that most ILs have relatively large solubility in CO_2 and, at elevated pressures of 400+bar, are immeasurably insoluble in a compressed CO_2 phase[9-12]. This behavior is contrary to what is observed for organic compounds with CO_2 pressure [13-15], in that such compounds partition into the CO_2 phase; the CO_2

becomes miscible or critical with organic compounds and solvents at higher pressures. Thus for IL synthesis, reactants can be rendered miscible by choice of temperature, pressure and composition, however, the product IL will remain insoluble in this solvent. Thus, by varying CO_2 pressure, this phenomenon may be used to extract or purify the IL from residual reactants and impurities. This allows for separation of the CO_2 solvent without cross contamination between itself and the IL.

Concurrently with our work, Han *et al.*,[1] demonstrated in a batch reactor that the reaction between 1-methylimidazole and 1-bromobutane in supercritical CO_2 can produce high yields of imidazolium IL in CO_2 within 48 hours. The study correlated yield with time at two temperatures (50°C, 70°C) and 15.0 MPa for [BMim][Br], and at 32°C and 10 MPa for [Me_2Im][Br]. They observed that yields for [BMim][Br] varied for the two temperatures studied (50°C and 70°C) at 15.0 MPa: the rate of reaction was positively dependent on temperature. However, no relationship of the phase behavior to the reaction rate was presented, nor a kinetic rate published. At 70°C, Zhou *et al.*, synthesized [BMim][Cl] using CO_2 as a reaction medium over different pressures (0.1MPa- 15.0 MPa) [3]. They obtained different conversions at the various pressures and found that the rate of reaction increased with increasing pressures. No reference was made as to how the initial concentration of the reactants was corrected for the addition of CO_2 under pressure, especially for lower pressures below mixture critical point. Molarity is needed to compute rate constant. Molarity is the ratio of number of moles to volume. Initial volume of reactants considerably increased with pressure (CO_2 solubility) in the liquid phase; thus volume expansion data for the reacting mixture will be necessary to correct for true

volume of the reaction mixture used to compute molarity. Their reported k is questionable.

Chapter 4 presents measured phase equilibrium of reactants and IL product involved in the synthesis of 1-hexyl-3-methyl-imidazolium in compressed CO_2[6]. We reported experimental and modeled data for CO_2 solubility, volume expansion and mixture critical points for binary (1-bromohexane/CO_2, 1-methylimidazole/CO_2, [HMim][Br]) and ternary systems (1:1 mixture 1-bromohexane and 1-methylimidazole/CO_2) at 313.15 K and 333.15 K, between 5 and 150 bar. The solubility of CO_2 and the volume expansion were found to increase in the order of [HMim][Br] << 1-methylimidazole < 1:1 mixture of reactants < 1-bromohexane. The mixture critical points of the ternary system were 87.5 bar and 0.962 mole fractions of CO_2 at 313.15 K, and 111.8 bar and 0.913 CO_2 mole fraction at 333.15 K. The volume expansion data for the reacting system was important for concentration computation. The volume of this system was found to increase with increasing pressure, as seen with other organics.

Most kinetic expressions are based upon concentrations i.e. mole per unit volume. Above the mixture critical point, the volume expansion reaches infinity, as the fluid will fill whatever volume it occupies. Hence, the concentration is simply the moles divided by the total volume of the vessel. However, below the mixture critical point, the concentration must be computed using the relation between the pressure and volume of the liquid phase. The true volume can be determined from volume expansion data, the relative change in volume compared to the initial volume before CO_2 addition, i.e. $(V_m\text{-}V_0)/V_0$,

where the subscript *m* indicates mixture volume at any given pressure while subscript *0* is for the initial volume of the liquid phase. For example, at 313.15 K and 78.46 bar, the volume expansion was observed to be as much as 3.026 times of the initial volume. Consequently, the reported *k* values by Zhou *et al*., [3] using the initial concentrations computed without accounting for this expansion at pressures below the critical points, are questionable.

6.1.2. Reaction System Phase Behavior and Equilibria

Phase equilibrium in high pressure reactive systems is one of the most important controlling factors for the rate constant [10]. We previously reported phase behavior studies for this system. From our results, we showed that the composition of the reactants in the liquid phase is highly dependent on pressure, and can change significantly when operating near the mixture's critical point. For example, when operating above the mixture critical point (> 87.53 bar at 313.15 K, > 111.75 bar at 333.15 K), the reaction begins as a single phase, because the two reactants and CO_2 are miscible/critical with each other. There are two possible initial scenarios, depending on temperature and pressure: a single phase/supercritical mixture and a two-phase vapor-liquid equilibrium. The initial single phase becomes two as the reaction progresses: an IL rich phase, [HMIm][Br], separates from the solution. This is illustrated through the photographs in Figure 6. 1.[4] One note of safety when performing batch reactions in either of these scenarios: the pressure can increase throughout the reaction. The solubility of CO_2 in the reactants (0% conversion) and IL (100% conversion) can be quite different. For example

CO_2 has only about 0.285 mole fraction solubility in [HMIm][Br] at 40^oC and 75 bar. This can be compared to a mole fraction of 0.802 CO_2 in the 1:1 reactant mixture at the same conditions. Thus as the reaction proceeds, less CO_2 is soluble in the emerging IL phase which increases the system pressure.

However, when operating below the mixture's critical point, the reaction begins as VLE, an expanded liquid mixture rich in the reactants, along with a CO_2 rich phase. It proceeds to vapor-liquid-liquid equilibrium (VLLE), involving a CO_2-rich vapor phase, a reactant-rich phase, and an IL-rich phase (see Figure 6. 1). The critical pressures for the binary and ternary systems at the two temperatures studied are presented Table 6. 1. With multiple phases present during the reaction, the actual synthesis reaction has the possibility of occurring in each of these phases. This could significantly complicate the quantification of the reaction kinetics especially with experimental methods that are more suitable for overall kinetics. However, as we will illustrate here, under these conditions the reaction primarily occurs in one phase.

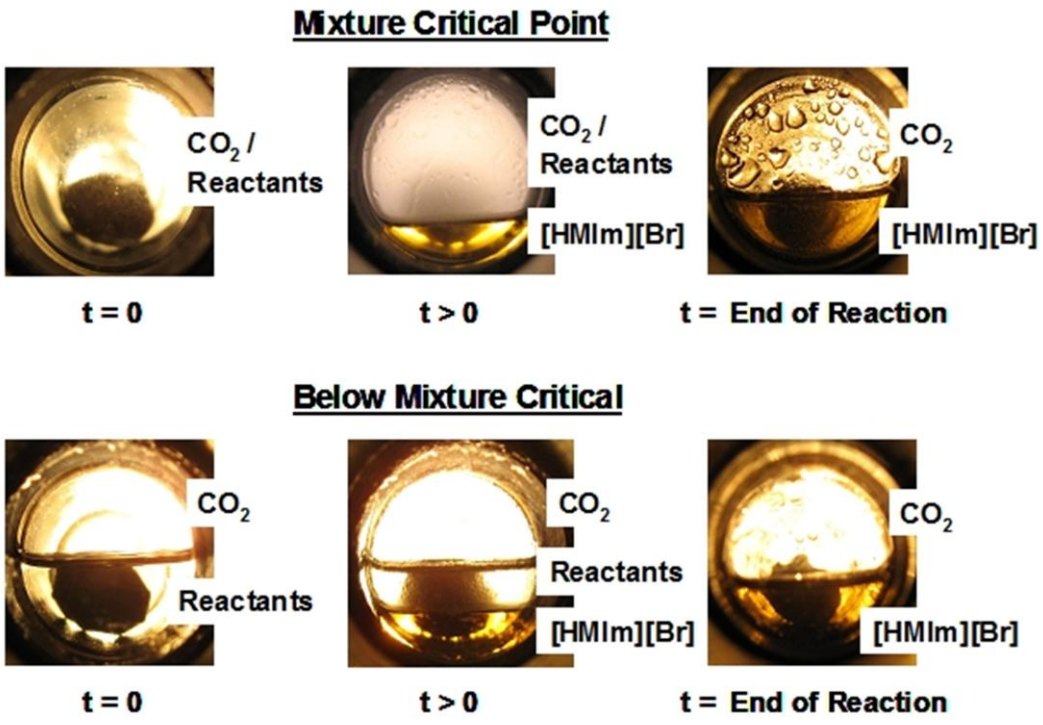

Figure 6. 1 Phase behavior at sub-critical conditions (top) and above the critical point for the reaction mixtures as the reaction proceeds (bottom) [4]. Note: magnetic stir-bar at the bottom of the viewcell.

Table 6. 1 Experimentally acquired mixture critical points for reactants in CO_2 taken at 313.15 K and 333.15 K Ref [6]

System	Critical Pressure (bar) 313.15 K	CO_2 mole fraction	Critical Pressure (bar) 333.15 K	CO_2 mole fraction
1-bromohexane / CO_2	84.90	0.9681 ± 0.0002	107.81	0.9289 ± 0.0001
1-methylimidazole / CO_2	91.77	0.9144 ± 0.0003	153.52	0.9521 ± 0.0003
1-methylimidazole / 1-bromohexane / CO_2[a]	87.53	0.9616 ± 0.0001	111.75	0.9128 ± 0.0006

a) Taken at a 1:1 mole ratio of reactants 1-methylimidazole:1-bromohexane

Table 6.2 Overall kinetic rate constants taken at different pressures at 313.5 K and 333.15 K using a 1:1 mole ratio of 1-methylimidazole to 1-bromohexane

313.15 K (40°C)

Phase Transition	Pressure (bar)	Initial x_{CO2}	k x10^6 (M^{-1} sec^{-1})
2→3→ 2 phases	30	0.1816	14.85 ± 0.49
2→3→2 phases	60	0.5654	8.24 ± 0.75
1→2 phases	90	0.980	7.97 ± 0.20
1→2 phases	140	[a]	5.91 ± 0.11

333.15 K (60°C)

Phase Transition	Pressure (bar)	Initial x_{CO2}	k x10^6 (M^{-1} sec^{-1})
2→3→2 phases	30	0.1629	107.0 ± 2.83
2→3→2 phases	60	0.4089	69.0 ± 0.97
2→3→2 phases	90	0.5900	59.9 ± 0.84
1→2 phases	140	[a]	49.2 ± 0.95

[a] occuring above mixture critical point of reactant/CO_2 mixture

As previously shown in chapters 2 and 5, these reaction rates, are 2^{nd} order and thus the reaction rate is dependent on the concentration of each species, C_i, in the particular phase of interest, p, and the intrinsic kinetic rate constant in the particular phase:

$$r_{IL}^{p} = \frac{dC_{IL}^{p}}{dt} = k^{p} C_{1-methylimidazole}^{p} C_{1-bromohexane}^{p}$$

The molar rate of formation of the IL for the entire system with π number of phases would be:

$$\frac{dN_{IL}}{dt} = \sum_{p=1}^{\pi} V_p r_{IL}^p = \sum_{p=1}^{\pi} V_p k^p C_{1-methylimidazole}^p C_{1-bromohexane}^p$$

where V_p is the total extensive volume of the phase, p. Thus, when only overall data for concentration with time are known, the phase-specific 2nd order kinetic rate constant is only equal to the overall rate constant when the reaction in only one phase is dominant. Obviously from the mathematics this may occur when one or more of the following is true: low concentration of one or both reactants in a given phase, low intrinsic rate constants of all but one phase, low total phase volume, etc.

In the supercritical scenario, the IL-rich phase progressively grows in volume, which allows the possibility that the reactants may partition from the CO_2 phase into the IL phase and potentially the overall reaction rate is the sum of the two phases. While the absolute volume of the IL phase is not negligible for high conversion data, it would be very small initially. Moreover at ambient pressure without CO_2, the solubility of 1-haloalkanes in the IL are relatively low [18] while 1-methylimidazole is miscible with the IL. However, the presence of CO_2 in the IL phase makes the solubility of even polar solutes decrease significantly in the IL phase; this has been described as using CO_2 pressure as a "separation switch" for IL mixtures [12]. Thus, the low concentration of one of the reactants renders the overall reaction rate to have little contribution to the overall kinetics.

For the sub-critical scenario that begins as two phases and then becomes three-phase during the reaction, the reaction in the upper CO_2 phase will be small due to low solubility of the reactants (<<1%) and an intrinsically low kinetic constant due to the low polarity. The low-volume of the newly formed IL-rich phase will, similar to above, have low solubility of at least one of the reactants and have negligible effect on the total reaction rate. Thus, only the reaction in the reactant-rich middle phase will the kinetic rate be important.

To confirm these qualitative conclusions, the phase behavior of the reaction was simulated for 0% and 50% conversion at 60 bar and 40^{o}C (reaction scenario*(below mixture critical point): 2 phase →3→2*) using the Peng-Robinson Equation of State based solely on the binary interaction parameters found in our previous study [6] Initially (0% conversion), the reactants with CO_2 are in a two-phase region (VLE). The vapor phase is predicted to have a mole fraction of each component of approximately 0.0007, while the liquid phase is predicted to have compositions for 1-methylimidazole and 1-bromohexane as approximately 0.21 for each. As the density of the vapor-phase is much lower than the liquid phase, the vapor phase concentrations are small at approximately 2.4 mM for each reactant. The liquid phase concentrations are approximately 2.66M, which are more than 3 orders of magnitude greater than the vapor phase. The resulting 2nd order reaction rates would thus be over 6 orders of magnitude higher in the liquid phase than vapor phase with a similar kinetic constant. At 50% conversion, the simulation for the vapor phase has similar conclusions as, now, there is even less of the reactants. The reactant-rich middle liquid phase will have similar concentrations as the initial mixture,

but now there is some small solubility of the IL (~350mM) in this phase that diminishes as the reactants are depleted. Thus, the observed rate constant in the organic phase is approximately equal to the overall k constant. Bowing and Jess [18] found similar results for the synthesis of [BMim][Cl] in ambient conditions, where a phase split occurred at conversions greater than 8%. The authors found that the organic phase was the key reactive phase. They also observed that the effective rate constant, k_{eff}, of the overall system was similar for a two-phase system compared to a single phase system; this is because as the reaction proceeds, the concentrations are maintained as the volume of the reaction phase decreases for a two phase system, while in a single phase system, the concentration decreases but the total volume stays constant.

While conventional multi-phase liquid systems may suffer from mass transport limitations resulting in an overall reduction in the kinetic rate: CO_2 has been shown to dramatically improve the mass transport properties of ILs[19, 20]. The viscosities of liquids are decreased with CO_2 addition, resulting in increased diffusivity, as well as enhanced inter-phase mass transfer [10, 21, 22]. In addition, we have previously established that the diffusion-limited kinetic rate constant at single-phase ambient pressure is 14 orders of magnitude faster than our kinetic rate constants, thus, mass transfer issues do not exist in these systems.

.

6.1.3. Reaction Kinetics

6.1.3.1. Temperature and Pressure effects

The properties of this system are sensitive to temperature, pressure and composition. Figure 6.2 illustrates the positive dependence of the rate of reaction on temperature, as expected. For the synthesis of [BMim][Br] at 150 bar, Han and coworkers [1] found that the yield at 50°C was about 18% over a 24 hour period, compared to a yield of about 86% at 70°C. From 313.15 K to 333.15 K, the rate of reaction for [HMim][Br] synthesis for all the pressures observed increased about an order of magnitude. Figure 6.2 also indicates that the overall rate of reaction changes considerably with altering pressures of CO_2. This not strictly a pressure effect, but more of a composition, phase equilibria, and polarity effect (see below).

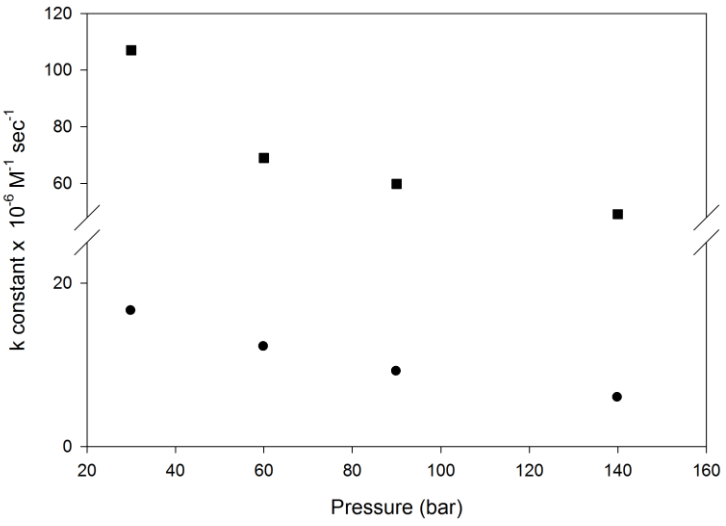

Figure 6.2 Rate constant with pressure at 313.15 K and 333.15 K

The molar concentration (mole/liter, etc.) of reactants decreases significantly with CO_2 addition, as the CO_2 dissolution causes a corresponding volume expansion, thus decreasing the constant mole per volume. As the 2nd order reaction rate is directly proportional to the concentration, the reaction rate decreases with the reduced concentration, given a constant 2nd order rate constant, *k*. Similar results have been observed by Subramaniam and coworkers [23] for the oxidation of cyclohexene in CO_2-expanded (CXL) acetonitrile, where no added benefits to rate constant were achieved at a CO_2 mole fraction higher than 30%. They found that at higher mole fractions, CO_2 becomes a diluent and has a negative effect on the apparent reaction rate.

Above the mixture critical point, the reactants' molarity is constrained by the reactor volume. Thus, with constant loading of the reactants, the concentration will remain constant at the various pressures, but the mole fraction of the reactants will decrease. However, reaction rate mechanisms are proportional to molar concentration and not mole fraction. Thus, given a similar starting concentration at two different pressures, the regressed 2nd order kinetic rate constant should be the same. However, at 313.15 K, the rate constant at 90 bar is approximately 35% higher than that at 140 bar, which is well beyond the experimental precision of the measurements. Does *k* thus have pressure dependence?

Wang *et al.,* [3] found that the rate of reaction was optimal at pressures close to the critical pressures/density of CO_2 (solvent). Over a pressure range of 1 to 150 bar, they found a dependence of the rate constant on the reduced density of pure CO_2. They

attribute this high rate constant with higher pressure to transition state theory phenomena. Transition state theory describes a thermodynamic equilibrium of the reactants in the transition state, assuming that once the transition state complex is formed, it proceeds directly to products. Hence, according to the transition state theory, the pressure dependence of the rate of reaction is proportional to the activation volume, $\Delta \underline{V}^{\neq}$ [24]:

$$\left(\frac{\partial \ln k_x}{\partial P}\right)_T = -\frac{\Delta \underline{V}^{\neq}}{RT} \qquad \text{Eqn 6. 1}$$

where *k* is expressed in pressure independent concentration units at a fixed temperature *T* and pressure *P*, and R is the gas constant. However, for most reactions, several hundred to a thousand bars of pressure are needed to significantly change *ln k* [25]. Temperature by far has a greater effect on rate of reaction than pressure. Despite the large partial molar volumes observed in SCFs, especially in the near-critical regime [26], partial molar volumes of liquids are on the order of 0-40cm^3/ mol. This pressure dependence of the rate constant is primarily due to the large compressibility of the solvent [27]. Thus, a strong pressure dependence on the reaction rate constant may be unlikely.

6.1.4. Polarity

From our previous study of this synthesis reaction in conventional solvents, the 2nd order rate constant is highly dependent on the polarity of the solvent media [16]. However, single parameter polarity scales could not qualitatively nor quantitatively describe the solvent effects. Only multi-parameter approaches such as Kamlet Taft (*KT*) could quantify the reaction rate constant. *KT* parameters differentiate various aspects of

"polarity", *viz.* acidity (α), basicity (β), and dipolarity/polarizability (π^*). Acidity, α, is a measure of the solvent's ability to donate a proton in a solvent-to-solute hydrogen bond [28]. β is the measure of the solvent's ability to accept a proton in a solvent-to-solute hydrogen bond [29], and π^* is a measure of the solvent's ability to stabilize a charge or dipole [30, 31]. For chlorinated solvents, another parameter, δ, is used; otherwise it is zero. The LSER for conventional solvents at 40°C is [4, 16]:

$$\ln k = -14.72 - 2.07\alpha + 0.07\beta + 4.99(\pi^* - 0.20\delta) \qquad R^2 = 0.95 \qquad \text{Eqn 6. 2}$$

From this equation it can be concluded that solvents containing small α, and large β and π^*, are desirable for maintaining high rates of reaction. Table 6. 3 illustrates the *KT* parameters of the reactants, reactant mixture, and [HMIm][Br] product found for the neat reaction.

The *KT* values for CO_2 are temperature and pressure (density) dependent [8, 32-34]. The solvent strength of supercritical fluids is found to vary, especially near the critical region. Kim and Johnston, while using solvachromatic probes in mixtures of CO_2 and co-solvents, found that local concentrations of co-solvent around a solute molecule (solvent-solute interactions) are sensitive to pressure and can be as high as seven times that of the bulk [35]. These large excesses of solvent-solute interactions can affect the rate constant, especially for bimolecular reactions [36, 37]. Sigman *et al.*, [38] have published *KT* values for CO_2 [8] showing π^* ranging from -0.01 to -0.90, from a pressures of 222.6 down to 88.8 bar at about 40^{o}C. Another study also presented α ranging from 0.000 to

0.195, over a pressure range of 96.2 to 81.1 bar, at 45°C [39]. The range of *KT* parameters for CO_2 from the literature is summarized in Table 6. 3.

By increasing the pressure induced by CO_2, the solubility of CO_2 in the liquid phase increased, altering the *KT* values, as well as, the polarity of the liquid phase. These values decreased slightly with both pressure and CO_2 composition, while α increased. However, the β values remained relatively constant over most of the pressure range investigated. This is similar to what Sigman *et al*., observed for pure CO_2, where β, unlike the π^* and α values, does not show any correlation with the density of CO_2 [38]. This trend has been observed in studies performed on CO_2/n-alcohol mixtures [40], as well as, in Diels-Alder type reactions using CO_2. [39, 41] Since for most of the pressure range, β remains constant, π^* decreases and α increases, the kinetic constant for the synthesis of [HMIm][Br] with CO_2 should be expected to decrease slightly with increasing amounts of CO_2 per [16]:

$$\ln k = -14.72 - 2.07\alpha + 0.07\beta + 4.99(\pi^* - 0.20\delta) \qquad R^2 = 0.95 \qquad \text{Eqn 6. 2}$$

.

This is what is observed for the kinetic constants in Table 6.2. For the kinetic runs that are conducted in single-phase supercritical conditions, the increase in pressure is accomplished by increasing the amount of CO_2 added to the mixture. Thus, while the molarities of the reactants are roughly similar, the mole fractions of the reactants decrease with the pressure as more CO_2 is added. As CO_2 decreases the polarity of the mixture to a relatively small extent, the kinetic rate constants should also decrease.

Table 6. 3 *KT* parameters for CO_2, reactants, and product

Component	α	β	π^*
CO_2	0.000-0.195[a]	(-0.09) – (-0.14)[b]	(-0.01) – (-0.90)[b]
1-Methylimidazole	0.232 ± 0.012	0.712 ± 0.016	0.961 ± 0.014
1-Bromohexane	0.014 □ 0.07	(-0.009) ± 0.011	0.500 ± 0.001
[HMIm][Br][c]	0.453 □0.069	0.562 □ 0.066	0.983 □ 0.037
1:1 1-Methylimidazole: 1-Bromohexane	0.280	1.07	0.650
1:1 Reactant CO_2 30 bar	0.433	1.096	0.632
1:1 Reactant CO_2 90 bar	0.508	1.120	0.611

a.) taken from ref.[5] for a pressure range of 96.2-81.1 bar b.) taken from ref.[8] for a pressure range 222.6-88.8 bar c.) taken from ref. [16]

Table 6.4 presents the *k* constants for this reaction in selected organic solvents [16], along with those obtained in CO_2. Compared to traditional solvents, the rate constants observed for CO_2 are found to be moderate. At the maximum pressure studied, 140 bar, the CO_2 composition in the liquid is about 66% at 40°C and 54% at 60°C. At the lower pressures, it is comparable to using cyclopentanone, while at higher pressures above the mixture's critical pressure, the rate of reaction is similar to that observed for ethyl formate.

Table 6.4 Comparison of rates of reactions for CO_2 with those obtained in organic solvents at 40°C and 60°C.[6]

	k x10^6 (M^{-1} sec^{-1})	
Solvent[b]	313.15 K	333.15 K
Dimethyl Sulfoxide[c]	77.89 ± 1.72	322.31 ± 3.53[a]
Acetonitrile	21.56 ± 0.21	110.64 ± 1.42
Neat (1:1 mixture)	17.63 + 0.06	106.34 ± 13.2
Cyclopentanone	15.11 ± 0.11	76.11 ± 1.72
Acetone	12.67 ± 0.06	63.67 ± 0.61
2-Butanone	11.56 ± 0.08	53.75 ± 0.28
CO_2 30 bar	14.85 ± 0.49	107.0 ± 2.83
CO_2 60 bar	8.24 ± 0.75	69.0 ± 0.97
CO_2 90 bar	7.97 ± 0.20	59.9 ± 0.84
CO_2 140 bar	5.91 ± 0.11	49.2 ± 0.95
Dichloromethane	8.47 ± 0.11	- [a]
Ethyl Formate	7.97 ± 0.14	- [a]
Methanol	2.03 ± 0.08	17.14 ± 0.11

a) Exceeds boiling point of solvent b) 1:1:20 c)1:1:80 of solvent due to exothermicity of the reaction.

Despite having only moderate kinetic rates compared with conventional solvents, CO_2 has a number of advantageous properties. The quaternization reaction is strongly exothermic. For a similar reaction between 1-methylimidazole and 1-bromobutane, the heat of reaction (ΔH^{rxn}) is -96 KJ/mol [42]. Such a large heat of reaction is often handled with large amounts of solvent, and/or by the use of heat exchangers (chillers, etc.). CO_2 is well known to have a high heat capacity, C_p, which increases dramatically in the near-

critical regime [43, 44]. For example, the heat capacity of CO_2 at 40°C and 88.4 bar is 594 J/mol-K [45]; at 140 bar it is 125 J/mol-K. Therefore, a large amount of energy released during an exothermic reaction can be absorbed by either the CO_2 phase or the enhanced heat capacity of the gas-expanded liquid. In addition, the presence of CO_2 dissolved in ILs decreases viscosity dramatically, sometimes by over 80% [46-50]. This decrease in viscosity is accompanied by a corresponding increase in the diffusivity of all species in the mixture. As demonstrated, the phase behavior of CO_2 with the IL and its corresponding reactions often lead to facile separations, as the IL is immeasurably insoluble in CO_2 at any pressure. We have previously performed a rigorous analysis on the human and environmental impact of various organic solvents for potential IL production, such as those found Table 6.4 [51]. CO_2 would be the most benign of all solvents previously investigated, especially if obtained from non-sequestered sources.

6.1.5. Summary: Synthesis of 1-Hexyl-3-Methyl-Imidazolium Bromide, with CO_2

We believe that CO_2 has great potential for the sustainable/"green" production of ILs, as shown later for the synthesis of [HMIm][Br]. Compressed CO_2 allows for control of phase behavior (dissolutions of reactants or precipitation of products) with small changes in operating conditions. The effect of phase behavior does have some impact on the 2nd order kinetic rate constant. Higher CO_2 pressure and composition decrease the kinetic rate constant. These rate constants were found to be comparable to those in reactions using conventional organic solvents. However, the phase behavior with CO_2 allows for

facile separation. The presence of CO_2 also improves mass transport. The high heat capacity of CO_2 would mitigate the high heat of reaction found for these reactions. Finally, CO_2 has one of the lowest human and environmental impacts of all solvents, especially if the CO_2 comes from non-sequestered sources.

6.2 Kinetics of [HMim][Br] in Gas Expanded CO_2 (GXL)

6.2.1. Introduction

Gas Expanded Liquids (GXLs) media are organic liquid solvents that have been expanded due to the dissolution of a gas, for example, CXLs are organic liquid solvents that are expanded using CO_2. These promising solvent media offer the flexibility of a highly tunable reaction media for use in various applications. For example, CXLs' solvent strength and transport properties can be significantly altered or optimized by simply manipulating pressure, temperature and composition of CO_2. Since the CO_2 expands the volume of the organic liquid by up to 80%, the amount of the solvent (usually a volatile organic compound) needed for a process can be substantially reduced, lessening human exposure to toxic chemicals and adverse environmental impact. Further, the CO_2 better improves mass transport compared to the pure organic liquid, while the CXL has solvating properties superior to those of the pure CO_2. Typically, optimal CXL conditions in the literature are at lower pressures (~30bar), compared to supercritical fluids (>100 bar), alleviating energy and safety concerns that plague SCF systems.[52] Distillation methods of separation are cost and energy intensive, CXL technology alleviate several issues associated with distillation; (1) Significant reduction of solvent

amounts that would be eventually recovered from product, should distillation become inevitable (2) when CO_2 is extraction is sufficient for product recovery, energy demand is drastically reduced as simple depressurization can be utilized for recovery of the product. Brennecke [53] summarized the different ways in which GXL media or SCFs can affect reactions as:

1) Improved diffusion reaction rates
2) Improved mass transfer
2) Increased reactant solubility (ies)
3) Simpler separations
4) Pressure effect on the rate constant
5) Effects of local density
6) Effects of local composition

Previously, our group found DMSO (one of the most environmentally benign organic solvents) to have the highest kinetic rate, among ten other organic solvents, for the synthesis of 1-hexyl-3-methylimidazolium bromide ([HMIm][Br]), a model IL.[4, 54] However, DMSO is beset with a very high boiling point (189^{o}C) and heat of vaporization, rendering it both economically and environmentally non-feasible as a solvent option. Synthesis and processing of ILs in gas-expanded DMSO liquid media may alleviate these issues. This work, for the first time, leverages the kinetic benefits of DMSO and the thermodynamic advantage of environmentally benign CO_2 for the production of ILs. CO_2 is known to induce many IL-solvent mixtures to split into IL-rich and solvent-rich phases that can be decanted, or, at higher pressures, extracted by near-,

or super-, critical CO_2.[55] In this study, we explore the use of CO_2 expanded DMSO as a reaction media for the synthesis of [HMIm][Br] at different pressures and at two temperatures 313.15 K and 333.15 K.

6.2.2. Kinetic Data

Figure 6.3 presents conversion over time for the synthesis of [HMIm][Br] from 1-bromohexane and 1-methylimidazole in CO_2 expanded DMSO at 30 bar and 40°C. The reaction rate constants in CXL (DMSO) are reported in Table 6.5. The rates of reaction was found to increase over tempreture by a factor of two, at all concentrations. Only a moderate decrease was observed for rate constant with pressure and CO_2 composition. Some decrease in the rate constant is not surprising, as CO_2 typically lowers the rate of reactions that have a relatively polar transition state [52] - CO_2 reduces the polarity of the organic solvents. So, polarity decreases with increasing CO_2 concentrations, as illustrated in Figure 6. 4. However, the reaction rate was not drastically lowered by addition of CO_2 until a very high concentration of CO_2 was attained (above the mixture critical point of the DMSO/CO_2 system). We attribute this trend to local composition effects. Spectroscopic investigations of reactions in the GXLs have been useful in elucidating solvent effects at a molecular scale. Past studies show that both bulk (pressure, such as increase in CO_2 composition), and local (local compositions of the solvent), properties can affect reaction rates. [6, 17, 53] To understand this trend, we conducted spectroscopic investigations for the CO_2 expanded DMSO system. With varied CO_2 composition/pressures, the CO_2 expanded solvent medium changes in polarity, as illustrated in Figure 6. 5. The Kamlet Taft (*KT*) parameters α, β and $E_T(30)$ were found to

decrease very little over the CO_2 composition range investigated, while the polarizability/dipolarity (π^*) had a larger decrease with CO_2. The polarity data for this CXL emphasizes the ability to tune the solvent property of gas expanded liquids that is exploitable. *KT* parameters are the environment that the probe feels (i.e. the ratio of the two solvent molecules around the probe). This may be similar to the transition state of the reaction. The effects of local compositions have been studied experimentally and through molecular dynamic simulations. At times, bulk solvent properties do not adequately describe overall observed behavior due to preferential solvation of solute molecules by one of the components in the mixture[35, 56] The cybotactic region (local composition) is characterized by the volume immediately surrounding a solute molecule, and in which the local solvent structure is strongly affected by intermolecular forces between the solute and the solvent.[41] This local composition varies with the bulk solvent composition and can drastically affect reaction rates. Kim and Johnston showed concentration of the co-solvent around a solute molecule to be as high as 7 times that in the bulk. In the same study, they observed the shift of the solvachromatic dye, phenol blue, in mixtures of carbon dioxide and co-solvent (1-5.25% acetone, methanol, ethanol, octane), as function of pressure.[17] Preferential solvation of the probes by DMSO (i.e., the probe sees mostly DMSO molecules around it) causes only a minimal change in the Kamlet Taft (*KT*) parameters α, β and $E_T(30)$ up to $x\mathrm{CO_2} > 0.6$. Literature data for pure CO_2 suggests a sharp decrease in $E_T(30)$ at $x\mathrm{CO_2} > 0.85$.[36]

The π^* value (see Figure 6. 5a) only decreases from 1 ($x\mathrm{CO_2} = 0$, pure DMSO) to 0.61 at more than half molar composition of CO_2 ($x\mathrm{CO_2} = 0.63$). Although this lowered π^* by

40%, a π^* value of 0.61 indicates a still relatively polar medium, comparable to acetone's π^* value of 0.62 and that of acetonitrile at 0.66. Literature data for methanol, acetone and acetonitrile suggests a sharp decrease at $xCO_2 > 0.85$ to the pure CO_2 value. [6, 36, 41]

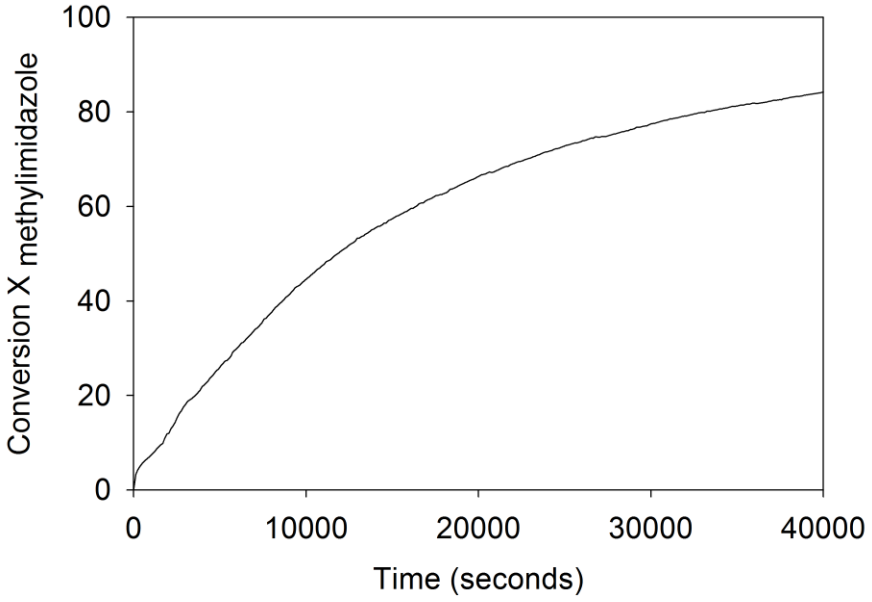

Figure 6.3 Conversion over time for the synthesis of [HMIm][Br] from 1-bromohexane and 1-methylimidazole in CO2 expanded DMSO at 30 bar and 40°C, CMIM,0=1.390 mol/L

Table 6.5 Overall kinetic rate constants taken at different pressures at 313.5 K and 333.15 K, using a 1:1:5 mole ratio of 1-methylimidazole to 1-bromohexane to 5DMSO

313.15 K (40^{o}C)

Pressure (bar)	Initial x_{CO2}	k x10^{6} (M^{-1} sec^{-1})
0	0.000	111.3±2.51
24	0.102	70.2 ± 5.83
30	0.184	65.17 ± 1.67
60	0.595	53.67 ±3.49
90	~0.99[a]	9.90 ± 1.56

333.15 K (60^{o}C)

Pressure (bar)	Initial x_{CO2}	k x10^{6} (M^{-1} sec^{-1})
0	0.000	571.0 ± 15.52
30	0.125	416.9 ± 48.17
50	0.259	391.2 ± 22.62
60	0.326	271.0 ± 8.65
100	0.594	100.0 ± 1.41

'a at above mixture critical point of reactant

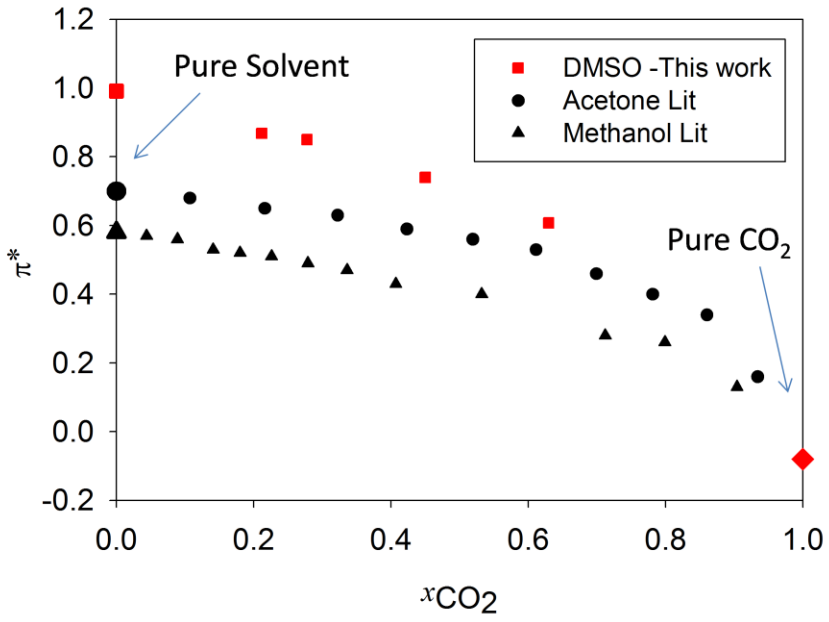

Figure 6. 4 π* with xCO2 in CO2 expanded DMSO (this work), Acetone[6] and Methanol[6], Pure CO2[17]

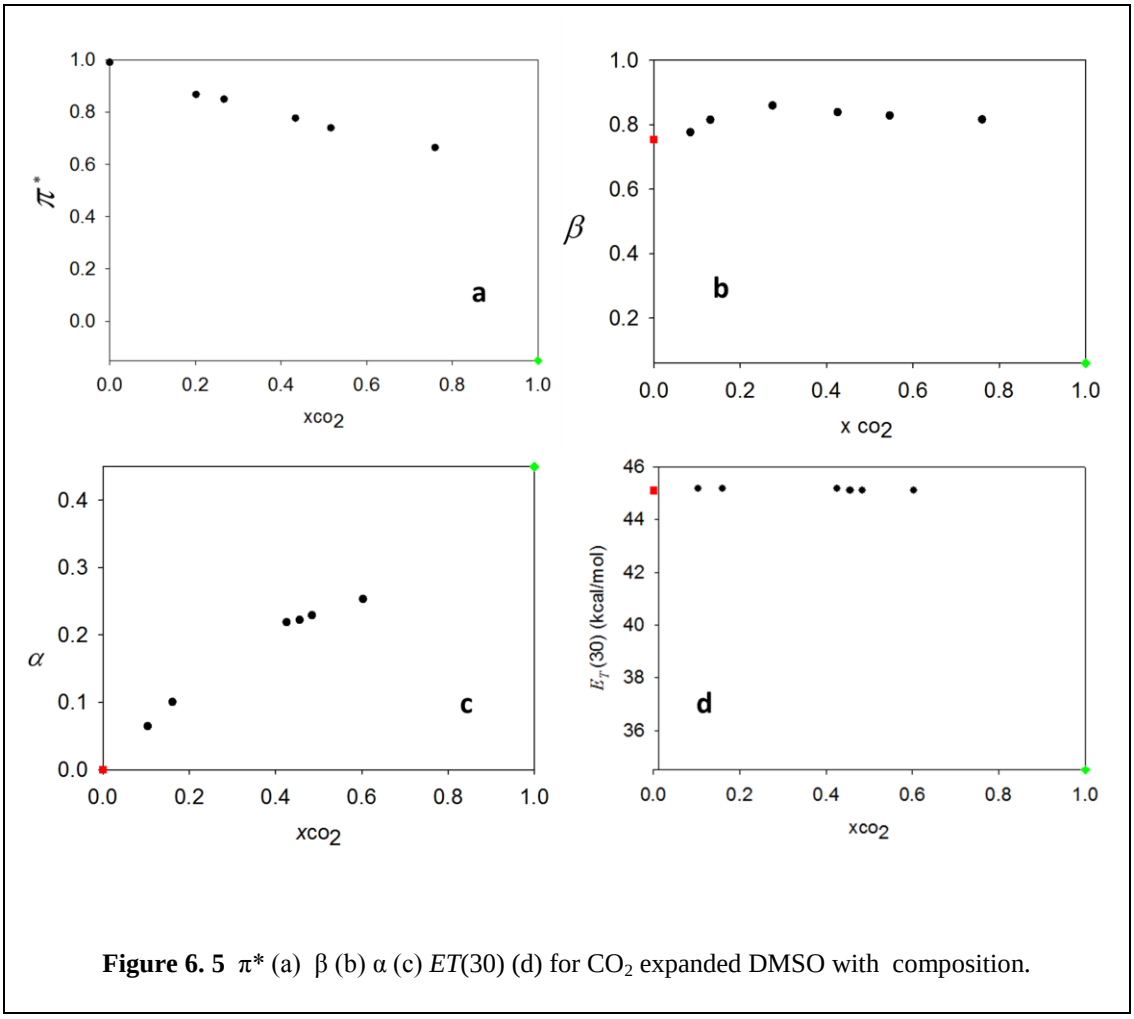

Figure 6. 5 π* (a) β (b) α (c) *ET*(30) (d) for CO_2 expanded DMSO with composition.

Further, the local composition enhancement of DMSO (xDMSO$_{local}$) around the probes was estimated using literature methods, based on our π^* measurements. [17, 22, 35, 41, 56, 57] A mixture with no local composition effects, would have spectral shifts linearly related to the shifts of their pure components weighted by their mole fractions in the mixture, so that:

$$\pi^* = x_1\pi_1^* + x_2\pi_2^* \qquad \text{Eqn 6. 3}$$

Thus local composition effects can expressed as the deviation from Eqn 6. 3 as,

$$\Delta\pi^* = \pi^* - (x_1\pi_1 + x_2\pi_2) \qquad \text{Eqn 6. 4}$$

Were (1) = xDMSO, (2) = $x$$CO_2$, so that, to determine $x_{DMSOlocal}$, the deviation in π^* ($\Delta\pi^*$) is computed from Eqn 6. 3, based on the values of pure acetonitrile (π^*_{DMSO}) and pure CO_2 (π^*CO_2). Then, $\Delta\pi^*$ is assumed to be zero so that, $x_{DMSO,local}$ becomes:

$$x_1 = \frac{\pi^* - \pi_2^*}{\pi_1^* - \pi_2^*} \qquad \text{Eqn 6.5}$$

A composition enhancement factor (CEF) is defined, similar to Ford et al.[41], where

$$CEF = \frac{x_{DMSO,local}}{x_{DMSO,bulk}}$$

Although Maroncelli and coworkers [58] have shown, by molecular dynamics simulations, that this methodology exaggerates the extent of preferential solvation, especially when electrostatic interactions cannot be neglected, they note that this a good first approximation. Figure 6. 6 (a) presents CEF with $x$$CO_2$: we find that the CEF exhibits a modest change for $x$$CO_2$ < 0.60. It shows that the local mole fraction of DMSO is larger than that in the bulk solution. For example, at $x$$CO_2$ = 0.45, $x$$DMSO_{local}$ = 0.68, and is 30% greater than the bulk concentration of DMSO ($x$$DMSO_{bulk}$ = 0.55). Although the local composition was enhanced with bulk CO_2 composition, large CO_2 composition reduces the concentration of the solvent, diluting the bulk and consequently the number of DMSO molecules around the probe (shown in Figure 6. 6 b), thus causing a reaction rate decrease.[27] The net of these two countering effects (increasing CEF with bulk CO_2 composition and the diluting effect of CO_2) explains the relatively high rate constants observed for the CO_2-DMSO systems even at higher pressures. Although the

rate of reaction in CXL systems go down with the composition of less polar CO_2, the reaction rate constant remain relatively high for this reaction. This trend emphasizes opportunities presented by CO_2 expanded liquids; one can successfully replace significant amounts of the organic solvent (green initiative) while maintaining strong solvent properties.

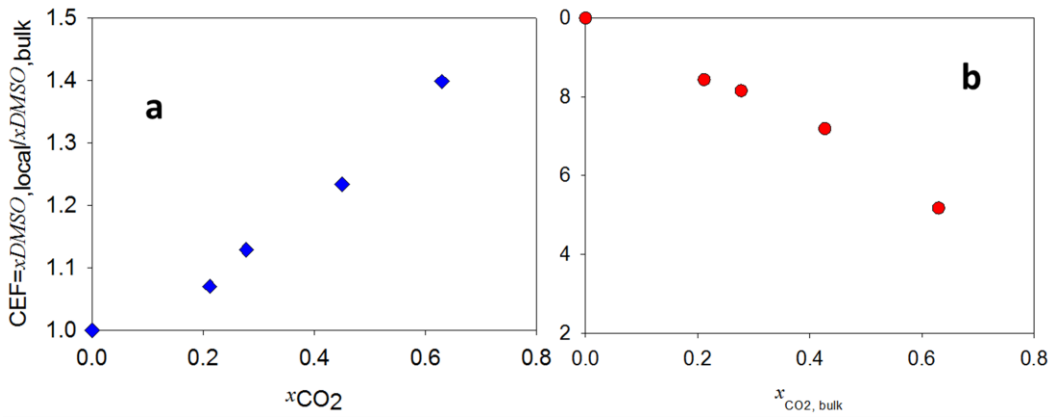

Figure 6. 6 (a) Composition Enhancement Factor (CEF) for CO2 expanded DMSO (b)) local composition of DMSO with bulk CO2 composition

Chen and coworkers attribute this behavior around the critical region to large isothermal compressibility and low density of the fluid at close to critical conditions. [10, 27] .

6.2.3. Separations/CO_2 extraction

Although the amount of solvent needed for reaction is drastically reduced by using CO_2, at the end of reaction, the IL still has to be recovered from the reaction mixture. Distillation methods would incur significant cost, as this method of separation can be energy intensive. In chapter 4, we showed unique phase behavior that might be leveraged

for separation. Table 6.5 summarizes phase transitions and mixture critical points in CO_2 expanded DMSO IL synthesis systems at various loadings and pressure. In the IL/DMSO/CO_2 system, we find that a three-phase (VLLE) equilibrium can occur: for example, at 40^oC and 81.32 bar, VLLE occurs. The first liquid is IL rich and the second rich in CO_2; at 85.87 bar, VLLE goes back to VLE. If the IL rich phase is separated from the system, CO_2 extraction can then be used to purify the new concentrated system. Extraction runs in the laboratory demonstrate that a separation greater than 98% purity of the IL can be achieved. For example, an extraction experiment achieved 98% purity from 0.5grams of a 2 HMimbr: 5DMSO system at 60^oC and at 150 bar, using 120mL of CO_2. A more rigorous setup that optimizes extraction factors such as mass transfer would be better than these runs carried out in an autoclave, with a stirring bar for mixing. We also appreciate that, often, the last percent of purity is often the most expensive to achieve. While these are first pass attempts to explore this potential, in an optimized case, mass transfer would be greatly enhanced. The important factor is that the CO_2 and DMSO recovered will be recycled back into the system, adding to the overall efficiency of this route. More studies will have to be carried to out identify optimal recovery amounts. Life cycle analysis and detailed economic analysis will be insightful to real benefits of synthesizing ILs via this route, see chapter 7.

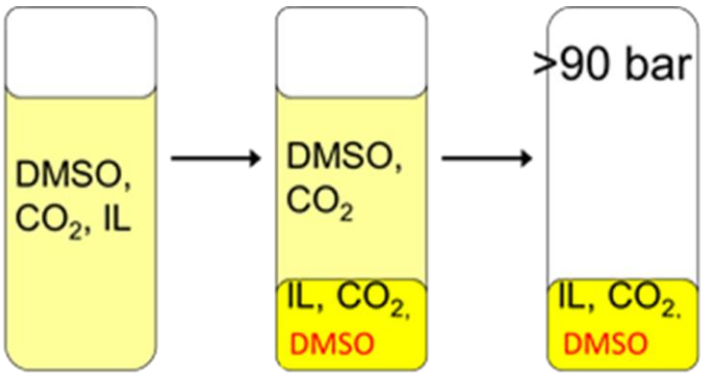

Figure 6. 7: Illustrating multiphase phase transition in gas expanded DMSO

Table 6. 6 Summary of Phase transitions and Mixture Critical Points in CO_2 expanded DMSO IL Synthesis Systems at 40C

Systems	*Phase Transitions (Pressure (Bar), * Mixture Critical Point)*
1:1 Reactants : 5DMSO + CO_2	2→3(VLLE, 86) →1* (89.19)
2 [HMim][Br] : 5 DMSO + CO_2	2→3(VLLE, 81.32) →2 (VLE, 85.87)
1:1 Reactants : 20 DMSO + CO_2	2→3(VLLE, 84.3) →1* (86.14)
2[HMim][Br] : 20 DMSO + CO_2	2→3(VLLE, 94.64) →2(VLE, 121.57)
1-Methylimidazole + CO_2	2→3(VLLE, 82.97) →1* (91.77)
Bromohexane + CO_2	2→ 1* (84.90)
1:1 Reactants + CO_2	2→ 1* (87.53)

6.2.4. Summary

CO_2 has been demonstrated to be a potential solvent for the synthesis of 1-hexyl-3-methylimidazolium bromide ([HMIm][Br]), at different pressures, and at temperatures 313.15 K and 333.15 K. This synthesis route affords easy separations simply by

controlling the pressure loading of CO_2. The rate of reaction under certain conditions was found to be as attractive as using conventional organic solvent. The rate of reaction decreases with increasing CO_2 pressure for imidazolium-based ILs, especially when operating above the mixture critical point. Also, it has been demonstrated that phase equilibrium, as well as the solubility of CO_2, plays a significant role in understanding kinetics by decoupling the various effects of compressed CO_2.

The synthesis of ILs in CO_2 expanded DMSO systems is a potential solvent route for IL synthesis. Although increasing CO_2 concentration decreases the polarity of polar aprotic DMSO, high reaction rates are still attainable for this solvent media, up until about greater than 80 percent CO_2 mole fraction, and are attributed to local composition effects. Compared to all the CO_2 systems for IL synthesis studied in this research, CXL-DMSO has the highest rate of reaction. Further, we demonstrated that the kinetic benefits of DMSO and the thermodynamic advantage of environmentally benign CO_2 can be leveraged for the production of ILs.

References

[1] W. Wu, W. Li, B. Han, Z. Zhang, T. Jiang, Z. Liu, A green and effective method to synthesize ionic liquids: supercritical CO_2 route, Green Chem., 7 (2005) 701-704.

[2] Z. Zhou, T. Wang, H. Xing, Preparation of ionic liquid N,N'-dialkylimidazolium halide, in: F.Z.S.G. Shuomingshu (Ed.), China, 2005.

[3] Z. Zhou, T. Wang, H. Xing, Butyl-3-methylimidazolium Chloride Preparation in Supercritical Carbon Dioxide, Ind. Eng. Chem. Res., 45 (2006) 525-529.

[4] J. Schleicher, in, University of Kansas, Lawrence, Kansas, USA, 2007.

[5] Y. Ikushima, N. Saito, M. Arai, K. Arai, Solvent Polarity Parameters of Supercritical Carbon Dioxide as Measured by Infrared Spectroscopy, Bull. Chem. Soc. Jpn., 64 (1991) 2224-2229.

[6] S.O. Nwosu, J.C. Schleicher, A.M. Scurto, High-pressure phase equilibria for the synthesis of ionic liquids in compressed CO2 for 1-hexyl-3-methylimidazolium bromide with 1-bromohexane and 1-methylimidazole, J. Supercrit. Fluids, 51 (2009) 1-9.

[7] M. Poliakoff, J.M. Fitzpatrick, T.R. Farren, P.T. Anastas, Green chemistry: science and politics of change, Science, 297 (2002) 807-810.

[8] M.E. Sigma, S.M. Linley, J.E. Leffler, Supercritical Carbon Dioxide: Behavior of pie* and beta Solvatochromic Indicators in Media of Different Densities, J. Amer. Chem. Soc., 107 (1985) 1471-1472.

[9] L.A. Blanchard, Z. Gu, J.F. Brennecke, High-Pressure Phase Behavior of Ionic Liquid/CO2 Systems, J. Phys. Chem. B, 105 (2001) 2437-2444.

[10] M. Nunes da Ponte, Phase equilibrium-controlled chemical reaction kinetics in high pressure carbon dioxide, J. Supercrit. Fluids, 47 (2009) 344-350.

[11] W. Ren, B. Sensenich, A.M. Scurto, High-Pressure Phase Equilibria of Carbon Dioxide (CO2)+ n-Alkyl-Imidazolium Bis (trifluoromethylsulfonyl) amide Ionic Liquids, The Journal of Chemical Thermodynamics, (2009).

[12] A.M. Scurto, S. Aki, J.F. Brennecke, CO2 as a separation switch for ionic liquid/organic mixtures, J. Am. Chem. Soc, 124 (2002) 10276-10277.

[13] R. Dohrn, G. Brunner, High-pressure fluid-phase equilibria: experimental methods and systems investigated (1988–1993), Fluid Phase Equil., 106 (1995) 213-282.

[14] T. Kraska, K.O. Leonhard, D. Tuma, G.M. Schneider, Correlation of the solubility of low-volatile organic compounds in near-and supercritical fluids. Part I: applications to adamantane and ß-carotene, J. Supercrit. Fluid., 23 (2002) 209-224.

[15] D.J. Miller, S.B. Hawthorne, Determination of Solubilities of Organic Solutes in Supercritical CO2 by Online Flame Ionization Detection, Anal. Chem., 67 (1995) 273-279.

[16] J. Schleicher, A.M. Scurto, Kinetics and solvent effects in the synthesis of ionic liquids: imidazolium, Green Chem., Published Online: DOI: 10.1039/b808364a (2009) in press.

[17] Y. Ikushima, N. Saito, M. Arai, K. Arai, Solvent polarity parameters of supercritical carbon dioxide as measured by infrared spectroscopy, Bull. Chem. Soc. Jpn., 64 (1991) 2224-2229.

[18] A.G. Böwing, A. Jess, Kinetics of single-and two-phase synthesis of the ionic liquid 1-butyl-3-methylimidazolium chloride, Green Chem., 7 (2005) 230-235.

[19] A. Ahosseini, E. Ortega, B. Sensenich, A.M. Scurto, Viscosity of n-alkyl-3-methyl-imidazolium bis (trifluoromethylsulfonyl) amide ionic liquids saturated with compressed CO2, Fluid Phase Equilibria, 286 (2009) 62-68.

[20] A. Ahosseini, W. Ren, A.M. Scurto, Understanding Biphasic Ionic Liquid/CO2 Systems for Homogeneous Catalysis: Hydroformylation, Industrial & Engineering Chemistry Research, 95-101.

[21] M. Arai, S.-i. Fujita, M. Shirai, Multiphase catalytic reactions in/under dense phase CO2, J. Supercrit. Fluids, 47 (2009) 351-356.

[22] J.P. Hallett, C.L. Kitchens, R. Hernandez, C.L. Liotta, C.A. Eckert, Probing the Cybotactic Region in Gas-Expanded Liquids (GXLs), Acc. Chem. Res., 39 (2006) 531-538.

[23] B. Kerler, R.E. Robinson, A.S. Borovik, B. Subramaniam, Application of CO2-expanded solvents in heterogeneous catalysis: a case study, Appl. Catal., B 49 (2004) 91-98.

[24] M.G. Evans, M. Polanyi, Some applications of the transition state method to the calculation of reaction velocities, especially in solution, Transactions of the Faraday Society, 31 (1935) 875-894.

[25] C. Reichardt, Solvents and solvent effects in organic chemistry, 3rd ed., Wiley-VCH, Weinheim, Germany, 2003.

[26] K.P. Johnston, C. Haynes, Extreme solvent effects on reaction rate constants at supercritical fluid conditions, AIChE Journal, 33 (1987) 2017-2026.

[27] C.A. Eckert, B.L. Knutson, P.G. Debenedetti, Supercritical fluids as solvents for chemical and materials processing, Nature, 383 (1996) 313-318.

[28] M.J. Kamlet, R.W. Taft, The Solvatochromic Comparison Method. 2. The alpha-scale of Solvent Hydrogen-Bond Donor (HBD) Acidities, J. Amer. Chem. Soc., (1976) 2886-2894.

[29] M.J. Kamlet, R.W. Taft, The Solvatochromic Comparison Method. I. The beta-scale of Solvent Hydrogen-Bond Acceptor (HBA) Basicities, J. Amer. Chem. Soc., (1976) 377-383.

[30] M.J. Kamlet, J.L. Abboud, R.W. Taft, The Solvatochromic Comparison Method. 6. The pie star Scale of Solvent Polarity, J. Amer. Chem. Soc., 99 (1977) 6027-6037.

[31] C. Laurence, P. Nicolet, M.T. Dalati, The Empirical Treatment of Solvent-Solute Interactions: 15 Years of pi*, J. Phys. Chem., (1994) 5807-5816.

[32] J.A. Hyatt, Liquid and Supercritical Carbon Dioxide as Organic Solvents, J. Org. Chem., 49 (1984) 5097-5101.

[33] M. Maiwald, G.M. Schneider, Solvatochromism in supercritical fluids, Berichte der Bunsen-Gesellschaft, 102 (1998) 960-964.

[34] A.P. Abbott, C.A. Eardley, J.E. Scheirer, Analysis of dipolity/polarizability parameter, pie*, for a range of supercritical fluids, Phys. Chem. Chem. Phys., 2001 (2001) 3722-3726.

[35] S. Kim, K.P. Johnston, Molecular interactions in dilute supercritical fluid solutions, Ind. Eng. Chem. Res. , 26 (1987) 1206-1213.

[36] T.W. Randolph, J.A. O'Brien, S. Ganapathy, Does Critical Clustering Affect Reaction Rate Constants? Molecular Dynamics Studies in Pure Supercritical Fluids, J. Phys. Chem., 98 (2002) 4173-4179.

[37] C.B. Roberts, J.E. Chateauneuf, J.F. Brennecke, Unique pressure effects on the absolute kinetics of triplet benzophenone photoreduction in supercritical carbon dioxide, J. Am. Chem. Soc., 114 (2002) 8455-8463.

[38] M.E. Sigman, S.M. Lindley, J.E. Leffler, Supercritical carbon dioxide: behavior of .pi.* and .beta. solvatochromic indicators in media of different densities, J. Am. Chem. Soc., 107 (1985) 1471-1472.

[39] Y. Ikushima, N. Saito, M. Arai, Supercritical carbon dioxide as reaction medium: examination of its solvent effects in the near-critical region, J. Phys. Chem., 96 (1992) 2293-2297.

[40] D.S. Bulgarevich, T. Sako, T. Sugeta, K. Otake, Y. Takebayashi, C. Kamizawa, Y. Horikawa, M. Kato, The Role of General and Hydrogen-Bonding Interactions in the Solvation Process of Organic Compounds by Supercritical CO2/n-alcohol Mixtures, Ind. Eng. Chem. Res., 41 (2002) 2047-2081.

[41] J.W. Ford, J. Lu, C.L. Liotta, C.A. Eckert, Solvent Effects on the Kinetics of a Diels-Alder Reaction in Gas-Expanded Liquids, Ind. Eng. Chem. Res., 47 (2008) 632-637.

[42] D.A. Waterkamp, M. Heiland, M. Schluter, J.C. Sauvageau, T. Beyersdorff, J. Thoming, Synthesis of ionic liquids in micro-reactors-a process intensification study, Green Chem., 9 (2007) 1084-1090.

[43] H. Jin, B. Subramaniam, Exothermic oxidations in supercritical CO2: effects of pressure-tunable heat capacity on adiabatic temperature rise and parametric sensitivity, Chem. Eng. Sci., 58 (2003) 1897-1901.

[44] R. Span, W. Wagner, A new equation of state for carbon dioxide covering the fluid region from the triple-point temperature to 1100 K at pressures up to 800 MPa, J. Phys. Chem. Ref. Data, 25 (1996) 1509.

[45] E.W. Lemmon, M.L. Huber, M.O. McLinden, REFPROP Referene Fluid Thermodynamic and Transport Properties, in, 2007, pp. NIST Standard Reference Database 23

[46] A. Ahosseini, A.M. Scurto, Viscosity of Imidazolium-Based Ionic Liquids at Elevated Pressures: Cation and Anion Effects, International Journal of Thermophysics, 29 (2008) 1222-1243.

[47] K.R. Harris, M. Kanakubo, L.A. Woolf, Temperature and pressure dependence of the viscosity of the ionic liquids 1-methyl-3-octylimidazolium hexafluorophosphate and 1-methyl-3-octylimidazolium tetrafluoroborate, Journal of chemical and engineering data(Print), 51 (2006) 1161-1167.

[48] K.R. Harris, M. Kanakubo, L.A. Woolf, Temperature and pressure dependence of the viscosity of the ionic liquid 1-butyl-3-methylimidazolium tetrafluoroborate: Viscosity and density relationships in ionic liquids, J. Chem. Eng. Data, 52 (2007) 2425-2430.

[49] K.R. Harris, L.A. Woolf, M. Kanakubo, Temperature and pressure dependence of the viscosity of the ionic liquid 1-butyl-3-methylimidazolium hexafluorophosphate, J. Chem. Eng. Data, 50 (2005) 1777-1782.

[50] D. Tomida, A. Kumagai, K. Qiao, C. Yokoyama, Viscosity of 1-Butyl-3-methylimidazolium Hexafluorophosphate+ CO2 Mixture, J. Chem. Eng. Data, 52 (2007) 1638-1640.

[51] J.C. Schleicher, A.M. Scurto, Kinetics and solvent effects in the synthesis of ionic liquids: imidazolium, Green Chem., 11 (2009) 694-703.

[52] K.W. Hutchenson, A.M. Scurto, B. Subramaniam, Gas-Expanded Liquids (GXLs): Fundamentals and Applications, in: Gas Expanded Liquids and Near-Critical Media: Green Chemistry and Engineering Washington, D.C., 2009, pp. 3-37.

[53] J.F. Brennecke, E.J. Maginn, Ionic liquids: innovative fluids for chemical processing, AIChE J., 47 (2001) 2384-2389.

[54] A.A. Chrisochoou, K. Schaber, K. Stephan, Phase Equilibria with Supercritical Carbon Dioxide for the Enzymatic Production of an Enantiopure Pyrethroid Component. Part 1. Binary Systems, J. Chem. Eng. Data, 42 (1997) 551-557.

[55] S. Nwosu, J. Schleicher, A.M. Scurto, Kinetics and Polarity Effects for the synthesis of ionic liquids in compressed CO_2 Manuscript in preparation, (2009).

[56] S. Kim, K.P. Johnston, Clustering in supercritical fluid mixtures, AIChE J., 33 (1987) 1603-1611.

[57] J. Zhang, D.P. Roek, J.E. Chateauneuf, J.F. Brennecke, A Steady-State and Time-Resolved Fluorescence Study of Quenching Reactions of Anthracene and 1,2-Benzanthracene by Carbon Tetrabromide and Bromoethane in Supercritical Carbon Dioxide, J. Am. Chem. Soc., 119 (1997) 9980-9991.

[58] P.T. Anastas, J.B. Zimmerman, Peer Reviewed: Design Through the 12 Principles of Green Engineering, Environ. Sci. Tech., 37 (2003) 94A-101A.

7. "Greening" Ionic Liquid Production

7.1. Introduction

Many factors are involved in the critical activity of selecting an "appropriate" solvent for syntheses, based upon principles of "green"/sustainable chemistry and engineering,. When selecting a solvent for an ionic liquid (IL) alkylation reaction, issues such as sustainability, environmental impact, cost (separation and raw material) and kinetics (polarity) come into play. ILs are often synthesized in toxic, volatile and environmentally harmful solvents. To date, the alkylation step has been carried out in a variety of traditional, volatile organic compounds (VOCs). For example, Ford *et al.*[1], used petroleum ether and acetonitrile to synthesize quaternary ammonium ILs. Selvan *et al.*[2], used tetrahydrofuran (THF), and hexane as solvents for synthesizing imidazolium based ILs. Neve *et al.*[3], used pyridine and diethyl ether for pyridinium based ILs. Dichloromethane has been used to process quaternary ammonium, imidazolium, and pyrrolidinium ILs.[4, 5] Bonhôte *et al.*[6], used methanol, acetonitrile, and trichloroethane in processing imidazolium ILs. Karodia *et al.*[7], used toluene to synthesize phosphonium based ILs.

This chapter considers the economic feasibility of, and penalties associated with three solvent platforms: 1) conventional organic solvents; 2) compressed and supercritical CO_2; 3) CO_2-Expanded DMSO. At the early design stages of alternative technology development, it is useful to perform comparative quantitative assessments to identify key economic and environmental drivers.[8] To date, it represents the most complete body of

work on the alkylation step of IL synthesis. The rate of reaction is influenced heavily by the "polarity" of the reaction mixture or solvent. [9, 10] Although high kinetic rates are preferred, straightforward and low-energy separations are needed to purify the IL. The environmental impact, cost and kinetic yield are critical factors for solvent selection in IL production processes. Additionally, the human health impact, especially of the solvent, is an important aspect of designing safer and more sustainable processes.

Here, four different routes for the alkylation step for IL synthesis are compared. The first three routes, acetone as an optimal organic solvent at ambient pressure (1), a CO_2 expanded reactant system (2) and a CO_2 expanded DMSO (CXL) route (3), are compared to a conventional solvent route dichloromethane (DCM) most often used in literature studies. Environmental impact analyses are carried out based on computer-aided material and energy simulations of processes. Inventory data involving IL synthesis is scarce in the literature: only a few groups have attempted or considered the environmental impact of segments of, or complete, IL synthesis processes. Kralisch *et al.* [11, 12], analyzed the synthesis of some ILs using estimated data. Zhang *et al.*, carried out a comparative life cycle analysis (LCA) for the manufacture of cyclohexane in 1-butyl-3methyl-imidazolium tetrafluoroborate ([BMim][BF_4]). Righi *et al.*, also looked at comparative cradle-to-grave LCAs of cellulose dissolution with 1-butyl-3-methylmidazolium chloride and N-methyl-morpholine-n-oxide. The errors in estimates used for IL synthesis are very high, due to limited data availability.

To evaluate proposed novel routes for IL production, this section marries results from experimental kinetic studies, and thermodynamic computation and modeling. Potential

"hot" spots i.e., unit operations that have the most impact on environment and profitability, in the life cycle of the processes are identified. While optimized design configurations for these processes is beyond the scope of this current work, resulting engineering recommendations will serve as 'green' design best practice for consideration in future applications.

7.2. IL Process Development

7.2.1. Background

Only a few studies have considered reaction engineering or process intensification for the production of ILs. Micro-reactors have been investigated for IL synthesis [13, 14]: WaterKamp *et al.*[13, 14] present a technique for the synthesis of 1-butyl-3-methylimidazolium bromide ([BMIM][Br]) in a continuously operating micro-reactor system in a solvent-free modus. While the results achieved were promising, micro-reactors may only be used for relatively low viscosity liquids, requiring sufficient pumping for the high-viscosity liquefied product. For instance the melting point of [BMIm][Cl] is 66.95^{o}C which means that the temperature of the microreactor must be set well above that temperature. They note that, even for micro-reactors used in large scale batch synthesis of [BMIM][Br], safety risks and concerns dictate that reactions be carried out in a solvent. Jess and Grosse-Böwing have also described important reactor engineering issues and properties for the neat synthesis of 1-ethyl-3-methyl-imidazolium ethylsulfate and [BMim][Cl] ILs.[15] Their kinetic modeling yielded recommendations for IL synthesis in an adiabatic loop reactor. They confirm that IL synthesis, without

solvent use, would require extensive heat exchange for cooling in order to avoid a runaway reactor scenario: they set a maximum temperature of 100^{o}C, where IL discoloration typically occurred. Further previously from our group, Schleicher carried out an analysis of IL synthesis in a continuous-flow stirred reactor, using acetone as the solvent of choice (both from an environmental stand point and for separation): he investigated reactions in adiabatic and non-adiabatic conditions. [16, 17] Results of engineering computations for both reactor configurations were compared by energy requirement and size for a specified conversion rate and outlet temperature. The non-adiabatic process was found to be superior, as it required smaller reactor volumes. These studies recommend a continuous process for the quaternization step of IL synthesis. Using the Linear Solvation Energy Relationship (LSER) with environmental and toxicity databases, our group found acetone, of 10 organic solvents studied, optimal for favorable kinetics as well as minimal human and environmental impact. In the long term, large scale production of ILs will need continuous schemes, making solvent use necessary for the synthesis process. The exothermicity of quaternization reactions (ΔH_r for 1-methylimidazole and 1-bromobutane is -96 kJ/mol, with an estimated run-away adiabatic temperature greater than 48°C [13, 14]) is a source of safety concerns. Solvent use would manage the heat generated from the reactions, as well alleviate viscosity issues.[18, 19] However, the use of a solvent introduces tail-end separation issues: the amount of solvent must be minimal, yet sufficient to address heat, viscosity, processing, etc., issues. Depending on the amount of solvent used, the viscosity of the system increases as the IL conversion progresses, driving up utility costs for pumping the product. Further, we have shown that the choice of a solvent is very critical for this type of reaction, as the rate of

reaction is a function of polarity, concentration and temperature; all these factors must be weighed and balanced when designing production processes for an IL.

7.2.2. Design Heuristics for IL Process Development- An Overview

A simplified pictorial process flow diagram is summarized in the superstructure presented in Figure 7. 1. The proposed alkylation process will start in a mixer, where the reactants and solvents are mixed and preheated. The mixture proceeds to the reaction vessel and then a separating vessel, which could be flash drum, distillation column, gas stripper, etc., depending on the choice of the solvent. At each stage, efficient design of each unit operation requires judicious selection of engineering parameters and properties for eventual scale up. In specifying a mixer, for example, density of the mixture, thermal conductivity, heat capacities and enthalpy of mixing will be considered in developing an optimal design.

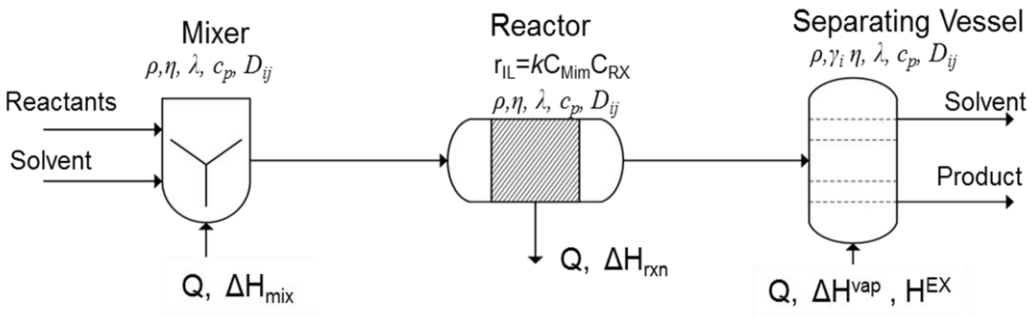

Figure 7. 1 Process sheet for IL production

Analysis of experimental and pilot scale data is key in achieving successful implementation of commercial size processes. A common factor affecting scale-up is the resulting increased energy dissipation in larger vessel volumes: heat transfer surface area per unit volume decreases, which could lead to hot spots, consequently resulting in unwanted runaway conditions. As we have previously shown, feed conditions (molar ratios, temperature, etc.) are among the important factors that inherently affect conversion/yield. Care must be taken at the mixer stage to ensure little or no reaction takes place before mixing is completed. Chemical engineering and design texts are rich with accounts of such variations (such as energy dissipation) in going from pilot to commercial sizes, which can have effects on scale-up success by a factor greater than 10. Dimensionless numbers are used in engineering designs to estimate parameters using physical properties.

7.2.2.1. Mixer

For the mixer, the Damkoehler number, $D_{a,M}$ is typically employed for engineering scale up for mixer design as it usually remains the same for different vessel sizes; concentration, feed location and impeller rotation rate are additional useful parameters for scale-up, as they provide information about the mixing effects that need to be considered.

$$D_{a,M} = \frac{\tau_M}{\tau_R}$$

where τ_M is the mixing time and τ_R is the reaction rate. $D_{a,M}$ is less than 0.001, the reaction rate is slower than the mixing rate and the chemical kinetics is the limiting phenomena. When $D_{a,M}$ > 1000, the reaction rate is much faster than mixing rate; when

$0.001 < D_{a,M} < 1000$, the reaction and mixing rates compete and both micro-mixing and chemical kinetics must be considered. Schleicher, [16, 17] used self-diffusion measurements by ^{1}H NMR of 1-methylimidazole and 1-bromohexane in DMSO to compute the diffusion-controlled reaction rate and compared it to the experimentally determined rate. At 25^{o}C, the predicted diffusion-controlled reaction rate, k_d , is 1.66x10^9 M^{-1}sec^{-1} while the reaction in DMSO has reaction rate constant k of 2.22x10^{-5} M^{-1}sec^{-1} [17]. Thus, the actual rate of reaction is four orders-of-magnitude below that of diffusion controlled regime ($D_{a,M}$ is much less 0.001) and is not limited by diffusion limitations.

7.2.2.2. Separations

For separation (using high pressure CO_2 solvent platform, operating pressure above mixture critical point of reactants and CO_2), the reaction starts out at one phase (critical) and then, as the product (IL) is generated, it forms a different phase (refer to chapter 6). At the desired conversion, the product can be sequestered by simply separating the mixture in a separation/flash vessel. In designing a simple flash vessel, it is assumed that the vapor and liquid are in equilibrium, and that the vessel is adiabatic (no heat lost or gained). Additionally, a material balance, a heat balance, and equilibrium data are necessary. Several design heuristics are available for traditional solvent distillation (encountered in the case of acetone solvent route). Typically, operating pressure is determined by the temperature of the most economically available condensing medium (for example, 100-120^{o}F for cooling water), or by the maximum allowable reboiler temperature (150 psig steam and 366 F). The economically optimal reflux ratio is about

1.2 times the minimum reflux ratio R_m. Several thermodynamic properties will be essential in the design of an optimal distillation process.

7.2.2.3. Reactor

In a plug flow reactor (PFR), reactants are fed to the inlet and the products are removed at the outlet. The reaction takes place within the reactor as the reacting mixture moves through the pipe; its (the mixture's) properties are assumed to be uniformly distributed across the cross-section of the reactor. The design equation for a reactant, *a*, in the PFR is obtained by writing its mass balance over a deferential volume of the reacting mixture *dV*. The theoretical model used to simulate the reaction is based on a second rate kinetic system, described in chapter 2. The second order kinetic rate expression can be described, given a: 1-methylimidazole while b: 1-bromohexane, as:

$$r = k(T)c_a c_b$$

where, $c_a = c_{ao}(1 - X)$. The temperature dependent rate constant is given by the Arrhenius relationship

$$k(T) = Ae^{\left(\frac{-Ea}{RT}\right)}$$

Assuming ideal plug flow, and neglecting radial concentration and temperature gradients inside the pipe, and axial dispersion of heat and mass, the resulting mass and energy balances in terms of reactant n-methyl imidazole (*a*) are:

$$\frac{dn_a}{dV} = -r(T), \quad dX = -\frac{dn_a}{\dot{n}_{a,0}} \quad then \quad \frac{dX}{dV} = \frac{-r}{n_{a,0}}$$

$$\frac{dT}{dV} = \frac{U_a \Delta T + (-r_a(T))(-\Delta H_{Rxn}(T))}{\sum (n_i c_{pi})}$$

where U_a is the overall heat transfer coefficient, $\Delta H_{Rxn}(T)$ is the enthalpy of reaction and the n_i, c_{pi} are the molar flow and heat capacities, respectively, of each specie (reactants and solvent, if any). For practical applications, the overall heat transfer is a function of flow velocity, system geometry, fluid properties, and operating temperatures. It accounts for all resistances, both by conduction and convection. A generalized overall heat transfer coefficient can be expressed as :

$$U_a = \frac{1}{A\sum \text{Resistance}}$$

For this plug flow configuration, it becomes

$$U_a = \frac{1}{\frac{1}{h_i} + \frac{\Delta x_a}{\lambda_{wall}} + \frac{1}{h_o}} \left(\frac{W}{m.K} \right)$$

The external heat transfer coefficient h_o accounts for the heat transfer from the wall to the cooling water. The internal heat transfer coefficient h_i is the heat resistance between the reaction mixtures and the internal wall. Δx_a is the difference of two radii where the inner and outer radii are used to define the thickness of a pipe carrying the fluid. These coefficients may be obtained using empirical correlations based on dimensionless numbers such as the Reynolds number N_{Re}, Nusselts number $N_{Nu,}$ and Prandtl's number N_{Pr}. The Reynolds number is the ratio of inertial forces to viscous forces, and measures

the relative importance of these two types of forces for given flow conditions. It can be expressed as

$$N_{\mathrm{Re}} = \frac{Dv\rho}{\mu}$$

It is particularly useful for characterizing flow regimes, such as laminar or turbulent flow: laminar flow occurs at low Reynolds numbers, where viscous forces are dominant, while turbulent flow occurs at high Reynolds numbers, and is dominated by inertial forces.

The Prandtl number is ratio of the shear component of diffusivity for momentum, μ/ρ, to the diffusivity for heat $\lambda/\rho c_p$, so

$$N_{\mathrm{Pr}} = \frac{\mu / \rho}{\lambda / \rho c_p} = \frac{c_p \mu}{\lambda}$$

The Nusselt number is used to relate data for the heat transfer coefficient h to thermal conductivity λ of the fluid, given a characteristic dimension D (for a pipe, D is its diameter).

$$N_{Nu} = \frac{hD}{\lambda}$$

Heat transfer coefficient correlations abound in design and chemical engineering literature. To employ these types of correlations, mixtures must be thoroughly evaluated to ensure appropriate correlations are being applied, and it is the burden of the design engineer to ensure that assumptions are not violated, and hold true under operating conditions. For instance, to estimate the heat transfer coefficient for laminar flow inside a pipe, one such correlation by Sieder and Tate is given as

$$(N_{Nu})_a = \frac{hD}{\lambda} = 1.86\left(N_{\mathrm{Re}} N_{\mathrm{Pr}} \frac{D}{L}\right)^{1/3}\left(\frac{\mu_b}{\mu_w}\right)^{0.14}$$

where $N_{Re} < 2100$ and $(N_{Re}\, N_{Re}\, D/L) > 100$; L is the length of the pipe, μ_b is the fluid viscosity at bulk average temperature and μ_w is the viscosity at the wall temperature. Several estimations can be made where no data is available; however, accurate fluid property data are essential for optimizing reactor design. Jess and Grosse-Böwing [15] found up to a 50% difference in value for overall heat transfer correlations based on correlation computations (with estimated fluid property data) versus those based on regressed data from experiments. Fluid property data for mixtures encountered in various IL synthesis routes are presented in Chapter 4.

7.3. Principles of Green Engineering

The Environmental Protection Agency (EPA) defines 'green engineering' as the design, commercialization and use of processes and products that are profitable, while minimizing source pollution and environment and human risks. The exciting aspect of green engineering is the marriage of the, sometimes conflicting, concepts of human health and environmental protection, with cost effectiveness. The key factor is early implementation or adoption of green engineering thinking at the design and development phase of a process or product. Annastas and Zimmerman[20] illustrate this in twelve, now widely accepted, principles/guidelines of Green Engineering, as follows:

1. Designers need to strive to ensure that all material and energy inputs and outputs are as inherently nonhazardous as possible.

2. It is better to prevent, than to treat or clean up waste after it is formed.
3. Separation and purification operations should be designed to minimize energy consumption and materials use.
4. Products, processes, and systems should be designed to maximize mass, energy, space, and time efficiency.
5. Products, processes, and systems should be "output pulled" rather than "input pushed" through the use of energy and materials.
6. Embedded entropy and complexity must be viewed as an investment when making design choices on recycling, reuse, or beneficial disposition.
7. Targeted durability, not immortality, should be a design goal.
8. Design for unnecessary capacity or capability (e.g., "one size fits all") should be considered a flaw.
9. Material diversity in multicomponent products should be minimized to promote disassembly and value retention.
10. Design of products, processes, and systems must include integration and interconnectivity with available energy and materials flows.
11. Products, processes, and systems should be designed for performance in a commercial "afterlife".
12. Material and energy inputs should be renewable rather than depleting.

The Twelve Principles of Green Chemistry [21]:

1. **Prevention**: It is better to prevent waste than to treat or clean up waste after it has been created.

2. **Atom Economy**: Synthetic methods should be designed to maximize the incorporation of all materials used in the process into the final product.

3. **Less Hazardous Chemical Syntheses**: Wherever practicable, synthetic methods should be designed to use and generate substances that possess little or no toxicity to human health and the environment.

4. **Designing Safer Chemicals**: Chemical products should be designed to effect their desired function while minimizing their toxicity.

5. **Safer Solvents and Auxiliaries**: The use of auxiliary substances (e.g., solvents, separation agents, etc.) should be made unnecessary wherever possible and innocuous when used.

6. **Design for Energy Efficiency**: Energy requirements of chemical processes should be recognized for their environmental and economic impacts and should be minimized. If possible, synthetic methods should be conducted at ambient temperature and pressure.

7. **Use of Renewable Feedstocks**: A raw material or feedstock should be renewable rather than depleting whenever technically and economically practicable.

8. **Reduce Derivatives**: Unnecessary derivatization (use of blocking groups, protection/ deprotection, temporary modification of physical/chemical processes) should be minimized or avoided if possible, because such steps require additional reagents and can generate waste.

9. **Catalysis**: Catalytic reagents (as selective as possible) are superior to stoichiometric reagents.

10. **Design for Degradation**: Chemical products should be designed so that at the end of their function they break down into innocuous degradation products and do not persist in the environment.

11. **Real-time analysis for Pollution Prevention**: Analytical methodologies need to be further developed to allow for real-time, in-process monitoring and control prior to the formation of hazardous substances.

12. **Inherently Safer Chemistry for Accident Prevention**: Substances and the form of a substance used in a chemical process should be chosen to minimize the potential for chemical accidents, including releases, explosions, and fires.

The ultimate goal of this area of engineering is achieving sustainability. In many cases, one, or more, of the principles becomes challenging to adhere to: the more applicable principle then supersedes the others. In attempting to optimize processes with regards to minimizing waste, environmental and human impact, while maximizing profit, scientists and engineers struggle to balance these principles. The first listed principle, along with LCA, is the key approach for "greening" engineering processes. In this study, we strive to achieve **Principles 1, 2**, **3,** possibly **4, 5** and **10** of green engineering by systematically selecting green solvents, or solvents with the least environmental impact, while also heavily weighing energy input for the process. Additionally, in meeting these goals, we meet **Principles 1 through 5** of green chemistry.

Separation design is the most energy intensive segment of many chemical processes; energy is required for purifying products or for compressing CO_2 to high pressure. Resulting emissions and cost are identified as the key impacts of the chosen processes. Here, CO_2 is found to be kinetically competitive for IL synthesis: it requires no other separation beyond flashing off CO_2, which is then recycled. However, the LCA approach dictates that the cost and energy input into the CO_2 compression must be considered to check overall "net" sustainable advantage (cost of solvent, solvent choice's need for pumps, compression cost and energies required, kinetic rates and downstream separations).

7.4. Risk Impact Categories

Environmental risk assessment measures the probability of adverse effects.[22] Physico-chemical properties of substances such as boiling point, melting point, vapor pressure, Henry's law constant and solubility are used to quantify the risk categories. Example of risk impact categories include: *ozone depletion* (change in the amount of ozone, O_3, in the stratosphere resulting from the release of a given solvent; related to the same amount released by trichlorofluoromethane's emission[23]) and *global warming potential* (accumulation of infrared energy released by 1 kg of solvent relative to 1 kg CO_2.[23]). *Smog formation* is the capacity of a given solvent to create smog formation agents.[23] *Bio-concentration factor* is the ratio of a chemical's concentration in the tissue of an aquatic organism, compared to its concentration in water. Ranking these indicators by

order of importance in the choice of a solvent is arguably debatable and often adds vagueness or ambiguity to green impact studies. At all times, less toxic chemicals should be used in processes. This ensures minimal to zero worker exposure and reduces adverse effects of potential emission or spills **(Green Chemical Engineering Principles 1** and **2).** Techniques for processing these impacts factors are widely available. In the area of ILs, the sheer enormity of the number of possible compounds further frustrates IL toxicity data availability. Unknown properties for organic compounds can be estimated using models such as group contribution methods.

7.5. E-Factor

The E-Factor is a green chemistry metric that measures the efficiency of a chemical process. It is computed as the ratio of waste generated per kilogram product obtained, where waste is described as everything but the

desired product. The ideal E-factor is zero, and higher This can be expressed as:

$$E - Factor = \frac{Total\ waste(kg)}{\mathrm{Pr}oduct(kg)}$$

E-factors are indicative of higher environmental burden. Table 7. 1 is an overview of typical E-factors associated with different chemical industries.

Table 7. 1 E-factor analysis for industry

Industry[a]	Product tonnage[a]	E-factor[a]
Oil Refining	10^6-10^8	~0.1
Bulk Chemicals	10^4-10^6	1-5
Fine Chemicals	10^2-10^4	5-50
Pharmaceuticals	10^1-10^3	50->50

a.) Taken from ref.[12]

Higher throughput industries, such as oil refining, have lower amounts of waste; the fine chemicals sector (pharmaceuticals, etc.) show high amounts of waste per unit amount of desired product. By examining process efficiency, this metric can be a useful tool in determining "greener" synthesis design for ILs. While it considers material flow, the E-factor approach neglects energy streams, limiting its use for processes in which energy requirements dominate. For instance, in the quaternization reaction used to produce [HMIm][Br], the E-factor is essentially ~0 if no solvents were used in the synthesis, since every mole of reactant is converted to the desired product when stoichiometric amounts of starting material are used. However, due to high viscosities[24-26], low melting points (solid products)[27, 28], heats of reaction[13, 14], etc., the neat synthesis is typically undesirable as it will add to higher energy requirements. Further, ILs are typically produced via a further anion exchange step after the quaternization reaction of halo-anion ILs, such as the [HMIm][Br], studied here. The anion exchange step can add significantly large amounts of organic solvent and/or water to the overall IL production, dramatically changing the E-factor. Additionally, the E-factor does not account for recycled materials,

such as solvent and catalyst, and therefore only relates the total amount of mass needed for processing to the desired output. This is noteworthy, as in this study, the main advantage of using a gas expanded solvent rests heavily on the ability to recycle CO_2.

For an IL synthesis with acetone as the solvent platform, the ratio of the mass of sum of reactants and solvents to the amount of ionic liquid system, computed E-factor was found to be within the range for bulk chemicals (see Table 7. 1). Since Sheldon's first presentation of E-factor about two decades ago, environmental impact assessment investigations in the literature attempt to account for energy, using different approaches. For example, Kralisch and coworkers [11, 12] employed an energy efficiency methodology of accounting for energy E_{EF} in four categories: cumulative energy demand for solvent supply, heating of the solvent to reaction temperature, workup energy, and thermal disposal of the solvent, required in the production of 1-butyl-3-methylimidazollium tetrafluoroborate implemented in Umberto. [11, 12] While this methodology can be potentially useful, the study did not quantify separation energy for the corresponding solvents. Another method, employed by Fang *et al.*, for an environmental impact analysis of catalytic olefin hydroformylation in a CO_2 expanded liquid media, accounts for energy requirements by including CO_2 emissions due to energy consumptions in E-factor waste computation.

7.6. Rowan Solvent Selection Table (RSST)

The Rowan Solvent Selection Table (RSST) [23, 29] attempts to quantify the human and environmental impact of solvent factors. Our group has previously used this for analyzing IL production processes. The RSST yields an overall index obtained by normalizing and weighting each impact factor. In the original formulation, the human impact factors were weighted higher than the environmental factors as it was originally developed for the pharmaceutical industry. Our group set the weightings equal. The RSST uses chemical and environmental properties of a given chemical or solvent for the calculation of an overall "greenness" score, by taking into account various environmental parameters and determining an overall solvent index. Further, RSST software gives the user the flexibility of comparing processes using a user-defined index, that is, an overall weighted factor such as solvent type, quantity, and environmental impact.

In determining the Index, the values obtained for solvents are compared to that of water, which has an Index of zero.[23] Thus, the larger the value of the Pharmaceutical Index, the less "green", or sustainable, the solvent is for a given application. Additionally, by incorporating a weighting factor to account for amount of solvent used, the RSST index allows for a comparison of processes based on the amount of solvent required. Table 7. 2 presents the Rowan Green index with ten solvents, ranked by kinetic rate constant, for the synthesis of [HMim][Br] at 40^{o}C. [17] The RSST Index indicates DMSO as the best solvent at 0.42, while acetone has a 2.15 index (worst). The neat solvent route has an estimated highest index of 5, which is similar to the toxicity of synthesizing the IL in a solvent such as chlorobenzene (o-dichlorobenzene), found to be the worst solvent choice

based on how “green” it is for the quaternization reaction. Carbon dioxide has a negligible index value, and would be considered from this impact category as the best solvent choice.

Table 7. 2 Rowan Green index with ten solvents, ranked by kinetic rate constant, for the synthesis of [HMim][Br] at 40oC [17]

Solvent	**k x10^{6} (M^{-1} sec^{-1})**	***Rowan* "Green Index" (0= Best)**
Dimethyl Sulfoxide	77.89	0.42
Acetonitrile	21.56	3.21
Neat (1→2→1 phase)	*17.63*	>5 (Est.)
Cyclopentanone	15.11	3.6
Carbon Dioxide	7-17	0
Acetone	12.67	2.15
2-Butanone	11.56	3.6
Dichloromethane	8.47	5.36
Ethyl Formate	7.97	3.11
Chlorobenzene (1 → 2 phases)	3.64	>5 (est.)
Ethyl Lactate	2.86	1.57
Methanol	2.03	2.52

7.7. Environmental Assessment Methodology

The systematic risk assessment methodology developed by Allen and Shonnard is employed here for this environmental impact assessment. This is the first time this

methodology has been extended to ILs systems. Environmental Fate and Risk Assessment Tool (EFRAT) is a process design software for estimating environmental and health impact of designs through screening fate and transport calculations and risk assessment indices. EFRAT, which resides within the SCENE software implements the systematic risk assessment methodology. First, a mass balance and energy balance is performed, using process simulation software Aspen HYSIS 7.3 (Aspen Technology Incorporated). Then, Chemical Partition Estimation is performed for four environments, namely air, water, soil, and sediment. The method computes/predicts the emission distribution in four compartments (air, surface water, soil, and sediment), assuming constant emissions are released to the environment. Parameters are obtained from chemical structures using the EPI (Estimation Programs Interface) Suite™, a collection of physical/chemical property and environmental fate estimation programs, developed by the EPA's Office of Pollution Prevention Toxics and Syracuse Research Corporation (SRC). One segment of the EPI converts emissions into environmental concentrations via a modified "level III" multimedia fugacity model. Once all parameters are available, an overall process Composite Index can be computed. EFRAT computes a Relative Risk Index for a given process. The air emissions calculator within EFRAT uses emission factors along with stream data to compute emissions specific to unit operations and fugitive air emissions rates for each chemical within a process. Risk assessment indices computed from the EFRAT which resides within the SCENE software are employed here. As many parameters used in these synthesis platforms are not experimentally available, estimated parameters used for toxicity were obtained using the EPA Toxicity Estimation Software Tool (TEST). Chemical partition, persistence and bioaccumulation

data that are not readily available were computed/estimated using the Environmental Protection Agency's EPI (Estimation Programs Interface) Suite™.[30] Figure 7. 2 is an overview map of the method employed in this study.

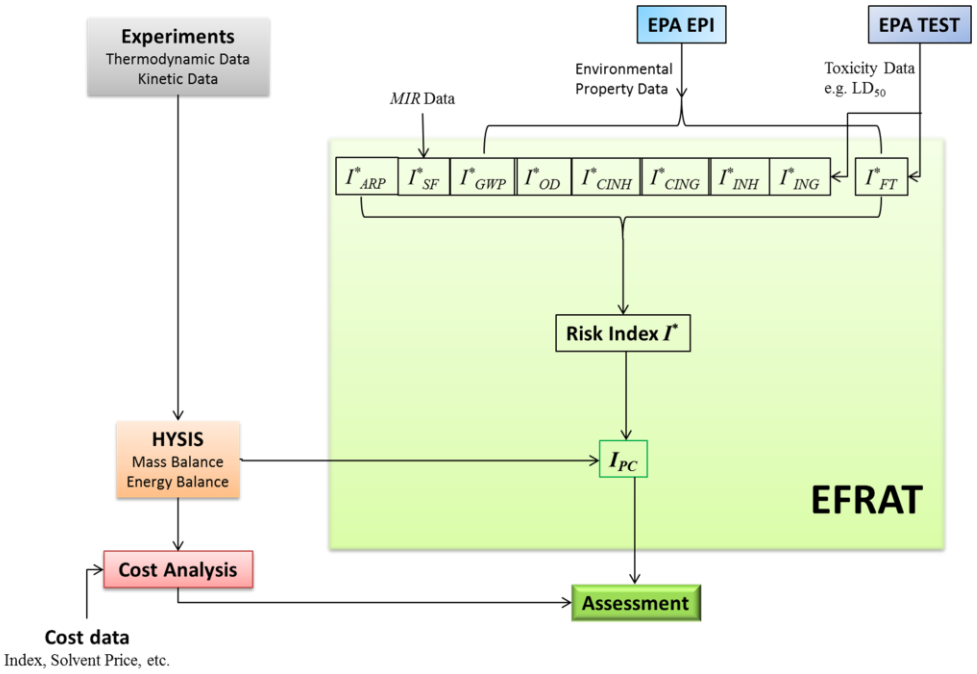

Figure 7. 2 Systematic Risk Assessment Method Map for this Study

7.7.1. Fate and Emission Estimation

Several parameters are needed for each chemical in risk analysis study. These include vapor pressure, Henry's Law constant (*H*), octanol-water partition coefficient (K_{OW}), bio-concentration factor (*BCF*), as well as several distribution coefficients such as the water/solids coefficient (K_{ds}), soil/plant coefficient (K_{SP}) and air/solids coefficient (K_{da}). In scenarios where emitted chemicals may enter or leave compartments via different processes, we must take such information into consideration. This is often described by a partitioning of chemical between different environmental phases - air, water, solids (soil, sediment, and suspended sediment), fish, and aerosol. The inter-media transport between environmental compartments (air/water, air/soil, water/sediment etc.) can be by diffusive and non-diffusive mechanisms are described by models such as the Fugacity Model.[31-33] The mole fraction or amounts partitioned to the air, water, soil, or sediment compartments can then be approximated. EPI Suite software implements this model, using data from other programs and an accompanying database.

7.7.1.1. Fugacity Model

The Fugacity Model is widely accepted for quantifying the partitioning of chemicals in the different environmental compartments. There are 3 series in the Fugacity Model described by McKay.[34] These models describe the partitioning of an organic chemical in a control environment with area of 1 km^2 at 25 ^oC. The 3 fugacity level account for two environment, where (a) is an environment of only air, water, soil, sediments and (b)

is the media fish and suspended solids. Level I estimate the equilibrium partitioning of a known amount of organic chemical between the homogeneous environmental media with defined volumes, densities, organic carbon contents, and lipid fraction. This model assumes that there are no in- or out-flows of chemical, and no loss by reactions. Level II is similar to Level I, however, it assumes steady state with a constant input rate. There is both advective in- and out-flow of chemical within the control volume boundary. Loss of chemical through degrading reactions may occur. Although steady state is also assumed, for Level III, the system is not in equilibrium. In this level, conventional expressions and typical parameters for intermedia transfer by processes such as wet deposition from the air and sediment deposition in the water would be used.

The fugacity model Level I quantifies the partitioning of chemicals in the different environmental compartments, as follows:

- Air: $f = y\phi P_T \approx \mathrm{P}$

The term y is the mole fraction in the air phase, ϕ is the dimensionless fugacity that accounts for non-ideality at low pressures encountered at ambient conditions (1atm) - it is assumed to be unity. P is the total pressure. Concentration is related to partial pressure by the ideal gas law.

- Water phase: $f = x\gamma P^s$

Here, γ is the activity coefficient (evoking Raoult's law), x is the mole fraction and P^s is the saturation vapor pressure of the pure liquid chemical. Assuming a very dilute concentration, Henry's law constant, H, is used to relate concentration and fugacity in

$$\frac{x}{v_w} = \frac{f}{v_w \gamma P^s} = \frac{f}{H}.$$

v_w is the molar volume of solution.

- Soil phase:

It is assumed compounds are sorbed to organic matter in the soil, and are in equilibrium with water phase concentration, hence the distributed coefficient, which is seen to correlate with K_{ow}.

7.7.1.2. Environmental Protection Agency's EPI (Estimation Programs Interface) Suite™

The Estimation Programs Interface (EPI) Suite is a Windows®-based suite of physical/chemical property and environmental fate estimation programs developed by the EPA's Office of Pollution Prevention Toxics and Syracuse Research Corporation (SRC). A comprehensive search for chemical property data was carried out before using EPI Suite. In addition, EPI Suite implements a database search (called PHYSPROP©).

EPI Suite implements several estimation programs.

- Dermwin™ estimates the dermal permeability coefficient K_p.
- ECOSAR™ predicts aquatic toxicity. ECOSAR™ can also be downloaded as a separate program that estimates toxicity of chemicals discharged into water using structural activity relationships (SARs).
- KOWWIN™ estimates the log octanol water partition coefficient of compounds using group contribution methods.
- AOPWIN™ estimates gas-phase reaction rate chemicals and hydroxyl radicals.

- HENRYWIN™ predicts the Henry's Law constant using both bond and group contribution methods.
- MPBPWIN™ estimates melting point, boiling point and vapor pressure.
- BIOWIN™ estimates aerobic and anaerobic biodegradability of organic chemicals using seven different models.
- BioHCwin estimates biodegradation half-life for hydrocarbons only.
- KOCWIN™ estimates the K_{oc}, organic carbon-normalized sorption coefficient for soil and sediment, via two methods, one of which is based on log K_{OW}.
- WATERNT™ and WSKOWWIN™ estimate a compound's solubility in water.
- BCFBAF™ estimates fish bioconcentration factor.
- HYDROWIN™ estimates aqueous hydrolysis rate constants and half-lives for the following chemical classes: esters, carbamates, epoxides, halomethanes, selected alkyl halides, and phosphorus esters. It identifies a variety of chemical structure classes for which hydrolysis may be significant (e.g. carbamates) and gives relevant experimental data.
- KOAWIN estimates K_{OA}, the octanol/air partition coefficient, using the ratio of the octanol/water partition coefficient (K_{OW}) from KOWWIN™ and the dimensionless Henry's Law constant (K_{AW}) from HENRYWIN™.
- AEROWIN™ estimates the fraction of airborne substance sorbed to airborne particulates, i.e. the parameter phi (φ).
- The fate models WVOLWIN™ and STPWIN™ use several outputs from EPI Suite™ to predict the removal of a chemical in a typical activated sludge-based sewage treatment plant. Values are given for total removal and three processes

that may contribute to removal: biodegradation, sorption to sludge, and air stripping.

- LEV3EPI™ contains a level III multimedia Fugacity Model and predicts partitioning of chemicals among air, soil, sediment, and water under steady state conditions for a default model "environment".
- ECOSAR™ estimates ecotoxicity.

The EPI output for all the compounds analyzed are presented in the appendix section.

7.7.2. Relative Risk Index Calculator

The Relative Risk Index Calculator computes nine environmental and health impact indexes for overall process: 1) global warming, 2) ozone depletion, 3) smog formation, 4) acid rain, 5) and 6) human inhalation and human ingestion route non-carcinogenic toxicities, 7) and 8) human inhalation and human ingestion route carcinogenic toxicities, and 9) ecotoxicity (fish mortality). The general formula for calculating indexes is given by,

$$I_i^* = \frac{\left[(D)(\tau)(P)\right]_i}{\left[(D)(\tau)(P)\right]_{benchmark}}$$

Here, D is a dimensionless mole fraction partitioned to the air, water, soil, or sediment compartment (obtained from the Fugacity Model, for example) and τ is the reaction residence time of the chemical in the impacted compartment (unit of time) (EPI output). P is the inherent impact parameter of the index: for example, Global Warming Potential

(GWP) for the global warming index. So, the cumulative process index for the environmental impact category is given by:

$$I_i = \sum_{i=1}^{n} (I_i^* \times E_i)$$

E_i is the cumulative emission rate of chemical *i* from the entire process; *n* is the number of chemicals emitted from the process. Thus, the cumulative process index (I_i) has units of emission rate (mass/unit time), and represents the equivalent emission of the benchmark compound having the same impact as the actual process emissions.

Finally, a composite process index (I_{PC}) is calculated as the sum of the normalized indices,

$$I_{PC} = \sum_{i=1}^{n} (I_i^N \times W_i)$$

where $I_i^N = \frac{I_i}{\hat{I}}$, W_i is the weighting factor for each environmental impact category, and $\hat{I}$ is a published national index for each impact category (product of the annual national emission of the chemical representing the impact category and its average relative risk index in the national inventory). The weighting factor used is generated for quantification of environmental effects that negatively impact ecosystems or human health based on the distance to target principle, which assumes that 5% ecosystem damage is equal to one human death per million per year. Individual equations for impacts are summarized below [22]:

- Global Warming Potential

$$I^*_{GW} = GWP \times \frac{D_{i,A}}{D_{CO2,A}}$$

where the *D* values are obtained from the Fugacity Model. Compounds that mineralize readily to CO_2 account for indirect contribution due to carbon dioxide released upon atmospheric oxidation, I^*_{GW}, given by:

$$I^*_{GW} = N_C \times \frac{Mw_{CO_2}}{Mw_i}$$

N_c is the number of carbons in the compound and *Mw* are the molecular weights.

- Ozone depletion

$$I^*_{OD} = ODP \times \frac{D_{i,A}}{D_{CFC-11}}$$

Ozone depletion is computed from photochemical models. Here, data on reaction lifetimes, atomic oxygen reaction rate constant (*k*), both given in EPI output, and number of chlorine in each chemical are used to evaluate this model. Trichlorofluoromethane (CFC-11, CCl3F) is the benchmark compound.

- Smog formation

$$I^*_{SF} = \frac{MIR_i}{MIR_{Formaldehyde}} \times \frac{D_{A,i}}{D_{A,Formaldehyde}}$$

MIR is the tabulated maximum incremental reactivity of the compound. Photo-dissociation of NO_2 accounts for large portion of the ozone formed in the lower atmosphere, given by:

$$NO_2 + h\nu \rightarrow O^3(P) + NO$$
$$O(^3P) + O_2 + M \rightarrow O_3 + M$$
$$O_3 + NO \rightarrow NO_2 + O_2$$

where M can be nitrogen or molecular oxygen. Volatile organic compounds form radicals with NO_2 without destroying ozone, increasing ozone levels. Incremental reactivity was proposed to evaluate smog formation potential and is defined as changes in moles of ozone formed as a result of emission into one mole of the VOC emitted into air. Different scales can be used, and several models in the literature exist from estimating IR. EFRAT employs maximum incremental reactivity (MIR), occurring under NO_x conditions when the highest ozone formation occurs. Higher MIR is indicative of higher NO_x levels. The benchmark compound for this index is formaldehyde. MIR data was obtained from different databases: for 1-methylimidazole, the MIR for pyridine was used and for 1-bromohexane, the MIR for bromobutane was used.

- Acid rain index

$$I^*_{AR} = \frac{ARP_i}{ARP_{SO_2}} \times \frac{D_{A,i}}{D_{A,SO2}}$$

ARP is the acid rain potential of the chemical, given by:

$$ARP_i = \frac{\eta_i}{\eta_{SO_2}}$$

$$\eta_i = \frac{\alpha_i}{MW_i}$$

$$X + \ldots \rightarrow \alpha H^{+} + \ldots\ldots$$

α is the number of moles of the hydrogen ion created per number of moles of the compound emitted. *MW* is the molecular weight of the compound and SO_2 is the benchmark compound.

7.7.2.1. Accounting for Toxicity

Toxicity to humans and the ecosystem are both accounted for as functions of dose and response. Dose depends on the fate and transport of the chemical and its intake. Although quantifying this risk can be complicated, Shonnard and Allen[22] sufficiently simplify this category to quantify this impact for use in engineering design. Inhalation and ingestion are assumed to be the dominant mode of exposure. For this study, rat inhalation LC_{50} data were obtained from MSDS sheets when available. Rat ingestion LD_{50} data were obtained or estimated using the EPA's Toxicity Estimation Software Tool (TEST).

7.7.2.1.1. Environmental Protection Agency's Toxicity Estimation Software Tool (TEST)

The TEST tool enables researchers to estimate toxicity from a chemical's molecular structure. The program uses predictive models obtained from correlating existing toxicity data to estimated quantitative toxicity values, such as FLC_{50}, the concentration of a certain chemical (in mg/L) it would take to result in a 50% mortality rate for a commonly used study animal (such as fathead minnows) in a given amount of time (here, FLC_{50} 96

hr is used). Further, TEST houses a comprehensive database of experimental values and can output these with references. Each type of test contains its own library, which varies in size and composition, of comparison chemicals. In the case where experimental data is available, it was used instead of an estimated value.

- Inhalation non-carcinogenic human toxicity

$$I^*_{INH} = \frac{LC_{50,Toluene}}{LC_{50,i}} \times \frac{\tau_{i,A}}{\tau_{Toluene,A}} \times \frac{D_{i,A}}{D_{Toluene,A}}$$

- Ingestion non-carcinogenic human toxicity

$$I^*_{ING} = \frac{LD_{50,Toluene}}{LD_{50,i}} \times \frac{\tau_{i,W}}{\tau_{Toluene,W}} \times \frac{D_{i,W}}{D_{Toluene,W}}$$

LC_{50} and LD_{50} are the lethal concentration and lethal dose values for 50% mortality of animals (rats) in an acute exposure. τ is the reaction half-life in air (subscript *A*), obtained from EPI output and water (subscript *W*) .Toluene is used as the benchmark compound.

Cancer related risk is bench marked against benzene. The carcinogenic potential is determined using Hazard Value (HV) [35] obtained from the Weight of Evidence classification schemes of the EPA and of the International Agency for Research on Cancer (U.S. EPA, 1997 and OSHA, 1997),[36] shown in **Table 7. 3**:

Table 7. 3 Carcinogenicity scoring (Weight of Evidence Classifications (IRIS)) [22]

Group	Definition	HV
A	Human carcinogen	5
	Probable Human Carcinogen	
	B1: Limited data	B1:4.0
B	B2: Sufficient Data	B2:3.5
C	Possible Human Carcinogen	1.5
D	Not Classifiable	0
E	Evidence of Non-Carcinogenicity	0

- Inhalation non-carcinogenic human toxicity

$$I^{*}_{CINH} = \frac{HV_i}{HV_{Benzene}} \times \frac{\tau_{i,A}}{\tau_{Benzene,A}} \times \frac{D_{i,A}}{D_{Benzene,A}}$$

- Ingestion carcinogenic human toxicity

$$I^{*}_{CING} = \frac{HV_i}{HV_{Benzene}} \times \frac{\tau_{i,W}}{\tau_{Benzene,W}} \times \frac{D_{i,W}}{D_{Benzene,W}}$$

- Ecotoxicity (fish mortality)

$$I^{*}_{FT} = \frac{LC_{50f,PCP}}{LC_{50f,i}} \times \frac{\tau_i}{\tau_{PCP}} \times \frac{D_{i,W}}{D_{PCP,W}}$$

The subscript PCP represents pentachlorophenol, the benchmark compound.

Table 7. 4 Summarized definitions for relative risk indices (Curled from the EFRAT Manual)

Relative risk index	Equation
Global warming	$I^*_{GW,i} = N_{C,i} \times \frac{Mw_{CO_2}}{Mw_i}$ $\quad I^*_{GW,i} = GWP_i$
Ozone depletion	$I^*_{OD,i} = ODP_i$
Smog formation	$I^*_{SF,i} = \frac{MIR_i}{MIR_{Formaldehyde}}$
Acid rain	$I^*_{AR,i} = \frac{ARP_i}{ARP_{SO_2}}$
Human non-carcinogenic ingestion toxicity	$I^*_{ING,i} = \frac{LD_{50,Toluene}}{LD_{50,i}} \times \frac{\tau_{i,W}}{\tau_{Toluene,W}} \times \frac{D_{i,W}}{D_{Toluene,W}}$
Human non-carcinogenic inhalation toxicity	$I^*_{INH,i} = \frac{LC_{50,Toluene}}{LC_{50,i}} \times \frac{\tau_{i,A}}{\tau_{Toluene,A}} \times \frac{D_{i,A}}{D_{Toluene,A}}$
Human carcinogenic ingestion toxicity	$I^*_{CING,i} = \frac{HV_i}{HV_{Benzene}} \times \frac{\tau_{i,W}}{\tau_{Benzene,W}} \times \frac{D_{i,W}}{D_{Benzene,W}}$
Human carcinogenic inhalation toxicity	$I^*_{CINH,i} = \frac{HV_i}{HV_{Benzene}} \times \frac{\tau_{i,A}}{\tau_{Benzene,A}} \times \frac{D_{i,A}}{D_{Benzene,A}}$
Fish toxicity	$I^*_{FT,i} = \frac{LC_{50f,PCP}}{LC_{50f,i}} \times \frac{\tau_{i,W}}{\tau_{PCP,W}} \times \frac{D_{i,W}}{D_{PCP,W}}$

N_C: number of carbons; M_W: molecular weight; *ODP*: ozone depletion potential; *MIR*: maximum incremental reactivity; *ARP*: acid rain potential; τ_W : persistence of chemical in water; τ_A : persistence of chemical in air; LC_{50}: lethal concentration; *HV*: hazard value.

7.8. Assessing IL Synthesis Systems

Environmental evaluation of the *greenness* of any product or technology should consider the product life cycle in its entirety, since impacts may occur at, or shift to, various stages of the life cycle. Case in point: the question arises whether IL are "green", or truly nonvolatile, if many upstream processes in the life cycle of ILs and precursor chemicals do involve volatile and hazardous organic reactants. Although the environmental impact assessments here are focused on the IL synthesis process (reaction and separation of the product), we present a brief overview of the reactants and the IL human- and eco-toxicity. Jastorff *et al.,* [37] sketch out life cycle analyses for the multi-objective problem of designing ILs, focusing primarily on influence of side chain influence and anion choice on toxicity for imidazolium type ILs. Their work illustrates the complex nature and issues associated with IL use. Zhang *et al*., [38] carried out an LCA using IL 1-butyl-3-methyl-imidazolium tetrafluoroborate ([Bmim][BF_4]) for the manufacture of cyclohexane in a Diels–Alder reaction, comparing results with more conventional synthesis methods. They found that using the IL resulted in a higher life cycle environmental impact. In selecting ILs for processes, their stability will be important and can significantly increase environmental impact. For example, 1-alkyl-3-methylimidazolium tetrahaloaluminates, such as [Bmim][$AlCl_4$] can decompose to halomethane and alkylimidazole, while ILs containing $[PF_6]^-$ can be hydrolyzed to hydrogen fluoride. Recently, Righi *et al.*,[39] presented environmental impact analyses of industrial cellulose dissolution with the IL 1-butyl-3-methylimidazolium chloride ([Bmim][Cl]). They compared the IL system to the well-established *N*-methyl-morpholine-*N*-oxide (NMMO)/H_2O process. [Bmim][Cl] generates higher environmental loads via abiotic resource depletion (non-living chemical

and physical factors), emissions of volatile organic compounds and eco-toxicity than does the NMMO/H_2O process. They found the IL route to be advantageous in the human toxicity impact category, while major contributions to the environmental impacts come from precursor syntheses (parent organics, methyl imidazole, butyl chloride and work up solvents). Contribution to abiotic resource depletion is mainly due to the extraction of fossil fuels, in particular methane, used in electric and thermal energy production, and due to crude oil and methane being used as raw materials for these organic solvents. ILs have negligible volatility and will not have significant direct air emissions. Their toxicity is higher than that of acetone: halide ILs will have comparable toxicity to chlorinated organic compounds, as some studies indicate minimal degradation of [Bmim][Cl] in water. This evidence indicates that emissions of IL in fresh water would negatively impact the ecosystem. Kralish and coworkers [11] validated the ECO (ecological and economic optimization) method using IL synthesis. This method describes energy, environmental and economic requirements of routes as efficiencies, while also considering material costs of the synthesis of ILs in different conventional solvents. They showed that, for an IL to be advantageous from an environmental standpoint, efficiencies associated with its manufacture must be increased.

7.8.1. Assessing IL Synthesis Systems-EFRAT Result

Figure 7. 3 presents inherent risk indices for the nine impact categories computed in EFRAT for different solvents used in IL synthesis. From the figure, acetonitrile and chlorobenzene is associated with the highest inherent risk indices of all the solvents considered; DMSO, methanol, ethylacetate, DCM and acetone all have moderate risk

index which translate into lower environmental impact. CO_2 as a solvent, has the least environmental impact, with only a penalty for the Global Warming Potential index; in fact, CO_2 is the reference chemical for the GWP index (see GWP index computation above). Additionally, environmental credits can be claimed when CO_2 used are form non-sequestered sources. 1-methylimidazole, compared to 1-bromohexane, has a higher environmental impact, due to its high fish (aquatic) toxicity. The model predicts a preferential partition of 1-methylimidazole into the water and air environmental compartments. While these are mostly predicted properties, it is reassuring that the model predicts little air pollution for the non-volatile IL with the predominant pollution pathways of [HMim][Br] as partitioning to the water and soil. Its air partitioning fraction/percent is negligible, and is attributed mostly to aerosols that can form, or the IL adsorbing to airborne particles. Here, conservative estimates were used for the IL, since no data is available for its toxicity or IRIS ranking. The few available complete material safety data sheet (MSDS) for ILs are rated highly toxic. For this study, conservative carcinogenic ranking was used for the IL, resulting in a relatively high carcinogenic impact results. However, for the purposes of this study, this is does not affect comparative study as the IL is present across all systems. That most solvents preferentially partition into the water and air compartment does not come as a surprise. Most of these solvents are volatile organic compounds (VOC) and are known to be notorious for air emissions. It is these kinds of solvents that ILs can replace. From the EFRAT indices, CO_2 is the solvent with the least environmental impact. DMSO has also a low environmental impact, as does dimethylsulofoxide (DMSO), ethyl acetate and

acetone. While these indices are raw numbers without weighting, the breakdown is a useful tool to heuristically select a solvent for preliminary solvent choice/analysis.

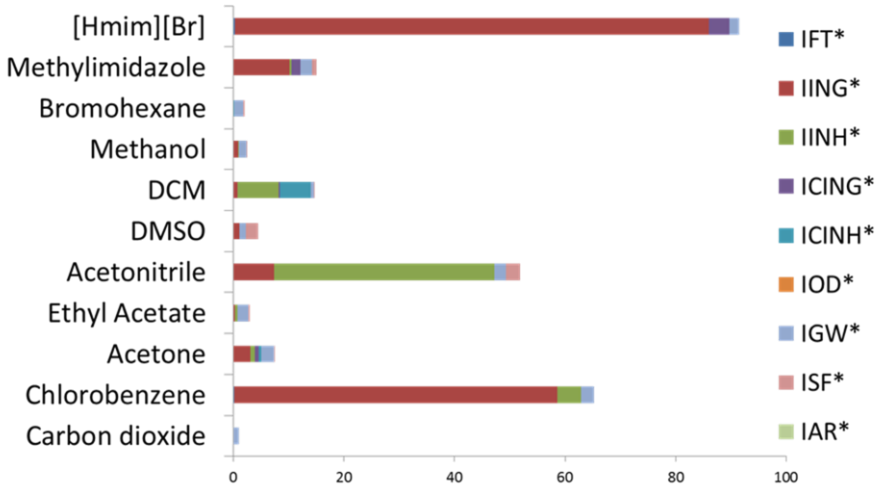

Figure 7. 3 Dimensionless Index for nine EFRAT Impact Categories for different Solvents for IL Synthesis

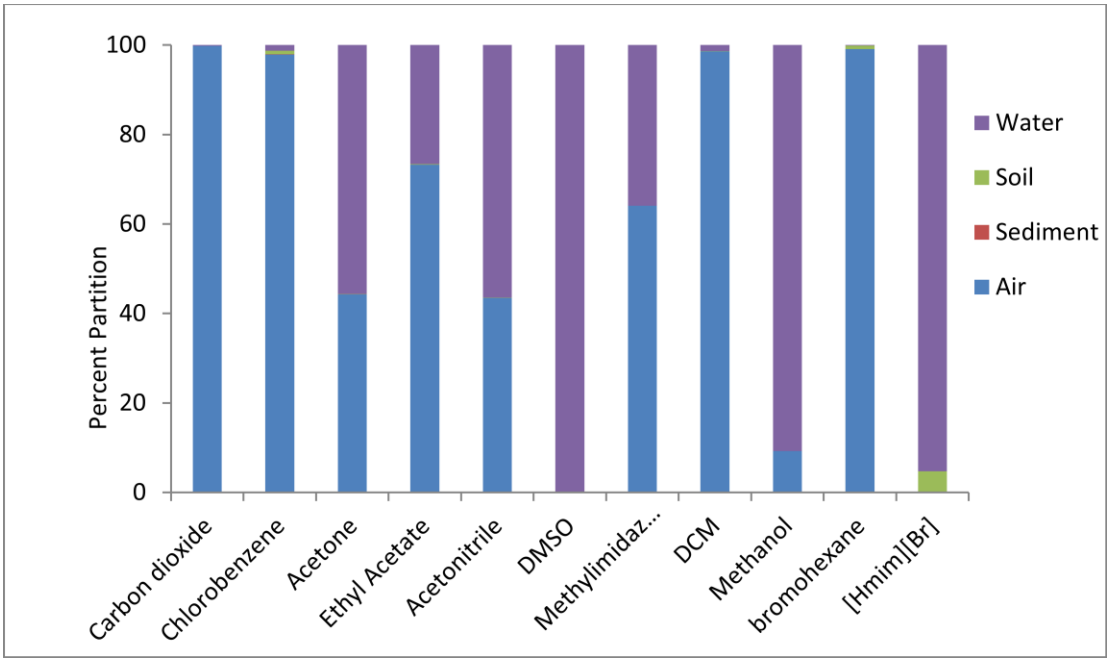

Figure 7. 4 Fate & Transport: Percent partitioning of compound into environmental compartments

Table 7. 5 Chemical Indices for various EFRAT Impact Categories

Chemical	IFT*	IING*	IINH*	ICING*	ICINH*	IOD*	IGW*	ISF*	IAR*
1-bromohexane	1.56E-04	2.46E-03	0.01	0.00	0.15	0	1.60	0.19	0
methylimidazole	1.26E-03	1.01E+01	0.32	1.63	0.01	0	2.14	0.83	0
Carbon dioxide	7.16E-06	0.00E+00	0.00	0.00	0.00	0	1.00	0.00	0
Chlorobenzene	1.99E-01	5.84E+01	4.31	0.00	0.00	1.76E-05	2.35	0.00	0
Acetone	1.74E-04	3.06E+00	0.78	0.72	0.48	0	2.27	0.14	0
Ethyl Acetate	8.09E-04	2.35E-01	0.48	0.00	0.00	0	2.00	0.23	0
Acetonitrile	1.41E-03	7.31E+00	39.88	0.00	0.00	0	2.14	2.52	0
DMSO	7.47E-05	1.13E+00	0.00	0.00	0.00	0	1.13	2.23	0
DCM	2.62E-04	6.78E-01	7.52	0.15	5.67	6.87E-05	0.52	0.01	0
Methanol	1.27E-05	8.48E-01	0.08	0.00	0.00	0	1.37	0.18	0
[Hmim][Br]	2.54E-01	8.58E+01	0.00	3.71	0.00	0	1.78	0.00	0

Table 7. 6 Chemical Partition Summary % (EFRAT Output)

Chemical	Percent in:			
	Air	Sediment	Soil	Water
Carbon dioxide	99.78	0.00	0.00	0.22
Chlorobenzene	97.90	0.02	0.79	1.29
Acetone	44.27	0.00	0.03	55.69
Ethyl Acetate	73.25	0.00	0.13	26.62
Acetonitrile	43.49	0.00	0.03	56.48
DMSO	0.00	0.00	0.01	99.99
1-methylimidazole	64.07	0.00	0.03	35.89
DCM	98.62	0.00	0.02	1.36
Methanol	9.21	0.00	0.02	90.76
1-bromohexane	99.09	0.02	0.76	0.14
[HMim][Br]	0.13	0.10	4.50	95.27

7.9. IL Synthesis Process Simulation-*Assumptions and Conditions*

To the best of our knowledge, no current industrial scale-up for IL synthesis has been published in the open or patent literature. Conditions are inferred from lab-scale studies on the basis of good engineering design practice. While extensive effort is required to achieve optimized scale up of these processes, the simplifications made here are adequate for the scope of current study, and will yield reasonable preliminary estimates of expected material and energy flows. HYSIS 7.3 is used to estimate overall process conversions, the energy consumption (both thermal and electric) and the waste stream production, as well as preliminary efficiency estimates of unit operations (reactor, compressors, separation etc.) for selected routes. The flow sheet for each process is illustrated in Figure 7. 6. Some of the component IL and reactants, such as 1-methylimidazole and 1-bromohexane, are not available in the HYSIS databank.

Hypothetical groups are created for these set of chemicals. Thermodynamic properties obtained from methods shown in chapter 3 are entered into HYSIS. The basis for the simulation is the production of the model IL [HMim][Br] at an assumed rate of 1 kg/hr, while assuming an equimolar amount of 1-methylimidazole and 1-bromohexane in the feed for all scenarios.

For the comparison study, heuristically optimized reaction and process conditions for the four routes presented earlier are selected. Best reactor case configurations for the different systems are employed. Complete conversion of the reactants here is arbitrarily set to 99 % in each process. Reaction constants are obtained from experimental kinetic studies. The simulation parameters unique to the processes are summarized in **Table 7. 7.** Process optimization and intensification (such as recycling energy or product streams) will add cost and energy savings. However, we assume that the gain from such optimization will be similar across the different paths and will not significantly change the overall results. Emissions to air are estimated on the assumption that 0.2% of the input materials were emitted to air as commonly done in other studies[40] Also, estimates of major unit emissions are developed using industry emission factors available in EFRAT. The impact of the construction and maintenance of the production plant and equipment is neglected. Chemical production plant infrastructure is commonly assumed to have low or insignificant impact. Carcinogenic impacts are heavily penalized in this model, as is the case for several environmental analysis techniques. This emphasizes the need to examine individual risk indices/components, beyond emission rates. A simplified

process boundary is illustrated in Figure 7. 5; analysis boundary is limited to the IL alkylation synthesis and separation steps.

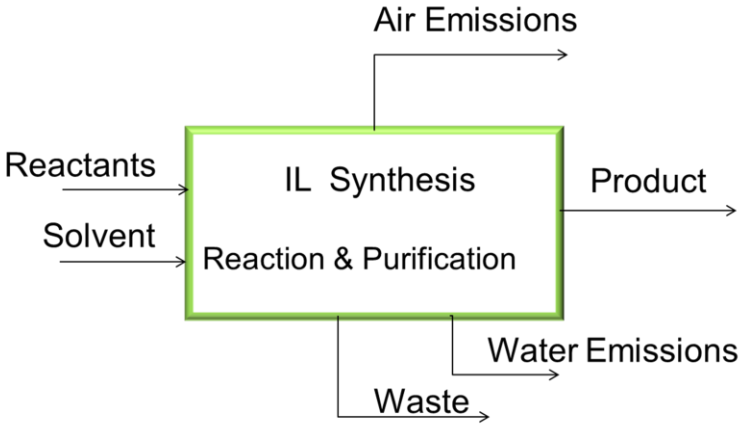

Figure 7. 5 Life Cycle Assessment Boundary for this IL Production Study

7.10. Process Conditions

Operating conditions were selected based on heuristics and experimental data presented in previous chapters. Reaction was allowed to occur at 60^{o}C (except for acetone and DCM at 40^{o}C, due to boiling point limitation); while higher temperatures can be used for faster reaction rates, experimental work shows that the quality of product IL can be significantly affected. Kinetic data are experimentally obtained (see chapters 5 and 6). Thermodynamic properties are obtained from Chapter 4. For Route 1, Synthesis in Acetone, acetone has a relatively high *k* (from Table 7. 2) and a low Rowan number. Schleicher [16, 17], through polarity studies and the Rowan table, selected acetone as an ideal synthesis candidate solvent. Further kinetic studies done for the acetone system

yielded kinetic data based on mole ratio of acetone to reactants (presented in chapter 5). Ideally, the least amount of solvent needed for reaction in one phase and reduced viscosity, while retaining high *k* rate constant should be sought. Based on rate constant data (chapter 5) and viscosity data for this system (chapter 4), $x_{acetone}$ = 0.25 met these criteria, and thus was selected. Acetone at this composition was found to reduce the viscosity of the system and improves transport properties of the product IL [HMIm][Br] For the desired separation, for the distillation simulations, acetone or DCM was selected as the light key components. For Route-1b, Traditional Solvent (DCM) Route, a 1mole 1-bromohexane to 1 mole 1-methylimidazole to 5 mole DCM molar ratio was selected as the feed ratio. Both Route 1a and 1b processes involve a reactor and distillation column (see Figure 7. 6). For the neat CO_2 routes, although the *k* are slightly lower for higher pressures (chapter 6), the ease of separation afforded by a flash vessel at these condition (savings from high energy demand associated with distillation (operating cost) was prioritized over the kinetic rate constant gain (where the penalty is a low rate of reaction and higher reactor volume - capital cost). This call will be evaluated in the economic analysis. In the CXL route, considering kinetic data (chapter 6), the fast rate constant and relatively moderate pressure (safety concern), we select 60 bar pressure with molar ratio of 1-bromohexane:1- methylimdazole:5-DMSO; the rate constant is highest in comparison to all solvent platforms considered. Solvent mole fraction input data for HYSIS were obtained from VLE data (Chapter 4). In the CXL process, CO_2 extraction is employed for purification of the product; this can be achieved in two steps at the desired purity. The flow sheet for all the processes is shown in Figure 7. 6.

Table 7. 7 Reaction and Separation Conditions for Simulated Processes

System	Solvent	P, T	k x 10^6 ($M^{-1}sec^{-1}$)
Synthesis in Acetone (Route 1)	Acetone	1atm, 50C	33.00
Synthesis in DCM (Route 1b)	DCM	1atm, 40C	8.47
CO_2 as a Solvent (Route 2)	CO_2	140 bar, 60C	49.2
CXL as Solvent (Route 3)	DMSO, CO_2	60 bar,60C	271
Neat Reaction (Route 4)	-	60C	106.34

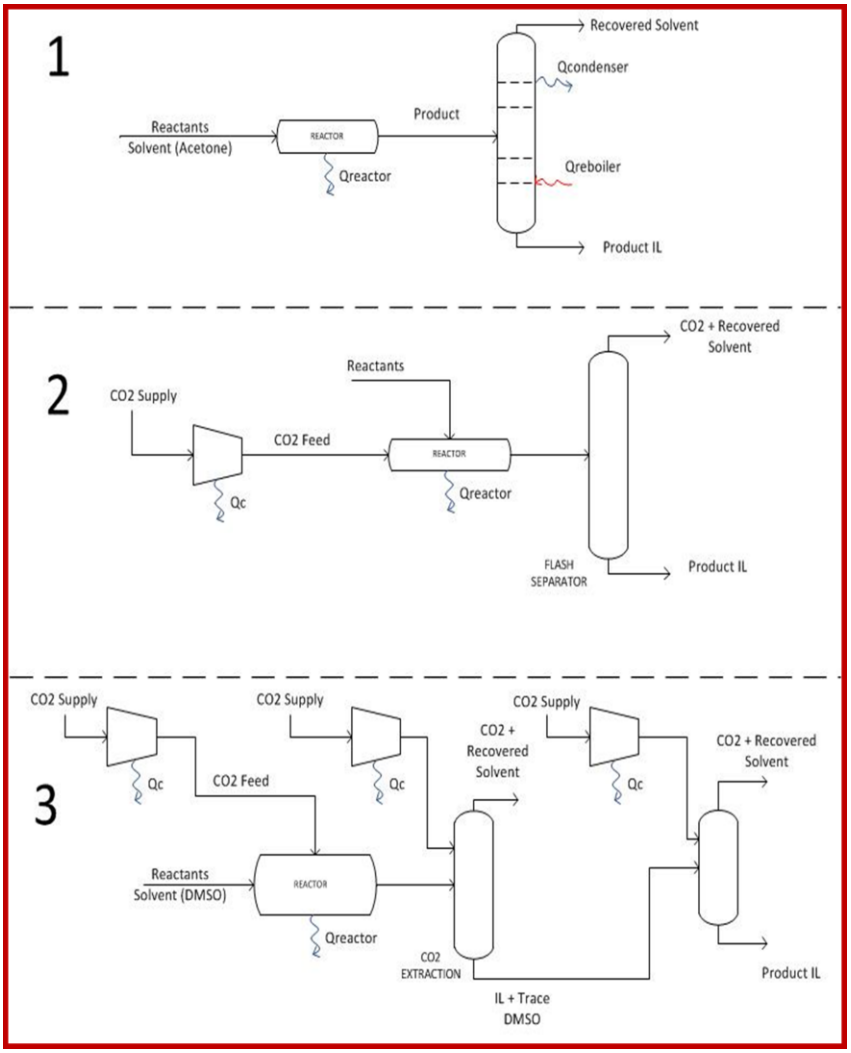

Figure 7. 6 Flowsheet for proposed Routes

7.11. Environmental Assessment

The environmental assessment considers multiple categories of impact on the natural environment and human health. The method, due to the properties in the database, associates the IL synthesis as carcinogenic emissions. Compared to acetone systems, CXL and CO_2 systems have reduced emissions in most impact categories. Figure 7. 7

show the total I_{PC} for all the proposed routes along with a conventional solvent DCM for illustration. Figure 7. 8 show the relative contributions of the nine environmental impact categories to the I_{PC}. The high *ICIH* value is caused by the use of conservative estimates for the product IL; this does not affect the overall trend as it is present across all the routes represented. The higher percentages of global warming and acid rain effects observed for the acetone and DCM routes are due to higher utility consumption for distillation needs.

The I_{PC} for the DCM conventional process is about 7 times greater than that of the CO_2 process, 3 times than that of the CXL process and 2.6 times that of acetone. The CXL process was an order of compared to conventional process using just DMSO as a solvent reduced the I_{pc} value by 50%. These are interesting results: quick heuristic optimization by Schleicher and Scurto, ranked acetone, above DCM as the optimal solvent using the rowan table. Fugitive emissions in the CO_2 and CXL routes (95% of the I_{PC}) are from emission rate factor for the CO_2 extraction flash vessel. For the CXL and CO_2 processes, the CO_2 solvent usage and associated emissions do not increase the environmental burden, since CO_2 is being utilized as a solvent and can be obtained from abundantly available existing sources. In addition, most of it is recycled back into the process. These results provide research and process engineering guidance for reducing potential environmental impact of IL synthesis.

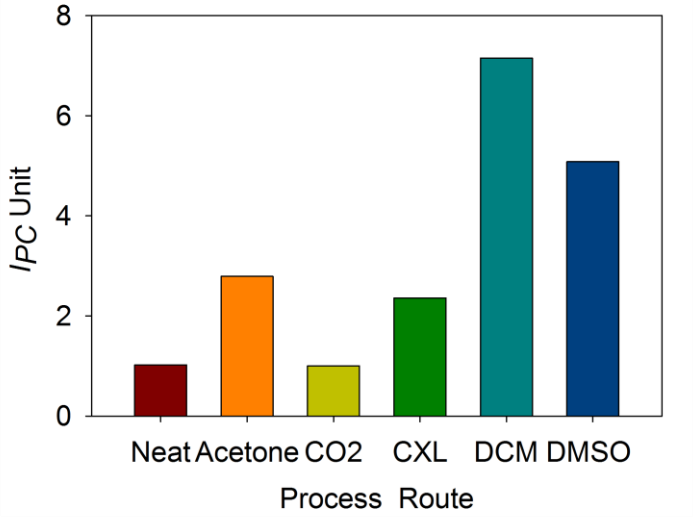

Figure 7. 7 Overall environmental index (I_{PC}) for different process routes (ambient DMSO as a solvent platform is added for comparison).

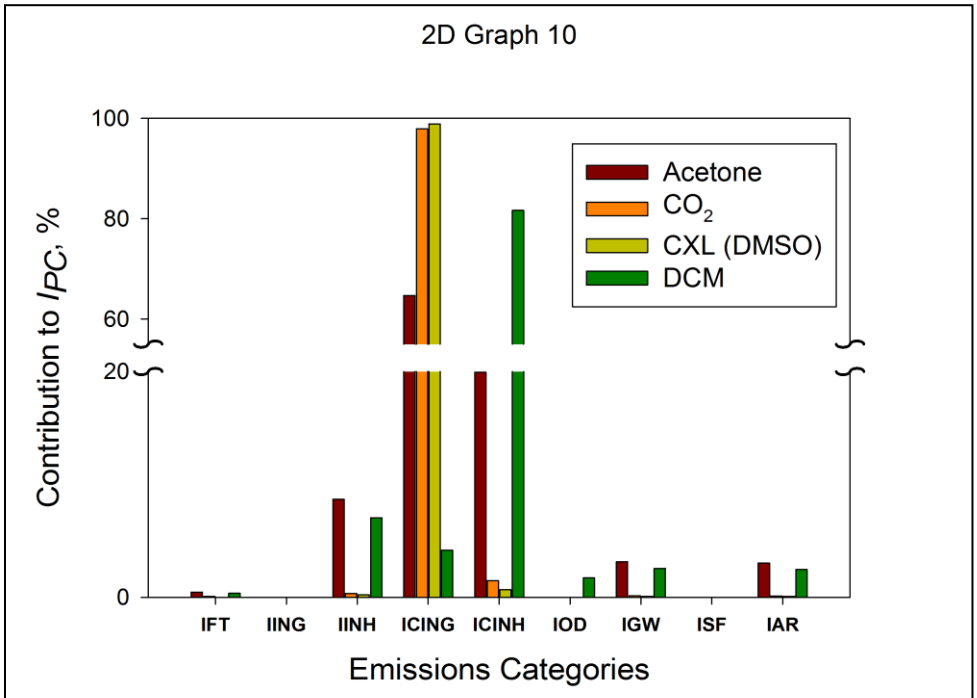

Figure 7. 8 Contribution to overall environmental index (I_{PC}) from various categories.

7.12. Economic Analysis

Unique costing indicators are used in making comparisons: operating costs, such as solvent cost and utilities, were used as the dominant cost indicator. Reactor volume cost was considered for this analysis, since the *k* constant was found to change for the different routes; depreciation is assumed to be negligible. The costs of solvents are taken from Chemical Industry News & Chemical Market Intelligence (ICIS).The Chemical Engineering Plant Cost index (CEI) is used to adjust, for inflation, to 2012 dollars: it was 593.1 in July 2012. Utility costs are obtained from the Energy Information Administration, Department of Energy (average industrial electricity rate 2012, 6.89¢/KW-hr).[41] Electricity is chosen for utility. The emission factors for the different unit operations are available within EFRAT and can be found in Shonnard and Allen.[22] Standard methods from Peter and Timmerhaus [8] are used to compute equipment cost, where:

$$\text{Cost equip.a} = \text{cost of equip.b}\left(\frac{\text{Capacity equip a}}{\text{Capacity equip.b}}\right)^{0.6}$$

Stainless steel was chosen as the material of construction. Based on the predicted economic and environmental impact outcomes, credit was assigned for the various performance criteria and summarized in Table 7.

Table 7.8. Positive and Negative Process Credits for Solvent Routes

Credits	CXL	CO_2	Acetone
Pressure/Safety	-	-	+
Solvent Cost	-	+	+
Reactor Size/cost	-	-	-
Energy Requirement	+	+	-

"+": environmentally or economically favorable; "−": unfavorable.

Cost analysis indicates that CXL is the most expensive option of the 3 proposed routes, Table 7. 8. A 98.8% energy cost savings can be attained for the production of 1kg of IL by synthesizing in CO_2, instead of using the conventional acetone method, while the energy cost difference with the CXL routes is 33.45% (shown in Table 7.10). Compression cost is found to be only 1% of the energy cost required for the whole process: most of the energy for the CO_2 route is spent in cooling the reactor. However, since the CO_2 rate of reaction is the lower than any of the three other routes, a larger cost is needed for the reactor volume,

Table 7. 9 present a comparison of volume size. Using Timmerhaus's methodology, the cost of high pressure equipment is higher by a power of 1.3. There is also the safety concern of operating a high pressure vessel.[8]

Table 7. 8 Cost Analysis for Solvent Routes

Solvent Platform		**CXL-DMSO**	**Acetone**	**Neat CO_2**
Compound	\$/kg[b]	kg	kg	kg
Acetone	0.95	-	1.98	-
CO_2	0.08	2366.53	-	11.00
DMSO	2.11	1.67	-	-
DCM	0.34	192.86	1.88	0.88
Energy Demand				
Cost \$/KWhr[a]	0.069			
Reactor (KW-hr)		0.61	0.61	0.36
Distillation (KW-hr)		-	1142	-
Compressor (KW-hr)		23.32	-	0.16
Total Energy Demand (KW-hr)		23.93	1142.61	0.52

a : U.S. Energy Information Administration, Form EIA-826, "Monthly Electric Sales and Revenue Report with State Distributions Report;" 1992-2005: Form EIA-861, "Annual Electric Power Industry Report."
b: http://www.icis.com/chemicals

Table 7. 9 Comparing Reactor Volume for IL Synthesis (1kg/hr)

Solvent Platform	Acetone	CXL	CO_2	Neat
Final product Flowrate (kg/h)	1	1	1	1
Product molar mass (g/mol)	247	247	247	247
Product Flowrate (mol/h)	4.05	4.05	4.05	4.05
initial reactant concentration, C_{ao} (mol/L)	3.569	1.611	0.797	4.8
conversion, X_a	0.999	0.999	0.999	0.999
rate constant, k ($M^{-1}hr^{-1}$)	0.1188	0.9756	0.17712	0.3828
initial reactant Flowrate (mol/h)	4.053	4.053	4.053	4.053
Volume (L)	2675.43	1598.97	35984.78	459.04
Volume (m^3)	2.68	1.60	35.98	0.46
Cost (\$)	64,300	285,234	1847431	22,358

CO_2 is very cheap: for this analysis, \$0.08/kg was used as the going pipeline rate. For the CXL system, DMSO is \$2.11/kg compared to CO_2 and acetone at \$0.95/kg. Acetone also operates at ambient pressure, lowering the cost of the reactor, compared to that required for going the CXL route. The acetone route is penalized most at the tail end of the process - separation of the product. Energy for distillation accounts for 99% of total energy requirement for the whole system. From both environmental and economic standpoints, the CO_2 route stands as the most competitive of any of the solvent routes studied. We find that these simple, early design, assessments capture the most important economic and environmental issues in a quantitative manner.

7.13. Summary

We have demonstrated throughout this study that a solvent is important for IL synthesis, and the selection process for an optimal solvent must consider several factors, discussed here in detail. The preliminary economic and environmental assessments of the proposed routes suggest that CO_2 is the desirable route for IL synthesis. While the CXL-DMSO process can be potentially competitive, optimized and new separation techniques will be critical to achieve this. The acetone reactor costs are significantly lower than those of the high pressure processes (CXL and CO_2), due to mild operating conditions. However, the CO_2 route is the most environmentally friendly and economically competitive, as it eradicates the need for energy intensive distillation. Also, CO_2 is a cheap and readily available solvent. We find that in our lab, because the reaction occurs more slowly, and the CO_2 acts as an extraction agent, the resulting product IL is clearer and cleaner. The critical factor will be recycling CO_2 and reactants back into the process. The conventional

synthesis of ILs in a common solvent, such as dichloromethane, is shown to have the worst environmental impact of all the solvent routes proposed evidenced by the I_{PC} unit, while the use of neat CO_2 is the route with the least environmental impact. Per Kralish's findings, we also find that the neat route has a very low environmental impact. However because of several issues outlined throughout this study, solvent use is almost inevitable.

Cradle-to-grave analysis will be needed to confirm that emissions are not simply being carried from one branch to another of the life cycle tree. The next step is considering how to perform rapid evaluations using free EPA software/tools. Commercial software such as Gabi, can be expensive especially for researchers in the academics and inventory data for ILs are often unavailable. Empirical methods/correlation must be considered to aid rapid environmental parameter estimation employed in environmental assessment software. Since there are still no industrial scale processes, many of these studies are still bench marked against hypotheticals. We succeeded in systematically evaluating a novel process versus traditional methods of making ILs (at least at the lab scale); we identified important issues. Separation is the most energy intensive segment of the process, at higher purities there is higher energy demand, and higher emissions. New processes must emerge to make the production of these solvents profitable. CO_2 (neat or as a co-solvent with an aprotic solvent like DMSO), has real advantages that translate into environmental benefits and cost savings. However, recovery and recycling of CO_2 will be imperative for these process routes.

References

[1] W.T. Ford, R.J. Hauri, D.J. Hart, Syntheses and properties of molten tetraalkylammonium tetraalkylborides, J. Org. Chem., 38 (1973) 3916-3918.

[2] M.S. Selvan, M.D. McKinley, R.H. Dubois, J.L. Atwood, Liquid-liquid equilibria for toluene plus heptane+1-ethyl-3-methylimidazolium triiodide and toluene plus heptane+1-butyl-3-methylimidazolium triiodide J. Chem. Eng. Data, 45 (2000) 841-845.

[3] F. Neve, O. Francescangeli, A. Crispini, J. Charmant, A(2)[MX4] copper(II) pyridinium salts. From ionic liquids to layered solids to liquid crystals Chem Mater, 13 (2001).

[4] S.V. Dzyuba, R.A. Bartsch, Influence of structural variations in 1-alkyl (aralkyl)-3-methylimidazolium hexafluorophosphates and bis (trifluoromethylsulfonyl) imides on physical properties of the ionic liquids, ChemPhysChem, 3 (2002) 161-166.

[5] D.R. MacFarlane, S.A. Forsyth, J. Golding, G.B. Deacon, Ionic liquids based on imidazolium, ammonium and pyrrolidinium salts of the dicyanamide anion, Green Chemistry, 4 (2002) 444-448.

[6] P. Bonhôte, A.-P. Dias, N. Papageorgiou, K. Kalyanasundaram, M. Grätzel, Hydrophobic, highly conductive ambient-temperature molten salts, Inorg. Chem., 35 (1996) 1168-1178.

[7] N. Karodia, S. Guise, C. Newlands, J.-A. Andersen, Clean catalysis with ionic solvents - phosphonium tosylates for hydroformylation Chem Comm, (1998) 2341-2342.

[8] M. Peter, K. Timmerhaus, R. West, Plant Design and Economics for Chemicals Engineering, Mc. Graw Hill Book Company, (2003).

[9] N. Menshutkin, Unknown, Z. Physik Chem., 5 (1890) 589.

[10] A. Skrzypczak, P. Neta, Rate constants for reaction of 1, 2-dimethylimidazole with benzyl bromide in ionic liquids and organic solvents, International Journal of Chemical Kinetics, 36 (2004) 253-258.

[11] D. Kralisch, D. Reinhardt, G. Kreisel, Implementing objectives of sustainability into ionic liquids research and development, Green Chemistry, 9 (2007) 1308-1318.

[12] D. Kralisch, A. Stark, S. Körsten, G. Kreisel, B. Ondruschka, Energetic, environmental and economic balances: Spice up your ionic liquid research efficiency, Green Chemistry, 7 (2005) 301-309.

[13] C.B. Minnich, L. Küpper, M.A. Liauw, L. Greiner, Combining reaction calorimetry and ATR-IR spectroscopy for the operando monitoring of ionic liquids synthesis, Catalysis Today, 126 (2007) 191-195.

[14] D.A. Waterkamp, M. Heiland, M. Schlüter, J.C. Sauvageau, T. Beyersdorff, J. Thöming, Synthesis of ionic liquids in micro-reactors—a process intensification study, Green Chemistry, 9 (2007) 1084-1090.

[15] A. Große Böwing, A. Jess, Kinetics and reactor design aspects of the synthesis of ionic liquids—Experimental and theoretical studies for ethylmethylimidazole ethylsulfate, Chemical engineering science, 62 (2007) 1760-1769.

[16] J. Schleicher, Masters Thesis, in, MS Thesis, University of Kansas, 2007.

[17] J.C. Schleicher, A.M. Scurto, Kinetics and solvent effects in the synthesis of ionic liquids: imidazolium, Green Chemistry, 11 (2009) 694-703.

[18] K.R. Harris, M. Kanakubo, L.A. Woolf, Temperature and Pressure Dependence of the Viscosity of the Ionic Liquids 1-Methyl-3-octylimidazolium Hexafluorophosphate and 1-Methyl-3-octylimidazolium Tetrafluoroborate, J. Chem. Eng. Data, 51 (2006) 1161-1167.

[19] J.M. Crosthwaite, M.J. Muldoon, J.K. Dixon, J.L. Anderson, J.F. Brennecke, Phase transition and decomposition temperatures, heat capacities and viscosities of pyridinium ionic liquids, J. Chem. Thermodyn., 37 (2005) 559–568.

[20] P.T. Anastas, J.B. Zimmerman, Peer reviewed: design through the 12 principles of green engineering, Environmental Science & Technology, 37 (2003) 94-101.

[21] P.T.W. Anastas, J.C, Green chemistry: Theory and Practice, Oxford University Press, New York, 1998.

[22] D.T. Allen, D.R. Shonnard, Green engineering: environmentally conscious design of chemical processes, Prentice Hall, 2001.

[23] Rowan University, Rowan Solvent Selection Table, in, http://www.rowan.edu/greenengineering, Accessed: April 08, 2007.

[24] H. Tokuda, K. Hayamizu, K. Ishii, M.A.B.H. Susan, M. Watanabe, Physicochemical Properties and Structures of Room Temperature Ionic Liquids. 1. Variation of Anionic Species, J. Phys. Chem. B, 108 (2004) 16593-16600.

[25] H. Tokuda, K. Hayamizu, K. Ishii, M.A.B.H. Susan, M. Watanabe, Physicochemical Properties and Structures of Room Temperature Ionic Liquids. 2. Variation of Alkyl Chain Length in Imidazolium Cation, J. Phys. Chem. B, 109 (2005) 6103-6110.

[26] H. Tokuda, K. Ishii, M.A.B.H. Susan, S. Tsuzuki, K. Hayamizu, M. Watanabe, Physicochemical Properties and Structures of Room Temperature Ionic Liquids. 3. Variation of Cationic Structure, J. Phys. Chem. B, 110 (2006) 2833-2839.

[27] P.A. Hunt, Why Does a Reduction in Hydrogen Bonding Lead to an Increase in Viscosity for the 1-Butyl-2,3-dimethyl-imidazolium-Based Ionic Liquids?, J. Phys. Chem. B, 111 (2007) 4844-4853.

[28] E.A. Turner, C.C. Pye, R.D. Singer, Use of ab Initio Calculations toward the Rational Design of Room Temperature Ionic Liquids, J. Phys. Chem. A, 107 (2003) 2277-2288.

[29] C.S. Slater, M.J. Savelski, A Method to Characterize the Greenness of Solvents used in Pharmaceutical Manufacture, J. Environ. Sci. Health., Part A, 42 (2007) 1595-1605.

[30] U. EPA, Estimation Programs Interface Suite™ for Microsoft® Windows, v 4.10, in, United States Environmental Protection Agency, Washington, DC, USA, 2011.

[31] D. Mackay, M. Diamond, Application of the QWASI (Quantitative Water Air Sediment Interaction) fugacity model to the dynamics of organic and inorganic chemicals in lakes, Chemosphere, 18 (1989) 1343-1365.

[32] D. Mackay, M. Joy, S. Paterson, A quantitative water, air, sediment interaction (QWASI) fugacity model for describing the fate of chemicals in lakes, Chemosphere, 12 (1983) 981-997.

[33] D. Mackay, S. Paterson, Evaluating the multimedia fate of organic chemicals: a level III fugacity model, Environmental Science & Technology, 25 (1991) 427-436.

[34] D. Mackay, Multimedia Environmental Models; The Fugacity Approach, Lewis Publishers, CRC Press, 1991.

[35] M.B. Swanson, G.A. Davis, L.E. Kincaid, T.W. Schultz, J.E. Bartmess, S.L. Jones, E.L. George, A screening method for ranking and scoring chemicals by potential human health and environmental impacts, Environmental Toxicology and Chemistry, 16 (1997) 372-383.

[36] U.S.E.P. Agency, Integrated Risk Information System (IRIS), Guidelines for Carcinogen Risk Assessment, in, Washington, DC, 2005.

[37] B. Jastorff, K. Mölter, P. Behrend, U. Bottin-Weber, J. Filser, A. Heimers, B. Ondruschka, J. Ranke, M. Schaefer, H. Schröder, Progress in evaluation of risk potential of ionic liquids—basis for an eco-design of sustainable products, Green Chem., 7 (2005) 362-372.

[38] Y. Zhang, B.R. Bakshi, E.S. Demessie, Life Cycle Assessment of an Ionic Liquid versus Molecular Solvents and Their Applications, Environmental Science & Technology, 42 (2008) 1724-1730.

[39] S. Righi, A. Morfino, P. Galletti, C. Samorì, A. Tugnoli, C. Stramigioli, Comparative cradle-to-gate life cycle assessments of cellulose dissolution with 1-butyl-3-methylimidazolium chloride and N-methyl-morpholine-N-oxide, Green Chem., 13 (2011) 367-375.

[40] J.D. Holbrey, W.M. Reichert, R.P. Swatloski, G.A. Broker, W.R. Pitner, K.R. Seddon, R.D. Rogers, Efficient, halide free synthesis of new, low cost ionic liquids: 1,3-dialkylimiadolium salts containing methyl- and ethyl-sulfate anions, Green Chem., 4 (2002).

[41] U.E.I. Administration, Data-Electric Power Monthly, in, eia, 2012.

8. Applications of Ionic Liquids: Biomass and Cellulose Processing and Separations

Introduction

In the chemical industry, there is increased emphasis on renewable resources as alternatives to fossil-fuel based raw materials.[4] Biofuels and value-added chemical products from biomass are the vanguard of the discussion on sustainable engineering. Lignocellulose (LC), an abundant(estimated yearly production of about 170–200 billion ton[6]), renewable feedstock that does not compete with food supplies, is of particular interest. To produce fuels and value-added chemicals from LC, several chemical and biochemical transformations have been proposed. However, the heterogeneous and recalcitrant nature of LC biomass hinders conversion processes that promise useful products. [1, 7] Although the area of pretreatment and processing of biomass is still in its infancy, there is heightened academic and industrial interest. This is evidenced by the exponential growth of new publications (patents, reviews and data) added to the literature.

The use of ILs in biomass processing presents many advantages over traditional processing methods or solvents.[8] Biomass hydrolysis in ILs has been catalyzed using transition metals,[2] mineral or solid acids, [9, 10] as well as the IL itself. [11] Researchers have found that, depending on the water content and the acidity of the medium, ILs enhance selectivity in the conversion of monosaccharides to platform chemicals. In laboratory scale processes, researchers realize that water content, viscosity, and separation issues are some of the major challenges that must be overcome.[8, 12-15] As the current cost of ILs is of some concern, this dissertation addresses sustainable

methods for the economic production of several ILs. This chapter presents the use of ILs in biomass processing.

8.2. Lignocellulose (LC) as a Bio refinery Feedstock

LC biomass consists of three main components, namely cellulose (35–50%), hemicellulose (20–35%) and lignin (10–25%).[16] Cellulose is a polymer composed of glucose units linked by β-1, 4-glycosidic bonds (see Figure 8. 1 [1]). It is highly crystalline with polymeric chains held together by hydrogen bonds and van der Waals forces[17]. Due to this crystallinity, cellulose is difficult to dissolution. Hemicellulose is a matrix of polysaccharides such as arabinoxylans, and occurs within plant cell walls. Unlike cellulose, it has a random, amorphous structure that is relatively easier to hydrolyze. Although hemicellulose composition varies between plant species, it primarily appears as xylan. Furfural and xylitols are derivatives of xylose, a major product of hemicellulose hydrolysis. Lignin is a bulky, highly branched, heterogeneous aromatic polymer, comprising mainly of three building blocks, guaiacylpropane, syringylpropane and p-hydroxyphenylpropane. It is the most recalcitrant of the three lignocellulosic components.[1] Pretreating lignocellulosic biomass disrupts the lignin−carbohydrate complex, decreasing cellulose crystallinity.

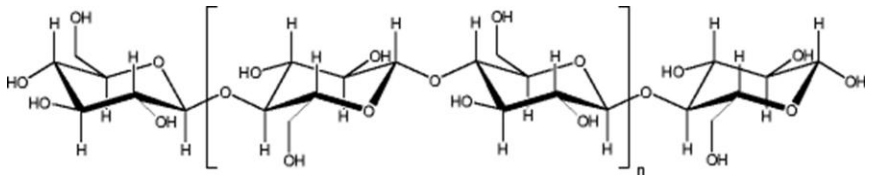

Figure 8. 1 Cellulose Structure [1]

8.3. Cellulose Conversion

Biomass conversion occurs in three main phases: cellulose is first converted to monomer sugars, and those sugars converted to platform bio-chemicals such as polyols and oxygenates, which can then be further transformed to fuels or chemicals. Oxygenate molecules such as fufural and 5-(hydroxymethyl)furfural (HMF) are derived from the dehydration of sugars, while polyols such as sorbitol are synthesized from the hydrogenation of sugars.

8.3.1. HMF and Its Derivatives

Experts speculate HMF will be a key player in the renewable chemical industry; its derivatives have valuable potential in industry (see Figure 8. 2[2]). In a recent evaluation of bio-refinery products of the highest industrial relevance, Pacific Northwest National Laboratory (PNNL) identified 2,5-dimethylfuran (DMF), a derivative of HMF, as a top-10 platform chemical.[18] Applications of HMF range from fuels to solvents and pharmaceuticals. DMF is touted as the next generation liquid transportation fuel, with

comparable energy content to present day gasoline, which is 40% greater than that of ethanol.

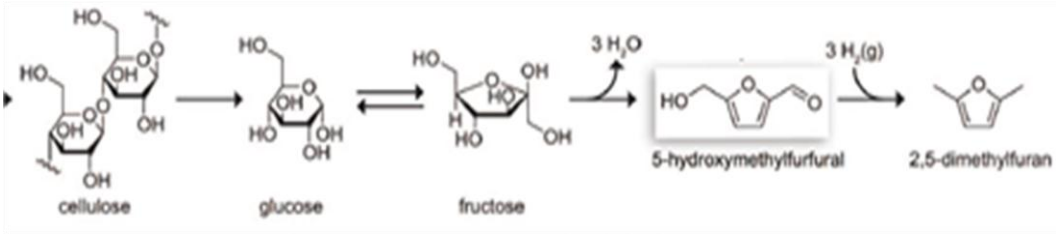

Figure 8. 2 Synthesis of 5-(Hydroxymethyl)furfural Chemicals from Cellulose [2]

Furthermore, HMF can potentially add value to the production of polyethylene terephthalate (PET) by offering a green substitute (2,5-furandicarboxylic acid) for petroleum-derived terephthalic acid. Currently, HMF can be synthesized from monomer sugars in highly polar solvents such as water, dimethyl sulfoxide (DMSO), dimethylformamide (DMF), and dimethylacetamide (DMA) in the presence of a catalyst. However, these reactions are often plagued with low yields and poor selectivity. Furthermore, HMF is easily further converted to humins that limit (inhibit) the desired conversion. When Binder and Raines[7] used a combination of metals and ILs to catalyze the conversion of glucose to HMF, they obtained a yield of up to 70% under mild conditions, and observed that the IL presented the advantage of high selectivity with negligible formation of byproducts (humins). They extended this study to a single reaction step conversion of LC biomass into furans and HMF, by using N,N-dimethylacetamide containing metal chlorides and 1-ethyl-3-methylimidazolium chloride as an additive.

Some studies have reported satisfactory yields for HMF using imidazolium chloride ILs as both solvents and catalysts in the conversion of fructose to HMF.[19, 20] Recently, Hu *et al.*,[11] converted fructose to HMF, with above 90% yield, using a relatively environmentally benign mixture of ethyl acetate (EA) and a cheap renewable choline chloride based IL. The results from these studies hold the promise of several opportunities for effective production of HMF from biomass feedstock, and feasible separation, while adhering to the principles of green engineering. Further study to understand the thermodynamics of these systems is essential to practical implementation.

8.3.2. Polyols and Derivatives

Polyols, otherwise known as sugar alcohols, are formed by the hydrogenation of sugars. Polyols are considered bio-platforms that can be converted to fuels and, in their own right, also have the potential to be key players in the polymer and food industries. Traditionally, the hydrogenation reaction is carried out in the presence of metal catalysts such as Pt, Ni and Ru, at moderate temperature and pressure. Dumesic's group[20] has replaced expensive precious metals with mineral acid to catalyze cellulose conversion to sorbitol and other polyols. However, this process is not *green* (not environmentally friendly) as it suffers from problems associated with mineral acid *viz* corrosion and acid disposal.

Some researchers [9, 10] have further replaced liquid acids with solid acids for cellulose conversion into polyols, but this route presents relatively low yields due to limited

available surface acid sites. Recently, Luo *et al.*,[21] reported a one-step catalytic conversion of cellulose into polyols using smaller amounts of Ru clusters dispersed in IL; they reported higher selectivity and yield. However, there is then the challenge of product and catalyst recovery from the IL.

8.3.3. Optimal Ionic Liquid for cellulose conversion systems

The "desired" IL for biomass processing must be able to dissolve a high amount of cellulose, while promoting reaction selectivity, conversion/yield and low viscosity. The inherent basicity or acidity of the IL allows it to perform as combined solvent and catalyst, eliminating the need for additional expensive transition metal catalysts or corrosive acids. This has been shown in the dehydration of monomer sugars to HMF. However, in the synthesis of polyols from biomass derivatives, a non-IL catalyst might be required. In this situation, immobilization of the catalyst in the IL phase would potentially allow for easy separation of the product and recycling of the catalyst. When used, co-solvents or catalysts should be readily recoverable from the IL.

Stability is intertwined with cost and toxicity factors, as recyclability will minimize cost and tail-end water contamination. Interfacial tension is a key consideration, as this can drastically increase cost by the necessitation of larger contact time or the formation of a stable emulsion, which can be even harder to separate. By the same token, the selected IL must be relatively cheap and widely available. Product extraction and IL recycling should thus be considered when designing IL for such processes.

8.4. Biomass/Cellulose Pretreatment

Pretreatment is the conversion of LC biomass from its native crystalline to a more amorphous form, of which processing is much more effective. Pretreatment results in structural changes that yield increased surface area, promoting cellulose conversion kinetics; researchers have observed up to thirty (30) times faster rates for amorphous cellulose than for the high-crystalline form. Many methods are currently used for biomass pretreatment - physical, biological, thermal, chemical, electrical, or a combination of these methods.

Thermochemical processes utilize heat, pressure and chemical methods to change the molecular structure of the native biomass. Biological methods utilize selected microorganisms to convert biomass: while such approaches have low chemical and energy demands, they are time consuming and plagued with low yields. Physical pretreatment, such as ball milling[22], is often energy intensive and inefficient. Chemical pretreatments are by far the most employed and are often preceded by mechanical methods. Common chemical pretreatment techniques include acid catalyzed processes [23], pH-controlled hot water, dilute acid pretreatment, lime [24] and the use of organic solvent [25] processes. However, these processes are accompanied with the disadvantages of low selectivity, high costs and severe processing conditions.[26]

Chemical processes often utilize solvents for dissolution, enabling homogeneous phase reactions which circumvent mass transfer and kinetic limitations; however, very few solvents can dissolve cellulose. In the literature, studies show that inorganic molten salt hydrates, such as $ZnCl_2$, $CaCl_2$, and LiCl can be used to convert cellulose and hemicellulose to monosaccharides under mild conditions [27-30]; however, these methods are harsh to the environment and are not environmentally friendly. Other studies use aqueous solutions or organic mixtures such as DMSO/water, N-methyl-morpholine-N-oxide for processing.[31] Separating mixtures of these non-green, high boiling solvents presents yet another dilemma. There continues to be an overwhelming need for improved solvent media for biomass processes.

8.5. IL Cellulose dissolution

ILs have high potential as powerful cellulose solvents. Remarkably, selected ILs have been found effective for dissolving not only isolated components, but also for native mixtures without any prior treatment and at high concentrations.[1, 8, 32] Dissolution processes for cellulose (refined or natural) derivatives and their applications have been described in the literature;[1, 8, 33, 34]

Rogers and co-workers extensively studied the dissolution of high concentrations of cellulose (without derivation) in a wide range of ILs at 100°C. Fukaya and co-workers prepared a 10 wt% cellulose solution using several ILs. They dissolved 2-4 wt% cellulose N-ethyl-N'-methylimidazolium methylphosphate at moderate 45°C. Kilpelainen et al.,[33] dissolved Norway spruce sawdust in [BMim][Cl] at 80-120°C. They found that

water content in the sawdust affected its solubility in the ILs. We conducted dissolution studies with several ILs at 100^{o}C and with agitation. We found that the solubility of cellulose increased with temperature and was very dependent on the kind of IL (anion and cation choice). Figure 8. 3 present a visual contrast of a pure IL against an IL with cellulose.

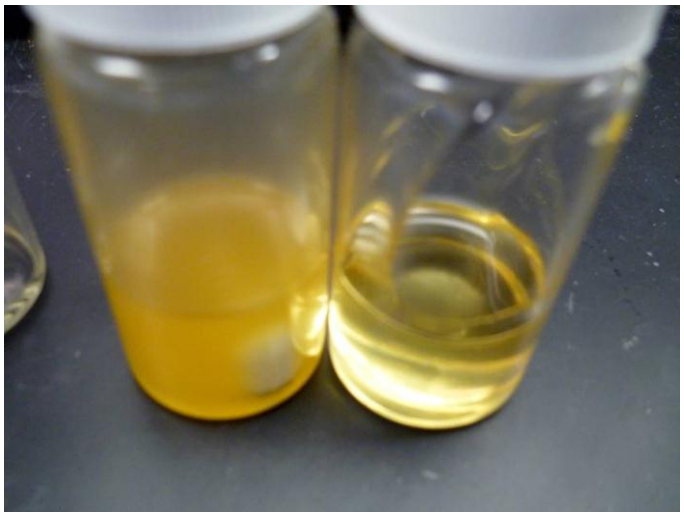

Figure 8. 3 [Hmim][Br] with cellulose (left), [Hmim] [Br] ionic liquid (right)

8.5.1. Anion Effect

The ability to tune hydrophobicity or hydrophilicity of the IL by choice of the anion is an important tool, providing design flexibility. Compared to other ILs tested, chloride and acetate anions are the prime choices, so far, in the biomass related area; they dissolve higher amounts of cellulose. Bromide ILs typically have cellulose solubility of less than

10 wt%, while Tf_2N ILs have a solubility of 0-0.5 wt% and [EMIM]Ac ILs can have a solubility of >30 wt%. In this study, for instance, [HMim][Cl] dissolved three (3) times more weight percent of cellulose compared to [HMim][Br], under the same conditions. In contrast, there was no cellulose dissolution in [HMim][Tf_2N]. Swatloski *et al.*,[8] have shown via NMR studies that ILs with strong hydrogen accepting anions were most effective for cellulose dissolution, as they interact with the hydroxyl group of the cellulose.

8.5.2. Cation Effect

Although cation effect on IL properties is less well studied, simulation work points to a weak relationship between the choice of cation and cellulose dissolution. **Table 8. 1** presents solubility data for different ILs: we see that increasing the alkyl chain length on imidazolium cations in identical chloride-containing ILs leads to a decrease in cellulose solubility, corroborating findings from previous work.[35-37] This evidence suggests the importance of cation choice and the role they may play in not only dissolution mechanisms, but in conversion catalysis and separations. Pyridinium and imidazolium cations are believed to have higher cellulose solubility.

Table 8. 1 Resulting from Dissolution study at T=100^{o}C and with vigorous stirring

Ionic Liquid	Percent weight (%)
[EMIM] Br	8.71
[BMIM] Br	9.00
[HMIM] Br	4.96
[DMIM] Br	0.86
[HMIM] Tf_2N	0.00
[BMIM][Cl]	13.5
[HMIM] [Cl]	9.24

Mass transfer and diffusion considerations affect solubility studies: mixing limitations that occur as a result of high viscosity in IL/cellulose solutions often introduce ambiguity. Since IL-cellulose solutions begin to form gels and the system becomes overly viscous (mass transfer limitations), it is not clear if the IL is truly saturated with cellulose at these high cellulose concentrations. Regardless, for cellulose processes, an ideal IL would allow for moderate operating viscosity at mild temperature conditions. For example, while [BMIM]Cl is one of the best ILs for dissolving cellulose, its viscosity and high melting point (60^{o}C) present a technical drawback for use as a processing solvent, due to costs of energy needed for pumps. While lower viscosity and melting point make acetate-based ILs seem more attractive than chloride-based ILs, the choice will come down to economics.

8.6. IL for Separations in Biomass Systems

Separating processes, in general, play an important role in almost every chemical industry. Distillation remains the most commonly used method; energy accounts for 60 to 80% of cost in most mature chemical processes. [26] Product recovery from IL mixtures remains a significant challenge and is a major obstacle to their wide scale industrial application. Recent advances have embraced non-conventional solvents and extraction techniques for the separation and purification of various biomolecules via partitioning of liquid phases. Biphasic homogeneous catalysis presents the advantages of easy product and catalyst recovery. Figure 8. 2 presents a schematic for the synthesis of 5-(Hydroxymethyl)furfural in an IL using a biphasic system.[3] Weingarten *et al.*,[38] have studied the dehydration of xylose to furfural in an aqueous methyl isobutyl ketone system. Interestingly, they report minimal decomposition of 5-hydroxymethylfurfural, a feature unique to biphasic systems for this reaction. Also, they found that the biphasic system did not alter the overall kinetics of this reaction when compared to its monophasic analogue. Hu *et al.*, [11] studied the conversion of fructose to HMF in a biphasic system that used ethyl acetate and choline chloride based ILs. They reported a distribution of the target, HMF, between the organic-rich phase and the IL-rich phase. Both studies found that better extraction of the target chemical was achieved with continued addition of co-solvent. This indicates that reactor design will be critical in obtaining better yields of target bio-molecules. Hence, optimizing a biphasic scheme for maximum product recovery will require an insightful balance of choices in solvent, recycling, and amount of the solvent

needed and impurity (e.g. water) tolerance. Even more so, a full understanding of system thermodynamics is critical.

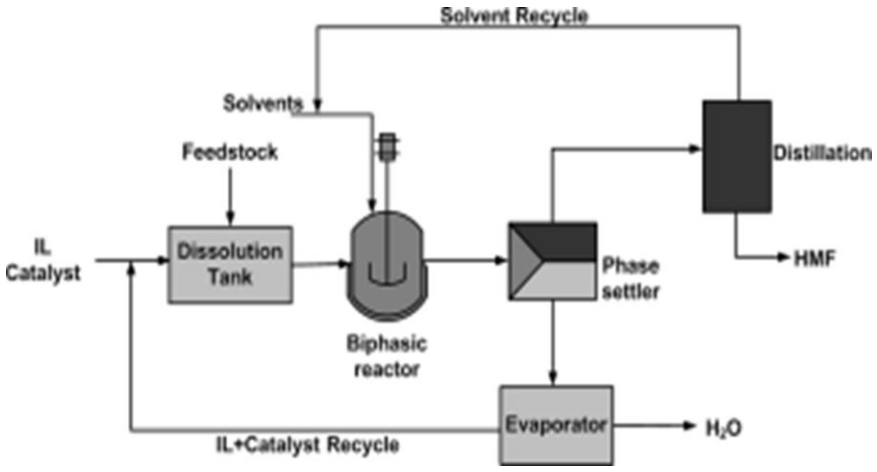

Figure 8. 4 Biphasic Synthesis of 2, 5 (Hydroxymethyl)furfural in Ionic Liquids. [3]

8.6.1. Ethyl Acetate as a Co-solvent

In the literature, several traditional solvents have been employed for biomass and cellulose conversion catalysis. Here, ethyl-acetate (EA) is explored as a model co-solvent for the design-optimized reaction/separation multiphase system of biomass conversion to HMF, a highly functional bio-platform. EA is hydrophobic and made from ethanol and acetic acid, both bio-renewable sources; its solvent impact indexes are presented in chapter 8. Studies have used EA for biomass processes - EA's relatively low boiling point advantageously reduces energy cost and avoids thermal decomposition or polymerization of the products because of product isolation. While HMF and DMF are

soluble in EA, hydrophilic ILs and monomer sugars (such as fructose) have negligible solubility. Our group found experimentally that a common halide IL, 1-hexyl-3-methylimidazolium bromide, has less than 0.13% w/w solubility in EA. Preliminary studies show that rare LLLE behavior is observed for IL/EA/DMF systems at specified concentrations of the three components (x_{DMF}, x_{EA} and x_{IL}); data is presented in **Table 8. 2**. Two such systems are illustrated in Figure 8. 5 'a' and 'b' with DMF- (1), EA- (2) and IL- (3) rich phases. This type of behavior is characteristic of the rare Type 2 system shown in Figure 8. 6.[5] A three phase Type 2 system has one three-phase region, three two-phase regions, and two one-phase regions.[39] In IL/EA/DMF systems, two binaries, IL/EA and IL/DMF have miscibility gaps, while the third, DMF/EA, is completely miscible. Triethylene/glycol/monooctyl, and ether/dodecane/water systems exhibit three phase Type 2 behavior at 25°C.[5] Practical exploitation of this unique thermodynamic behavior for separation processes will not be possible until fundamental mechanisms are understood.

Thermodynamic knowledge is needed for these complex multicomponent systems: to date, full characterizations of these systems are nonexistent in the literature. Can this kind of thermodynamic information be used in designing a system to continuously facilitate a DMF-rich phase as the reaction progresses? Will such a system be feasible regarding reasonable amounts of solvents? Is the DMF-rich phase stable in the presence of other biomass processing components**?** What predictive thermodynamic tools can be employed for these regions and behaviors? Furthermore, water is a byproduct of many biomass conversion reactions and should be expected in these systems. For example,

there are three water molecules produced for every glucose molecule converted to HMF.[1] It is therefore important to understand the effects of water on these systems and how it would affect partitioning of the targets into the different phases. Solvents must be selected carefully as addition of co-solvents into IL systems, already with several unknowns, introduces yet another engineering complexity that must be handled.

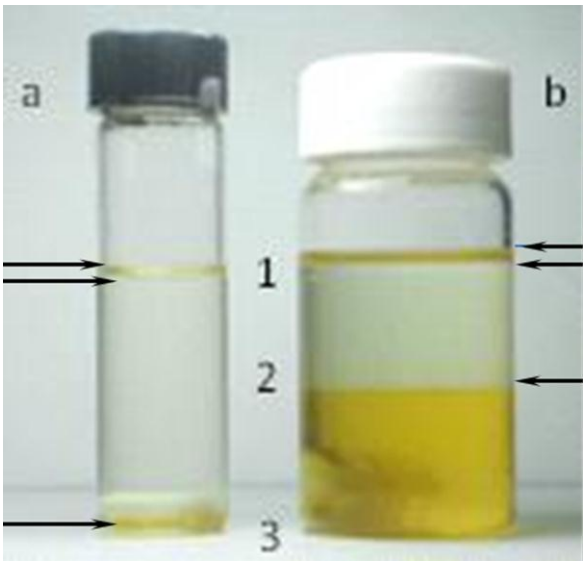

Figure 8. 5 LLE in IL/EA/DMF mixtures at ambient conditions, 1-DMF rich phase, 2-EA rich phase 3- ILrich phase (arrows indicate meniscus)

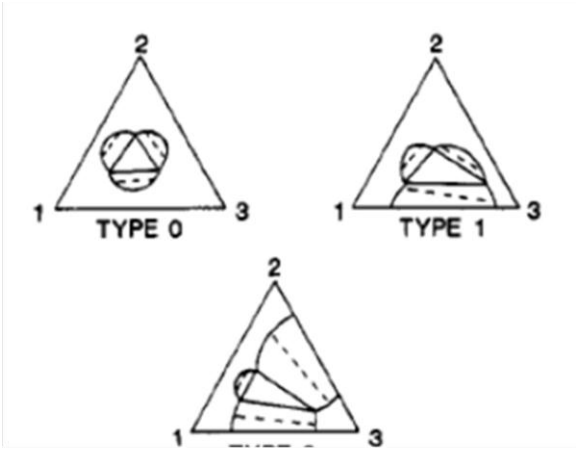

Figure 8. 6 Phase formation in type 0, 1 and 2 systems [5]

Table 8. 2 Resulting number of phases with Feed composition data for ternary system at 25°C

Number of Phases	DMF	EA	IL
2	0.13	0.00	0.87
2	0.99	0.00	0.01
2	0.00	0.98	0.02
2	0.00	0.08	0.92
1	0.94	0.00	0.06
2	0.83	0.00	0.17
2	0.19	0.78	0.03
2	0.00	0.08	0.92
1	0.11	0.07	0.82
2	0.20	0.06	0.74
3	0.37	0.05	0.58
2	0.00	0.98	0.02
2	0.08	0.90	0.02
3	0.52	0.47	0.01
1	0.20	0.80	0.00
2	0.19	0.78	0.03

8.7.Conclusion

Ionic liquids have great promise and great potential in biomass processes. While several studies continue to emerge for application of these designer solvents for cellulose processing, there is a need to address separation and characterization method issues. These concerns need to be addressed before IL biomass technologies can become sufficiently economical to be implemented wide scale. New methods for quantitatively measuring cellulose solubility in ionic liquids are important. Emerging methodology must account for water effects in the solubility efficiency of the choice IL. Further, new solvent platforms such as GXLs may present green solutions like significantly reduce the amount of solvent required for processing regenerated cellulose. In biomass valorization, utilizing unique phase behavior of ionic liquids and solvents (such as ethyl acetate) can potentially reduce intensive energy used for separations. Although, it is not yet clear which biomolecule will be the future's dominant bio-fuel: approaches presented here are transferrable solutions that address critical separation challenges, thus advancing several other states of art.

References

[1] S. Tan, D. MacFarlane, Ionic Liquids in Biomass Processing, Ionic Liquids, (2010) 311-339.

[2] J.B. Binder, R.T. Raines, Simple chemical transformation of lignocellulosic biomass into furans for fuels and chemicals, Journal of the American Chemical Society, 131 (2009) 1979-1985.

[3] T. Ståhlberg, W. Fu, J.M. Woodley, A. Riisager, Synthesis of 5 (Hydroxymethyl) furfural in Ionic Liquids: Paving the Way to Renewable Chemicals, ChemSusChem, 4 (2011) 451-458.

[4] M. Himmel, S. Ding, D. Johnson, W. Adney, M. Nimlos, J. Brady, T. Foust, Biomass recalcitrance: engineering plants and enzymes for biofuels production, Science, 315 (2007) 804.

[5] P.A. Gupte, R.P. Danner, Prediction of liquid-liquid equilibria with UNIFAC: a critical evaluation, Industrial & Engineering Chemistry Research, 26 (1987) 2036-2042.

[6] Y.H.P. Zhang, Reviving the carbohydrate economy via multi-product lignocellulose biorefineries, Journal of industrial microbiology & biotechnology, 35 (2008) 367-375.

[7] J.B. Binder, R.T. Raines, Fermentable sugars by chemical hydrolysis of biomass, Proceedings of the National Academy of Sciences, 107 (2010) 4516.

[8] R.P. Swatloski, S.K. Spear, J.D. Holbrey, R.D. Rogers, Dissolution of Cellose with Ionic Liquids, Journal of the American Chemical Society, 124 (2002) 4974-4975.

[9] N. Ji, T. Zhang, M. Zheng, A. Wang, H. Wang, X. Wang, Y. Shu, A.L. Stottlemyer, J.G. Chen, Catalytic conversion of cellulose into ethylene glycol over supported carbide catalysts, Catalysis Today, 147 (2009) 77-85.

[10] A. Fukuoka, P.L. Dhepe, Catalytic conversion of cellulose into sugar alcohols, Angewandte Chemie International Edition, 45 (2006) 5161-5163.

[11] S. Hu, Z. Zhang, Y. Zhou, B. Han, H. Fan, W. Li, J. Song, Y. Xie, Conversion of fructose to 5-hydroxymethylfurfural using ionic liquids prepared from renewable materials, Green Chemistry, 10 (2008) 1280-1283.

[12] A.P. Dadi, S. Varanasi, C.A. Schall, Enhancement of cellulose saccharification kinetics using an ionic liquid pretreatment step, Biotechnology and Bioengineering, 95 (2006) 904-910.

[13] T.V. Doherty, M. Mora-Pale, S.E. Foley, R.J. Linhardt, J.S. Dordick, Ionic liquid solvent properties as predictors of lignocellulose pretreatment efficacy, Green Chemistry, 12 (2010) 1967-1975.

[14] D.A. Fort, R.C. Remsing, R.P. Swatloski, P. Moyna, G. Moyna, R.D. Rogers, Can ionic liquids dissolve wood? Processing and analysis of lignocellulosic materials with 1-< i> n</i>-butyl-3-methylimidazolium chloride, Green Chem., 9 (2006) 63-69.

[15] D.A. Fort, R.C. Remsing, R.P. Swatloski, P. Moyna, G. Moyna, R.D. Rogers, Can ionic liquids dissolve wood? Processing and analysis of lignocellulosic materials with 1-n-butyl-3-methylimidazolium chloride, Green Chemistry, 9 (2007) 63-69.

[16] L.R. Lynd, P.J. Weimer, W.H. van Zyl, I.S. Pretorius, Microbial Cellulose Utilization: Fundamentals and Biotechnology, Microbiol. Mol. Biol. Rev., 66 (2002) 506-577.

[17] S. Datta, B. Holmes, J.I. Park, Z. Chen, D.C. Dibble, M. Hadi, H.W. Blanch, B.A. Simmons, R. Sapra, Ionic liquid tolerant hyperthermophilic cellulases for biomass pretreatment and hydrolysis, Green Chem., 12 (2010) 338-345.

[18] J.J. Bozell, G.R. Petersen, Technology development for the production of biobased products from biorefinery carbohydrates—the US Department of Energy's "Top 10" revisited, Green Chem., 12 (2010) 539-554.

[19] C. Moreau, A. Finiels, L. Vanoye, Dehydration of fructose and sucrose into 5-hydroxymethylfurfural in the presence of 1-H-3-methyl imidazolium chloride acting both as solvent and catalyst, Journal of Molecular Catalysis A: Chemical, 253 (2006) 165-169.

[20] Y. Román-Leshkov, C.J. Barrett, Z.Y. Liu, J.A. Dumesic, Production of dimethylfuran for liquid fuels from biomass-derived carbohydrates, Nature, 447 (2007) 982-985.

[21] C. Luo, S. Wang, H. Liu, Cellulose Conversion into Polyols Catalyzed by Reversibly Formed Acids and Supported Ruthenium Clusters in Hot Water, Angewandte Chemie International Edition, 46 (2007) 7636-7639.

[22] D.B. Rivers, G.H. Emert, Lignocellulose pretreatment: a comparison of wet and dry ball attrition, Biotechnology letters, 9 (1987) 365-368.

[23] R. Torget, P. Walter, M. Himmel, K. Grohmann, Dilute-acid pretreatment of corn residues and short-rotation woody crops, Applied biochemistry and biotechnology, 28 (1991) 75-86.

[24] W.E. Kaar, M.T. Holtzapple, Using lime pretreatment to facilitate the enzymic hydrolysis of corn stover, Biomass and Bioenergy, 18 (2000) 189-199.

[25] H. Chum, D. Johnson, S. Black, J. Baker, K. Grohmann, K. Sarkanen, K. Wallace, H. Schroeder, Organosolv pretreatment for enzymatic hydrolysis of poplars: I. Enzyme hydrolysis of cellulosic residues, Biotechnology and Bioengineering, 31 (1988) 643-649.

[26] G. Stephanopoulos, Challenges in engineering microbes for biofuels production, Science, 315 (2007) 801.

[27] H. Leipner, S. Fischer, E. Brendler, W. Voigt, Structural changes of cellulose dissolved in molten salt hydrates, Macromolecular Chemistry and Physics, 201 (2000) 2041-2049.

[28] S. Fischer, H. Leipner, E. Brendler, W. Voigt, K. Fischer, Molten inorganic salt hydrates as cellulose solvents, in, ACS Publications, 1999, pp. 143-150.

[29] S. Fischer, H. Leipner, K. Thümmler, E. Brendler, J. Peters, Inorganic molten salts as solvents for cellulose, Cellulose, 10 (2003) 227-236.

[30] S. Fischer, K. Thümmler, K. Pfeiffer, T. Liebert, T. Heinze, Evaluation of molten inorganic salt hydrates as reaction medium for the derivatization of cellulose, Cellulose, 9 (2002) 293-300.

[31] R.C. Brown, Thermochemical Processing of Biomass, John Wiley & Sons, West Sussex, 2011.

[32] M. Schrems, A. Brandt, T. Welton, F. Liebner, T. Rosenau, A. Potthast, Ionic liquids as media for biomass processing: opportunities and restrictions, Holzforschung, 65 (2011) 527-533.

[33] I. Kilpeläinen, H. Xie, A. King, M. Granstrom, S. Heikkinen, D.S. Argyropoulos, Dissolution of Wood in Ionic Liquids, Journal of Agricultural and Food Chemistry, 55 (2007) 9142-9148.

[34] H. Tadesse, R. Luque, Advances on biomass pretreatment using ionic liquids: An overview, Energy Environ. Sci., (2011).

[35] T. Erdmenger, C. Haensch, R. Hoogenboom, U.S. Schubert, Homogeneous Tritylation of Cellulose in 1-Butyl-3-methylimidazolium Chloride, Macromolecular Bioscience, 7 (2007) 440-445.

[36] R. Swatloski, J. Holbrey, R. Rogers, Ionic liquids are not always green: hydrolysis of 1-butyl-3-methylimidazolium hexafluorophosphate, Green Chemistry, 5 (2003) 361-363.

[37] J. Wu, J. Zhang, H. Zhang, J. He, Q. Ren, M. Guo, Homogeneous Acetylation of Cellulose in a New Ionic Liquid, Biomacromolecules, 5 (2004) 266-268.

[38] R. Weingarten, J. Cho, J.W.C. Conner, G.W. Huber, Kinetics of furfural production by dehydration of xylose in a biphasic reactor with microwave heating, Green Chemistry, 12 (2010) 1423-1429.

[39] T.F. Anderson, J.M. Prausnitz, Application of the UNIQUAC Equation to Calculation of Multicomponent Phase Equilibria. 2. Liquid-Liquid Equilibria, Industrial & Engineering Chemistry Process Design and Development, 17 (1978) 561-567.

9. Conclusion and Recommendations

9.1. Conclusion

Ionic liquids (ILs) have several advantages over traditional solvents. For one, ILs offer enormous design flexibility, with theoretically over 10^{14} possible molecular combinations of cations and anions. Clearly, unless they can be produced in an economically and sustainably feasible manner, wide-scale application will remain remote. Still, very little work in the literature has been dedicated to this goal. Most literature reports of IL syntheses are primarily concerned with making relatively small quantities for studying physiochemical properties, or for other small-scale applications. This work represents significant progress towards finding environmentally benign, and economically viable, IL synthesis and production methods.

New solvent routes were explored for IL synthesis, *viz* CO_2 and GXL DMSO. CO_2 was found to be a potentially sustainable, 'green', replacement for traditional volatile organic solvents in the production of ILs, as shown here for the synthesis of [HMIm][Br]. Compressed CO_2 allowed for control of phase behavior (dissolution of reactants, or precipitation of products) through small changes in operating conditions. While we found that higher CO_2 pressure and composition decreased the kinetic rate constant, the phase behavior with CO_2 allows for facile separation.

The global phase behavior of 1-methylimidazole was investigated from 275.15K to 333.5K. It was found to be a Type V system (or potentially IV), per the scheme of Scott

and van Konynenburg, with regions of vapor-liquid equilibrium, vapor-liquid-liquid equilibrium, liquid-liquid equilibrium, an upper and lower critical endpoint, and mixture critical points. The solubility and volume expansion of CO_2 in 1-methylimidazole, 1-bromohexane, DMSO, 1:1 mixture of 1-methylimidazole and 1-bromohexane, and [HMIm][Br] was determined at 313.15 K and 333.15 K, for pressures ranging from 10-160 bar. The Peng-Robinson equation of state, along with van der Waals 2-parameter mixing rules, was used with estimated critical properties to well correlate the vapor-liquid equilibrium. The phase equilibrium data allowed for a thorough understanding of the reacting system's phase behavior, in addition to kinetic characterization for the synthesis of ILs with CO_2. Experimentally obtained kinetic, thermodynamic and thermo-physical data needed to engineer efficient continuous processes for IL synthesis were presented. The results have important ramifications on the kinetics and process constraints of an actual IL synthesis.

Carbon dioxide (CO_2) was found to induce many IL-solvent mixtures to split into IL-rich and solvent-rich phases that can be decanted, or, at higher pressures, extracted by near- or super-critical CO_2. The synthesis and processing of ILs in a CO_2-expanded media allows for facile separations and reduced solvent amounts. Non-complex separation schemes are proposed from mixture phase behavior. CO_2 has been demonstrated to be a potential solvent for the synthesis of 1-hexyl-3-methylimidazolium bromide ([HMIm][Br]), at different pressures, and at temperatures 313.15 K and 333.15 K. This synthesis route affords the flexibility of tuning the rate of reaction by simply controlling the pressure loading of CO_2. The rate of reaction under certain conditions was found to be as attractive

as using conventional organic solvent. The rate of reaction decreases with increasing CO_2 pressure for imidazolium-based ILs, especially when operating above the mixture critical point. Also, it has been demonstrated that phase equilibrium, as well as the solubility of CO_2, plays a significant role in understanding kinetics by decoupling the various effects of compressed CO_2.

The synthesis of ILs in CO_2 expanded DMSO systems is a potential solvent route for IL synthesis. Although increasing CO_2 concentration decreases the polarity of polar aprotic DMSO, high reaction rates are still attainable for this solvent media, up until about greater than 80 percent CO_2 mole fraction, and are attributed to local composition effects. Further, we demonstrated that the kinetic benefits of DMSO and the thermodynamic advantages of environmentally benign CO_2 can be leveraged for the production of ILs. Kamlet Taft (*KT*) polarity parameters were obtained for CO_2 expanded DMSO over various CO_2 compositions.

Quantitative second (2^{nd}) order rate constants for the synthesis of 1-alkyl-3-methyl-imidazolium halide, 1-hexyl-pyridium bromide and 1-hexyl-1-methylpyrrolidinium bromide ILs are reported here. Additionally, LSER regression results using *KT* polarity parameters are presented. New IL synthesis systems can be rapidly estimated from these empirical correlations. There are numerous types of substituents (R-groups) that yield different physical and chemical properties of ILs, using a variety of different starting materials.

Comparative environmental and economic assessments were carried out for the different IL synthesis routes proposed. Potential "hot" spots (unit operations that have the most impact on the environment and profitability) in the life cycle of the processes were identified. CO_2 emerged as the most economic route and has the least environmental impact. We have demonstrated throughout this study that a solvent is important for IL synthesis, and the selection process for an optimal solvent must consider several factors, discussed here in detail. The preliminary economic and environmental assessments of the proposed routes suggest that CO_2 is the desirable route for IL synthesis. While the CXL-DMSO process can be potentially competitive, optimized and new separation techniques will be critical to achieve this. The acetone reactor costs are significantly lower than those of the high pressure processes (CXL and CO_2), due to mild operating conditions. However, the CO_2 route is the most environmentally friendly and economically competitive, as it eradicates the need for energy intensive distillation. Also, CO_2 is a cheap and readily available solvent. The conventional synthesis of ILs in a common solvent, such as dichloromethane have the worst environmental impact of all the solvent routes proposed, while the use of neat CO_2 is the route with the least environmental impact. These results serve as engineering recommendations for design best practice in future green and economic IL synthesis.

9.2. Recommendations and Future Work

- To move beyond the preliminary stage (lab scale experiments and estimations) of IL production, more thermodynamic data and transport data will be needed to complete technical design optimizations necessary for implementation in a pilot scale study.
-
- There is a need to consider easier evaluations using free EPA software/tools for IL systems. Commercial software, such as GaBi®, can be expensive, especially for researchers in academia; inventory data for ILs are often unavailable. Since there are still no industrial scale processes, many of these studies are benchmarked against hypotheticals. Cradle-to-grave LCA analysis will be important for the next stages of IL deployment. Researchers have shown that cradle-to-gate LCA are more comprehensive and thus give a better picture of the true greenness of processes. Sometimes, emissions/impacts can be simply shifted from one branch/node of the life cycle tree to another. To date, very limited inventory data remains a road block for this kind of analysis for IL systems; it can get expensive to accumulate commercial inventory databases such as GaBi®.

- ILs synthesis typically involves two steps: (1) an alkylation and an (2) anion exchange step. This work focused on the first step, as most ILs can be synthesized from halide ILs such as [HMim][Br], the model IL in this study. Work should be extended to anion exchange techniques, so that overall process may be optimized for sustainable and economic production of the IL.

- The age-old petrochemical industry utilizes conventional thermodynamic methods (such as UNIFAC) to model, correlate, and predict separations for various mixtures of well characterized compounds. However, very little experimental and modeling precedent exists in the literature for IL synthesis systems. The design and selection of optimal ILs for chemical processes can be realized by optimizing phase equilibrium thermodynamics. However, the binary and ternary data for systems involving ILs is meager. It is impractical to experimentally test individual ILs, and with binary or ternary systems involving ILs being even greater in number, it is to be expected that little to no data exists for such systems. Hence, there is an increasingly urgent need for predictive tools in the study of ILs. Molecular based models would be highly useful in the design of ILs, and in screening for specific properties advantageous to separations.

- IL data is lacking: the sheer enormity of the available cations makes it daunting to experimentally test all IL systems. Empirically derived correlations (LSER) will be most helpful to the engineering community for estimating parameters needed in design and study in an *a priori* manner. Predictive methods must be employed. In the literature, few studies have considered the relationship between the structure of ILs and their properties. Reliable and well-populated sample data for physiochemical properties are needed for these kinds of empirical correlations. Only through more in-depth knowledge of the solution chemistry (solubility properties, activity coefficient of ILs in different solvent media, etc.) can practical, reliable correlations emerge.

New empirical correlations to open literature for quick property estimation are crucial for solving engineering problems.

- Ethyl acetate (EA) has been identified as a potential green solvent for IL synthesis processes. Thermodynamic data involving different kinds of IL and EA will be useful across the entire IL community. Logically, one is expected to derive savings and lower environmental impact from switching to liquid-liquid extraction systems, however, large amounts of solvent are often required to achieve desired purity. These must be factors in the overall "greenness" analysis. When employing EA as a solvent for IL production, costs will need to be quantified before the process truly be said to be greener than alternative routes.

- For feasible implementation in biomass processes, recyclability of the IL is imperative: 1g of cellulose to 10 g of IL to 100g of water is not sustainable. The first step for determining IL recyclability is identifying the minimal amount of water required to maintain optimum or workable cellulose solubility efficiency. Currently, solubility data remains qualitative, and so, new methodologies must emerge for a quantitative method that will allow researchers to optimize cellulose solubility and impurity (such as water and other biomolecules) effects on these systems. Ongoing work within Scurto's group is investigating new methods to quantify these effects.

Appendix A: Kinetic Data and Mixture Densities

Reaction-Mixture Densities

Solvent	ρ(25°C) (g/cm^3)	ρ(40°C) (g/cm^3)	ρ(60°C) (g/cm^3)
Acetone	0.81627	0.79953	0.77850
ACN	0.82092	0.80868	0.79015
DMSO	1.08401	1.07340	1.05890
Methanol	0.84150	0.82690	0.80700

Table 1.

Density Measurements for Pyridine and 1-bromohexane 1:1: 20 solvents			
Solvents	**25°C (g/cm^3)**	**40 °C (g/cm^3)**	**60 °C (g/cm^3)**
Acetone	0.8296	0.8123	-
acetonirtile	0.8300	0.8133	0.7902
2-Butanone	0.8308	0.8147	0.7929
Chlorobenzene	1.1016	1.0853	1.0633
Cyclopentanon	0.9604	0.9457	0.9258
DCM	1.2730	1.1144	-
DMSO (25 & 40)	1.0960	1.0807	1.0598
Ethyl formate	0.9383	0.9186	-
Ethyl Lactate	1.0338	1.0173	0.9948
Methanol	0.8525	0.8377	-

Density Data for 1:1 1-bromohexane & 1-methylimidazole with $x_{acetone}$

T=25°C			
Solvent Ratio	Actual Temp (°C)	Density (g/cm^3)	Density (mg/L)
75%	24.99	0.90172	901720
50%	24.99	0.99063	990630
25%	25	1.06248	1062480
10%	25	1.0956	1095600

T=40°C			
Solvent Ratio	Actual Temp (°C)	Density (g/cm^3)	Density (mg/L)
75%	39.98	0.89616	896160
50%	39.98	0.97991	979910
25%	39.98	1.04879	1048790
10%	39.99	1.08766	1087660

T=50°C			
Solvent Ratio	Actual Temp (°C)	Density (g/cm^3)	Density (mg/L)
75%	49.97	0.88586	885860
50%	49.98	0.97239	972390
25%	49.98	1.04176	1041760
10%	50	1.08097	1080970

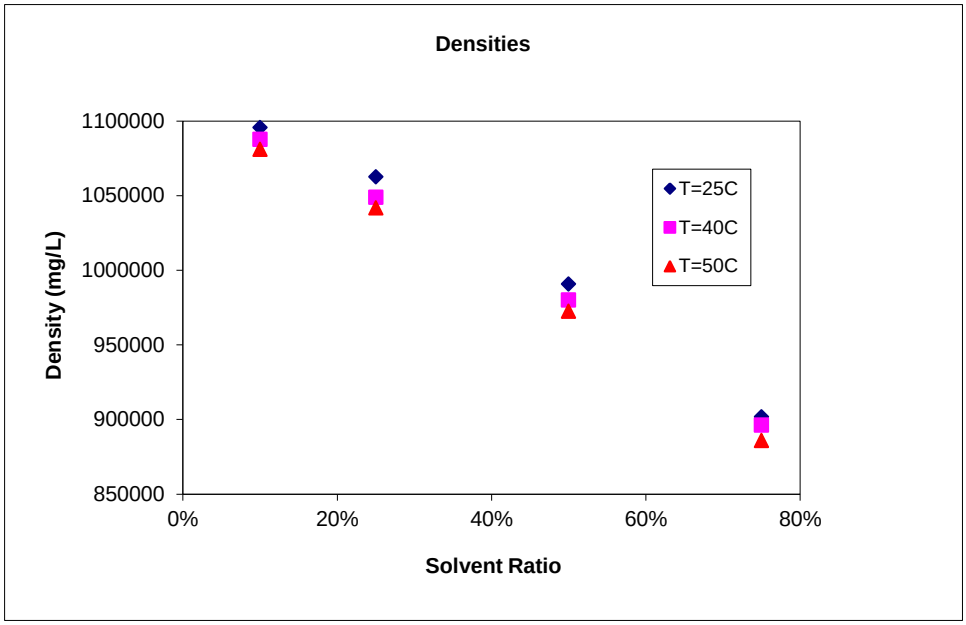

Appendix B: Sigma Plot Code

LSER regression in the form: $\ln k = \ln k^o + a\alpha + b\beta + p(\pi^* - d\delta)$

Use code for solvents when correction parameter is used for chlorinated solvents

```
f=y0+a*x+b*y+c*(w+d*v)    'regression equation in the form of LSER equation
fit f to z

x = col(3) ' {{prevmin: 0.000000}} {{prevmax: 10.000000}} 'column for pi*
y = col(4) ' {{prevmin: 0.000000}} {{prevmax: 5.000000}}   'column for alpha
w = col(5) ' {{prevmin: 0.000000}} {{prevmax: 5.000000}}  'column for beta
v = col(6) ' {{prevmin: 0.000000}} {{prevmax: 5.000000}} 'delta, correction for chlorinated solvents
z = col(2)   'ln k

'Automatic Initial Parameter Estimates
F(q,r)=ape(q,r,1,0,1)

y0 = F(x,z)[1] ''Auto {{previous: -17.8646}}
a = F(x,z)[2] ''Auto {{previous: -2.58233}}
b = F(y,z)[2] ''Auto {{previous: 2.20916}}
c = F(w,z)[2] ''Auto {{previous: 8.28937}}
d = F(v,z)[2] ''Auto {{previous: 8.28937}}

1000      'number of iteration
1
0.0001     'tolerance
```

LSER regression in the form: $\ln k = \ln k^o + a\alpha + b\beta + p\pi^*$

```
f=y0+a*x+b*y+c*w
fit f to z

x = col(3) ' {{prevmin: 0.000000}} {{prevmax: 10.000000}}
y = col(4) ' {{prevmin: 0.000000}} {{prevmax: 5.000000}}
w = col(5) ' {{prevmin: 0.000000}} {{prevmax: 5.000000}}
z = col(2)
'Automatic Initial Parameter Estimates
F(q,r)=ape(q,r,1,0,1)

y0 = F(x,z)[1] ''Auto {{previous: -17.8646}}
a = F(x,z)[2] ''Auto {{previous: -2.58233}}
b = F(y,z)[2] ''Auto {{previous: 2.20916}}
c = F(w,z)[2] ''Auto {{previous: 8.28937}}

1000
1
0.0001
```

2nd Order Kinetic Rate Regression code

```
C=1/(1/y0+k*t)
fit C to y

t = col(1) ' {{prevmin: 0.000000}} {{prevmax: 5.000000}} 't is time
y = col(2)                                                    'C at any
time
y0= col(3)                                                  'C at t=0
'Automatic Initial Parameter Estimate Functions
F(q)=ape(t,y,1,0,1)

k = F(0)[1] ''Auto {{previous: 0.0130703}}

100
100
0.00000000100
```

LSER Regression 25 C-Pyridine + bromohexane (10 solvents)

f = y0+ a*x+ b*y+ c*(w+d*v)

R	Rsqr	Adj Rsqr	Standard Error of Estimate
0.9938	0.9876	0.9778	0.1693

	Coefficient	Std. Error	t	P
y0	-19.5843	0.3957	-49.4877	<0.0001
a	0.1021	0.1938	0.5272	0.6206
b	-1.6067	0.4208	-3.8182	0.0124
c	8.4958	0.5041	16.8537	<0.0001
d	-0.2177	0.0355	-6.1302	0.0017

Analysis of Variance:

Analysis of Variance:

	DF	SS	MS
Regression	5	2063.6503	412.7301
Residual	5	0.1434	0.0287
Total	10	2063.7936	206.3794

Corrected for the mean of the observations:

	DF	SS	MS	F	P
Regression	4	11.4567	2.8642	99.8925	<0.0001
Residual	5	0.1434	0.0287		
Total	9	11.6000	1.2889		

Statistical Tests:

Normality Test (Shapiro-Wilk) Passed (P = 0.3582)

W Statistic= 0.9201 Significance Level = 0.0500

Constant Variance Test Passed (P = 0.6068)

Appendix C: ReactIR

To align ReactIR and improve peak height and contrast

- Check Interferometer alignment
    - Attach the smapling technology tto the conduit
    - Check that the proper smapling technology and detector has been set in the system menu
- In the reactIR software system menu, select contrast command, if there no gains proceed to next step.
- Using a small hex driver, slowly make a small turn of one of the adjustment screw clockwise or counter clock wise while observing the peak height value in display.
- Move to the other adjustment screw and repeat steps until peak height has been maximized.
- Keep data of maximum peak height regularly for reference.

NOTE: Make small adjustments at a time and Keep track of all moves, or you could worsen alignments. When there is no gain after all attempt, contact Vendor.

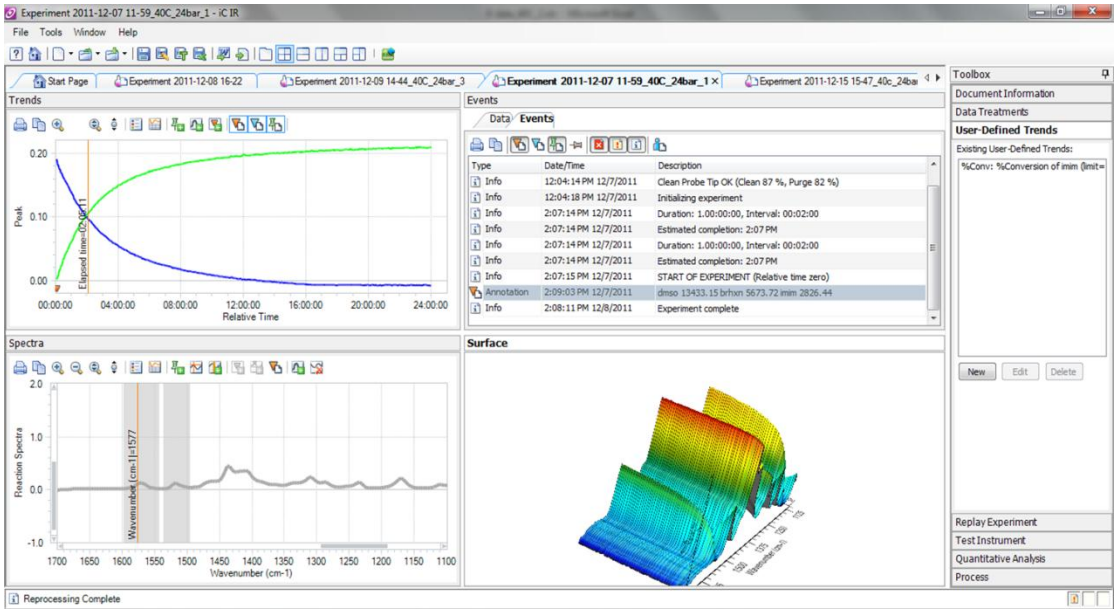

Calibrating Lab view

- Enter Laview, go to measurement and automation tab in start menu
- Locate appropriate folder for version (CP-AI-110@4), click start change to obtain calibration information. Assign and select Channels, note. (T- Channel 0, P- Channel 2 and Rotator-Channel 1)
- After calibration, determine slope and intercepts
- Enter Data in back panel (ctrl + E)

Appendix D: EPI Suite™ output for Chemicals Studied

The Estimation Programs Interface (EPI) Suite is a Windows®-based suite of physical/chemical property and environmental fate estimation programs developed by the EPA's Office of Pollution Prevention Toxics and Syracuse Research Corporation (SRC). A comprehensive search for chemical property data was carried out before using EPI Suite. In addition, EPI Suite implements a database search (called PHYSPROP©).

Acetone:

```
CAS Number: 000067-64-1
SMILES : O=C(C)C
CHEM   : 2-Propanone
MOL FOR: C3 H6 O1
MOL WT : 58.08
------------------------------ EPI SUMMARY (v4.10) --------------------------
 Log Octanol-Water Partition Coef (SRC):
    Log Kow (KOWWIN v1.68 estimate) =  -0.24
    Log Kow (Exper. database match) =  -0.24
       Exper. Ref:  HANSCH,C ET AL. (1995)

Boiling Pt, Melting Pt, Vapor Pressure Estimations (MPBPVP v1.43):
    Boiling Pt (deg C):  44.80  (Adapted Stein & Brown method)
    Melting Pt (deg C):  -93.58  (Mean or Weighted MP)
    VP(mm Hg,25 deg C):  249  (Mean VP of Antoine & Grain methods)
    VP (Pa, 25 deg C) :  3.32E+004  (Mean VP of Antoine & Grain methods)
    MP  (exp database):  -98.3 deg C
    BP  (exp database):  55.5 deg C
    VP  (exp database):  2.32E+02 mm Hg (3.09E+004 Pa) at 25 deg C

 Water Solubility Estimate from Log Kow (WSKOW v1.42):
    Water Solubility at 25 deg C (mg/L):  2.199e+005
       log Kow used: -0.24 (expkow database)
       no-melting pt equation used
     Water Sol (Exper. database match) =  1e+006 mg/L (25 deg C)
        Exper. Ref:  RIDDICK,JA ET AL. (1986)

 Water Sol Estimate from Fragments:
    Wat Sol (v1.01 est) =  2.6753e+005 mg/L

 ECOSAR Class Program (ECOSAR v1.00):
    Class(es) found:
       Neutral Organics

 Henrys Law Constant (25 deg C) [HENRYWIN v3.20]:
   Bond Method :   4.96E-005  atm-m3/mole  (5.02E+000 Pa-m3/mole)
   Group Method:   3.97E-005  atm-m3/mole  (4.02E+000 Pa-m3/mole)
   Exper Database: 3.50E-05  atm-m3/mole  (3.55E+000 Pa-m3/mole)
 For Henry LC Comparison Purposes:
   User-Entered Henry LC:  not entered
   Henrys LC [via VP/WSol estimate using User-Entered or Estimated values]:
      HLC:  8.653E-005 atm-m3/mole  (8.768E+000 Pa-m3/mole)
      VP:   249 mm Hg (source: MPBPVP)
      WS:   2.2E+005 mg/L (source: WSKOWWIN)

 Log Octanol-Air Partition Coefficient (25 deg C) [KOAWIN v1.10]:
  Log Kow used:  -0.24  (exp database)
  Log Kaw used:  -2.844  (exp database)
```

```
      Log Koa (KOAWIN v1.10 estimate):  2.604
      Log Koa (experimental database):  2.310

 Probability of Rapid Biodegradation (BIOWIN v4.10):
   Biowin1 (Linear Model)         :   0.7267
   Biowin2 (Non-Linear Model)     :   0.8495
 Expert Survey Biodegradation Results:
   Biowin3 (Ultimate Survey Model):   3.0483  (weeks       )
   Biowin4 (Primary Survey Model) :   3.7417  (days-weeks  )
 MITI Biodegradation Probability:
   Biowin5 (MITI Linear Model)    :   0.6579
   Biowin6 (MITI Non-Linear Model):   0.8483
 Anaerobic Biodegradation Probability:
   Biowin7 (Anaerobic Linear Model):  0.2850
 Ready Biodegradability Prediction:   YES

Hydrocarbon Biodegradation (BioHCwin v1.01):
    Structure incompatible with current estimation method!

 Sorption to aerosols (25 Dec C)[AEROWIN v1.00]:
  Vapor pressure (liquid/subcooled):  3.09E+004 Pa (232 mm Hg)
  Log Koa (Exp database): 2.310
   Kp (particle/gas partition coef. (m3/ug)):
       Mackay model           :  9.7E-011
       Octanol/air (Koa) model:  5.01E-011
   Fraction sorbed to airborne particulates (phi):
       Junge-Pankow model     :  3.5E-009
       Mackay model           :  7.76E-009
       Octanol/air (Koa) model:  4.01E-009

 Atmospheric Oxidation (25 deg C) [AopWin v1.92]:
   Hydroxyl Radicals Reaction:
      OVERALL OH Rate Constant =   0.2040 E-12 cm3/molecule-sec
      Half-Life =    52.431 Days (12-hr day; 1.5E6 OH/cm3)
   Ozone Reaction:
      No Ozone Reaction Estimation
   Fraction sorbed to airborne particulates (phi):
      5.63E-009 (Junge-Pankow, Mackay avg)
      4.01E-009 (Koa method)
    Note: the sorbed fraction may be resistant to atmospheric oxidation

 Soil Adsorption Coefficient (KOCWIN v2.00):
      Koc    :  2.364  L/kg (MCI method)
      Log Koc:  0.374       (MCI method)
      Koc    :  9.726  L/kg (Kow method)
      Log Koc:  0.988       (Kow method)

 Aqueous Base/Acid-Catalyzed Hydrolysis (25 deg C) [HYDROWIN v2.00]:
    Rate constants can NOT be estimated for this structure!

 Bioaccumulation Estimates (BCFBAF v3.01):
   Log BCF from regression-based method = 0.500 (BCF = 3.162 L/kg wet-wt)
   Log Biotransformation Half-life (HL) = -1.4496 days (HL = 0.03551 days)
   Log BCF Arnot-Gobas method (upper trophic) = -0.032 (BCF = 0.929)
   Log BAF Arnot-Gobas method (upper trophic) = -0.032 (BAF = 0.929)
       log Kow used: -0.24 (expkow database)

 Volatilization from Water:
    Henry LC:  3.5E-005 atm-m3/mole  (Henry experimental database)
    Half-Life from Model River:      13.53  hours
    Half-Life from Model Lake :      211.5  hours   (8.811 days)

 Removal In Wastewater Treatment:
    Total removal:               3.69  percent
    Total biodegradation:        0.09  percent
    Total sludge adsorption:     1.73  percent
    Total to Air:                1.87  percent
      (using 10000 hr Bio P,A,S)

 Level III Fugacity Model:
```

```
           Mass Amount    Half-Life    Emissions
            (percent)        (hr)       (kg/hr)
   Air       12.3           1.17e+003    1000
   Water     42.1           360          1000
   Soil      45.5           720          1000
   Sediment  0.0813         3.24e+003    0
     Persistence Time: 336 hr
```

Dimethylsulfoxide (DMSO)

```
CAS Number: 000067-68-5
SMILES : O=S(C)C
CHEM   : Methane, sulfinylbis-
MOL FOR: C2 H6 O1 S1
MOL WT : 78.13
------------------------------ EPI SUMMARY (v4.10) --------------------------

 Physical Property Inputs:
    Log Kow (octanol-water):   ------
    Boiling Point (deg C)  :   ------
    Melting Point (deg C)  :   ------
    Vapor Pressure (mm Hg) :   ------
    Water Solubility (mg/L):   ------
    Henry LC (atm-m3/mole) :   ------

 Log Octanol-Water Partition Coef (SRC):
    Log Kow (KOWWIN v1.68 estimate) =  -1.22
    Log Kow (Exper. database match) =  -1.35
       Exper. Ref:  HANSCH,C ET AL. (1995)

Boiling Pt, Melting Pt, Vapor Pressure Estimations (MPBPVP v1.43):
    Boiling Pt (deg C):  128.63  (Adapted Stein & Brown method)
    Melting Pt (deg C):  -49.71  (Mean or Weighted MP)
    VP(mm Hg,25 deg C):  0.622  (Mean VP of Antoine & Grain methods)
    VP (Pa, 25 deg C) :  82.9  (Mean VP of Antoine & Grain methods)
    MP  (exp database):  18.5 deg C
    BP  (exp database):  189 deg C
    VP  (exp database):  6.10E-01 mm Hg (8.13E+001 Pa) at 25 deg C

 Water Solubility Estimate from Log Kow (WSKOW v1.42):
    Water Solubility at 25 deg C (mg/L):  1e+006
       log Kow used: -1.35 (expkow database)
       no-melting pt equation used
     Water Sol (Exper. database match) =  1e+006 mg/L ( deg C)
        Exper. Ref:  DORIGAN,J ET AL. (1976A);@2ND

 Water Sol Estimate from Fragments:
    Wat Sol (v1.01 est) =  1e+006 mg/L

 ECOSAR Class Program (ECOSAR v1.00):
    Class(es) found:
       Neutral Organics

 Henrys Law Constant (25 deg C) [HENRYWIN v3.20]:
   Bond Method :   4.96E-008  atm-m3/mole  (5.02E-003 Pa-m3/mole)
   Group Method:   1.90E-003  atm-m3/mole  (1.92E+002 Pa-m3/mole)
   Exper Database: 1.51E-09  atm-m3/mole  (1.53E-004 Pa-m3/mole)
 For Henry LC Comparison Purposes:
   User-Entered Henry LC:  not entered
   Henrys LC [via VP/WSol estimate using User-Entered or Estimated values]:
      HLC:  6.394E-008 atm-m3/mole  (6.479E-003 Pa-m3/mole)
      VP:   0.622 mm Hg (source: MPBPVP)
      WS:   1E+006 mg/L (source: WSKOWWIN)

 Log Octanol-Air Partition Coefficient (25 deg C) [KOAWIN v1.10]:
  Log Kow used:  -1.35  (exp database)
  Log Kaw used:  -7.209  (exp database)
      Log Koa (KOAWIN v1.10 estimate):  5.859
      Log Koa (experimental database):  4.960
```

```
 Probability of Rapid Biodegradation (BIOWIN v4.10):
   Biowin1 (Linear Model)         :   0.7104
   Biowin2 (Non-Linear Model)     :   0.8698
 Expert Survey Biodegradation Results:
   Biowin3 (Ultimate Survey Model):   3.0265  (weeks       )
   Biowin4 (Primary Survey Model) :   3.7350  (days-weeks  )
 MITI Biodegradation Probability:
   Biowin5 (MITI Linear Model)    :   0.4805
   Biowin6 (MITI Non-Linear Model):   0.5766
 Anaerobic Biodegradation Probability:
   Biowin7 (Anaerobic Linear Model):  0.6769
 Ready Biodegradability Prediction:   NO

Hydrocarbon Biodegradation (BioHCwin v1.01):
    Structure incompatible with current estimation method!

 Sorption to aerosols (25 Dec C)[AEROWIN v1.00]:
  Vapor pressure (liquid/subcooled):  81.3 Pa (0.61 mm Hg)
  Log Koa (Exp database): 4.960
   Kp (particle/gas partition coef. (m3/ug)):
       Mackay model           :  3.69E-008
       Octanol/air (Koa) model:  2.24E-008
   Fraction sorbed to airborne particulates (phi):
       Junge-Pankow model     :  1.33E-006
       Mackay model           :  2.95E-006
       Octanol/air (Koa) model:  1.79E-006

 Atmospheric Oxidation (25 deg C) [AopWin v1.92]:
   Hydroxyl Radicals Reaction:
      OVERALL OH Rate Constant =  62.1216 E-12 cm3/molecule-sec
      Half-Life =     0.172 Days (12-hr day; 1.5E6 OH/cm3)
      Half-Life =     2.066 Hrs
   Ozone Reaction:
      No Ozone Reaction Estimation
   Fraction sorbed to airborne particulates (phi):
      2.14E-006 (Junge-Pankow, Mackay avg)
      1.79E-006 (Koa method)
    Note: the sorbed fraction may be resistant to atmospheric oxidation

 Soil Adsorption Coefficient (KOCWIN v2.00):
      Koc    :  2.082  L/kg (MCI method)
      Log Koc:  0.319       (MCI method)
      Koc    :  1.877  L/kg (Kow method)
      Log Koc:  0.273       (Kow method)

 Aqueous Base/Acid-Catalyzed Hydrolysis (25 deg C) [HYDROWIN v2.00]:
    Rate constants can NOT be estimated for this structure!

 Bioaccumulation Estimates (BCFBAF v3.01):
   Log BCF from regression-based method = 0.500 (BCF = 3.162 L/kg wet-wt)
   Log Biotransformation Half-life (HL) = -1.6621 days (HL = 0.02177 days)
   Log BCF Arnot-Gobas method (upper trophic) = -0.048 (BCF = 0.8952)
   Log BAF Arnot-Gobas method (upper trophic) = -0.048 (BAF = 0.8952)
       log Kow used: -1.35 (expkow database)

 Volatilization from Water:
    Henry LC:  1.51E-009 atm-m3/mole  (Henry experimental database)
    Half-Life from Model River: 3.427E+005  hours   (1.428E+004 days)
    Half-Life from Model Lake : 3.739E+006  hours   (1.558E+005 days)

 Removal In Wastewater Treatment:
    Total removal:               1.85  percent
    Total biodegradation:        0.09  percent
    Total sludge adsorption:     1.75  percent
    Total to Air:                0.00  percent
      (using 10000 hr Bio P,A,S)

 Level III Fugacity Model:
           Mass Amount    Half-Life    Emissions
            (percent)        (hr)       (kg/hr)
```

```
   Air       0.0325          4.14         1000
   Water     37              360          1000
   Soil      62.8            720          1000
   Sediment  0.071           3.24e+003    0
     Persistence Time: 573 hr
```

Bromohexane

```
CAS Number: 000111-25-1
SMILES : BrCCCCCC
CHEM   : Hexane, 1-bromo-
MOL FOR: C6 H13 Br1
MOL WT : 165.07
------------------------------ EPI SUMMARY (v4.10) -------------------------

 Physical Property Inputs:
    Log Kow (octanol-water):   ------
    Boiling Point (deg C)  :   ------
    Melting Point (deg C)  :   ------
    Vapor Pressure (mm Hg) :   ------
    Water Solubility (mg/L):   ------
    Henry LC (atm-m3/mole) :   ------

 Log Octanol-Water Partition Coef (SRC):
    Log Kow (KOWWIN v1.68 estimate) =  3.63
    Log Kow (Exper. database match) =  3.80
       Exper. Ref:  HANSCH,C ET AL. (1995)

Boiling Pt, Melting Pt, Vapor Pressure Estimations (MPBPVP v1.43):
    Boiling Pt (deg C):  148.07  (Adapted Stein & Brown method)
    Melting Pt (deg C):  -41.59  (Mean or Weighted MP)
    VP(mm Hg,25 deg C):  4.06  (Mean VP of Antoine & Grain methods)
    VP (Pa, 25 deg C) :  541  (Mean VP of Antoine & Grain methods)
    MP  (exp database):  -84.7 deg C
    BP  (exp database):  155.3 deg C
    VP  (exp database):  3.90E+00 mm Hg (5.20E+002 Pa) at 25 deg C

 Water Solubility Estimate from Log Kow (WSKOW v1.42):
    Water Solubility at 25 deg C (mg/L):  36.88
       log Kow used: 3.80 (expkow database)
       no-melting pt equation used
     Water Sol (Exper. database match) =  25.7 mg/L (25 deg C)
        Exper. Ref:  YALKOWSKY,SH & DANNENFELSER,RM (1992)

 Water Sol Estimate from Fragments:
    Wat Sol (v1.01 est) =  77.93 mg/L

 ECOSAR Class Program (ECOSAR v1.00):
    Class(es) found:
       Bromoalkanes

 Henrys Law Constant (25 deg C) [HENRYWIN v3.20]:
   Bond Method :   3.50E-002  atm-m3/mole  (3.55E+003 Pa-m3/mole)
   Group Method:   3.22E-002  atm-m3/mole  (3.27E+003 Pa-m3/mole)
   Exper Database: 3.28E-02  atm-m3/mole  (3.32E+003 Pa-m3/mole)
 For Henry LC Comparison Purposes:
   User-Entered Henry LC:  not entered
   Henrys LC [via VP/WSol estimate using User-Entered or Estimated values]:
      HLC:  2.391E-002 atm-m3/mole  (2.423E+003 Pa-m3/mole)
      VP:   4.06 mm Hg (source: MPBPVP)
      WS:   36.9 mg/L (source: WSKOWWIN)

 Log Octanol-Air Partition Coefficient (25 deg C) [KOAWIN v1.10]:
  Log Kow used:  3.80  (exp database)
  Log Kaw used:  0.127  (exp database)
      Log Koa (KOAWIN v1.10 estimate):  3.673
      Log Koa (experimental database):  None

 Probability of Rapid Biodegradation (BIOWIN v4.10):
   Biowin1 (Linear Model)         :   0.7312
   Biowin2 (Non-Linear Model)     :   0.1262
```

```
 Expert Survey Biodegradation Results:
   Biowin3 (Ultimate Survey Model):   3.1617  (weeks       )
   Biowin4 (Primary Survey Model) :   3.9140  (days        )
 MITI Biodegradation Probability:
   Biowin5 (MITI Linear Model)    :   0.5653
   Biowin6 (MITI Non-Linear Model):   0.3477
 Anaerobic Biodegradation Probability:
   Biowin7 (Anaerobic Linear Model):  0.9278
 Ready Biodegradability Prediction:   YES

Hydrocarbon Biodegradation (BioHCwin v1.01):
    Structure incompatible with current estimation method!

 Sorption to aerosols (25 Dec C)[AEROWIN v1.00]:
  Vapor pressure (liquid/subcooled):  520 Pa (3.9 mm Hg)
  Log Koa (Koawin est  ): 3.673
   Kp (particle/gas partition coef. (m3/ug)):
       Mackay model           :  5.77E-009
       Octanol/air (Koa) model:  1.16E-009
   Fraction sorbed to airborne particulates (phi):
       Junge-Pankow model     :  2.08E-007
       Mackay model           :  4.62E-007
       Octanol/air (Koa) model:  9.25E-008

 Atmospheric Oxidation (25 deg C) [AopWin v1.92]:
   Hydroxyl Radicals Reaction:
      OVERALL OH Rate Constant =   4.9923 E-12 cm3/molecule-sec
      Half-Life =     2.142 Days (12-hr day; 1.5E6 OH/cm3)
      Half-Life =    25.710 Hrs
   Ozone Reaction:
      No Ozone Reaction Estimation
   Fraction sorbed to airborne particulates (phi):
      3.35E-007 (Junge-Pankow, Mackay avg)
      9.25E-008 (Koa method)
    Note: the sorbed fraction may be resistant to atmospheric oxidation

 Soil Adsorption Coefficient (KOCWIN v2.00):
      Koc    :  239.7  L/kg (MCI method)
      Log Koc:  2.380       (MCI method)
      Koc    :  1984  L/kg (Kow method)
      Log Koc:  3.298       (Kow method)

 Aqueous Base/Acid-Catalyzed Hydrolysis (25 deg C) [HYDROWIN v2.00]:
  Total Kb for pH > 8 at 25 deg C :  3.176E-009  L/mol-sec
  Kb Half-Life at pH 8: 6.915E+006  years
  Kb Half-Life at pH 7: 6.915E+007  years
    (Total Kb applies only to esters, carbmates, alkyl halides)

 Bioaccumulation Estimates (BCFBAF v3.01):
   Log BCF from regression-based method = 2.174 (BCF = 149.4 L/kg wet-wt)
   Log Biotransformation Half-life (HL) = -0.1189 days (HL = 0.7605 days)
   Log BCF Arnot-Gobas method (upper trophic) = 2.335 (BCF = 216.4)
   Log BAF Arnot-Gobas method (upper trophic) = 2.335 (BAF = 216.5)
       log Kow used: 3.80 (expkow database)

 Volatilization from Water:
    Henry LC:  0.0328 atm-m3/mole  (Henry experimental database)
    Half-Life from Model River:      1.334  hours
    Half-Life from Model Lake :      122.3  hours   (5.095 days)

 Removal In Wastewater Treatment:
    Total removal:              93.44  percent
    Total biodegradation:        0.07  percent
    Total sludge adsorption:    12.94  percent
    Total to Air:               80.44  percent
      (using 10000 hr Bio P,A,S)

 Level III Fugacity Model:
           Mass Amount    Half-Life    Emissions
            (percent)        (hr)       (kg/hr)
```

```
   Air       28.7            43.9         1000
   Water     56.8            360          1000
   Soil      13.9            720          1000
   Sediment  0.621           3.24e+003    0
     Persistence Time: 109 hr
```

Methylimidazole

```
SMILES : c1nccn1C
CHEM   : C:\Users\Sylvia\Documents\Sylvia Phd work\CO2_kinetics paper\methylim
         idazole.mol
MOL FOR: C4 H6 N2
MOL WT : 82.11

------------------------------ EPI SUMMARY (v4.10) --------------------------
    Henry LC (atm-m3/mole) :   ------
    Log Kow (octanol-water):   ------
    Boiling Point (deg C)  :   ------
    Water Solubility (mg/L):   ------
 Physical Property Inputs:
    Vapor Pressure (mm Hg) :   ------
    Melting Point (deg C)  :   ------

 Log Octanol-Water Partition Coef (SRC):
    Log Kow (KOWWIN v1.68 estimate) =  0.61
    Log Kow (Exper. database match) =  -0.06
       Exper. Ref:  HANSCH,C ET AL. (1995)

Boiling Pt, Melting Pt, Vapor Pressure Estimations (MPBPVP v1.43):
    Boiling Pt (deg C):  194.34  (Adapted Stein & Brown method)
    Melting Pt (deg C):  2.62  (Mean or Weighted MP)
    VP(mm Hg,25 deg C):  0.451  (Mean VP of Antoine & Grain methods)
    VP (Pa, 25 deg C) :  60.2  (Mean VP of Antoine & Grain methods)
    MP  (exp database):  -6 deg C
    BP  (exp database):  195.5 deg C

 Water Solubility Estimate from Log Kow (WSKOW v1.42):
    Water Solubility at 25 deg C (mg/L):  1.458e+005
       log Kow used: -0.06 (expkow database)
       no-melting pt equation used
     Water Sol (Exper. database match) =  1e+006 mg/L (20 deg C)
        Exper. Ref:  YALKOWSKY,SH & DANNENFELSER,RM (1992)

 Water Sol Estimate from Fragments:
    Wat Sol (v1.01 est) =  77219 mg/L

 ECOSAR Class Program (ECOSAR v1.00):
    Class(es) found:
       Imidazoles

 Henrys Law Constant (25 deg C) [HENRYWIN v3.20]:
   Bond Method :   8.01E-005  atm-m3/mole  (8.12E+000 Pa-m3/mole)
   Group Method:   Incomplete
 For Henry LC Comparison Purposes:
   User-Entered Henry LC:  not entered
   Henrys LC [via VP/WSol estimate using User-Entered or Estimated values]:
      HLC:  3.342E-007 atm-m3/mole  (3.386E-002 Pa-m3/mole)
      VP:   0.451 mm Hg (source: MPBPVP)
      WS:   1.46E+005 mg/L (source: WSKOWWIN)

 Log Octanol-Air Partition Coefficient (25 deg C) [KOAWIN v1.10]:
  Log Kow used:  -0.06  (exp database)
  Log Kaw used:  -2.485  (HenryWin est)
      Log Koa (KOAWIN v1.10 estimate):  2.425
      Log Koa (experimental database):  None

 Probability of Rapid Biodegradation (BIOWIN v4.10):
   Biowin1 (Linear Model)         :   0.7085
   Biowin2 (Non-Linear Model)     :   0.8633
 Expert Survey Biodegradation Results:
   Biowin3 (Ultimate Survey Model):   3.0177  (weeks       )
```

```
  Biowin4 (Primary Survey Model) :   3.7293  (days-weeks  )
MITI Biodegradation Probability:
  Biowin5 (MITI Linear Model)    :   0.4929
  Biowin6 (MITI Non-Linear Model):   0.6307
Anaerobic Biodegradation Probability:
  Biowin7 (Anaerobic Linear Model):  0.4702
Ready Biodegradability Prediction:   NO

Hydrocarbon Biodegradation (BioHCwin v1.01):
    Structure incompatible with current estimation method!

Sorption to aerosols (25 Dec C)[AEROWIN v1.00]:
 Vapor pressure (liquid/subcooled):  54.9 Pa (0.412 mm Hg)
 Log Koa (Koawin est  ): 2.425
  Kp (particle/gas partition coef. (m3/ug)):
      Mackay model           :  5.46E-008
      Octanol/air (Koa) model:  6.53E-011
  Fraction sorbed to airborne particulates (phi):
      Junge-Pankow model     :  1.97E-006
      Mackay model           :  4.37E-006
      Octanol/air (Koa) model:  5.23E-009

Atmospheric Oxidation (25 deg C) [AopWin v1.92]:
  Hydroxyl Radicals Reaction:
     OVERALL OH Rate Constant =  36.1360 E-12 cm3/molecule-sec
     Half-Life =     0.296 Days (12-hr day; 1.5E6 OH/cm3)
     Half-Life =     3.552 Hrs
  Ozone Reaction:
     No Ozone Reaction Estimation
  Fraction sorbed to airborne particulates (phi):
     3.17E-006 (Junge-Pankow, Mackay avg)
     5.23E-009 (Koa method)
   Note: the sorbed fraction may be resistant to atmospheric oxidation

Soil Adsorption Coefficient (KOCWIN v2.00):
     Koc    :  32.5  L/kg (MCI method)
     Log Koc:  1.512       (MCI method)
     Koc    :  19.51  L/kg (Kow method)
     Log Koc:  1.290       (Kow method)

Aqueous Base/Acid-Catalyzed Hydrolysis (25 deg C) [HYDROWIN v2.00]:
   Rate constants can NOT be estimated for this structure!

Bioaccumulation Estimates (BCFBAF v3.01):
  Log BCF from regression-based method = 0.500 (BCF = 3.162 L/kg wet-wt)
  Log Biotransformation Half-life (HL) = -0.7218 days (HL = 0.1898 days)
  Log BCF Arnot-Gobas method (upper trophic) = -0.011 (BCF = 0.9752)
  Log BAF Arnot-Gobas method (upper trophic) = -0.011 (BAF = 0.9752)
      log Kow used: -0.06 (expkow database)

Volatilization from Water:
   Henry LC:  8.01E-005 atm-m3/mole  (estimated by Bond SAR Method)
   Half-Life from Model River:      7.548  hours
   Half-Life from Model Lake :      158.3  hours   (6.597 days)

Removal In Wastewater Treatment:
   Total removal:               5.80  percent
   Total biodegradation:        0.09  percent
   Total sludge adsorption:     1.70  percent
   Total to Air:                4.02  percent
     (using 10000 hr Bio P,A,S)

Level III Fugacity Model:
          Mass Amount    Half-Life    Emissions
            (percent)        (hr)       (kg/hr)
  Air       1.34           7.1          1000
  Water     33             360          1000
  Soil      65.6           720          1000
  Sediment  0.105          3.24e+003    0
    Persistence Time: 330 hr
```

Carbon dioxide

```
CAS Number: 000124-38-9
SMILES : O=C=O
CHEM   : Carbon dioxide
MOL FOR: C1 O2
MOL WT : 44.01
------------------------------ EPI SUMMARY (v4.10) --------------------------

 Physical Property Inputs:
    Log Kow (octanol-water):   ------
    Boiling Point (deg C)  :   ------
    Melting Point (deg C)  :   ------
    Vapor Pressure (mm Hg) :   ------
    Water Solubility (mg/L):   ------
    Henry LC (atm-m3/mole) :   ------

 Log Octanol-Water Partition Coef (SRC):
    Log Kow (KOWWIN v1.68 estimate) =  0.83
    Log Kow (Exper. database match) =  0.83
       Exper. Ref:  HANSCH,C ET AL. (1995)

Boiling Pt, Melting Pt, Vapor Pressure Estimations (MPBPVP v1.43):
    Boiling Pt (deg C):  -16.00  (Adapted Stein & Brown method)
    Melting Pt (deg C):  -105.19  (Mean or Weighted MP)
    VP(mm Hg,25 deg C):  1.78E+004  (Mean VP of Antoine & Grain methods)
    VP (Pa, 25 deg C) :  2.37E+006  (Mean VP of Antoine & Grain methods)
    MP  (exp database):  -56.5 deg C
    BP  (exp database):  -78.48 deg C
    VP  (exp database):  4.83E+04 mm Hg (6.44E+006 Pa) at 25 deg C

 Water Solubility Estimate from Log Kow (WSKOW v1.42):
    Water Solubility at 25 deg C (mg/L):  2.572e+004
       log Kow used: 0.83 (expkow database)
       no-melting pt equation used
     Water Sol (Exper. database match) =  1480 mg/L (25 deg C)
        Exper. Ref:  YALKOWSKY,SH & DANNENFELSER,RM (1992)

 Water Sol Estimate from Fragments:
    Wat Sol (v1.01 est) =  1474.9 mg/L

 ECOSAR Class Program (ECOSAR v1.00):
    Class(es) found:
       Neutral Organics

 Henrys Law Constant (25 deg C) [HENRYWIN v3.20]:
   Bond Method :   1.52E-002  atm-m3/mole  (1.54E+003 Pa-m3/mole)
   Group Method:   Incomplete
   Exper Database: 1.52E-02  atm-m3/mole  (1.54E+003 Pa-m3/mole)
 For Henry LC Comparison Purposes:
   User-Entered Henry LC:  not entered
   Henrys LC [via VP/WSol estimate using User-Entered or Estimated values]:
      HLC:  1.711E-003 atm-m3/mole  (1.734E+002 Pa-m3/mole)
      VP:   1.78E+004 mm Hg (source: MPBPVP)
      WS:   2.57E+004 mg/L (source: WSKOWWIN)

 Log Octanol-Air Partition Coefficient (25 deg C) [KOAWIN v1.10]:
  Log Kow used:  0.83  (exp database)
  Log Kaw used:  -0.207  (exp database)
      Log Koa (KOAWIN v1.10 estimate):  1.037
      Log Koa (experimental database):  None

 Probability of Rapid Biodegradation (BIOWIN v4.10):
   Biowin1 (Linear Model)         :   0.7266
   Biowin2 (Non-Linear Model)     :   0.9156
 Expert Survey Biodegradation Results:
   Biowin3 (Ultimate Survey Model):   3.1019  (weeks       )
   Biowin4 (Primary Survey Model) :   3.7842  (days        )
 MITI Biodegradation Probability:
   Biowin5 (MITI Linear Model)    :   0.5812
```

```
   Biowin6 (MITI Non-Linear Model):   0.7782
 Anaerobic Biodegradation Probability:
   Biowin7 (Anaerobic Linear Model):  0.8361
 Ready Biodegradability Prediction:   YES

Hydrocarbon Biodegradation (BioHCwin v1.01):
    Structure incompatible with current estimation method!

 Sorption to aerosols (25 Dec C)[AEROWIN v1.00]:
  Vapor pressure (liquid/subcooled):  6.44E+006 Pa (4.83E+004 mm Hg)
  Log Koa (Koawin est  ): 1.037
   Kp (particle/gas partition coef. (m3/ug)):
       Mackay model           :  4.66E-013
       Octanol/air (Koa) model:  2.67E-012
   Fraction sorbed to airborne particulates (phi):
       Junge-Pankow model     :  1.68E-011
       Mackay model           :  3.73E-011
       Octanol/air (Koa) model:  2.14E-010

 Atmospheric Oxidation (25 deg C) [AopWin v1.92]:
   Hydroxyl Radicals Reaction:
      OVERALL OH Rate Constant =   0.0000 E-12 cm3/molecule-sec
      Half-Life =   -------
   Ozone Reaction:
      No Ozone Reaction Estimation
   Fraction sorbed to airborne particulates (phi):
      2.7E-011 (Junge-Pankow, Mackay avg)
      2.14E-010 (Koa method)
    Note: the sorbed fraction may be resistant to atmospheric oxidation

 Soil Adsorption Coefficient (KOCWIN v2.00):
      Koc    :  1  L/kg (MCI method)
      Log Koc:  0.000       (MCI method)
      Koc    :  14.29  L/kg (Kow method)
      Log Koc:  1.155       (Kow method)

 Aqueous Base/Acid-Catalyzed Hydrolysis (25 deg C) [HYDROWIN v2.00]:
    Rate constants can NOT be estimated for this structure!

 Bioaccumulation Estimates (BCFBAF v3.01):
   Log BCF from regression-based method = 0.500 (BCF = 3.162 L/kg wet-wt)
   Log Biotransformation Half-life (HL) = -1.3948 days (HL = 0.04029 days)
   Log BCF Arnot-Gobas method (upper trophic) = 0.123 (BCF = 1.328)
   Log BAF Arnot-Gobas method (upper trophic) = 0.123 (BAF = 1.328)
       log Kow used: 0.83 (expkow database)

 Volatilization from Water:
    Henry LC:  0.0152 atm-m3/mole  (Henry experimental database)
    Half-Life from Model River:     0.7025  hours   (42.15 min)
    Half-Life from Model Lake :      63.29  hours   (2.637 days)

 Removal In Wastewater Treatment:
    Total removal:              85.60  percent
    Total biodegradation:        0.03  percent
    Total sludge adsorption:     0.48  percent
    Total to Air:               85.08  percent
      (using 10000 hr Bio P,A,S)

 Level III Fugacity Model:
           Mass Amount    Half-Life    Emissions
            (percent)        (hr)       (kg/hr)
   Air       55.7           1e+005       1000
   Water     42.6           360          1000
   Soil      1.64           720          1000
   Sediment  0.0797         3.24e+003    0
     Persistence Time: 146 hr
```

1-hexyl-3-methylimidazolium bromide

```
SMILES : C1=CN(CCCCCC)CN1CBr
CHEM   : C:\Users\Sylvia\Documents\Sylvia Phd work\hmimbr.m
```

```
        ol
MOL FOR: C10 H19 Br1 N2
MOL WT : 247.18

------------------------------ EPI SUMMARY (v4.10) -------------------------
 Log Octanol-Water Partition Coef (SRC):
    Log Kow (KOWWIN v1.68 estimate) =  1.72

Boiling Pt, Melting Pt, Vapor Pressure Estimations (MPBPVP v1.43):
    Boiling Pt (deg C):  282.70  (Adapted Stein & Brown method)
    Melting Pt (deg C):  75.88  (Mean or Weighted MP)
    VP(mm Hg,25 deg C):  0.0016  (Modified Grain method)
    VP (Pa, 25 deg C) :  0.214  (Modified Grain method)
    Subcooled liquid VP: 0.00487 mm Hg (25 deg C, Mod-Grain method)
                       : 0.649 Pa (25 deg C, Mod-Grain method)

 Water Solubility Estimate from Log Kow (WSKOW v1.42):
    Water Solubility at 25 deg C (mg/L):  8547
       log Kow used: 1.72 (estimated)
       no-melting pt equation used

 Water Sol Estimate from Fragments:
    Wat Sol (v1.01 est) =  25039 mg/L

 ECOSAR Class Program (ECOSAR v1.00):
    Class(es) found:
       Aliphatic Amines
       Vinyl/Allyl Amines

 Henrys Law Constant (25 deg C) [HENRYWIN v3.20]:
   Bond Method :   3.31E-006  atm-m3/mole  (3.35E-001 Pa-m3/mole)
   Group Method:   Incomplete
 For Henry LC Comparison Purposes:
   User-Entered Henry LC:  not entered
   Henrys LC [via VP/WSol estimate using User-Entered or Estimated values]:
      HLC:  6.088E-008 atm-m3/mole  (6.169E-003 Pa-m3/mole)
      VP:   0.0016 mm Hg (source: MPBPVP)
      WS:   8.55E+003 mg/L (source: WSKOWWIN)

 Log Octanol-Air Partition Coefficient (25 deg C) [KOAWIN v1.10]:
  Log Kow used:  1.72  (KowWin est)
  Log Kaw used:  -3.869  (HenryWin est)
      Log Koa (KOAWIN v1.10 estimate):  5.589
      Log Koa (experimental database):  None

 Probability of Rapid Biodegradation (BIOWIN v4.10):
   Biowin1 (Linear Model)         :   0.2816
   Biowin2 (Non-Linear Model)     :   0.0005
 Expert Survey Biodegradation Results:
   Biowin3 (Ultimate Survey Model):   2.4706  (weeks-months)
   Biowin4 (Primary Survey Model) :   3.2196  (weeks       )
 MITI Biodegradation Probability:
   Biowin5 (MITI Linear Model)    :   0.2329
   Biowin6 (MITI Non-Linear Model):   0.0188
 Anaerobic Biodegradation Probability:
   Biowin7 (Anaerobic Linear Model): -1.4630
 Ready Biodegradability Prediction:   NO

Hydrocarbon Biodegradation (BioHCwin v1.01):
    Structure incompatible with current estimation method!

 Sorption to aerosols (25 Dec C)[AEROWIN v1.00]:
  Vapor pressure (liquid/subcooled):  0.649 Pa (0.00487 mm Hg)
  Log Koa (Koawin est  ): 5.589
   Kp (particle/gas partition coef. (m3/ug)):
       Mackay model           :  4.62E-006
       Octanol/air (Koa) model:  9.53E-008
   Fraction sorbed to airborne particulates (phi):
       Junge-Pankow model     :  0.000167
       Mackay model           :  0.000369
```

```
      Octanol/air (Koa) model:  7.62E-006

 Atmospheric Oxidation (25 deg C) [AopWin v1.92]:
   Hydroxyl Radicals Reaction:
      OVERALL OH Rate Constant = 156.6757 E-12 cm3/molecule-sec
      Half-Life =     0.068 Days (12-hr day; 1.5E6 OH/cm3)
      Half-Life =     0.819 Hrs
   Ozone Reaction:
      OVERALL Ozone Rate Constant =     0.175000 E-17 cm3/molecule-sec
      Half-Life =     6.549 Days (at 7E11 mol/cm3)
   Fraction sorbed to airborne particulates (phi):
      0.000268 (Junge-Pankow, Mackay avg)
      7.62E-006 (Koa method)
    Note: the sorbed fraction may be resistant to atmospheric oxidation

 Soil Adsorption Coefficient (KOCWIN v2.00):
      Koc    :  437.3  L/kg (MCI method)
      Log Koc:  2.641       (MCI method)
      Koc    :  55.69  L/kg (Kow method)
      Log Koc:  1.746       (Kow method)

 Aqueous Base/Acid-Catalyzed Hydrolysis (25 deg C) [HYDROWIN v2.00]:
    Rate constants can NOT be estimated for this structure!

 Bioaccumulation Estimates (BCFBAF v3.01):
   Log BCF from regression-based method = 0.799 (BCF = 6.301 L/kg wet-wt)
   Log Biotransformation Half-life (HL) = -2.2176 days (HL = 0.006059 days)
   Log BCF Arnot-Gobas method (upper trophic) = 0.243 (BCF = 1.752)
   Log BAF Arnot-Gobas method (upper trophic) = 0.243 (BAF = 1.752)
       log Kow used: 1.72 (estimated)

 Volatilization from Water:
    Henry LC:  3.31E-006 atm-m3/mole  (estimated by Bond SAR Method)
    Half-Life from Model River:      279.7  hours   (11.65 days)
    Half-Life from Model Lake :       3183  hours   (132.6 days)

 Removal In Wastewater Treatment:
    Total removal:               2.24  percent
    Total biodegradation:        0.09  percent
    Total sludge adsorption:     1.96  percent
    Total to Air:                0.19  percent
      (using 10000 hr Bio P,A,S)

 Level III Fugacity Model:
           Mass Amount    Half-Life    Emissions
            (percent)        (hr)       (kg/hr)
   Air       0.078          1.62         1000
   Water     19.4           900          1000
   Soil      80.1           1.8e+003     1000
   Sediment  0.47           8.1e+003     0
     Persistence Time: 1.01e+003 hr
```

Ethyl Acetate

```
CAS Number: 000141-78-6
SMILES : O=C(OCC)C
CHEM   : Acetic acid ethyl ester
MOL FOR: C4 H8 O2
MOL WT : 88.11
------------------------------ EPI SUMMARY (v4.10) --------------------------

Log Octanol-Water Partition Coef (SRC):
    Log Kow (KOWWIN v1.68 estimate) =  0.86
    Log Kow (Exper. database match) =  0.73
       Exper. Ref:  HANSCH,C ET AL. (1995)

Boiling Pt, Melting Pt, Vapor Pressure Estimations (MPBPVP v1.43):
    Boiling Pt (deg C):  77.91  (Adapted Stein & Brown method)
    Melting Pt (deg C):  -82.08  (Mean or Weighted MP)
    VP(mm Hg,25 deg C):  98.3  (Mean VP of Antoine & Grain methods)
    VP (Pa, 25 deg C) :  1.31E+004  (Mean VP of Antoine & Grain methods)
```

```
   MP  (exp database):  -83.6 deg C
   BP  (exp database):  77.1 deg C
   VP  (exp database):  9.32E+01 mm Hg (1.24E+004 Pa) at 25 deg C

Water Solubility Estimate from Log Kow (WSKOW v1.42):
   Water Solubility at 25 deg C (mg/L):  2.993e+004
      log Kow used: 0.73 (expkow database)
      no-melting pt equation used
    Water Sol (Exper. database match) =  8e+004 mg/L (25 deg C)
       Exper. Ref:  BANERJEE,S (1984)

Water Sol Estimate from Fragments:
   Wat Sol (v1.01 est) =  38942 mg/L

ECOSAR Class Program (ECOSAR v1.00):
   Class(es) found:
      Esters

Henrys Law Constant (25 deg C) [HENRYWIN v3.20]:
  Bond Method :   2.33E-004  atm-m3/mole  (2.36E+001 Pa-m3/mole)
  Group Method:   1.58E-004  atm-m3/mole  (1.60E+001 Pa-m3/mole)
  Exper Database: 1.34E-04  atm-m3/mole  (1.36E+001 Pa-m3/mole)
For Henry LC Comparison Purposes:
  User-Entered Henry LC:  not entered
  Henrys LC [via VP/WSol estimate using User-Entered or Estimated values]:
     HLC:  3.808E-004 atm-m3/mole  (3.858E+001 Pa-m3/mole)
     VP:   98.3 mm Hg (source: MPBPVP)
     WS:   2.99E+004 mg/L (source: WSKOWWIN)

Log Octanol-Air Partition Coefficient (25 deg C) [KOAWIN v1.10]:
 Log Kow used:  0.73  (exp database)
 Log Kaw used:  -2.261  (exp database)
     Log Koa (KOAWIN v1.10 estimate):  2.991
     Log Koa (experimental database):  2.700

Probability of Rapid Biodegradation (BIOWIN v4.10):
  Biowin1 (Linear Model)         :   0.8798
  Biowin2 (Non-Linear Model)     :   0.9971
Expert Survey Biodegradation Results:
  Biowin3 (Ultimate Survey Model):   3.1447  (weeks       )
  Biowin4 (Primary Survey Model) :   3.9496  (days        )
MITI Biodegradation Probability:
  Biowin5 (MITI Linear Model)    :   0.8440
  Biowin6 (MITI Non-Linear Model):   0.9477
Anaerobic Biodegradation Probability:
  Biowin7 (Anaerobic Linear Model):  0.8748
Ready Biodegradability Prediction:   YES

Hydrocarbon Biodegradation (BioHCwin v1.01):
    Structure incompatible with current estimation method!

Sorption to aerosols (25 Dec C)[AEROWIN v1.00]:
 Vapor pressure (liquid/subcooled):  1.24E+004 Pa (93.2 mm Hg)
 Log Koa (Exp database): 2.700
  Kp (particle/gas partition coef. (m3/ug)):
      Mackay model           :  2.41E-010
      Octanol/air (Koa) model:  1.23E-010
  Fraction sorbed to airborne particulates (phi):
      Junge-Pankow model     :  8.72E-009
      Mackay model           :  1.93E-008
      Octanol/air (Koa) model:  9.84E-009

Atmospheric Oxidation (25 deg C) [AopWin v1.92]:
  Hydroxyl Radicals Reaction:
     OVERALL OH Rate Constant =   1.7038 E-12 cm3/molecule-sec
     Half-Life =     6.278 Days (12-hr day; 1.5E6 OH/cm3)
     Half-Life =    75.331 Hrs
  Ozone Reaction:
     No Ozone Reaction Estimation
  Fraction sorbed to airborne particulates (phi):
```

```
      1.4E-008 (Junge-Pankow, Mackay avg)
      9.84E-009 (Koa method)
    Note: the sorbed fraction may be resistant to atmospheric oxidation

 Soil Adsorption Coefficient (KOCWIN v2.00):
      Koc    :  5.583  L/kg (MCI method)
      Log Koc:  0.747       (MCI method)
      Koc    :  18.34  L/kg (Kow method)
      Log Koc:  1.263       (Kow method)

 Aqueous Base/Acid-Catalyzed Hydrolysis (25 deg C) [HYDROWIN v2.00]:
  Total Kb for pH > 8 at 25 deg C :  1.208E-001  L/mol-sec
  Kb Half-Life at pH 8:      66.387  days
  Kb Half-Life at pH 7:       1.818  years
    (Total Kb applies only to esters, carbmates, alkyl halides)

 Bioaccumulation Estimates (BCFBAF v3.01):
   Log BCF from regression-based method = 0.500 (BCF = 3.162 L/kg wet-wt)
   Log Biotransformation Half-life (HL) = -1.7848 days (HL = 0.01641 days)
   Log BCF Arnot-Gobas method (upper trophic) = 0.047 (BCF = 1.114)
   Log BAF Arnot-Gobas method (upper trophic) = 0.047 (BAF = 1.114)
       log Kow used: 0.73 (expkow database)

 Volatilization from Water:
    Henry LC:  0.000134 atm-m3/mole  (Henry experimental database)
    Half-Life from Model River:      5.059  hours
    Half-Life from Model Lake :      133.9  hours   (5.579 days)

 Removal In Wastewater Treatment:
    Total removal:               8.07  percent
    Total biodegradation:        0.09  percent
    Total sludge adsorption:     1.68  percent
    Total to Air:                6.30  percent
      (using 10000 hr Bio P,A,S)

 Level III Fugacity Model:
           Mass Amount    Half-Life    Emissions
            (percent)        (hr)       (kg/hr)
   Air       15.2           160          1000
   Water     41.1           360          1000
   Soil      43.7           720          1000
   Sediment  0.0848         3.24e+003    0
     Persistence Time: 264 hr
```

Acetonitrile

```
CAS Number: 000075-05-8
SMILES : C(#N)C
CHEM   : Acetonitrile
MOL FOR: C2 H3 N1
MOL WT : 41.05
------------------------------ EPI SUMMARY (v4.10) --------------------------

 Log Octanol-Water Partition Coef (SRC):
    Log Kow (KOWWIN v1.68 estimate) =  -0.15
    Log Kow (Exper. database match) =  -0.34
       Exper. Ref:  HANSCH,C ET AL. (1995)

Boiling Pt, Melting Pt, Vapor Pressure Estimations (MPBPVP v1.43):
    Boiling Pt (deg C):  71.84  (Adapted Stein & Brown method)
    Melting Pt (deg C):  -83.79  (Mean or Weighted MP)
    VP(mm Hg,25 deg C):  200  (Mean VP of Antoine & Grain methods)
    VP (Pa, 25 deg C) :  2.67E+004  (Mean VP of Antoine & Grain methods)
    MP  (exp database):  -45 deg C
    BP  (exp database):  59.6 deg C
    VP  (exp database):  8.88E+01 mm Hg (1.18E+004 Pa) at 25 deg C

 Water Solubility Estimate from Log Kow (WSKOW v1.42):
    Water Solubility at 25 deg C (mg/L):  1.367e+005
       log Kow used: -0.34 (expkow database)
       no-melting pt equation used
```

```
    Water Sol (Exper. database match) =  1e+006 mg/L (25 deg C)
       Exper. Ref:  RIDDICK,JA ET AL. (1986)

Water Sol Estimate from Fragments:
   Wat Sol (v1.01 est) =  2.2266e+005 mg/L

ECOSAR Class Program (ECOSAR v1.00):
   Class(es) found:
      Neutral Organics

Henrys Law Constant (25 deg C) [HENRYWIN v3.20]:
  Bond Method :   3.06E-005  atm-m3/mole  (3.10E+000 Pa-m3/mole)
  Group Method:   3.46E-005  atm-m3/mole  (3.50E+000 Pa-m3/mole)
  Exper Database: 3.45E-05  atm-m3/mole  (3.50E+000 Pa-m3/mole)
For Henry LC Comparison Purposes:
  User-Entered Henry LC:  not entered
  Henrys LC [via VP/WSol estimate using User-Entered or Estimated values]:
     HLC:  7.902E-005 atm-m3/mole  (8.007E+000 Pa-m3/mole)
     VP:   200 mm Hg (source: MPBPVP)
     WS:   1.37E+005 mg/L (source: WSKOWWIN)

Log Octanol-Air Partition Coefficient (25 deg C) [KOAWIN v1.10]:
 Log Kow used:  -0.34  (exp database)
 Log Kaw used:  -2.851  (exp database)
     Log Koa (KOAWIN v1.10 estimate):  2.511
     Log Koa (experimental database):  2.310

Probability of Rapid Biodegradation (BIOWIN v4.10):
  Biowin1 (Linear Model)         :   1.0350
  Biowin2 (Non-Linear Model)     :   0.9992
Expert Survey Biodegradation Results:
  Biowin3 (Ultimate Survey Model):   3.0261  (weeks       )
  Biowin4 (Primary Survey Model) :   3.7233  (days-weeks  )
MITI Biodegradation Probability:
  Biowin5 (MITI Linear Model)    :   0.6621
  Biowin6 (MITI Non-Linear Model):   0.8312
Anaerobic Biodegradation Probability:
  Biowin7 (Anaerobic Linear Model):  0.7565
Ready Biodegradability Prediction:   YES

Hydrocarbon Biodegradation (BioHCwin v1.01):
    Structure incompatible with current estimation method!

Sorption to aerosols (25 Dec C)[AEROWIN v1.00]:
 Vapor pressure (liquid/subcooled):  1.18E+004 Pa (88.8 mm Hg)
 Log Koa (Exp database): 2.310
  Kp (particle/gas partition coef. (m3/ug)):
      Mackay model           :  2.53E-010
      Octanol/air (Koa) model:  5.01E-011
  Fraction sorbed to airborne particulates (phi):
      Junge-Pankow model     :  9.15E-009
      Mackay model           :  2.03E-008
      Octanol/air (Koa) model:  4.01E-009

Atmospheric Oxidation (25 deg C) [AopWin v1.92]:
  Hydroxyl Radicals Reaction:
     OVERALL OH Rate Constant =   0.0258 E-12 cm3/molecule-sec
     Half-Life =   413.931 Days (12-hr day; 1.5E6 OH/cm3)
  Ozone Reaction:
     No Ozone Reaction Estimation
  Fraction sorbed to airborne particulates (phi):
     1.47E-008 (Junge-Pankow, Mackay avg)
     4.01E-009 (Koa method)
   Note: the sorbed fraction may be resistant to atmospheric oxidation

Soil Adsorption Coefficient (KOCWIN v2.00):
     Koc    :  4.67  L/kg (MCI method)
     Log Koc:  0.669       (MCI method)
     Koc    :  13.46  L/kg (Kow method)
     Log Koc:  1.129       (Kow method)
```

```
 Aqueous Base/Acid-Catalyzed Hydrolysis (25 deg C) [HYDROWIN v2.00]:
    Rate constants can NOT be estimated for this structure!

 Bioaccumulation Estimates (BCFBAF v3.01):
   Log BCF from regression-based method = 0.500 (BCF = 3.162 L/kg wet-wt)
   Log Biotransformation Half-life (HL) = -1.3475 days (HL = 0.04493 days)
   Log BCF Arnot-Gobas method (upper trophic) = -0.034 (BCF = 0.9244)
   Log BAF Arnot-Gobas method (upper trophic) = -0.034 (BAF = 0.9244)
       log Kow used: -0.34 (expkow database)

 Volatilization from Water:
    Henry LC:  3.45E-005 atm-m3/mole  (Henry experimental database)
    Half-Life from Model River:      11.53  hours
    Half-Life from Model Lake :      179.5  hours   (7.478 days)

 Removal In Wastewater Treatment:
    Total removal:               3.67  percent
    Total biodegradation:        0.09  percent
    Total sludge adsorption:     1.73  percent
    Total to Air:                1.85  percent
      (using 10000 hr Bio P,A,S)

 Level III Fugacity Model:
           Mass Amount    Half-Life    Emissions
            (percent)        (hr)       (kg/hr)
   Air       11.9           1.54e+003    1000
   Water     40.3           360          1000
   Soil      47.8           720          1000
   Sediment  0.0816         3.24e+003    0
     Persistence Time: 347 hr
```

Chlorobenzene

```
CAS Number: 000108-90-7
SMILES : c(cccc1)(c1)CL
CHEM   : Benzene, chloro-
MOL FOR: C6 H5 CL1
MOL WT : 112.56
------------------------------ EPI SUMMARY (v4.10) --------------------------

 Log Octanol-Water Partition Coef (SRC):
    Log Kow (KOWWIN v1.68 estimate) =  2.64
    Log Kow (Exper. database match) =  2.84
       Exper. Ref:  SANGSTER (1994)

Boiling Pt, Melting Pt, Vapor Pressure Estimations (MPBPVP v1.43):
    Boiling Pt (deg C):  139.63  (Adapted Stein & Brown method)
    Melting Pt (deg C):  -45.78  (Mean or Weighted MP)
    VP(mm Hg,25 deg C):  9.27  (Mean VP of Antoine & Grain methods)
    VP (Pa, 25 deg C) :  1.24E+003  (Mean VP of Antoine & Grain methods)
    MP  (exp database):  -45.2 deg C
    BP  (exp database):  131.7 deg C
    VP  (exp database):  1.20E+01 mm Hg (1.60E+003 Pa) at 25 deg C

 Water Solubility Estimate from Log Kow (WSKOW v1.42):
    Water Solubility at 25 deg C (mg/L):  400.5
       log Kow used: 2.84 (expkow database)
       no-melting pt equation used
     Water Sol (Exper. database match) =  498 mg/L (25 deg C)
        Exper. Ref:  HORVATH,AL (1982)

 Water Sol Estimate from Fragments:
    Wat Sol (v1.01 est) =  392.21 mg/L

 ECOSAR Class Program (ECOSAR v1.00):
    Class(es) found:
       Neutral Organics

 Henrys Law Constant (25 deg C) [HENRYWIN v3.20]:
   Bond Method :   3.99E-003  atm-m3/mole  (4.04E+002 Pa-m3/mole)
```

```
  Group Method:   4.55E-003  atm-m3/mole  (4.62E+002 Pa-m3/mole)
  Exper Database: 3.11E-03  atm-m3/mole  (3.15E+002 Pa-m3/mole)
For Henry LC Comparison Purposes:
  User-Entered Henry LC:  not entered
  Henrys LC [via VP/WSol estimate using User-Entered or Estimated values]:
     HLC:  3.428E-003 atm-m3/mole  (3.473E+002 Pa-m3/mole)
     VP:   9.27 mm Hg (source: MPBPVP)
     WS:   401 mg/L (source: WSKOWWIN)

Log Octanol-Air Partition Coefficient (25 deg C) [KOAWIN v1.10]:
 Log Kow used:  2.84  (exp database)
 Log Kaw used:  -0.896  (exp database)
     Log Koa (KOAWIN v1.10 estimate):  3.736
     Log Koa (experimental database):  3.310

Probability of Rapid Biodegradation (BIOWIN v4.10):
  Biowin1 (Linear Model)         :   0.6396
  Biowin2 (Non-Linear Model)     :   0.7674
Expert Survey Biodegradation Results:
  Biowin3 (Ultimate Survey Model):   2.7658  (weeks       )
  Biowin4 (Primary Survey Model) :   3.5249  (days-weeks  )
MITI Biodegradation Probability:
  Biowin5 (MITI Linear Model)    :   0.4245
  Biowin6 (MITI Non-Linear Model):   0.4153
Anaerobic Biodegradation Probability:
  Biowin7 (Anaerobic Linear Model):  0.1748
Ready Biodegradability Prediction:   NO

Hydrocarbon Biodegradation (BioHCwin v1.01):
    Structure incompatible with current estimation method!

Sorption to aerosols (25 Dec C)[AEROWIN v1.00]:
 Vapor pressure (liquid/subcooled):  1.6E+003 Pa (12 mm Hg)
 Log Koa (Exp database): 3.310
  Kp (particle/gas partition coef. (m3/ug)):
      Mackay model           :  1.87E-009
      Octanol/air (Koa) model:  5.01E-010
  Fraction sorbed to airborne particulates (phi):
      Junge-Pankow model     :  6.77E-008
      Mackay model           :  1.5E-007
      Octanol/air (Koa) model:  4.01E-008

Atmospheric Oxidation (25 deg C) [AopWin v1.92]:
  Hydroxyl Radicals Reaction:
     OVERALL OH Rate Constant =   1.3716 E-12 cm3/molecule-sec
     Half-Life =     7.798 Days (12-hr day; 1.5E6 OH/cm3)
     Half-Life =    93.575 Hrs
  Ozone Reaction:
     No Ozone Reaction Estimation
  Fraction sorbed to airborne particulates (phi):
     1.09E-007 (Junge-Pankow, Mackay avg)
     4.01E-008 (Koa method)
    Note: the sorbed fraction may be resistant to atmospheric oxidation

Soil Adsorption Coefficient (KOCWIN v2.00):
     Koc    :  233.9  L/kg (MCI method)
     Log Koc:  2.369       (MCI method)
     Koc    :  291.4  L/kg (Kow method)
     Log Koc:  2.464       (Kow method)
      Experimental Log Koc:  2.15  (database)

Aqueous Base/Acid-Catalyzed Hydrolysis (25 deg C) [HYDROWIN v2.00]:
   Rate constants can NOT be estimated for this structure!

Bioaccumulation Estimates (BCFBAF v3.01):
  Log BCF from regression-based method = 1.541 (BCF = 34.74 L/kg wet-wt)
  Log Biotransformation Half-life (HL) = -0.2740 days (HL = 0.532 days)
  Log BCF Arnot-Gobas method (upper trophic) = 1.398 (BCF = 25)
  Log BAF Arnot-Gobas method (upper trophic) = 1.398 (BAF = 25)
      log Kow used: 2.84 (expkow database)
```

```
Volatilization from Water:
   Henry LC:  0.00311 atm-m3/mole  (Henry experimental database)
   Half-Life from Model River:      1.282  hours
   Half-Life from Model Lake :      102.9  hours   (4.29 days)

Removal In Wastewater Treatment:
   Total removal:              56.63  percent
   Total biodegradation:        0.06  percent
   Total sludge adsorption:     3.00  percent
   Total to Air:               53.57  percent
     (using 10000 hr Bio P,A,S)

Level III Fugacity Model:
           Mass Amount    Half-Life    Emissions
            (percent)        (hr)       (kg/hr)
  Air        25.4            333          1000
  Water      28.1            360          1000
  Soil       46.1            720          1000
  Sediment   0.302           3.24e+003    0
    Persistence Time: 230 hr
```

Appendix E: EFRAT Data Input for Chemicals

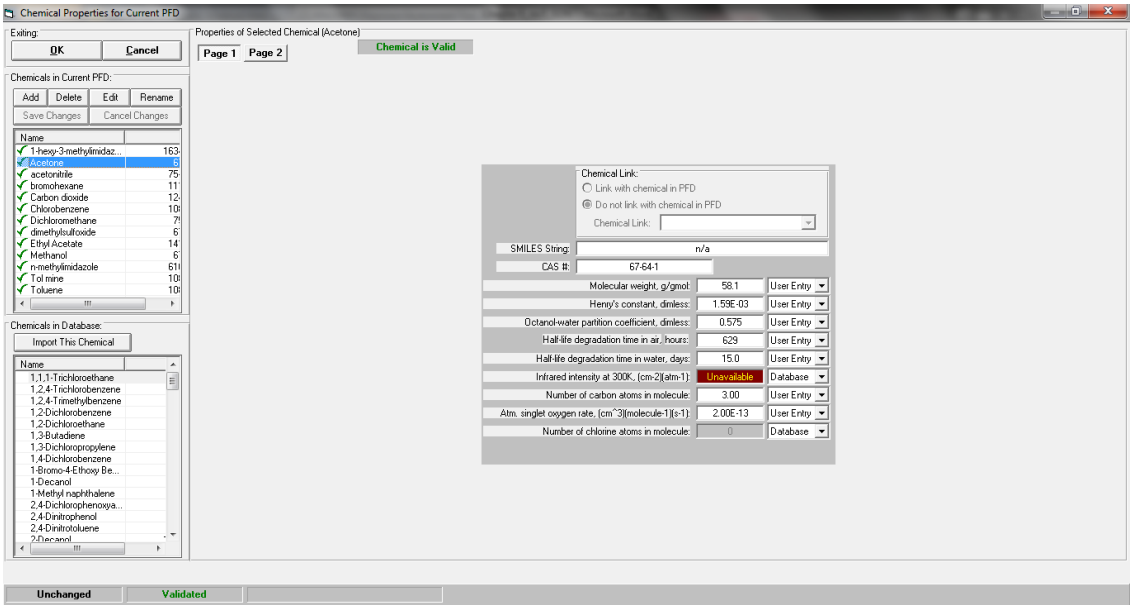

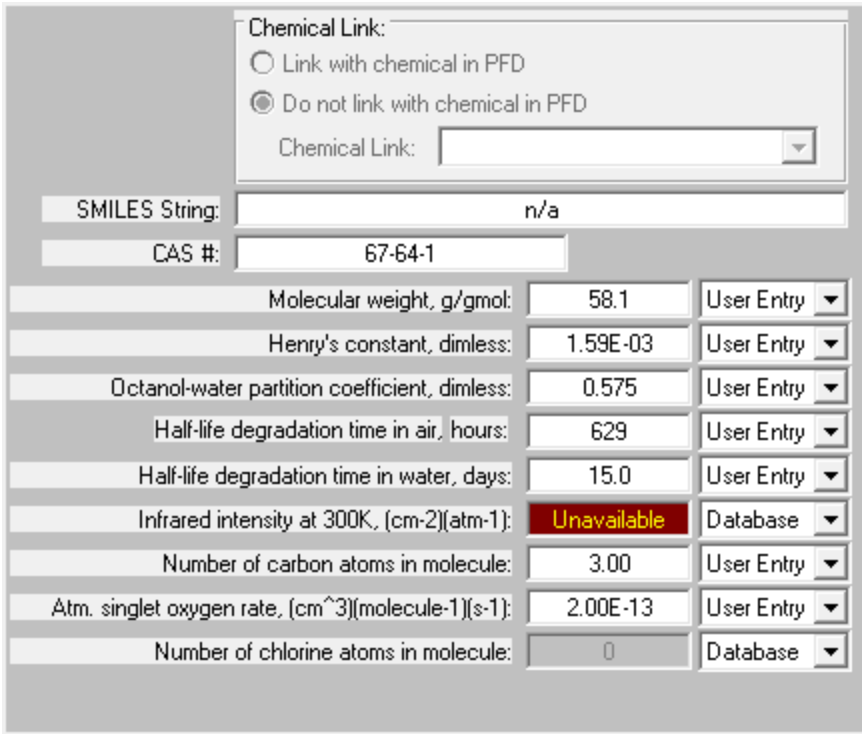
Chemical Link:
Link with chemical in PFD
Do not link with chemical in PFD
Chemical Link:
SMILES String: n/a
CAS #: 67-64-1
Molecular weight, g/gmol: 58.1 User Entry
Henry's constant, dimless: 1.59E-03 User Entry
Octanol-water partition coefficient, dimless: 0.575 User Entry
Half-life degradation time in air, hours: 629 User Entry
Half-life degradation time in water, days: 15.0 User Entry
Infrared intensity at 300K, (cm-2)(atm-1): Unavailable Database
Number of carbon atoms in molecule: 3.00 User Entry
Atm. singlet oxygen rate, (cm^3)(molecule-1)(s-1): 2.00E-13 User Entry
Number of chlorine atoms in molecule: 0 Database

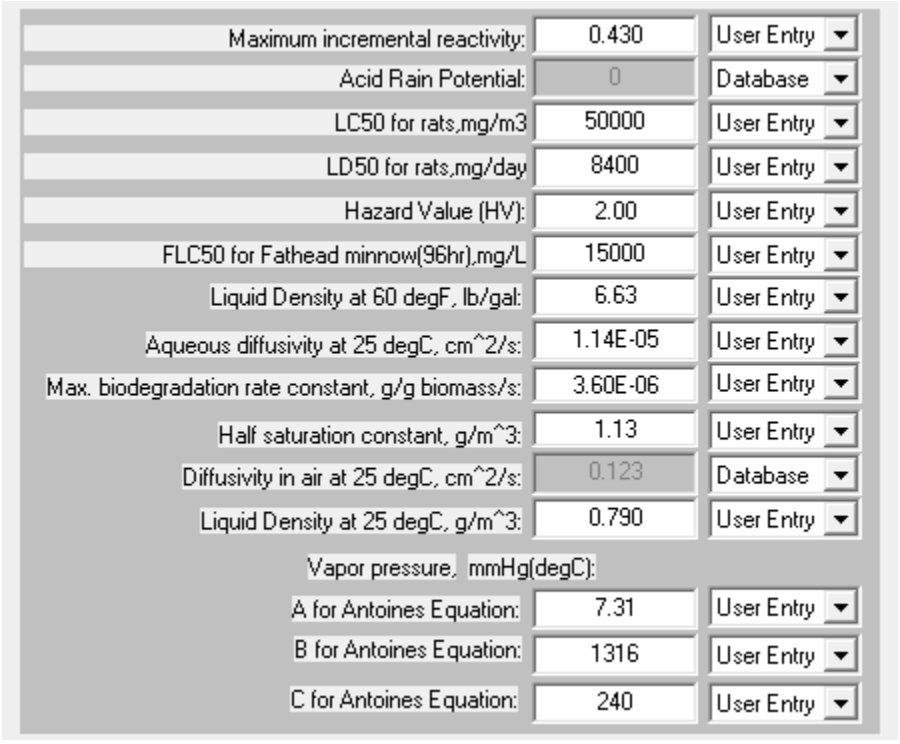
Maximum incremental reactivity: 0.430 User Entry
Acid Rain Potential: 0 Database
LC50 for rats,mg/m3 50000 User Entry
LD50 for rats,mg/day 8400 User Entry
Hazard Value (HV): 2.00 User Entry
FLC50 for Fathead minnow(96hr),mg/L 15000 User Entry
Liquid Density at 60 degF, lb/gal: 6.63 User Entry
Aqueous diffusivity at 25 degC, cm^2/s: 1.14E-05 User Entry
Max. biodegradation rate constant, g/g biomass/s: 3.60E-06 User Entry
Half saturation constant, g/m^3: 1.13 User Entry
Diffusivity in air at 25 degC, cm^2/s: 0.123 Database
Liquid Density at 25 degC, g/m^3: 0.790 User Entry
Vapor pressure, mmHg(degC):
A for Antoines Equation: 7.31 User Entry
B for Antoines Equation: 1316 User Entry
C for Antoines Equation: 240 User Entry

Appendix F: Lambda Cell

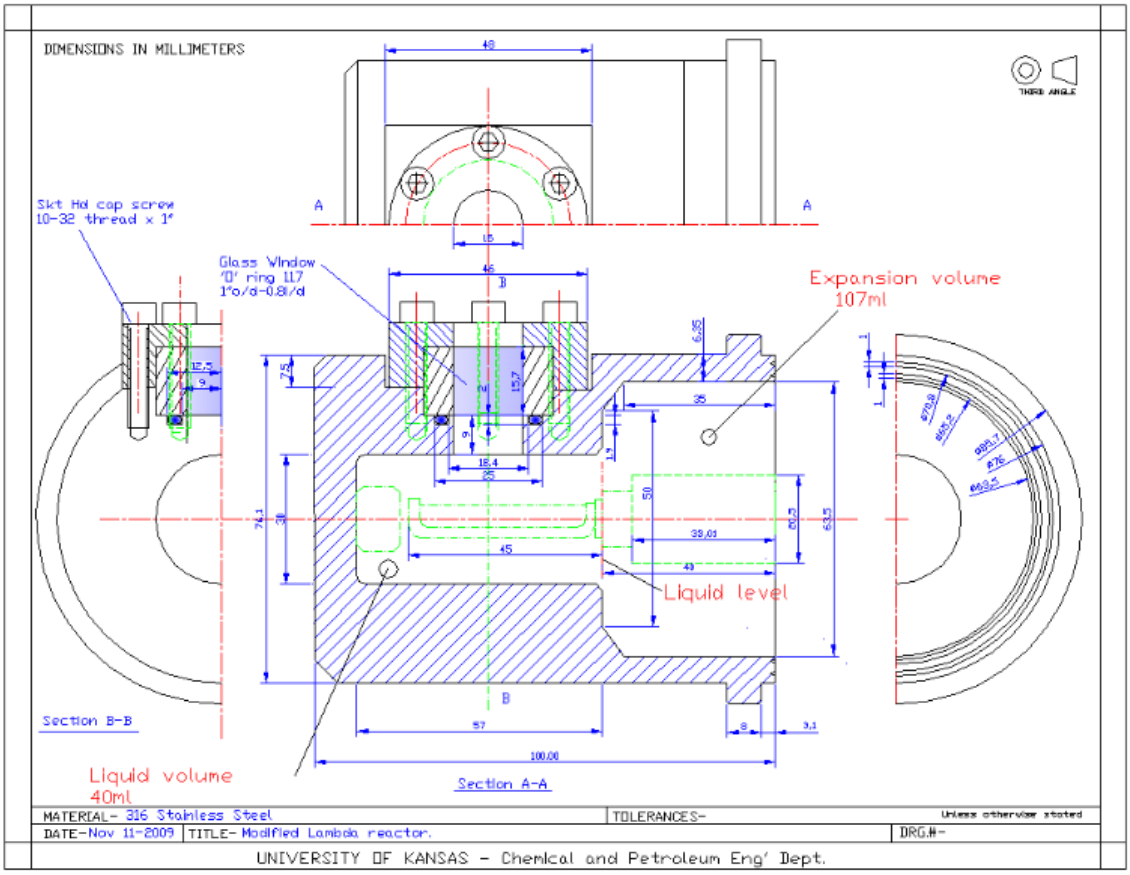

Appendix G: Processing PE2000 data using Excel Macro file

1. Save PE output as text
2. Open new sheet in data processor file document
3. In new sheet import PE data (text file) see illustration

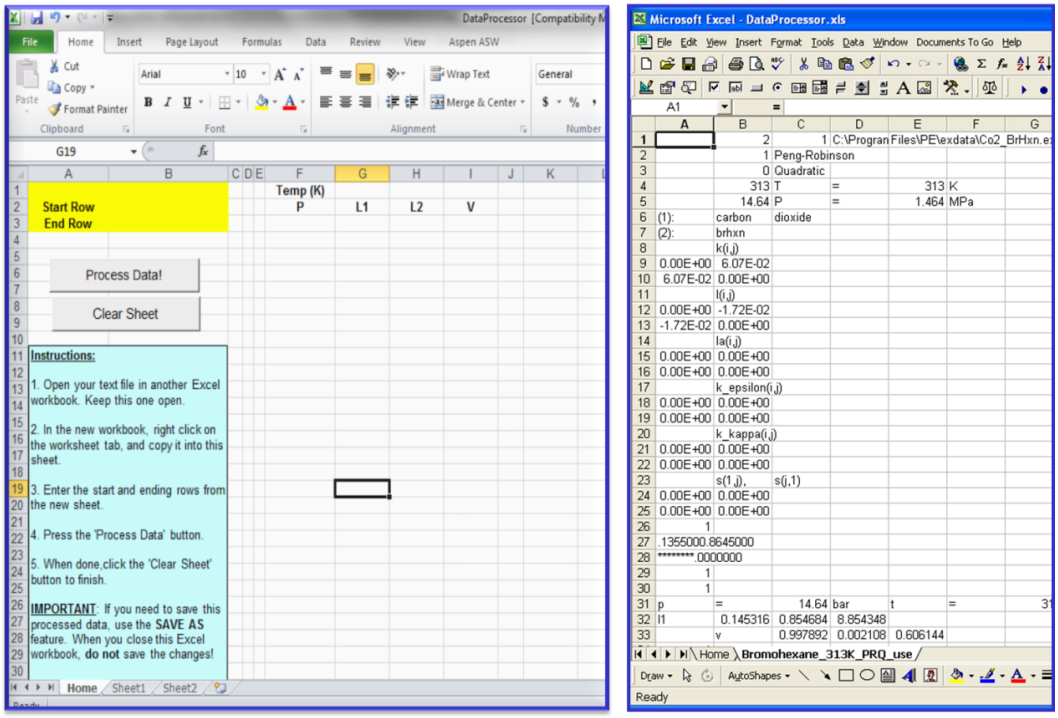

4. Enter start and ending rows from data sheet, then press “process data” button